DELIVERY OF PROAPOPTOTIC BIOMOLECULES AND DRUGS USING AMPHIPHILIC BLOCK COPOLYMER NANOPARTICLES FOR ANTI-CANCER THERAPY

ASHLYNN LINGZHI LEE

NATIONAL UNIVERSITY OF SINGAPORE
2011

DELIVERY OF PROAPOPTOTIC BIOMOLECULES AND DRUGS USING AMPHIPHILIC BLOCK COPOLYMER NANOPARTICLES FOR ANTI-CANCER THERAPY

ASHLYNN LINGZHI LEE
(B.Eng. (Chemical), Hons., NUS)

A THESIS SUBMITTED
FOR THE DEGREE OF DOCTOR OF PHILOSOPHY
DEPARTMENT OF PHYSIOLOGY
NATIONAL UNIVERSITY OF SINGAPORE
2011

ACKNOWLEDGMENTS

First and foremost I want to express gratitude towards my supervisor, Dr. Yi Yan Yang, for her continuous support and encouragement throughout my Ph.D. study. I would also like to thank my co-supervisor, Prof. Shazib Pervaiz, for being so encouraging of my research and for all the valuable advice he has given.

My research was based in the Drug and Gene Delivery group of the Institute of Bioengineering and Nanotecnhology (IBN). The members of this group have contributed immensely to my professional and personal development throughout my studies. They have provided constant support, friendships as well as good advice and collaborations. I would also like to thank Dr. Shu Jun Gao, for his help in my animal studies. Special mention also goes out to Kirthan Shenoy, graduate student in Prof. Pervaiz group, who has given me many useful suggestions on my TRAIL delivery work.

I would also like to express sincere appreciation to the members of my Ph.D. committee who monitored my work and took effort to read and provide precious comments on my thesis.

I am also grateful to the BioMedical Research Council (BMRC)**,** Agency for Science, Technology and Research (A*STAR) and Institute of Bioengineering and Nanotecnhology (IBN), which have been supportive in funding my research as well as providing an excellent working environment for me during the past few years.

Lastly, I would like to thank my family for all their love and encouragement. To my parents who supported me in all my pursuits. And also to my loving, patient and cheering husband Zhi Yuan, who has been my pillar of strength during the ups and downs of my research. Thank you.

Ashlynn Lingzhi Lee
July 2011

TABLE OF CONTENTS

SUMMARY

Nano-sized particles formed from amphiphilic block copolymers have shown great advantages as delivery agents for anti-cancer therapy, such as improving localization in tumor tissues *via* the enhanced permeability and retention (EPR) effect from the hyperpermeable angiogenic vasculature surrounding tumors. Self-assembled cationic polymer nanoparticles with well-defined core/shell structure are promising carriers for synergistic codelivery of small molecule drugs and nucleic acids/proteins against cancer. These particles can encapsulate hydrophobic drugs in the core and bind to biomolecules such as nucleic acids or proteins on the shell. In my research, cationic core/shell nanoparticles self-assembled from a biodegradable amphiphilic copolymer poly{*N*-methyldietheneamine sebacate)-co-[(cholesteryl oxocarbonylamido ethyl) methyl bis(ethylene) ammonium bromide] sebacate}P(MDS-*co*-CES) have been fabricated and used for the codelivery of various anti-cancer drugs and therapeutic proteins for improved cancer therapy.

The first part of this thesis focuses on the evaluation of these cationic nanoparticles as carriers for the delivery of therapeutic proteins. Studies have been performed to determine the *in vitro* cytotoxicity and delivery efficiency of a model therapeutic protein, Lectin-A (MW: 30.7 kDa) through adsorption of the protein on the cationic surface of the P(MDS-*co*-CES) nanoparticles. The results show that the nanoparticles deliver Lectin-A much more efficiently compared to the commercially-available protein carrier, BioPorter.

The core/shell structure of these nanoparticles allows the physical entrapment of hydrophobic drugs in the core. Hence, further studies have been performed by using

P(MDS-*co*-CES) nanoparticles to codeliver another therapeutic protein with a similar molecular weight, i.e. recombinant human tumor necrosis factor-related apoptosis-inducing ligand (TRAIL, MW: 20 kDa), together with an anticancer drug doxorubicin (Dox) simultaneously. TRAIL is a promising anticancer agent as it is selectively toxic to cancer cells and exerts limited toxicity to normal tissues when introduced systemically *in vivo*. Cellular response towards the P(MDS-*co*-CES) nanoparticle/TRAIL nanocomplexes has been investigated in both wild type and TRAIL-resistant SW480 cells (a human colon adenocarcinoma cell line). Cytotoxicity studies have shown that the co-delivery system synergistically enhances cytotoxic and anti-proliferative effects in both wild type and TRAIL-resistant SW480 cells. Receptor-blocking studies have demonstrated that the cellular uptake of Dox-loaded P(MDS-*co*-CES) nanoparticle/TRAIL complexes occurs through specific interactions between the death receptors on the cells and TRAIL present on the nanoparticle surface. Importantly, Dox-loaded nanoparticle/TRAIL nanocomplexes are toxic towards the cancer cells, but they do not exhibit significant cytotoxicity against non-cancerous cells (i.e. WI38, a human lung fibroblast cell line). In a separate study, the codelivery of TRAIL with another anti-cancer drug, paclitaxel (Pac), using P(MDS-*co*-CES) nanoparticles also induced synergistic anti-cancer effects on various human breast cancer cell lines with different TRAIL-sensitivity. The cytotoxicity of the codelivery system is significantly higher compared to free Pac+TRAIL combination in two out of the three cell lines tested.

The versatility of the P(MDS-co-CES) nanoparticles to codeliver larger therapeutic proteins together with anticancer drugs is also investigated. The combination of a therapeutic antibody, Herceptin (MW: 145 kDa) and Pac is used to treat human

breast cancer cells with overexpression of human epidermal growth factor receptor-2 (HER2/neu). Physical characterization shows that the Pac-loaded nanoparticle/herceptin nanocomplexes remain stable under physiologically-simulating conditions with sizes at around 200 nm. Anticancer effects of this co-delivery system have been investigated in human breast cancer cell lines with varying degrees of HER2/neu expression. Targeting ability of this co-delivery system is demonstrated through confocal imaging, which shows significantly higher cellular uptake in HER2-overexpressing BT474 cells as compared to HER2-negative HEK293 cells.

Animal studies were first carried out by investigating the differences in tissue biodistribution between intravenous *vs.* intratumoral injections of nanocarriers through *in vivo* imaging experiments. The latter method shows better tumour accumulation without distribution into major tissue organs. Finally, tumor efficacy studies are performed using the Pac and Herceptin codelivery system to treat female athymic mice that bear BT474 tumor xenografts. Mice that are treated with Pac-loaded nanoparticle/herceptin nanocomplexes experience significantly slower tumor growth compared to those treated with Pac-loaded nanoparticle alone. Lesser tumor growth difference was observed between the codelivery system and herceptin delivered using drug-free nanoparticles.

In all, P(MDS-co-CES) nanoparticles has demonstrated excellent properties as codelivery carriers of multiple therapeutics to cancer cells. Despite the inadequate *in vivo* success of the P(MDS-*co*-CES) nanoparticles, the research presented here contributes to the realization and development of protein-and-drug codelivery in a single therapeutic system. Huge potential can be seen in such polymeric carriers to play an increasingly important role in the future advancement of combination therapy against cancer.

LIST OF TABLES

LIST OF FIGURES

Keuls Multiple Comparison Test after analysis of variance (ANOVA). P≤0.05 was considered statistically significant. (D) An isobologram analysis representing the synergy between the two drugs at combination dose of paclitaxel-loaded nanoparticles (10 mg/l) and TRAIL (10 nM) in MCF7.

Figure 4.6 Cell cycle analysis of (A) MCF7 and (B) MDA-MB-231 cells after 48 hours incubation with (1) medium alone, (2) blank nanoparticles, (3) TRAIL, (4) blank nanoparticle/TRAIL complexes, (5) paclitaxel-loaded nanoparticles (6) paclitaxel-loaded nanoparticle/TRAIL complexes. P(MDS-*co*-CES), TRAIL and paclitaxel concentrations were fixed at 10 mg/l, 10 nM and 1.67 µM for both cell lines. Cell culture was performed in serum-containing medium. The error bars represent the mean ± S.D. (n=3).

Figure 4.7 Viability of (A) MCF7, (B) T47D and (C) MDA-MB-231 cells in the presence or absence of pan-caspase inhibitor ZVAD-FMK (20µM) pretreatment prior to 48 hour incubation with (1) blank nanoparticles, (2) TRAIL, (3) nanoparticle/TRAIL complexes, (4) paclitaxel-loaded nanoparticles and (5) paclitaxel-loaded nanoparticle/TRAIL complexes. P(MDS-*co*-CES), TRAIL and paclitaxel concentrations were fixed at 10 mg/l, 10 nM and 1.67 µM respectively, for all cell lines. Cell culture was performed in serum-containing medium. The error bars represent the mean ± S.D. (n=4). Statistical significance in differences was evaluated by Student's t-Test. P≤0.05 was considered statistically significant.

Figure 4.8 Viability of WI38 cells after 48 hours incubation with (1) blank nanoparticles, (2) TRAIL, (3) blank nanoparticle/TRAIL complexes, (4) Pac-loaded nanoparticles, (5) free Pac, (6) free Pac + TRAIL, (7) Pac-loaded nanoparticle/TRAIL complexes. Cell culture was performed in serum-containing medium. P(MDS-*co*-CES) (10 mg/l), TRAIL (10 nM) and Pac (1.67 µM) were used. The standard deviation is shown by error bars that represent the mean ± S.D. (n=3). Statistical significance in differences was evaluated by Newman–Keuls Multiple Comparison Test after analysis of variance (ANOVA). P≤0.05 was considered statistically significant.

Figure 4.9 (A) Colony formation at Day 17 and 11 in MCF7 and MDA-MB-231 cell lines respectively subsequent to 48 hours treatment with (1) control, (2) blank nanoparticles, (3) TRAIL, (4) blank nanoparticle/TRAIL complexes (5) paclitaxel-loaded nanoparticles (6) paclitaxel-loaded nanoparticle/TRAIL complexes. Colonies were stained with 0.5% w/v crystal violet. Cell culture was performed in serum-containing medium. P(MDS-*co*-CES) (10 mg/l), TRAIL (10 nM) and paclitaxel (1.67 µM) were used. The error bars represent the mean ± S.D. (n=3). Statistical

DOX-loaded micelle concentrations (1 to 20 mg/l) (B). Dox loading level: 8.6%. The standard deviation is shown by error bars that represent the mean ± S.D. (n=3).

Figure 5.6 Viability of parental SW480 (A) and TRAIL-resistant SW480-TR (B) cells after 48 hours incubation with various formulations (TRAIL concentration fixed at 10 nM; Dox-loaded nanoparticle concentrations varied from 1 to 10 mg/l; Dox loading level: 8.6%; Free Dox concentrations: 0.086 and 0.43 mg/l (Equivalent Dox concentration in 1 and 5 mg/l of Dox-loaded nanoparticles) for SW480 and SW480-TR respectively. The standard deviation is shown by error bars that represent the mean ± S.D. (n=3). Cell cycle analysis of parental SW480 (C) and TRAIL-resistant SW480-TR (D) cells after 48 hours incubation. For parental SW480, the concentration of P(MDS-*co*-CES) nanoparticles was 5 mg/l. For TRAIL-resistant SW480-TR, a higher concentration of P(MDS-*co*-CES) nanoparticles (10 mg/l) was used. Dox loading level: 8.6%. TRAIL concentration was fixed at 10 nM. All cell culture experiments were performed in serum-containing medium. The standard deviation is shown by error bars that represent the mean ± S.D. (n=3). Statistical significance in differences was evaluated by Newman–Keuls Multiple Comparison Test after analysis of variance (ANOVA). $P \leq 0.05$ was considered statistically significant. An isobologram analysis representing the synergy between the two drugs at combination dose (colored squares) of Dox-loaded nanoparticles (1 mg/l) and TRAIL (10 nM) in parental SW480 (E) and Dox-loaded nanoparticles (5 mg/l) and TRAIL (10 nM) in TRAIL-resistant SW480-TR (F) cells.

Figure 5.7 Viability of parental SW480 cells in the presence or absence of pan-caspase inhibitor ZVAD-FMK pretreatment (50 µM) prior to 48 hour incubation with nanocomplexes. P(MDS-*co*-CES) and TRAIL concentrations were fixed at 5 mg/l and 10 nM respectively. Dox loading level: 8.6%. Cell culture was performed in serum-containing medium. The error bars represent the mean ± S.D. (n=3). Statistical significance in differences was evaluated by Student's t-Test. $P \leq 0.05$ was considered statistically significant.

Figure 5.8 Viability of WI38 cells after 48 hours incubation with various formulations. Cell culture was performed in serum-containing medium. P(MDS-*co*-CES) (5 mg/l) and TRAIL (10 nM) were used. Dox loading level: 8.6%. Free Dox concentration: 0.43 mg/l (Equivalent Dox concentration in 5 mg/l of Dox-loaded nanoparticles). The standard deviation is shown by error bars that represent the mean ± S.D. (n=3).

Figure 5.9 Colony formation at Day 9 and 13 in parental SW480 and TRAIL-resistant SW480-TR cell lines respectively subsequent to 48 hours

ABBREVIATIONS

Caspase	Cysteine-dependent aspartate-specific protease
DCM	Dichloride methane
DISC	Death-inducing signalling complex
DMAc	Dimethylacetamide
DMEM	Dulbecco's Modified Eagle's Medium
DMF	Dimethylformamide
DMSO	Dimethyl sulfoxide
DNA	Deoxyribonucleic acid
DOX	Doxorubicin.HCl, anticancer drug
DR	Death receptor
FACS	Fluorescence-activated cell sorter
FBS	Fetal bovine serum
FDA	Food and Drug Administration
FLIP	FLICE-like inhibitory protein
HER2	Human Epidermal growth factor receptor-2
HPLC	High Pressure Liquid Chromatography
IAP	Inhibitor of apoptosis protein
MDR	Multi-drug resistance
Mw	Molecular weight
PAC	Paclitaxel, anticancer drug
PEG	Poly(ethylene glycol)
PBS	Phosphate buffered saline
PI	Propidium iodide
PLGA	Poly(L-lactide-co-glycolide)
PLLA	Poly(L-Lactide)
RES	Reticulo Endothelial System
RNA	Ribonucleic acid
Rnase	Ribonuclease
SDS	Sodium dodecyl sulfate
TRAIL	TNF-related apoptosis inducing ligand
zVAD	benzyoxycarbonyl valanyl alanyl aspartyl

LIST OF PUBLICATIONS & PATENTS

Journal Publications

1. **A.L.Z. Lee**, S.H.K. Dhillon, Y. Wang, S. Pervaiz, W. Fan, and Y.-Y. Yang, "Synergistic Anti-Cancer Effects via Co-Delivery of TNF-Related Apoptosis-Inducing Ligand (TRAIL/Apo2L) and Doxorubicin using Micellar Nanoparticles," Molecular BioSystems, 7 (2011) 1512-1522

2. **A.L.Z. Lee**, Y. Wang, S. Pervaiz and Y.Y. Yang, "Synergistic Anticancer Effects Achieved by co-Delivery of TRAIL and Paclitaxel using Cationic Polymeric Micelles," Macromolecular Bioscience, 11 (2011) 296-307

3. **A.L.Z. Lee**, Y. Wang, H.Y. Cheng, S. Pervaiz, Y.Y. Yang, "The Co-Delivery of Paclitaxel and Herceptin using Cationic Micellar Nanoparticles," Biomaterials, 30 (2009) 919-27

4. **A.L.Z. Lee**, Y. Wang, W.H Ye, H.S.Yoon, S.Y. Chan and Y.Y. Yang, "Efficient Intracellular Delivery of Functional Proteins Using Cationic Core/Shell Polymer Nanoparticles," Biomaterials, 29 (2008) 1224-32

Conference Publications

1. **A.L.Z. Lee**, Y. Wang, S. Pervaiz and Y.Y. Yang, ‘Synergistic Effects in Suppressing Cancer Cell Survival and Proliferation by Co-Delivery of TRAIL and Paclitaxel Using Micellar Polymer Nanoparticles’’ 23th European Conference on Biomaterials (ESB) 2010, 11 – 15 Sept 2010, Finland

2. **A.L.Z. Lee**, Y. Wang, H.Y. Cheng, S. Pervaiz and Y.Y. Yang, "The Co-Delivery of Paclitaxel and Herceptin Using Cationic Micellar Nanoparticles," 36th Annual Meeting & Exposition of the Controlled Release Society (CRS) 2009, 18th July – 22 July 2009, Denmark

3. **A.L.Z. Lee**, Y. Wang, H.Y. Cheng, S. Pervaiz and Y.Y. Yang, "The Co-Delivery of Paclitaxel and Herceptin Using Cationic Micellar Nanoparticles," 5th International Conference on Materials for Advanced Technologies (ICMAT) 2009, 28th June - 3rd July 2009, Singapore

4. **A.L.Z. Lee**, Y. Wang, W.H Ye, H.S.Yoon, S.Y. Chan and Y.Y. Yang, "Efficient Intracellular Delivery of Functional Proteins Using Cationic Core/Shell Polymer Nanoparticles," 9th US-Japan Symposium on Drug Delivery System 2007, 16-20 December 2007, USA

5. **A.L.Z. Lee**, Y. Wang, W.H Ye, H.S.Yoon, S.Y. Chan and Y.Y. Yang, "Efficient Intracellular Delivery of Functional Proteins Using Cationic Core/Shell Polymer Nanoparticles," SBE's 3rd International Conference on Bioengineering and Nanotechnology (ICBN) 2007, August 12-15, 2007, Singapore

6. **A.L.Z. Lee**, Y. Wang, W.H Ye, H.S.Yoon, S.Y. Chan and Y.Y. Yang, "Efficient Intracellular Delivery of Functional Proteins Using Cationic Core/Shell Polymer Nanoparticles," 4th International Conference on Materials for Advanced Technologies (ICMAT) 2007, 1 - 6 July 2007, Singapore

Patent

1. Y. Y. Yang, Y. Wang, **A.L.Z. Lee**, "Method of Delivering a Protein into a Cell (Novel Biodegradable Cationic Core Shell Nanoparticles for Delivery of Anionic Therapeutics)" Singapore Patent Granted on July 30, 2010

CHAPTER 1

LITERATURE REVIEW

1.1 Brief Background

Cancer treatment through chemotherapy began as early as the 1940s with the first discovery of nitrogen mustard [1] and folic acid antagonist drugs [2] as anti-cancer agents. Since then, the developments made in cancer therapy have been expanding with tremendous improvements in the understanding of cancer biology and pharmacology, as well as the utilization of this knowledge to improve clinical strategies. One of the most important breakthroughs in cancer treatment occurred in the mid 50s, when the use of combination therapy was first demonstrated by Emil Frei, Emil Freireich and James Holland. They found that the combination of Purinethol (mercaptopurine), Oncovin (vincristine sulfate), methotrexate, and prednisone— which together were referred to as the POMP regimen — could induce long-term remissions in children with acute lymphoblastic leukemia [3]. As research on combination therapy progresses, the clinical benefits of employing such treatment regimes become evident as the appropriate permutation of combined drugs on cancer cells is able to give rise to augmented effects with reduction of dose-related side effects of individual agents.

As the understanding of oncogenic mechanisms deepens, alongside with the development of recombinant technologies, the use of biopharmaceuticals came into light as an alternative to small-molecule drugs for cancer treatment. Biopharmaceutical drugs refer to a wide range of medicinal products created by biotechnology processes and these include nucleic acids (DNA, RNA or antisense oligonucleotides) and recombinant

therapeutic proteins. Over the past several decades, extensive efforts have been placed into exploring the different varieties of these biopharmaceuticals as a cure for cancer. By far, protein therapeutics has been the most successful class of biopharmaceutical drugs for cancer therapy with approximately one quarter of all biotechnology products in development being monoclonal antibodies, and some have already been approved by the U.S.A. F.D.A. for the treatment of cancer [4].

The application of anti-cancer agents in clinical settings is often met with many difficulties. For small-molecule drugs, common impedence include poor solubility as most of such drugs are often hydrophobic in nature; damage to surrounding tissue upon extravastion of the drugs; lack of selectivity for target tissues and poor biodistribution resulting in dose-limiting side-effects; rapid plasma clearance and degradation *in vivo* and the latter two problems are prevalent with use of protein therapeutics.

To circumvent the problems associated with conventional ("free") drugs, the use of drug delivery systems (with diameters around 200 nm or less) has been extensively explored to help improve the pharmacokinetics and biodistribution of the associated therapeutic agents [5]. These systems include liposomes and other lipid-based carriers such as lipid emulsions, and lipid-drug complexes; also included are micelles, polymer-drug conjugates and immunoconjugates. The potential of using drug delivery systems for cancer treatment have been demonstrated as early as 1974 for liposomes [6], and 1980 for polymeric nanoparticles [7]. Till this date, several drug delivery systems have moved into clinical application. Examples include liposomal doxorubicin (Myocet) which has shown less cardiotoxicity than doxorubicin for the treatment of metastatic breast cancer [8], and PEG-L-asparaginase [9, 10] with significantly longer plasma half life than the

unpegylated enzyme (357 hr *vs.* 20 hr) for acute lymphoblastic leukemia treatment. However, despite the advancements that drug delivery systems have made in improving cancer treatment, it is also important to realize that there are still concerns associated with its use. In spite of the reports on evasion of multi-drug resistance by drug delivery systems [11, 12], the possibility cannot be ruled out for the emergence of drug resistant variants during prolonged treatment. In a study reported by Panyam et al., treatment of multidrug resistant (MDR) cells showed that cytotoxicity of nanoparticle-encapsulated Paclitaxel (Pac) can only be restored under the influence of P-glycoprotein (P-gp) inhibitor, verapamil, and sustained inhibition of P-gp is required for sustained therapeutic efficacy of the encapsulated drug [13].

Another approach to reduce the chances of developing MDR that is better accomodated for clinical application is by combining different drugs with synergisitic or additive therapeutic effects that are non-cross resistant with one another. However, some of the main drawbacks include multiple administrations and uncertainty in the distribution of the different drugs to various body tissues. This leaves us room for improving drug formulations for better therapeutic efficacies and clinical convenience. In particular, it is exceedingly attractive to use nanoparticulate delivery systems for combinational therapy as these vehicles are able to co-deliver multiple drugs simultaneously in a single administration. One of the earlier studies involving co-delivery systems was conducted by Janoff et al. [14] where different small molecule anti-cancer drugs (irinotecan/floxuridine, cytarabine/daunorubicin, and cisplatin/daunorubicin) were co-delivered using liposomal systems and showed synergisitic therapeutic effects in mice models [15]. With structural versatility of nanoparticulate delivery vehicles, the

therapeutic agents that can be loaded into the carriers are not limited to only small molecule drugs, macromolecules such as nucleic acids and proteins can also be codelivered together using these vehicles.

1.2 Combinational Therapy

1.2.1 Introduction to combination therapy

The era of combination therapy began in mid 1950s, in the National Cancer Institute (NCI), when three physician-scientists, Holland, Frei and Freireich, proposed a revolutionary alternative approach to single drug therapy—by using combinations of multiple drugs to eliminate cancer cells before they developed resistance. Several years later, this group of researchers reported successful clinical studies which showed that the POMP regimen can treat pediatric patients with acute lymphoblastic leukemia and lower the chances of cancer relapse. This approach was also taken on by another group of researchers from the same institute, Vincent DeVita, George Canellos, who showed that the combination of nitrogen mustard, vincristine, procarbazine and prednisone — together referred to as the MOPP regimen — could provide a cure against both Hodgkin's lymphoma and non-Hodgkin's lymphoma [16]. These two successful combination regimens have since been actively used in clinics and has become the standard of care for patients with such cancers.

Following these landmark discoveries, new drugs and potent combinations for cancer treatment have been discovered, including taxanes, campthothecin, platinum-based agents, nitrosoureas and anthracyclines [17]. In scenarios where single agents are unable to produce satisfactory results in patients with advanced cancer, their use in combination are usually considered. In clinical settings, when several drugs have been

demonstrated to be therapeutic against a particular type of cancer, combining them becomes almost intuitive for clinicians. Table 1.1 shows some of the various combinations of small molecule drugs and antibodies that have been used in clinical studies.

Table 1.1 Examples of clinical studies conducted using various combinations of anti-cancer agents.

Treatment	Cancer type	Time to disease progression (Mth)	Overall survival (Mth)	Ref.
Cetuximab	Colorectal	1.5	6.9	[18]
Cetuximab/Irinotecan		4.1	8.6 (p =0.48)	
Docetaxel	Breast	4.2	11.5	[19]
Capecitabine/Docetaxel		6.1	14.5 (p = 0.126)	
Irinotecan (I)/Fluourouracil (FU)/leucovorin (LV) FU/Lv or IFL	Colorectal	5.6	14.6	[20]
Bevacizumab/FU/LV		8.8	17.9 (p =0.008)	
Docetaxel	Breast	6.1	22.7	[21]
Trastuzumab/Docetaxel		11.7	31.2 (p = 0.0325)	
Cyclophosphamide, Vincristine, and Prednisone (CVP)	Follicular lymphoma	14	30 (85% of the patients)	[22]
Rituximab/CVP		35	30 (89% of the patients)	
Paclitaxel (Pac)	Breast	–	22.2	[23]
Doxorubicin (Dox)			18.9	
Pac/Dox			22 (p = not significant)	

Strong emphasis is placed on the importance of selection of drugs for combination purpose. This is because, even though some drugs are potent when used individually, administrating them together does not guarantee enhancement in therapeutic efficacies. For instance, the combined use of two of the commonly used anti-cancer drugs, paclitaxel (Pac) and doxorubicin (Dox) did not increase the overall survival of patients compared to when the drugs were administered alone [23].

In most cases, the empirical approach is usually employed to test the effectiveness of different drug combinations on patients. This has been justified by the lack of methods to identify the sensitivity of tumors to individual agents or to a combination of agents [24]. In the recent decade, with the increasing knowledge regarding the complexity of cancer biology and the existence of multiple targets in the same or different interactive pathways in cancer cells, combinations of molecularly targeted agents have been investigated. However, due the specificity of such agents, focusing on a single target would usually give rise to modest clinical effects except during rare circumstances in which the cancer development is dominated by the abnormality or defect of a single gene [25]. Furthermore, due to the adaptability and variations in oncogenic pathways, 'cross-talk' between different pathways can occur to signal survival requirements of the cancer cells, leading to the activation of other molecular targets [26, 27]. Hence, the combination of therapeutic agents targeting a combination of various pathways may give rise to greater anti-cancer effects compared to monotherapy using single agents. Given the vast number of possible combinations of agents that can be used, the opportunities to develop effective combinations for improving therapeutic efficacy is attractive and abundant.

1.2.2 Rational for combining drugs

1.2.2.1 To evade drug resistance

In cancer therapy, the combination of drugs with different modes of biological action has been used in order to evade the development of drug resistance. When single agents are used to treat cancer, the repeated exposure of cancer cells to drugs can result in the development of clinical resistance. Drugs that are used as monotherapy are usually

those that target specific proteins involved in cancer development. These drugs can also lose their effects in advanced stages of cancer as the some cells acquire independence from such proteins [28]. There is a wide range of mechanisms through which cancer cells can acquire drug-resistance, including the mutation or overexpression of the molecular target, inactivation of the drug, or elimination of the drug from the cells [29]. For instance, tumors may become refractory to monotherapeutic anti-angiogenic drugs which targets only one angiogenic protein (e.g. VEGF) [30]. Another example is that in mice models that have been engineered with controllable oncogenes, the tumors that initially relied on the oncogene eventually lose this dependency as they develop [31].

There are two main aspects of the problem: firstly, the re-proliferation of cancer cells between therapy cycles and the development of resistant cells with each cycle, resulting in lower number of cells being eliminated. Another major issue with monotherapy is that when cancer cells develop resistance to some drugs of a particular class, the resistance has likelihood to be extended to the entire class of similar drugs. To evade the occurrence of multi-drug resistance, drug combinations are often used. The motion behind such practice is based on the postulation that the probability of cancer cells developing resistance to a combination of non-cross-resistant drugs varies as the product of the probabilities of resistance to each of the individual drug [24]. Thus, by lowering the chances of developing multi-drug resistance through the use of drug combinations, therapeutic regimens can be continued for longer period of time without losing the drug efficacy.

1.2.2.2 To enhance anti-cancer activity

Clinical prediction of drug efficacy and toxicity from theoretical knowledge or preclinical studies is often difficult and imprecise. As the efficacies of anti-cancer agents, particularly for small molecule-drugs, vary with the dosage used, clinicians usually administer drugs at levels at or close to the maximum tolerated dose (MTD) (Box 1.1) to achieve optimal therapeutic effects with tolerable side-effects. Therefore, there is a limitation as to the amount of single agents that can be used for treatment. The therapeutic window of any given drug refers to the range of dose of a drug or of its concentration in a bodily system that provides safe and effective therapy. The differences in therapeutic windows of different drugs are related to their functions, as in whether they inhibit the essential of non-essential functions of the human body. With reference to this context, inhibitors of essential functions will affect the survival of at least one vital cell type in the body. As a result, such drugs may be more potent but are likely to have narrow therapeutic windows. On the contrary, drugs that inhibit non-essential functions would likely be well tolerated, but their efficacy may be lower unless the appropriate cancer types are targeted [28]. To achieve enhanced therapeutic efficacy while maintaining side-effects at manageable levels, clinicians often combine two or more drugs in the treatment. This approach is useful only if the combination maintains or widens the therapeutic window and also, if the modulatory effects of one drug on another occur at a dose that is much lower than the MTD of either drug [32]. For instance, in a phase 3 clinical trial, when paclitaxel and bevacizumab were combined at levels below the MTDs, progression-free survival was significantly increased as compared to Pac alone, from 5.9 to 11.8 months [33].

Box 1.1 Studies that lead to the concept of maximum tolerate dose (MTD)

In 1955, the National Cancer Chemotherapy Service Center (NCCSC) was set up at the National Cancer Institute (NCI) in the U.S.A. to promote cancer drug discovery. The NCCSC established the necessary tests and indicators for the discovery, development, toxicology and clinical evaluation of candidate drugs. Later in the 1960s, Frank Schabel and Howard Skipper at the Southern Research Institute added on to the NCI's efforts by developing *in vivo* assays for analyzing toxicity of anti-cancer agents [34, 35]. In their studies, they demonstrated that anti-cancer agents display fractional killing effect on tumor cells that is dependent on the dose of agents used. In addition, they were also the first to propose that high dose of anti-cancer agents should be used to cure patients in order to prevent the likelihood of drug resistance development. This concept led to the current clinical practice of administering drugs at dosages close to or at the maximum tolerated dose (MTD).

1.2.3 Types of drug combinations and mechanisms

When two or more anti-cancer agents are combined, the resultant therapeutic effects may vary over a wider range compared to the summed effects of the individual agents. Drug combinations may produce effects that are pharmacodynamically synergistic, additive or antagonistic if the effect is larger, equal to, or lower than the summed effects of the single drugs [36]. The addition of drug to another can modulate the therapeutic activities of the partner drug by affecting the pharmacokinetics of the drugs in terms of absorption, distribution, metabolism and excretion.

Researchers and clinicians aim to discover drug combinations that produce synergistic therapeutic effects, where the 'whole' is greater than sum of the action of its parts [37]. Synergistic and potentiative combinations will allow favorable outcomes including enhanced therapeutic effectiveness; reduced drug dosages (hence related-side effects) at equal or higher level of efficacy; and/or decreased or postponed acquirement of drug resistance [38, 39]. The use of non-synergistic combinations is not favored clinically and these have been mostly replaced by single agents [40].

1.2.3.1 Pharmacodynamically synergistic combinations

There are mainly three groups of synergistic drug combinations that work based on different pharmacodynamic mechanisms: firstly, anti-counteractive actions of drugs that decrease the molecular pathway's counteractive behaviour to repel a drug's therapeutic effects; secondly, complementary actions of drugs that involves a positive modulation of a target or process by approaching the pathway at different points; thirdly, facilitating actions whereby one drug can help in enhancing the activity of another drug [40]. Table 1.2 shows some examples of synergistic drug combinations.

Table 1.2 Examples of pharmacodynamically synergistic drug combinations.

Types of action	Drug A	Drug B	Possible mechanism of synergism	Ref.
Anti-counteractive	ZD-1839	Doxorubicin, etoposide, cisplatin, carboplatin, or paclitaxel	Cellular damage by chemotherapy can result in the conversion of EGFR ligands from growth factors into survival factors for EGFR-expressing cancer cells. Blockage of EGFR mitogenic signaling by ZD-1839 in combination with cytotoxic drugs could irreversibly damage cells, leading to apoptosis.	[41]
	Paclitaxel	Flavopiridol (after administering paclitaxel)	Pac results in transient mitotic arrest with activation of cdc-2 kinase. After which, the cells exit mitosis with a reduction in cdc-2 kinase activity and MPM-2 labeling. Flavopiridol accelerates the mitotic exit when administered after pac treatment by inhibiting cdc-2 kinase and in association with a more rapid decrease in MPM-2 labeling.	[42]
	Cetuximab	Gefitinib or Erlotinib	Distinct classes of EGFR inhibitors, providing greater inhibition of the EGFR signalling and great down-regulation of p-MAPK and p-AKT expression.	[43]
Complementary	Angiostatin	Endostatin	Synergisitic inhibition of endothelial cell proliferation in the presence of both angiostatic proteins.	[44]
	Trastuzumab	Pertuzumab	Both antibodies target HER2 receptors. Pertuzumab sterically blocks HER-2 dimerization with other HER receptors and blocks ligand-activated signaling from HER-2/EGFR and HER-2/HER-3 heterodimers.	[45]

Facilitating	Angiotensin II	Chemotherapeutic drugs	Tumor blood flow increases in angiotensin II-induced hypertensive state but maintains constant in normal blood vessels. Hence, delivery of drugs to tumors can be increased using angiotensin II.	[46, 47]
	Trifluoperazine	Adriamycin	Trifluoperazine is an inhibitor of calmodulin and can alter membrane permeability. Treatment with it can significantly increase adriamycin accumulation and retention in cells.	[48]

1.2.3.2 Pharmacodynamically additive combinations

Additive combinations often have similar activity or overlapping effects on different targets of the same signaling pathways, and as a result they regulate the same molecular target in an equivalent manner. Otherwise, they can have interactions that directly or indirectly affect the same site of the same target. For example, additive drug interactions were observed in human colon cancer cell lines after treatment with 17-allylamino-17-demethoxygeldanamycin (17-AAG) and oxaliplatin. 17-AAG inhibits the activity of transcription factor NF-κB through the abrogation of upstream components of the NF-κB pathway, and that this results in a shift of the balance from cell survival to cell death in response to oxaliplatin treatment.

1.2.3.3 Pharmacodynamically potentiative combinations

Another type of drug combination which provides the enhancement of therapeutic efficacy is one that potentiates the partner drug's effects through positive regulation of drug transport or permeation, distribution or localization and metabolism. Improvements of the transport of drug into target cells or organelles occur *via* the disruption of transport

barrier, delay of barrier recovery, or prevention of drug efflux. The distribution or localization of drugs to target tissues is improved by inhibiting metabolic processes that convert drugs into excretory products. Positive modulation of metabolism occurs via the stimulation of conversion of drugs into active forms, or inhibit the conversion of drugs into inactive forms [40]. One example is co-administration of a P-glycoprotein inhibitor, cyclosporin A, with Pac. As a single agent, orally administered Pac has poor bioavailability because of its high affinity for the multidrug transporter P-glycoprotein, which is present in abundant levels in the gastrointestinal tract. The combined formulation significantly increases the oral bioavailability and systemic exposure of orally administered Pac [49].

1.2.3.4 Combinations that lower therapeutic efficacy

Some drugs work against each other and such pharmacodynamically antagonistic drug combinations are unsuitable to be used in clinical applications. Antagonistic mechanisms include interference of drug actions at the same target, or indirectly by disrupting related pathways that regulate the same target. One example of antagonistic drug combination is Pac and flavopiridol, with actions closely related in the cell cycle process. Pac induces apoptosis during mitosis, whereas pretreatment of cells with flavopiridol inactivates the cdc-2 kinase, which prevents the mitotic arrest of Pac from occurring in the context of a properly activated cdc-2 kinase. Therefore, the treatment sequence of flavopiridol followed by Pac becomes inactive [42].

Another type of drug combination that lowers therapeutic efficacy is one which is pharmacokinetically reductive. Such combinations of drugs result in negative modulation

of drug transport, permeation, distribution or localization, and metabolism. For instance, cisplatin, by itself results in DNA inter- and intra- strand adduction. When another drug, procainamide hydrochloride is added, it results in the formation of less toxic cisplatin-procainamide complex. Thus, this reduces cisplatin-induced hepatotoxicity by the inactivation of cisplatin or its highly toxic metabolites and rearrangement to a different subcellular distribution of platinum [40].

1.2.4 Methods for analyzing drug interactions

To study the overall therapeutic effects of drug combinations, various methods have been developed and explored. One of the commonly used and preferred methods is the isobolographic analysis, which was first introduced by Loewe in 1953, where additivity was predicted between ethyl alcohol and chloral hydrate [50, 51]. This method has been employed in my work for the analysis of effects of various drug combinations.

The isobologram method evaluates the effect of interaction of two drugs at a specified effect level, such as half of the maximal inhibition and the concentration at which it occurs is defined as the IC_{50}. Using graphical analysis, the concentrations required to produce the given effect (for example, IC_{50}) are determined for each of the individual drugs, A ($IC_{x, A}$) and B ($IC_{x, B}$). These points, ($IC_{x, A}$, 0) and (0, $IC_{x, B}$), are then plotted on the x and y axes of a two-coordinate plot. A line is drawn to connect these two points and this is defined as the line of additivity. After which, treatment is then performed by using the drugs in combination with varying concentrations used. The concentrations of A and B in the combination that provide the same effect, denoted as ($C_{A, x}$, $C_{B, x}$), are placed in the same plot. Effect of the drug interaction is determined

according to the position of the points ($C_{A,\,x}$, $C_{B,\,x}$) with respect to the line of additivity. Synergy, additivity, or antagonism is represented when the point is located below, on, or above the line, respectively [52, 53]. This isobologram method evaluates drug interaction at chosen therapeutic effect levels and provides a more comprehensive analysis of the drug interaction at the corresponding concentrations.

The Loewe model is based on the assumption that there is no self interaction of each individual drug. It also takes into account of the non-linear display of drug concentration-effect relationship such as the commonly observed sigmoidal curve. This will provide an advantage for evaluating drugs demonstrating such a relationship. This model also assumes that two drugs act through a similar mechanism, and the effect of each drug and the drug combination are related through equipotent dose ratios. Comparatively, another model – the Bliss independence model, assumes that the drugs act through independent mechanisms and combined effect of two drugs equals to the multiplication product of the effects of individual drugs. This assumption place a limit on the capacity for analysis as it is only applicable for drugs that exhibits linear dose-dependent effect but not for those with nonlinear relationships [54, 55].

Because of the application versatility of the Loewe additivity model, many other methods have been developed based on it. These include the interaction index calculation, the median effect method, and several three-dimensional surface-response models [52, 56]. The surface response methods involve more complex and rigorous calculations and thus, have not gained wide usage.

1.2.5 Issues and strategies for combination therapy

1.2.5.1 Practical issues for consideration

Drug combinations can have a wide range of effects that are different from that of single agents and it is often difficult to predict the sensitivity of tumors to the different combinations. In clinical settings, the empirical approach is often employed to study drug interactions and therapeutic efficacies of different combinations of drugs. To design effective clinical trials for drug combinations, several issues have to be carefully considered. Firstly, substantial preclinical and clinical data showing therapeutic potential of the combination must be obtained prior to planning the trial. Secondly, as the prevalence of different cancers may vary with different populations [57], the selection of population to be studied is important to ensure good relevance to the disease. Thirdly, since anti-cancer agents are being developed by many different pharmaceutical companies, intellectual property issues may arise with successful drug combinations [24].

1.2.5.2 Mechanistic considerations

The main priority for development of drug combinations is to allow enhanced therapeutic efficacy while maintaining acceptable pharmacology and non-specific toxicity. As such, knowledge on the mechanisms of action and resistance development to single agents and interaction mechanisms of the drug combinations should be well explored. There should also be strong evidence of therapeutic enhancement (either synergistic, potentiative or additive) from preclinical studies. An important point to consider is that in some cases, monotherapy using single agents may not produce anti-cancer effect at desired therapeutic levels, but may result in substantial enhancement of therapeutic effects when used in combinations with other drugs. For instance, LY303511 (LY30) is an inactive analog of LY294002 (LY29), a widely used inhibitor of the

phosphatidylinositide-3-kinase (PI3K)/Akt survival pathway, and when LY30 is combined with tumor necrosis factor-related apoptosis inducing ligand (TRAIL), the combination is able to induce significant increment of cell death [58].

Selection of drugs used for combinations may be conducted in such a way whereby the therapeutic activity of the first agent can be enhanced by the second agent. This is often decided based a number of strategies. Firstly, in combination, the second agent chosen is able to affect the targeted molecule of the first agent more effectively; and/or it is able to affect additional targets or interfere with related pathways; and/or it can be used as a counteractive agent against cellular process that arises during multi-drug resistance development. For instance, the downregulation of genes that serves as anti-apoptotic or protective factor such as HER2, interleukin10, Bcl-2 [59-61] and restoration of tumor suppressor p53 functions [62] by either gene therapy or small molecule drugs can increase cancer cells sensitivity to conventional chemotherapeutic agents. Another example is the combination of interferon (IFN) with chemotherapeutic drugs. IFNs have weak cytotoxicity but are able to inhibit cell cycle progression, which mainly occurs as S phase accumulation. The cell cycle inhibition has been implicated in the antitumor effect of combinations of IFNs and chemotherapeutic drugs such as cisplatin and Pac [63, 64]. In anti-angiogenic therapy, treatment with angiogenesis inhibitor (TNP-470) together with an anti-cancer prodrug, cyclophosphamide, can enable the eradication of drug-resistant tumors [65].

Therapeutic effectiveness of single or combined drugs is usually achieved through the modulation of multiple molecular targets rather than single targets. Investigations of drug effects on the molecular interactions within cells are commonly performed using the

empirical approach. Besides this, the integration of network biology and computational technologies can provide the alternate means to conceptualize and analyze the entire regulation and signaling networks of different normal and cancer cells. The understanding of network system of gene expression profiles and interaction between different genes and proteins in oncogenesis can be improved by network models such as the Boolean genetic network. Boolean networks represent a simplification of the actual complicated cell system in which each gene is considered to be a binary variable and can either be active = 'on' or inactive = 'off ' through regulation by other genes as represented by logical or Boolean functions. The information obtained will enable the identification of oncogenic pathways of specific cancers or their subtypes, and provide guidance to the use of specific molecular targeted agents as well as appropriate drug combinations for specific patients [38, 66].

1.2.5.3 Strategies for determining regimens

The strategies for designing combination regimens is based on the following principles: firstly, the drugs should be preferably targeted against the cancer cells over normal cells; secondly, as the therapeutic efficacies of the drugs is likely to be correlated with the dosage and duration of drug administration, the drugs should be used at or close to their maximal tolerated dose (MTD); thirdly, optimal combinations utilize agents with different mechanisms of action; and lastly, drug combinations should be selected to minimize any overlapping toxicities of the individual agents [64].

When drug combinations have been carefully evaluated using the above guidelines, other related practical parameters have to be considered as well. When single

agents are used, clinicians often have to use doses that are close to the MTD. This is because the destruction of cells by drugs follows the first order kinetics and only a fixed fraction of cells can be killed with a given dose. The implication of the fractional killing effect is that to completely eradicate a population of cancer cells, it is necessary either to increase the dose of drug within the MTD, or to initiate the treatment when the initial cancer cell number is small enough. Since the opportunity to treat early stages of cancer is uncommon, clinicians are often left with the option to increase the dose of single agents used, which tends increase dose-related side effects and limits the possible dosage. As such, the use of drug combination can help evade such problems by reducing the dose of individual agents used [67].

Besides the dose used, one of the important factors that can greatly interfere with the success of the treatment is the dose scheduling of the drugs involved. Appropriate scheduling of drug exposure enables optimal interaction of chemotherapeutic agents. An example of such is the combinations of melphalan, BCNU (1,3 bis(2-chloroethyl)-1-nitrosourea), or cisplatin with topotecan, which were found to have highest effectiveness when cells were exposed to the alkylating agent or platinating agent prior to topotecan treatment [68].

Another important factor is the dose intensities used during treatment. Therapeutic drugs may be given at different frequencies and this can give rise to different efficacies of treatment. For instance, in a retrospective clinical study, association between relapse-free survival and dose intensity was observed in clinical trials involving cyclophosphamide, methotrexate, and fluorouracil-containing adjuvant chemotherapy of stage II breast cancer [69]. In another study, female patients with stage II breast cancer

treated with combinations of cyclophosphamide, doxorubicin, and 5-fluorouracil also showed therapeutic dependencies on the frequencies of dosages [70].

1.2.6 Reasons for failure of some regimens

Due to the vast number of mechanisms by which different agents can interact, the therapeutic outcomes of combination regimens are usually complex and unpredictable. In some cases, therapeutic benefits may not result from certain combination regimens. There are several possible reasons that can result in the failure of combination therapy. Firstly, the nature of the effects the agents have on the cells, either individually or in combination, may not lead to augmentative interactions. These drugs may have overlapping activities on the same molecular target or signaling pathways and as a result, they would not have addition clinical gain when combined in the same regimen. Secondly, some combinations may result in antagonistic or reductive biological effects, which may even give rise to reduced effectiveness, as compared the single agent. Thirdly, the expressed level or biological functionality of molecular target may be low in the cancer cells. If the intended target is absent or there are other irrelevant pathways that can provide alternative signaling to maintain essential functions in the cancer cells, the effect of the combination regimen will decreased significantly. Fourthly, even with combination regimen, drug resistance can also develop in cancer cells after repeated administration. For instance, the cancer cells may acquire alterations in drug metabolism and transport, resulting in lower drug levels in the cells. As a result, the therapeutic efficacy of the agents will be become significantly reduced [24].

1.3 Protein Therapeutics

Early development of cancer therapeutics had been based on drugs that can inhibit cancer cell growth through blockage of cellular events essential for proliferation. For instance, in 1963, researchers at Eli Lily discovered *Vinca* alkaloids as a new class of oncolytic agents as it can stop the proliferation of cancer cells during their original screening for anti-diabetic agents [71]. Several years later, further research then showed that the anti-cancer activity of the *Vinca* alkaloids is attributed to their ability to inhibit microtubule polymerization, and thereby blocking mitosis from occurring [72]. Likewise, such early anti-cancer agents are usually small molecules, which are able to block cancer cell proliferation by modifying DNA structure and impairing DNA accurate replication or other cellular events such as nucleotide biosynthesis. In all, the screening process to identify potential anti-cancer agents has been mostly carried out using an empirical approach up till now. This is because the anti-cancer efficacy of candidate agents during in *vitro* tests and animal tumor models may not accurately reflect the complexities of human cancer. Hence, it is often difficult to recognize the reasons behind the success and failure of different candidate agents and the varying degrees of sensitivity of cancer cell types to different drugs.

In the last few decades, with the widening application of molecular biology, target identification in cancer became important and high through-put screening of potential oncogenes could be performed. Till now, many genes have already been extensively explored and some found to affect oncogenesis and cancer cell proliferation. With regards to target selection, some of the key areas that are being studied include genes and gene products affecting apoptosis induction, cell-cycle regulation, signal transduction and

tumor angiogenesis [73]. Through molecular biology techniques, gene candidates can be cloned and expressed into recombinant proteins with therapeutic functions. The vast number of proteins with therapeutic potential opened up a wide area for research and advancement. Various cloning and expression approaches in different host systems have also been developed. Currently, there is more than 130 different protein or peptide therapeutics approved by the US Food and Drug Administration (FDA) for clinical applications. Some examples are given in Table 1.3. In commercial perspective, it has been predicted that the global market value for therapeutic proteins will grow from 34,000 million USD to 52,000 million USD and oncology-related proteins will be the second most important revenue generator with an increasing market share of 14% in 2004 to 18% in 2010 [74].

Table 1.3 Examples of U.S. F.D.A. approved protein or peptide-based therapeutics [75, 76].

Generic Name	Company	Type of therapeutic	Indication of first FDA approval	Year of first FDA approval
Rituximab	Genentech	mAB	Non-Hodgkin's lymphoma	1997
Trastuzumab	Genentech	mAB	Breast cancer	1998
Denileukin diftitox	Seragen	rDNA	Cutaneous T-cell lymphoma	1999
Gemtuzumab ozogamicin	Wyeth	mAB	Acute myeloid leukemia	2000
Ibritumomab tiuxetan	BiogenIDEC	mAB	Non-Hodgkin's lymphoma	2002
Abarelix depot	Praecis	Synthetic peptide	Prostate cancer	2003
Tositumomab-I131	Corixa Seattle	mAB	Follicular lymphoma	2003
Bevacizumab	Genentech	mAB	Colorectal cancer	2004
Cetuximab	Imclone Systems	mAB	Colorectal cancer	2004
Panitumumab	Amgen	mAB	Colorectal cancer	2006

1.3.1 Recombinant proteins

The success of protein therapeutics in disease treatment has been first recognized in 1922, when the collaborative efforts of 4 researchers - Frederick Banting, Charles Best, John J.R. Macleod, and James Collip, demonstrated that insulin, purified from bovine and porcine pancreas, was able to replace the biological activities of the protein hormone in patients suffering from diabetes mellitus type I (DM-I) [77]. Despite the clinical benefits, the extraction of the therapeutic protein from animal sources meant that the availability of such treatment may be limited and expensive, and immunogenicity would be a potential complication. Subsequently, with breakthroughs in genetic research and expression engineering, production of recombinant human insulin from *Escherichia coli* became possible. US FDA approval was then given in 1982 and large-scale production of recombinant insulin enabled widespread inexpensive DM-I treatment. More recently, some research groups have succeeded in deriving human insulin from transgenic plants with the anticipation that this technique will be able to reduce production costs [78, 79].

In view of the huge clinical potential of protein therapeutics, various systems have been developed for recombinant protein production. These include bacteria, yeast, insect cells, mammalian culture, and transgenic plants and animals [80-86]. Selection of production method is dependent on the cost or the post-translation modifications required for protein functions. For many proteins, it can be difficult to manufacture in recombinant form or expressed in microbial systems. For instance, the commonly used bacterial systems for protein production cannot perform glycosylation reactions while yeasts, baculovirus and transgenic plants produce glycosylated proteins that are different from the human version and are unsuitable for clinical use. Deviations in glycosylation patterns can lead to enormous differences in biological activity, serum half-life and

immunogenicity of the recombinant proteins when administered into the body [87]. To improve the physiochemical and biological properties of recombinant proteins, extensive research has been put into devising strategies to modify targets and oligosaccharides on particular therapeutic protein to produce glycoforms with enhanced therapeutic activities [88]. Another approach adopted to improve the pharmacokinetics of recombinant proteins is through pegylation – which is the process by which polyethylene glycol (PEG) chains are attached to protein and peptide agents. By conjugating to PEG, this will increase the molecular mass of the protein drugs and shield them from proteolytic enzymes. For instance, Pegaspargase (Oncaspar), an FDA approved recombinant protein, used clinically in combination with chemotherapy for the treatment of acute lymphocytic leukaemia contains the pegylated enzyme L-asparaginase. Without pegylation, the enzyme causes allergic reactions and has a short half life of 20 hr. Comparatively, with pegylation, its half life can be extended to 357 hours with lower immunogenicity problems [89].

1.3.2 Rationale for using protein therapeutics

There are many reasons behind the extensive research efforts put into developing protein therapeutics, most of which are based on the advantages they have over small-molecules drugs and gene therapy. First, as compared to the large number of protein therapeutics currently used for disease treatment, no human gene therapy product has yet been approved by U.S. F.D.A. as a standard-of-care in clinics and this technology is also currently unavailable for most diseases. On the contrary, in genetic conditions where there are alterations or mutations of particular genes, protein therapeutics can provide

effective replacement treatment without involving gene therapy. Second, as the effects of proteins are short-lived compared to genetic therapeutics, the risk of any adverse long term consequences would be much lower. Third, some molecular targets exhibits biphasic, U-shaped dose-related efficacy and these targets are unsuitable for gene therapy because of the difficulties in controlling and predicting the *in vivo* expression of the gene. For instance, Folkman et al. initially discovered in one of their studies that gene therapy of endostatin produced an excessively high level of the protein such that the anti-angiogenic effect was heavily reduced [90, 91]. Fourth, while protein therapeutics can be produced on cost-effective scale and administrated *in vivo* through straightforward intravenous (IV) infusion with low risk of immunogenicity [87], gene therapy can have various pros and cons depending on the methods used. While *in vivo* gene transfer is more cost-saving, it is not patient-specific and immune response can be evoked against the delivery vectors. In the *ex vivo* approach, cells have to removed from the patient for transfection, and although this method offers higher transfection efficiency, it is largely patient-specific due to cell immunogenicity, and in turn, this technique is also more costly because of the cell manipulation procedures [92]. Fifth, proteins are highly specific in terms of target interactions and biological functions and these properties are difficult for simple chemical entities to mimic. Sixth, as a result of the specificity of proteins, there is a lesser likelihood for protein therapeutics to disrupt normal physiological processes and cause unwanted side effects. Seventh, protein production strategies have matured through many decades of development and scale-up optimization studies, and this has allowed protein therapeutics to be produced in a cost-effective manner. With the large number of various systems available, the optimal production method can be made

according to the cost as well as modifications of the protein required for its therapeutic functions. Eighth, past records revealed that protein therapeutics development is also more advantageous in both approval time and success probabilities. For instance, it has been reported that the probabilities for successful transition from clinical evaluation to U.S. F.D.A. approval were higher for monoclonal antibodies compared to small molecule drugs (Figure 1.1) [75]. In another study, it was found that the clinical development and approval time was ~30 months faster for anti-neoplastic protein therapeutics compared to small molecule drugs approved in 1980-2001 [93]. Last, as proteins are unique in their biological functions, companies will be able to obtain patent protections for protein therapeutics they develop. The last three points illustrates the commercial advantages proteins have over small molecule drugs that have made the development of protein therapeutics appealing to pharmaceutical industries.

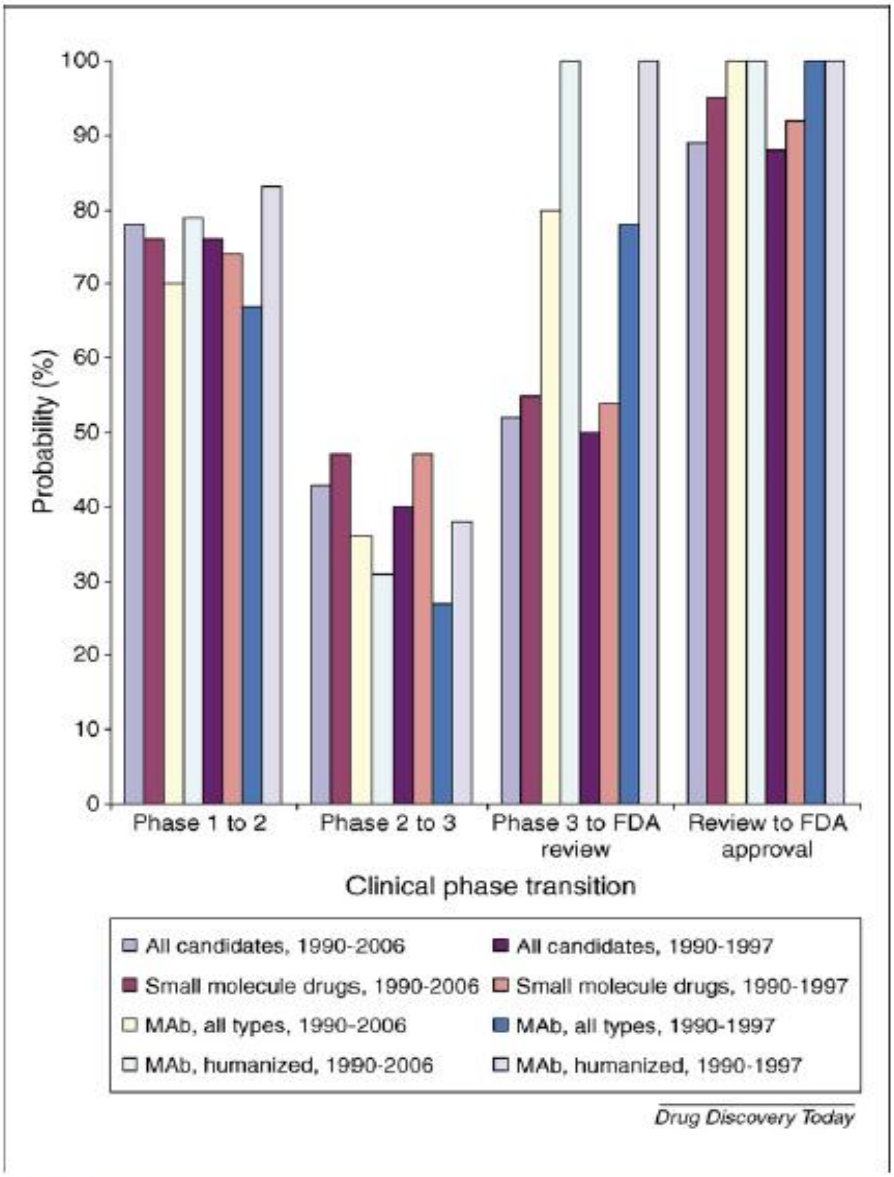

Figure 1.1 Probabilities of clinical phase transition for cancer therapeutics [75].

1.3.3 Challenges for protein therapy

Despite proteins having great potential to be used as therapeutic agents; they also have several limitations that will hinder their widespread usage in clinics. First, proteins typically have low stability and short *in vivo* half-lives, and their clinical application require either infusions or frequent repeated injections [94]. Such treatment methods are

unfavorable because of its invasiveness to human body and increased chances for other complications (e.g. treatment cost, patients' compliance and pathogenic infections). Second, another problem resulting from protein instability is the risk of administrating degraded protein as it could lead to undesirable side effects or loss of therapeutic effectiveness [95]. Third, while oral delivery has been proposed as an alternative method to administer protein therapeutics, a lot of improvement is necessary to increase the oral bioavailability of the proteins before the benefits of such systems can be realized. One of the main obstacles is that most proteins are hydrophilic with large molecule size and this prevents their partition into epithelial cell membranes and absorption *via* transcellular passive diffusion. Another problem is the inherent susceptibility of proteins to pre-systemic enzymatic degradation in the gastrointestinal tract [96]. To tackle these problems, many improvement strategies have been developed and these are further discussed in Box. 1.2. Fourth, immunogenicity against therapeutic proteins also poses a major challenge for its clinical application. Immune response can arise as anti-therapeutic protein antibodies (anti-drug antibodies) can development during treatment. These antibodies can either neutralize or reduce the therapeutic efficacies of the protein drug or in a worse scenario; it may cross-react with autologous proteins and lead to adverse side effects [97]. In most cases, immune responses are generated against proteins generated from non-human origin. Fortunately, the severity of this problem has been lowered through the development of humanized antibodies and also the production of fully human antibodies using transgenic animals or phage display technologies [87]. For example, Herceptin is a recombinant monoclonal antibody used to treat breast cancer patients with tumors that over-expressed HER2 receptors. This antibody was developed from a murine

monoclonal antibody that was later humanized to minimize the immunogenicity associated with the non-human therapeutic protein [98]. Fifth, the selection of production system for the protein also faces several issues. The system must be able to produce the protein with the correct post-translation modification needed for its biological functions. The convenience and cost involved for protein purification and storage must also be considered. In terms of storage, the system should also be assessed for protein misfolding, aggregation and instability. On top of these, the system must also generate sufficient quantity of the protein in a cost-effective manner to allow widespread clinical use [99-101].

Box. 1.2 Challenges faced in oral delivery of protein therapeutics.

The most convenient route for administering therapeutic agents into patients is *via* oral delivery. However, the attempts that have been made to deliver proteins and peptides drugs have not been widely successful. One of the reasons is their solubility characteristics and large molecular size. Most of these proteins are hydrophilic and are unable to get absorbed through passive transcellular diffusion. The paracellular route is also not available for protein absorption as the dimensions of the paracellular space of the human intestinal epithelium is < 10Å [102], and is therefore restricted only to small hydrophilic molecules (100-200 Da) [103]. Furthermore, proteins are vulnerable to hydrolysis and modification at the acidic gastric pH levels and proteloytic degradation in the gastrointestinal tract [104].

To increase the oral bioavailability of the therapeutic proteins, many strategies have been developed. One of such is the inclusion of additives in the drug formulations to enhance permeation of the proteins through the epithelium or inhibit proteases in the gastrointestinal (GI) tract. For instance, additives which modulates tight-junction permeability such as Zonula Occludens toxin [105] and Pz-peptide [106] have been shown to enhance protein absorption. However, there are also risks associated with this approach as the alteration of the tight junctions will not only enhance transport of the protein drug, but may also potentially increase the absorption of unwanted toxins/bacteria/immunogens present in the GI tract [107]. Another method that has been extensively researched upon is protein encapsulation technology in particulate carriers to minimize exposure of the protein to proteolytic enzymes. Till this date, polymeric drug delivery systems based on hydrogels, nanoparticles, microspheres, and lipid-based drug delivery systems (e.g. liposomes and microemulsions) have been developed for oral protein delivery [96]. In some reports, the potential of acrylic-based polymers and chitosan nanoparticles for oral protein delivery have been shown by several research groups [108-110]. In the GI tract, the proteolytic activity is highest in the stomach and duodenum, and is sharply reduced in the ileum and colon. Systems involving protein encapsulation with thick enteric coatings that delay the release of the drug until the drug reaches the ileum and colon has been devised. In addition, to target drug absorption in the large intestine, encapsulation of proteins with polymeric materials that can be specifically degraded by the human colonic microflora has been proposed [111]. However, the major disadvantage of these systems is the delay and reduction in time period for drug absorption, as well as the lack of control over absorption time due to the variability in intestinal motility and gastric emptying [103]. Other methods to improve oral bioavailability include structural modification of the proteins. For example, to increase the cellular uptake of the proteins, ligands such as vitamin B_{12} receptors [112] and

dipeptide that can be recognized by a peptide-influx transporter [113] have been chemically conjugated to the proteins for receptor-mediated endocytosis.

1.3.4 Current technologies in protein drug delivery

Over the past few decades, with the increasing identification of more therapeutic targets and developments made in the field of biotechnology, more protein and peptide pharmaceuticals have become commercially available. However, most of these drugs encounter difficulties in moving on to eventual clinical application as many obstacles still exist with regards to their delivery in a convenient, stable and cost-effective manner. The rising demand for improved methods for the delivery of protein agents has fuelled the development of numerous protein delivery systems. Selection and optimization of protein delivery systems involve several key issues. In particular, the system should allow a sufficiently high bioavailability after administration. The bioavailability of the therapeutic protein is dependent on the efficiency of the system as well as the properties of the delivery route. If only a small percentage of the protein is delivered to the circulation after administration, this would render the system ineffective as the significant loss of protein will lead to higher manufacturing and treatment cost. In addition, the delivery method may involve formulations/additives or routes of administration that could alter the pharmacology and/or toxicity of the protein and this may difficult to predict using preclinical animal models. Hence, thorough preclinical and clinical investigations would be required for the development of new delivery methods.

By far, the most convenient route for systemic delivery of most drugs is through the oral route. However, research efforts put into developing such systems for protein delivery have not been met with significant success due to the inherent properties of

proteins that results in low oral bioavailability (Box. 1.2). Parenteral delivery of protein drugs have been the most common method for systemic delivery due to the ease of administration and lower cost compared to other delivery methods [95]. It also allows the rapid onset and distribution of the proteins which is beneficial for maintaining protein activity. Furthermore, when compared to oral delivery systems, parenteral delivery provides an advantage through the evasion of gastrointestinal first-pass effect.

As preclinical studies and clinical trials are usually performed using parenteral delivery methods, the development of injectable formulations or devices tend to have a higher likelihood to succeed compared to alternative forms of delivery. Different strategies have been proposed to improve on parenteral delivery methods with regards to the enhancement of protein stability and therapeutic efficacy. These strategies can be broadly divided into 3 main classes: structural modification of protein, sustained-release formulations and modulation to delivery devices/systems. There is a large number of ways in which proteins can be modified; first, proteins may be pegylated to increase protein solubility and stability and also to reduce proteolysis and immunogenicity. However, pegylation can cause a decrease in the *in vitro* activity of proteins, but generally this negative effect can usually be offset in *in vivo* systems by the increase in circulation half-life of the protein. Pegylation may also reduce the binding affinity of therapeutic proteins to their cellular targets and alter the bioactivity of the proteins [89]. Modification of proteins through glycoengineering methods can also improve the protein folding, transport to specific tissues and binding affinity to receptors/targets [114]. Conjugation of proteins to other macromolecules such as serum albumin can help to increase protein stability *in vivo*. An example is Albuferon in which interferon alpha is

genetically fused to albumin. In primate studies, the rate of clearance of Albuferon was approximately 140-fold slower and the half-life 18-fold longer, than for interferon alpha [115]. Last, stimuli-sensitive polymers may be used to entrap or bind therapeutic proteins to increase their stability during delivery and release them in a regulated fashion. Many studies involving glucose-responsive polymers for insulin delivery has been carried out (Figure 1.2) [116, 117]. Insulin is first added to polymers with glucose-binding moieties for the formation of nanogel/microgels. After administration, when blood glucose level rises, insulin will be subjected to competitive binding with glucose molecules and release the insulin. This reduces the number of injections required and prevents hyper- or hypoglycaemic conditions.

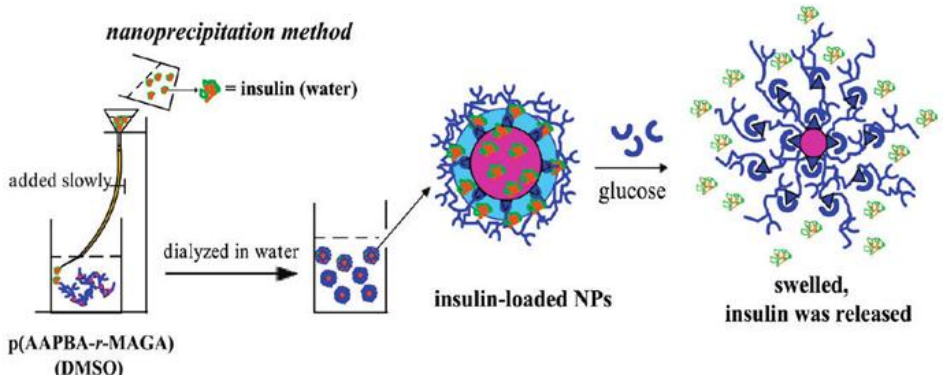

Figure 1.2 Self-Assembly of the glucose-responsive microgel and glucose-sensitive release of insulin [116].

Besides modifying protein structures and drug formulations, alterations can also be made to parenteral delivery device. To increase the ease of injections, a variety of devices such as prefilled syringes [118], pen devices [119, 120] and needle-free injectors [121] have been developed. With the exception of needle-free injectors, the pharmacology, toxicity and bioavailability of the proteins are likely to be the same for these systems as all of them involve direct injection into the body. As for needle-free

injectors, a high-velocity jet is typically used to deliver drugs across the skin into the subcutaneous or intramuscular region. These injectors have been used to deliver several therapeutic proteins such as insulin [122], growth hormones [122, 123] and erythropoietin [124]. One of the main concerns regarding their use is the shear force generated, which may be detrimental to protein integrity. Studies involving *in vitro* models have also shown significant variability in jet penetration in relation to the mechanical properties of the skin. Other issues include topical irritation, occasional pain and bleeding that is associated with the depth of penetration of the jet [121].

Another technique that has been extensively explored for delivering drugs into the systemic circulation is transdermal delivery. Delivering drugs through the skin is favorable as it can help to evade the gastrointestinal first-pass effect and is also more psychologically appealing to patients compared to the conventional injection/infusions using the hypodermic needle. A major product used for transdermal delivery is the transdermal therapeutic system (TTS), popularly known as patches. Despite the ease of application, the variety of drugs that can be administered using conventional TTS is highly limited. The main obstacle is that a large majority of drugs is unable to permeate skin at therapeutic rates due to the barrier imposed by stratum corneum layer of the skin. Drugs that can delivered using TTS should have low molecular mass (<500 Da), high lipophilicity and high therapeutic activity at a low dose. Therefore, this method is unsuitable for delivery of proteins.

Improvements to transdermal delivery methods have been focused on increasing skin permeability *via* temporary disruption to the structural integrity of stratum corneum. Several approaches has been studied, ranging from chemical enhancers [125] to physical

methods such as iontophoresis and electroporation [126, 127] and pressure waves generated by acoustic systems [128]. The extent of disruptions generated by these methods is believed to be nanosized, which allows the transport of small drugs and, in some cases, macromolecules, but not sufficiently large to cause damage of clinical significance. Iontophoresis involves the application of a low electrical current (~500 $\mu A/cm^2$) to the skin, allowing drugs to permeate through a combination of mechanisms: electrophoretic driving force, electro-osmotic driving force and transient increase in skin permeability. On the other hand, electroporation involves the use of short high-energy pulses to disrupt local areas of skin. Transport of drugs through skin has been shown to increase by several orders of magnitude with electroporation, with partial reversibility within seconds and full reversibility within minutes to hours. Large molecules of several thousand kDa can be successfully delivered using this technique [129]. More recently, ultrasound has been also used to deliver high molecular mass drugs such as insulin, erythropoietin and interferon [128]. This occurs mainly through the generation of cavitational events which causes the disruption of stratum corneum [130].

An alternative approach to the above methods involves creating larger transport pathways using arrays of microscopic needles. One of the main advantages of using microneedles for transdermal delivery is due to the anatomy of the stratum corneum. As this layer of the skin does contain nerves, the administration of drugs in this manner is unlikely to cause pain. Both *in vitro* and *in* vivo studies have shown that the administration of drugs using microneedles into skin can significantly increase permeability of small molecule drugs, proteins and nanoparticles [131, 132]. As yet, development in transdermal delivery systems has not been extended to treatment of

cancer. For cancer therapy, this mode of delivery is mostly used for long-term cancer pain management by replacing frequent dosing of pain-relievers with transdermal patches for sustained release of the drug [133, 134].

Another non-invasive approach for protein delivery that has also been explored is pulmonary delivery. Over decades, the lungs have been recognized as a potential entry-site for proteins and macromolecular drugs. This is because of the many favorable characteristics of the lungs to be used as a drug delivery site. These include low intrinsic proteolytic activity, large alveolar absorption area (about 100 m^2), extensive vasculature, thin layer alveolar epithelium (0.1–0.2Å) and short distance of air–blood exchange passage (15 μm) [135]. There are three commonly used pharmaceutical aerosols: jet or ultrasonic nebulizers, metered dose inhalers (MDIs) and dry powder inhalers (DPIs) [136]. Most studies on the pulmonary delivery of proteins are in favor of the use of DPIs because of the lower risk of protein instability compared to using MDIs and nebulizers. Dry-powder insulin inhalers have been used successfully to treat both type I and II diabetic patients and provided patients with greater treatment satisfaction than the control groups [137, 138]. Interesting, for cancer therapy, nebulization has been used to fabricate Aviscumine (recombinant mistletoe lectin) in a pulmonary delivery formulation. This protein has been successfully formulated for parenteral injections/infusions and current research is directed towards delivering it using alternative, non-invasive delivery systems. However, in one of the recent studies reported by Steckel et al., neubulization significantly affected protein stability and only 50% of the protein activity was retained after the process [139].

Besides protein instability, other challenges also exist for the development of pulmonary delivery systems. First, the efficiency of pulmonary delivery is inversely related to the molecular size of the proteins and the absorption of the macromolecules from the lungs into the bloodstream is usually low [140]. Side-effects may arise due to the pulmonary therapy. The administration of particulate matters to lungs could potentially affect lung function after prolonged duration and patients may also suffer from cough related to the therapy. Predictability of therapeutic efficacy from preclinical studies is also difficult as the bioavailability of proteins delivered through the pulmonary route in humans may differ greatly from animal models [141]. And furthermore, since the actual dosage of drug given using inhalers may not be precise, pulmonary delivery would be limited to drugs that have broad therapeutic windows. For anti-cancer therapy, studies on treatment with common small-molecule anti-cancer drugs have been carried out in hope of achieving region-specific delivery to lung tumors. However, such systems often met with problems associated with intra-arterial perfusion of organs, such as achieving a uniform distribution of the drug throughout the target tissue. Penetrability of the drugs in the tumor tissue also varies according to the physical and chemical characteristics of the drugs used as well as the tumor cell types [142].

Box. 1.3 Commonly used pharmaceutical aerosols.

Nebulizers deliver drugs in the form of inhalable fine mist. Compressed gas or ultrasound may be used to convert liquid to aerosol droplets in the respirable size range. Nebulizers are frequently used to deliver relatively large volumes of drug solutions and suspensions that cannot be easily formulated into MDI or DPI. One of the key concerns for its use in protein delivery is the production of heat during the generation of aerosol droplets that may be detrimental to the protein integrity [136].

MDIs contain therapeutic drugs that are contained in a propellant system, which contains liquefied gas in a pressurised container sealed with a metering valve. The drug is delivered as an aerosol spray in a metered dose. MDIs are typically inexpensive, portable, low cost and provide reproducible dose of the drug [143].

However, high velocity of the spray may result in significant loss of the drug through impact with oropharyngeal areas.

DPIs deliver drugs as clouds of dry and fine particulates. DPIs are inexpensive, portable, propellant-free and show enhanced stability of proteins as a due to storage in moisture-free state. Thus, they may be more preferable for the pulmonary delivery of peptide and protein therapeutics compared to nebulizers and MDIs [136, 144].

Amongst the various non-invasive modes of delivery, oral formulations of anti-cancer drugs have been most successful in clinical application. Many emerging oral pharmaceuticals are new formulations of drugs developed from those typically given through parenteral methods. Currently, some of the most widely used drugs delivered through the oral route are 6-mercaptopurine, methotrexate and busulphan in patients with leukaemia and lymphoma. Oral formulation of topotecan has shown similar therapeutic efficacy to parenteral administrations in small cell lung cancer and has better toxicity profile with less neutropenia [145, 146]. Despite the benefits that oral chemotherapy provides, such as ease of application and reduced cost, conventional infusion/injections still dominates over oral delivery. One of the main reasons is that these drugs are usually low-priced 'generic drugs' that have not been a high sales priority for the major pharmaceutical companies. Another reason could be the perception that both clinicians and drug developers generally have whereby chemotherapy is more effective when given through the parenteral route [147].

1.3.5 Proteins used in the studies (i.e. Lectin-A, TRAIL and Herceptin)

Various proteins have been used in this thesis at different phases to evaluate the protein delivery capabilities of P(MDS-*co*-CES) carriers. At the beginning, the focus has been placed on the accessing the prospect of using these nanoparticles as carriers for the

delivery of proteins. A model cytotoxic protein, Lectin-A (MW: 30.7 kDa) is selected as its main cytotoxic action is *via* the inactivation of ribosome in the cytosol, which in turn disrupts the cellular translation during protein biosynthesis [148-150]. Lectin-A, by itself, is unable to enter cells without assistance from delivery carriers but will induce significant cytotoxicity when it gets delivered into the cytosol. Therefore, *in vitro* cytotoxicity resulting from Lectin-A chain delivery is used as an indicator of the protein delivery efficiency of the nanoparticles.

In the later phase, the study was then moved on to the codelivery of another therapeutic protein, i.e. recombinant human tumor necrosis factor-related apoptosis-inducing ligand (TRAIL, MW: 20 kDa), together with an anticancer drug. TRAIL is selected as a promising anticancer protein as it is selectively toxic to cancer cells and only exerts limited toxicity to normal tissues *in viv*o. The core/shell structure of the P(MDS-*co*-CES) micelles allows the physical entrapment of hydrophobic drugs in the core and also the binding to proteins on the surface of the micelles.

With the codelivery system in place, it became desirable to enhance the therapeutic index of the nanocarriers through means of active targeting. A therapeutic antibody, Herceptin (MW: 145 kDa), targeted against human epidermal growth factor receptor-2, is codelivered with an anticancer drug, paclitaxel. Herceptin is selected for its specificity towards the HER-overexpressing cells and also for its availability as a FDA – approved therapeutic mAB. The binding of Herceptin onto the surface of the drug-loaded carriers can confer HER2-receptor specificity to the delivery system and sensitize the HER2+ cancer cells to anticancer drug treatment.

1.4 Nanoparticulate drug delivery systems

One of the main challenges in the development of anti-cancer drug formulations is the delivery of the drugs with sufficiently high bioavailability so as to achieve the therapeutic intention [5]. As many anti-cancer agents are hydrophobic, clinical administration of these drugs typically require dissolution using organic solvents. For instance, clinical application of paclitaxel (Pac) has been mostly hindered by its tremendously low aqueous solubility (0.3 μg/ml in water) [151]. This restricts its administration to a formulation comprising of 50:50 mixture of Cremophor EL (polyethoxylated castor oil):absolute ethanol. However, hypersensitivity reactions such as rashes and flushing occur in 41-44% of patients and also potentially-fatal reactions in 1.5-3%, even in those with cortisteriods premedication [152-154]. To reduce the dependence on this formulation, attempts have been made to modify the chemical structural of the drugs to increase their solubility, but limited success has been achieved [155-157].

Besides poor solubility, other challenges include the lack of target selectivity and poor biodistribution of small molecule drugs, whereby the anti-cancer agents are distributed non-specifically in the body and affect both cancerous and normal cells. This leads to dose-limiting side effects and lowers the dose-achievable in the cancer tissue. Small molecule drugs are also subjected to rapid plasma clearance and degradation *in vivo*, which will jeopardize the effectiveness of the therapy.

Over the past few decades, the development of drug delivery systems has been extensively explored as carriers of anti-cancer agents to help improve the pharmacokinetics and biodistribution. In relation to the context of my investigation, I will discuss the use of nanoparticles, as drug delivery systems. These nanosized carriers can

be made using a variety of materials including polymers (polymeric nanoparticles, micelles, or dendrimers), lipids (liposomes), viruses (viral nanoparticles), and organometallic compound (nanotubes). The key features of these nanoparticles and some examples are given in Table 1.4.

Table 1.4 Types and examples of nanoparticles for delivery of therapeutics agents.

Type of Nanoparticles	Key features	Examples	Ref.
Polymeric Micelles	a) Amphiphilic, self-assemble into nanoparticles	Doxorubicin-loaded PEG-aspartic acid micelles (NK911)	[158]
	b) Capacity to encapsulate hydrophobic drugs	Pac-loaded PEG-PLA micelles (Genexol-PM)	[159, 160]
	c) Versatility in structural manipulation for drug loading and release d) Surface modification possible, e.g. PEGylation, targeting moieties e) Relatively easy preparation	Doxorubicin-loaded PEG-PLGA micelles bearing folate	[161]
Polymer-drug conjugates	a) Water soluble	HPMA copolymer–Doxorubicin (PK1)	[162]
	b) Versatility in structural manipulation for molecular size, surface modification	HPMA copolymer–Pac (PNU1669845)	[163]
	c) Possibility to include bioresponsive elements	Polyglutamate–Pac (XYOTAX)	[164]
Dendrimers	a) Water soluble	Methotrexate-loaded PAMAM dendrimers	[165]
	b) Uniform and monodisperse	5-fluorouracil-loaded Folate−PEG−PAMAM dendrimers	[166]
	c) High stability due to covalent bonds d) High density of functional groups		
Liposomes	a) Biocompatible	Liposomal Doxorubicin (Myocet)	[167]
	b) Typically low toxicity	PEG–Liposomal Doxorubicin (Doxil)	[168]
	c) Surface modification possible, e.g. PEGylation, targeting moieties	PEG–Liposomal Pac conjugated to anti-HER2 antibody/antibody fragments	[169, 170]
Viral nanoparticles	a) High specificity	Viral capsid–DNA aptamer	[171]
	b) Biocompatible	Folate-PEG-Cowpea mosaic virus for DNA delivery	[172]
	c) Efficient cellular uptake and release of cargo d) Surface modification by mutagenesis or bioconjugation—multivalency		

Carbon nanotubes	a) Water soluble and biocompatible through chemical modification	Singled-wall carbon nanotubes (SWNTs)–Cisplatin prodrug conjugate	[173]
	b) Capacity to encapsulate drugs in hollow inner space	SWNT–Pac conjugate	[174]
		Doxorubicin-loaded SWNTs	[175]

1.4.1 Rationale of using nanoparticles

The use of nanoparticles as drug delivery systems offers several advantages as compared to using conventional free drugs. First, they serve as reservoirs to deliver hydrophobic anti-cancer drugs without organic solvents. Second, there is enormous flexibility in tuning the drug loading content and release rates by modifying the chemical nature of the nanoparticles. Third, functionalization of the carriers can carried out for the attachment of bioresponsive elements or targeting moieties. Fourth, nanoparticles can help to improve the pharmacokinetics of the drugs and reduce clearance. Furthermore, nanoparticles can have better tissue specificity than free drugs as they can accumulate within tumors by both passive and active targeting. When conventional anti-cancer agents are administered into the body, they are distributed nonspecifically in the body and they affect both cancerous and normal cells. The lack of target-specificity is a major barrier that limits the dose achievable within the tumor, and this result in suboptimal treatment with undesirable side effects. In other scenarios, efforts made in attempt to improve selectivity through the development of molecular targeted therapy [38]. However, the gradual lose of therapeutic effectiveness of such targeted agents is inevitable during clinical treatment due to the emergence of multi-drug resistance (MDR) [176, 177]. Nanoparticles have been reported to overcome MDR, as they enter cells *via* endocytosis,

thereby bypassing the recognition of P-glycoprotein efflux system – one of the main contributors of drug resistance [178].

1.4.2 Size and surface characteristics

One of the major reasons to develop nanoparticles as drug delivery carriers is to achieve longevity in blood circulation. Extended plasma half-life and delay in clearance will enable the therapeutic agent to be released from the carriers in a sustainable fashion without being eliminated and this will in turn; increase the chances of interaction with its therapeutic target. After administration into the bloodstream, opsonization (binding of serum proteins onto particles to identify as being foreign to the bodily system) of nanoparticles occurs and the particles become internalized by the macrophages of the RES (consisting mainly of liver, spleen, lungs and bone marrow). This results in a significant loss of nanoparticles from the circulation and is dependent on their size and surface characteristics. Small size and/or hydrophilic surfaces are necessary to reduce opsonization and elimination. The fate of injected nanoparticles can be controlled by adjusting their size and surface characteristics.

Size: The size of nanoparticles should lie within an optimal range whereby they should be sufficiently small enough to escape capture by the RES and also large enough to prevent renal clearance (~ 5.5 nm [179]) as well as leakage back into the blood vessels after entry into the tumor tissue. By modifying the chemical structure of the carriers (e.g. hydrophobic/hydrophilic composition, block lengths), the size of the nanoparticles can be adjusted.

Surface characteristics: The half-life and clearance of the nanoparticles are also strongly influenced by the surface characteristics of the nanoparticles. It has been

established in the early seventies that particles with hydrophilic surfaces tend to remain the circulation longer than those that are more hydrophobic [180]. To increase the hydrophilicity of the nanoparticles, hydrophilic groups such as PEG can either be chemically added or physically adsorbed onto the nanoparticle surface [181, 182].

1.4.3 Drug loading

Another important attribute of a successful drug delivery system is to have a high drug loading capacity. This will allow more drugs to be delivered per administration and thereby, lowering the number of administrations and amount of nanocarriers required. In general, small molecule drugs can be loaded into nanoparticles via two different ways – either by chemical conjugation of the drugs to the carriers or by physical entrapment of the drugs into the carriers through non-covalent interactions. The incorporation of the drug can be carried out during the process of nanoparticle fabrication or after the nanoparticles have been fabricated by immersing them in the drug solutions.

In terms of chemical conjugation of anti-cancer agents with nanocarriers, it is necessary to have functional groups that are accessible for the reactions to occur. For drugs that do not have functional groups available, derivative compounds and chemical linkers can be used. Careful selection of appropriate linkers is necessary for the creation of polymeric prodrugs remain inert during circulation but allows the drugs to be released when the targeted sites are reached. For instance, acid labile linkers such *cis*-aconityl, hydrazone and acetal have been widely used for conjugation of doxorubicin to polymers such as *N*-(2-hydroxypropyl)–methacrylamide copolymer (HPMA) [183], while ester linkages has been utilized in poly-(L)-glutamic acid-Pac conjugates (CT-2103) [184].

As for physical entrapment of drugs, the drug loading capacity in polymeric micellar nanoparticles *via* is dependent on various factors, such as the interaction between the polymer and drug and the length of repeating units in the polymer. Increasing the length of polymers tend to increase the association between the carrier and the drug [185] but may affect the aggregation behaviour of micelles. These results indicate that there is a need to optimize the length of polymer used for the drug entrapment. Other factors include the proportion of the core and shell-forming blocks in the copolymer, as well as the compatibility between the micellar core and the solubilizate (in this case, drug) [186, 187], assessed by the Flory–Huggins interaction parameter (χ_{sp}):

$$\chi_{sp}=(\delta_s-\delta_p)^2 V_s/RT$$

where δ_s and δ_p are the Scatchard–Hildebrand solubility parameter of the solubilizate and the core-forming polymer, respectively, V_s is the molar volume of the solubilizate, R is the gas constant and T the Kelvin temperature. Higher compatibility is indicated by lower χ_{sp} values. However, the Flory–Huggins interaction parameter is based on the regular solution theory and is unable to take into account the specific interactions between drugs and polymers. Furthermore, since polymers contain several different components, it is difficult to obtain of the Hildebrand–Scatchard solubility parameter of each component.

1.4.4 Drug release

Controlled drug release is an important feature for the development of useful drug delivery system. Nanocarriers should provide protection of its therapeutic load against leakage and degradation in circulation while enabling a sufficiently high local drug bioavailability in the target tissue. The release kinetics is dependent on several factors:

the rate of dissociation between the drug and the nanoparticles, breakdown of the linkages (in the case of polymer-drug conjugates), diffusion through the nanoparticle core and corona, and degradation/erosion of the carriers. Most drugs exhibit two-phase-release profiles, of which the drug is released at a relatively rapid rate in the early phase followed by a gradual and sustained release in the later phase. For some nanoparticle systems, there may be an initial burst release of drugs due to the dissociation of drug molecules that are weakly bound to the nanoparticle surface or corona. Following this, the drug release kinetics is mostly determined by the rate of diffusion across the nanoparticle barrier layer.

The rate of drug release is greatly influenced by both the physical and chemical properties of the carriers. Several reports have shown that nanoparticles comprising of higher molecular weight polymers with larger particle size generally can impede drug diffusion across the nanoparticle barrier and lower the rate of drug release. Interactions between the drugs and hydrophobic segments of the carrier may also affect drug release rates [188]. For example, Oh et al. reported the release of doxorubicin from poly(γ-benzyl-(L)-glutamate)/poly(ethylene oxide) (PBLG/PEO) polymeric nanoparticles with constant PEO length was dependent on the hydrophobic PBLG content. Significantly slower drug release and lesser cumulative release was observed over 24 hrs for the polymer with 60 mole% PBLB compared to those with 40 and 12.5 mole% [189].

1.4.5 Passive targeting

Nanoparticles typically have size ranging from 5 to 200 nm. The lower bound is based on the sieving coefficients for the glomerular capillary wall, which gives an

estimate for the threshold for renal elimination to be ~5 nm (diameter) [190]. The upper bound of particle size is mostly dependent on the microvascular permeability in tumors (~ 400 to 600 nm) [191]. Particles within the appropriate size range can preferentially target and accumulate in the tumor sites through the "Enhanced Permeation and Retention (EPR)" effect. This passive targeting phenomenon was first reported by Maeda et al. [192], who attributed it to two factors: the disorganized and leaky tumor vasculature which leads to hyperpermeability to macromolecules, alongside with poor lymphatic drainage in the tumor tissue to prevent escape of these macromolecules after entry. In greater detail, as fast-growing tumor cells reach a size of 2-3 mm, angiogenesis is induced to accommodate the increasing demand for oxygen and nutrients. Neovascularization or rerouting of existing blood vessels near the tumor tissue occurs to supply the tumor needs. As a result of the imbalance of angiogenic regulators such as growth factors and matrix metalloproteinases, tumor blood vessels are structurally and functionally abnormal. In contrast to normal blood vessels, tumor vessels are highly disorganized, defective or leaky with gap sizes varying from 100 nm to 2 μm [193, 194] as the endothelial cells are poorly aligned with large fenestrations [195]. This enables nanoparticles to escape easily from the blood stream and accumulate inside tumor tissue, while re-entry back into the bloodstream is prevented by the defective lymphatic drainage in the tumor [196]. With the appropriate drug carriers, the EPR effect can bring about 10 to 100 times higher tumor concentration of the therapeutic drug than that resulting from free drug administration [197].

Passive targeting can also be achieved by making use of certain properties of the nanoparticles, such as cationicity. Positively-charged liposomes have been shown to have

higher distribution into tumors as a result of the electrostatic interaction with negatively-charged phospholipid headgroups expressed at relatively higher levels on tumor endothelial cells than normal endothelial cells [198-200].

1.4.6 Active targeting

Besides passive targeting, chemotherapeutic agents can also be delivered to tumor cells through an active approach. The surface of nanoparticles can be functionalized and attached with ligands that can specifically recognize receptors expressed on the tumor cells. There are some criteria that need to be fulfilled in order to achieve effective active targeting of nanoparticles. First, the selected antigens and receptors surface should be expressed abundantly on tumor cells with little or no expression on normal cells. Second, the expression should be homogeneously expressed on all cells of the targeted tumor [201]. Last, there should not be any release of cell-surface antigens and receptors into the blood circulation. For instance, folate [202, 203], lectin/carbohydrate moieties and antibody/antibody-fragments are some of the types of ligands used for active targeting (Box. 1.4).

The binding of ligands to their cellular antigens/receptors will trigger internalization of the conjugates *via* receptor-mediated endocytosis. This mode of cellular entry is target-selective and useful for overcoming MDR by escaping recognition by efflux pump proteins on the cell surface [204]. However, in endocytotic processes, the recycling of endosomes back to the cell membrane may impede the efficient transport of the drug-loaded nanocarriers to the cytoplasm [205]. To prevent this, the release of drugs can be improved by disrupting the endosomal vesicles through the incorporation of

proton-buffering groups into the carrier structures. Subsequently, the endosomes be will destabilized *via* the 'proton-sponge effect' in the acidic microenvironment of the vesicles [206, 207], resulting in the release of the therapeutic drugs into the cytoplasm.

Box. 1.4 Affinity groups for active targeting.

Interactions between lectins and carbohydrate enable active targeting *via* the addition of carbohydrate moieties to nanoparticles that recognize specific lectins on the cells (direct lectin targeting) or the incorporation of lectins into nanoparticles that recognize cell surface carbohydrates (reverse lectin targeting). For instance, the interaction between galactose and the asialoglycoprotein receptor expressed at high levels in hepatocytes has been exploited in several liver cancer targeting systems [208, 209]. Transferrin, a glycoprotein that recognizes Transferrin receptors that are overexpressed in several cancer cell types, have also been incorporated into nanoparticle systems to deliver anti-cancer agents [210, 211]. However, the main challenge in these systems is that the interaction between carbohydrates and lectins is directed to entire organs. Therefore, the therapeutic agents will not only localize at the tumor sites but the normal tissues in the organ as well [212], and serious considerations have to be made to minimize damage to neighbouring tissues.

Interactions between antibody/antibody fragments and their complementary cellular receptors allow targeted delivery of the nanoparticles to the cancer tissue. Once the ligand-receptor interactions are achieved, the nanoparticles will be internalized by the cells via receptor-mediated endocytosis. These interactions can have positive effects on therapeutic activities either by enhancing the tumor localization or cellular uptake of these nanoparticles [213]. Besides targeting anti-cancer drugs to cancer cells, some antibodies (e.g. Herceptin [214, 215] also have inherent therapeutic properties which can bring about additive or synergistic interactions when delivered together to the cells. Currently, antibody fragments are more commonly used as targeting moieties for conjugation to nanosized drug carriers as they are smaller in size than antibodies. Furthermore, they do not contain the Fc effector region that could generate undesirable interaction with normal cells, and can lead to premature elimination through phagocytosis [216].

Angiogenesis-associated targeting is useful in developing targeted drug delivery systems to tumors. The advantages of targeting tumor blood vessels have been described by Kumar et al, In brief, first, the endothelial cells of angiogenic vessels are less likely to acquire phenotypic changes and drug resistance. Second, the physiological barriers that exist for drug delivery into tumors can be evaded by targeting the blood vessels. Third, the destruction of the tumor vasculature will greatly reduce the oxygen and nutrients supply to the tumor cells, hence, impeding the growth of the tumor. Last, such systems can be used unanimously for most tumors [217].

1.4.7 Augmentation of drug delivery

Structural and physiological disparities exist between tumor and normal tissues, and these differences have been explored to improve the therapeutic efficacy of drug delivery systems. For instance, compounds that affect blood vessels constriction/dilation can be added to nanocarriers to enhance vascular permeability and improve

biodistribution of drugs into tumor *via* the EPR effect. Vascular density in tumor tissues is typically higher than normal tissues and unlike normal blood vessels; tumor blood vessels do not have a smooth-muscle layer to regulate blood pressure and flow. When vasoconstrictor such as angiotensin-II (AT-II) is used to induce hypertension in normal blood vessels, the smooth-muscle layer constricts to maintain constant blood flow volume at higher blood pressure and flow rate. On the contrary, in AT-II-induced hypertension, tumor blood vessels cannot regulate the blood flow volume due to the lack of the smooth-muscle layer. As a result, the blood flow volume will increase as the blood pressure increases. In a report by Suzuki et al., tumor blood flow volume can increase 2–6 times by infusing tumor-bearing rats with AT-II [47]. The higher amount of blood volume reaching the tumor can bring about greater distribution and accumulation of drugs in the tumor tissue. At the same time, AT-II will induce constriction of normal blood vessels and tightening of endothelial gaps junctions which will then limit the extravasation of nanoparticles, leading to significantly lower amount of drug reaching healthy tissues [196].

Besides vasoconstriction, other means of modulating tumor blood vessels has also been explored. As such, vasodilators have been used to enhance vascular permeability by increasing the size of endothelial gaps of vessels. For instance, Bradykinin (BK), which is an endogenous vasodilator involved in tumor angiogenesis [218] and is upregulated in many tumors, can be degraded by angiotensin-converting enzyme (ACE). Therefore, the use of ACE inhibitors will increase the local concentration of BK in the tumor and enhance the delivery of nanocarriers to the tumor tissues [196].

1.4.8 Protein and peptide delivery using nanoparticles

As discussed earlier in section 1.3, there are many advantages of using proteins and peptides as therapeutics. Amongst which, the most attractive factors include the high specificity of target interactions and reduced risk of interference to normal physiological processes. Furthermore, the advancements in protein expression technology have made these compounds available on a larger and more economic scale than in the past. However, research progress in protein has far outpaced the ability to deliver these compounds effectively using delivery systems. Currently, the use of proteins/peptides for medical treatment has been mostly limited by their susceptibility to degradation and short plasma half-life. In this pursuit, the nanosized delivery systems have been explored for improving the stability of proteins against enzymatic degradation and thus, prolonging the lifespan of these therapeutic agents in circulation.

1.4.8.1 Protein loading into nanoparticles

For the preparation of protein-loaded nanoparticles, it is necessary to ensure that the therapeutic protein remains stable and subsequent dissociation from the nanoparticles is unhindered. Based on the preparation method chosen, the therapeutic agent can be entrapped in the polymer matrix, encapsulated in a hydrophobic core of micelles or adsorbed onto the particle surface. The methods that have been explored for protein loading include emulsification solvent evaporation [219], emulsion polymerization [220], nanoprecipitation [221] and salting out techniques [222]. As organic solvents are used in all the above procedures, a major challenge faced is the inevitable detrimental effects they will have on the stability and activity of the loaded protein. For instance, the w/o/w

double emulsion method has been widely used for encapsulating protein drugs into both nano- and microparticles. However, this technique not only requires the use of organic solvents, extended shearing/stirring rates and/or sonication [223-225] is also required for the fabrication of the particles. Subjecting proteins to such harsh conditions will inevitably lead to considerable loss in protein activity. In addition, it has also been reported that that such methods are also more suitable for loading compounds with hydrophobic nature to reduce drug leakage towards the outer aqueous medium [221]. In a study conducted by Barichello et. al., they observed that the encapsulation efficiency reduces with drug hydrophilicity and insulin, which is insoluble in organic solvents, was found be bound to the PLGA nanoparticles mostly *via* surface adsorption rather than encapsulation within the carriers [226].

Protein adsorption to nanoparticles can occur *via* electrostatic interactions, van der Waals forces and hydrogen bonding [227]. To enhance binding, nanoparticles with surface charges may be used. When proteins are added to charged nanoparticles, both the pH and ionic strength of the incubation medium can greatly affect the interaction and strength of association between the proteins and its carrier. pH influences the zeta potential of the both the proteins and nanoparticles and therefore, the charge neutralization and redistribution between the polymeric surface and protein molecule. Changes in ionic strength of the medium will affect the shielding effect on surfaces charges and the electrostatic interactions between the counter ions of the nanoparticles and protein [227]. Depending on the ionic strength and nature of the proteins, hydrophobicity of the polymeric carriers may also act as a governing parameter for protein binding. In a report by Bayraktar et al., they have suggested that the facial

specificity in binding of cytochrome *c* to carboxylate-functionalized nanoparticles is related to the balance between electrostatic association as well as hydrophobic interactions [228].

In some cases, binding between proteins and nanocarriers may not occur due to insufficient non-coulombic interactions or electrostatic repulsion between like-charges on the two entities. For such systems, chemical means can be used to manipulate the charge moieties to enable binding. For instance, Kataoka et al. [229] have reported the use of citraconic anhydride to convert positively-charged primary amines of polymeric nanoparticles to citraconic amides. The presence of carboxylate groups on the amides will confer negative charges to the nanoparticle and will allow binding with basic proteins.

1.4.8.2 Amphiphilic polymers used in protein/drug delivery systems

Research efforts made in the development of protein drug delivery have been mostly driven by the need to increase the bioavailability of therapeutic proteins by improving their stability. Various strategies that aim to prevent protein degradation as well as enhancing distribution to target sites have been explored. Through recombinant techniques, genetic fusions of protein/peptide ligands such as antibody fragments to therapeutic proteins [230, 231] have been created to alter the biodistribution of the native protein. For instance, in a study conducted by Pardridge and his co-workers, brain derived neurotrophic factor (BDNF) was fused to heavy chain of a chimeric monoclonal antibody that recognizes human insulin receptors (HIRMAb). The resultant HIRMAb-BDNF fusion protein had >100-fold longer mean residence time than native BDNF and

the interaction with HIR also enabled the therapeutic protein to cross the blood brain barrier [232]. Similar modification to proteins can also be made through chemical means whereby ligands/polymers can be covalently attached to free amine [233] or thiol [234] groups of proteins to produce conjugates with improved stability and tissue localization. Proteins-polymer conjugate systems have shown to increase protein stability and this can be attributed to enhanced protein surface activity, steric hindrance of protein-protein interactions, and increased viscosity limiting protein structural movement.

Biodegradable polymers

Besides enhancing protein stability, other properties such as solubility, biocompatibility and protein activity can also be adjusted through the chemical conjugation with synthetic polymers [235]. For therapeutic applications, there is an inclination towards the use of biodegradable polymers as the degradable products can be cleared from the body and are more likely to bring about improved patient compliance. Such polymers can be degraded by various ways, including hydrolysis (e.g. PLGA), solubilization (e.g. pluronics), bulk or surface erosion, or cleavage of labile bonds in the bioconjugates. There are several types of cleavable linkages that have been used for the formation of biodegradable polymers. In ascending orders of relative hydrolysis rates under physiological conditions:

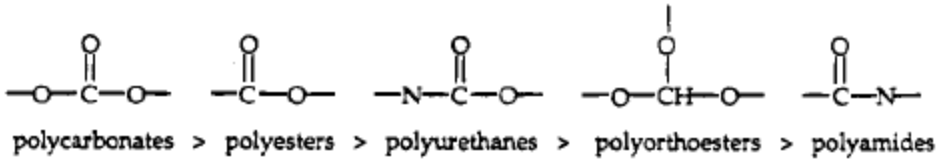

Figure 1.3 Labile bonds arranged in order of sensitivity to hydrolysis [235].

Besides the sensitivity of cleavage bonds to hydrolysis, polymer morphology is also another influencing factor in the degradability of the polymers. Hence, the relative rates at which polymers degrade cannot be predicted solely from the hydrolytic susceptibility of these bonds.

Stimuli-responsive polymers

Polymers that exhibit changes in behavior and physical properties have also been explored as they can impart stimuli-sensitivity to the delivery systems. In cancer research, the common stimuli involved are temperature and pH as differences in these two environmental factors exist between normal and tumour tissues. The latter has a slightly higher local temperature [236] and lower extracellular pH (6.8–7.2) compared to normal tissue (pH ~ 7.4) [237]. Therefore, the incorporation of stimuli-responsive polymers into drug delivery systems can assist in the selection of tumour against normal tissue and enable better targeting efficiency. For instance, one of the most widely studied thermo-responsive polymers is poly(N-isopropylacrylamide) (PNIPAM) [238-240], which undergoes a exhibit a coil to globule transition at 32 ^{o}C, changing from a hydrophilic state below this temperature to a hydrophobic state above it. PNIPAM becomes insoluble upon heating beyond 32 ^{o}C and this temperature is termed as the lower critical solution temperature (LCST). Other such polymers include those that contain N,N-diethylacrylamide (DEAM) [241], methylvinylether (MVE) [242] and N-vinylcaprolactam (NVCl) [243]. In addition, there are also polymer systems which become soluble upon heating, have an upper critical solution temperature (UCST). LCST

and UCST systems are not limited to aqueous solvent environment, but importantly, only polymers that are soluble in aqueous conditions and have transition temperature in physiologically acceptable range (~20–40^{o}C) are of interest for biomedical applications [244]. The temperature at which the transition occurs depends on various environmental factors such as the presence of surfactants, co-solvents and salt concentration [245]. Another way to alter the transition temperature is by changing the hydrophilic/hydrophobic balance of the polymer by copolymerization with a second monomer. Co-polymerizing with hydrophilic lowers the LCST and vice versa for hydrophobic monomers [246, 247]. In the case of drug delivery, increasing the precision of drug release can be done by in co-polymerizing both thermo- and pH-responsive monomers to create a dual-responsive system.

Physical interaction

Polymer systems have been widely explored as drug delivery agents and have demonstrated great potential as both chemical conjugates [248-251] or as physical carriers [252-255], mostly for small molecule drugs. In consideration of the delicate nature of proteins, chemical conjugation of polymers to proteins may be less preferential as the modification of protein structure may run into risks of changes to folding and in turn, the loss of protein specificity and activity. Instead, polymers may serve well as carriers of therapeutic proteins through various modes of physical interaction (as mentioned in section 1.4.5.1). This will more likely ensure that the folding structure of proteins is preserved and reduce any losses of protein integrity. For example, nanoparticles fabricated from polymers such as chitosan [256, 257] and poly(lactide-co-

glycolide) (PLGA) [258, 259] have been employed in many studies involving protein delivery. Such polymeric carriers utilize non-covalent interactions for protein adsorption which can prevent alterations to native protein structure. Importantly, they also protect the therapeutic proteins from degradation [260] and can also enable tunability of protein loading and release properties [256] of the delivery system through modification of polymer structures.

Amphiphilic copolymers used for therapeutic codelivery

Over the recent years, there has been a growing interest on the use of amphiphilic polymers to codeliver multiple therapeutic agents in a single carrier as more researchers recognize the appeal of targeting several oncogenic molecules for cooperative therapeutic effects.

My lab was one of the earliest to report the use of polymeric nanoparticles to codeliver therapeutic combinations for cancer treatment. A cationic amphiphilic copolymer, poly{(*N*-methyldietheneamine sebacate)-*co*-[(cholesteryl oxocarbonylamido ethyl) methyl bis(ethylene) ammonium bromide] sebacate} (P(MDS-*co*-CES)) has been synthesized by my previous lab member (Y. Wang) and has been successfully used for the codelivery of nucleic acids (DNA and siRNA) and anticancer drugs [261-264]. This polymer contains an amine-containing polyester main chain with cholesterol pendant groups. The amphiphilic structure enables it to self-assemble to form micelles with a core/shell structure. Such structure allows for the physical encapsulation of hydrophobic drugs within the core and the binding of hydrophilic biomolecules to the surface of the micelles.

Physical characterization of P(MDS-co-CES) shows that it has a low Critical Micelle Concentration (CMC) of ~1.9 mg/L which indicates good particle stability in extensive dilute conditions such as the bloodstream. Gel electrophoresis assays have shown that these cationic nanoparticles have excellent nucleic acids binding capacity and are able to induce high *in vitro* gene transfection. Animal studies conducted with the codelivery of Interleukin-12 gene and Paclitaxel (Pac) using the P(MDS-co-CES) nanoparticles displayed significant enhancement in tumor reduction compared to the individual therapeutic agents in 4T1-tumor bearing mice.

In other earlier work on codelivery, in 2007, Bae Y.H. and his co-workers reported that the use of branched poly(ε-caprolactone) (PCL) grafted branched polyethylenimine (PEI) [265] to form nanoparticles that can encapsulate doxorubicin. And at the same time, these nanoparticles can deliver luciferase gene and induce luciferase expression on liver cancer cells.

The codelivery of small molecule drugs has also been reported. In 2009, Panyam J. et al. [266] published an article on the codelivery of Paclitaxel and p-glycoprotein inhibitor which led to higher cellular accumulation of the anticancer drug and reduction in tumor growth. One of the latest developments in 2011 is on the use of dendritic polyamines conjugated with β-cyclodextrin to improve the solubility of hydrophobic drugs while the cationic amine component binds to Epidermal Growth Factor (EGFR) siRNA. This combination was delivered to brain tumor cells which overexpress the EGFR receptors and enhancement in cell death was reported [267].

1.5 Objectives and scope of the research

The ultimate goal of my study is to develop multifunctional co-delivery system from self-assembled polymeric core/shell nanoparticles that can be used ubiquitously for the simultaneous delivery of both anti-cancer drug and therapeutic proteins. Initial work has been started based on the hypothesis that amphiphilic polymers can enable the loading of both hydrophobic drugs and therapeutic proteins in a single nanosized therapeutic system and codeliver them together to cancer cells for enhanced anticancer effects. Investigations have been carried out progressively to understand various aspects of delivery vehicle. Prior to to my research, the polymer P(MDS-*co*-CES) has been synthesized by my previous lab member, Wang Y., [261-264]. The synthetic chemistry and characterization of P(MDS-*co*-CES) is described in Section 2.2 and Appendix I.

It is known that physical properties of nanoparticles such as size and charge will greatly influence the biocompatibility and biodistribution of the drug delivery systems to different organs. Therefore, at the initial phase, it is important to characterize the polymeric nanoparticle according to their particle size and zeta potential. To understand the capacity of these micelles to delivery therapeutic agents of different nature (i.e. small molecule drugs and proteins– molecular size and hydrophobicity/ hydrophilicity), separate assessments have been carried out to evaluation of their protein binding capacity as well as hydrophobic drug encapsulation efficiency and release behavior.

In order for the polymeric nanoparticles to function effectively as delivery vehicles, it is essential that they are biocompatible and can remain stable in physiological conditions. Size measurements of the nanoparticles are performed in physiologically-simulating conditions to investigate any changes in physical stability with time. *In vitro*

cell culture studies are conducted to evaluate the cytotoxicity of these micelles and in vivo studies in mice model are carried out to assess the dose-related physiological effects.

Next, a model protein, Lectin-A (MW: 30.7 kDa), is used for the initial study to evaluate the delivery efficiency of the nanoparticles. Lectin-A is unable to enter into cells without aid from delivery carriers but can induce significant cytotoxic when it is delivered intracellularly. Hence, *in vitro* cytotoxicity induced by Lectin-A delivery can be used as an indication of the protein delivery efficiency of the nanoparticles. Comparisons are also made against other commercially-available protein delivery agents such as BioPorter and ProJect according to the degree of cytotoxicity resulting from the different systems.

Combination therapy with two or more drugs in has been widely reported to show great improvements in cancer treatment efficacy and lower risk of multidrug resistance development. However, current treatment regimens are typically developed using free drugs without delivery carriers and may not be able to bring about the best possible therapeutic efficacy. In my study, one of the key aspects is to investigate the possibility of using polymeric micelles as co-delivery vehicles of anti-cancer drugs and proteins to impede cancer growth. From there, I will move on to delivering another therapeutic protein of similar molecular weight, i.e. recombinant human tumor necrosis factor-related apoptosis-inducing ligand (TRAIL, MW: 20 kDa) and anti-cancer drugs simultaneously. The main rationale for using TRAIL is because of its advantageous cytotoxic selectivity towards cancer cells with limited toxicity to normal tissues when introduced *in viv*o [268, 269]. Different delivery systems consisting of TRAIL-polymeric nanoparticles loaded with different drugs – Pac and Dox are studied. Cellular response to the co-delivery

systems is investigated in cancer cells with different degrees of TRAIL-sensitivity. Dox-loaded P(MDS-*co*-CES) nanoparticle/TRAIL complexes is used for treatment against both wild type and TRAIL-resistant SW480 cells and cytotoxicity studies is carried out to evaluate synergy in therapeutic effects. Comparison is made against free drug combinations to evaluate the differences in therapeutic effectiveness. To determine if the co-delivery systems exhibit unspecific cytotoxicity against non-cancerous cells, WI38, a human lung fibroblast cell line is used as a representative cell line for *in vitro* cell culture studies.

The final aim of this study is to develop a targeted delivery system that can simultaneously deliver both anti-cancer drug and proteins (Fig. 1.4) to cancer tissues. This is because targeted delivery of proapoptotic molecules to specific sites is likely to enable higher therapeutic effectiveness and lower the risk of damaging normal tissues in the body. A therapeutic antibody, Herceptin, was chosen as it can recognize HER2-receptors that are found to be overexpressed in 30% of human breast cancer patients. The binding of Herceptin onto the surface of the drug-loaded micelles will confer HER2-recognition to the delivery system and can increase sensitivity of the cancer cells to drug treatment. Investigations are made to evaluate if the co-delivery of both Herceptin and anti-cancer drug to the cells can lead to enhanced drug actions and increase therapeutic effectiveness.

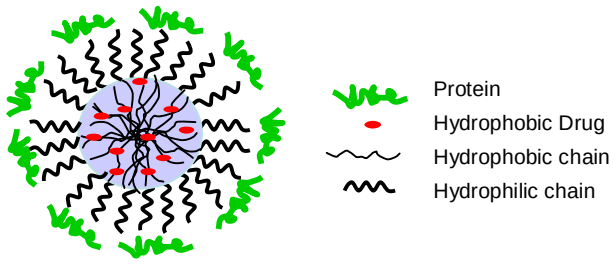

Figure 1.4. Nanocomplexes for codelivery of anti-cancer drug and protein therapeutics.

CHAPTER 2

MATERIALS AND METHODS

In my work, the possibility of utilizing various therapeutic proteins as monotherapy or in combination with different conventional chemotherapeutic drugs in nanoparticulate systems was evaluated. Physical characterization of nanocomplexes and enhancement of tumor cell death to combinational treatment were evaluated through various *in vitro* assays. The materials and methods used in this study are:

2.1 Materials

Therapeutic proteins

- Recombinant lectin A-chain of the heterodimeric lectin *from Viscum album coloratum* (Korean Mistletoe) was kindly provided by A/P Ho Sup Yoon, from Nanyang Technological University [270].
- Soluble human TRAIL (Mw: 20 kDa) was purchased from BioMol, U.S.A.
- Herceptin was purchased from Roche, Switzerland.

Chemotherapeutic drugs

- Paclitaxel was purchased from Sigma, U.S.A.
- Doxorubicin hydrochloride (Dox) was purchased from Boryung Pharmaceutical, Korea.

Organic solvents

Dimethyl sulfoxide (DMSO), dimethylacetamide (DMAC) and dimethyl formamide (DMF) were purchased from Sigma-Alrich, U.S.A.

Reagents

Polystyrene beads were obtained from Dukescientific, U.S.A. Dialysis buffer used for nanoparticle fabrication was self-prepared using sodium acetate and acetic acid (ACS grade, Merck, U.S.A.). 3-[4,5-Dimethylthiazol-2-yl]-2,5-diphenyl tetrazolium bromide (MTT), crystal violet, sodium azide and paraformaldehyde were obtained from Sigma, U.S.A. MTT was dissolved in phosphate-buffered saline (PBS, pH 7.4) with a concentration of 5 mg/ml, and the solution was filtered with a 0.22 μm filter to remove blue formazan crystals prior to use. Propidium iodide and 1,1'-dioctadecyl-3,3,3',3'-tetramethylindocarbocyanine perchlorate (DiL)was purchased from Invitrogen, U.S.A. BioPorter was purchased from Genlantis, U.S.A. and ProJect was purchased from Pierce Biotechnology, U.S.A. and both were used according to the manufacturer's instructions. Death receptors blocking antibodies (Anti-DR4 and Anti-DR5) were purchased from Enzo Life Sciences, U.S.A. Pan-caspase Inhibitor ZVAD-FMK was purchased from Promega, U.S.A. For *in vivo* studies, 17ß-Estradiol release pellets were obtained from Innovative Research of America, U.S.A. 1,1'-dioctadecyl-3,3,3',3'-tetramethylindotricarbocyanine iodide (DiR) was purchased from Caliper Lifesciences, USA. Unless stated otherwise, all reagents and solvents were of commercial grade, and were used as received.

Cell lines

The cell lines that were used are human breast cancer MDA-MB-231, MCF7, T47D and BT474, human cervical cancer HeLa, human liver carcinoma HepG2, human colorectal carcinoma SW480, mouse breast cancer 4T1 cell lines and human lung fibroblast WI38 and human embryonic kidney HEK293 cells. All cell lines were purchased from ATCC, U.S.A.

Cell culture medium

HepG2, HeLa and HEK293 were cultured in DMEM, MDA-MB-231 and SW480 in Leibovitz L-15, T47D, BT474, 4T1 and WI38 in RPMI 1640 and MCF7 in either MEM or RPMI 1640. All the culture media were supplemented with 10% fetal calf serum, 100 U/ml penicillin and 100 μg/ml streptomycin (HyClone, U.S.A.).

2.2 Synthesis of P(MDS-*co*-CES)

P(MDS-*co*-CES) (Figure 2.1A) was obtained by a three-step synthesis [261]. The detailed synthetic chemistry of the polymer is given the Appendix I. Briefly, the main chain, poly(*N*-methyldietheneamine sebacate) (PMDS), was first produced by condensation polymerization between *N*-methyldiethanolamine and sebacoyl chloride. Excess triethylamine was used to remove hydrochloride and limit protonation of the tertiary amine. Next, cholesteryl chloroformate was allowed to react with 2-bromoethylamine hydrobromide in an amidation reaction. The resulting hydrophobic *N*-(2-bromoethyl) carbarmoyl cholesterol was then grafted onto the hydrophilic poly(*N*-methyldietheneamine sebacate) main chain through a quaternization reaction to obtain the final product.

The main chain is a polyester, and the pendant chain contains hydrolytically labile urethano groups, rendering this copolymer degradable. The degree of cholesterol grafting was about 28.5%. P(MDS-*co*-CES) had a weight average molecular weight (M_w) of ~ 5.0 kDa with a polydispersity index of 1.7, as measured by gel permeation chromatography [Waters 2690, MA, U.S.A., with a differential refractometer detector (Waters 410, MA, U.S.A.); Mobile phase:water of HPLC grade with a flow rate of 1 mL/min; Polystyrene standards: molecular weight ranging from 1300 to 30,000]. The nitrogen content was determined to be 4.0 % in weight as estimated by elemental analysis using Perkin-Elmer Instruments Analyzer 2400.

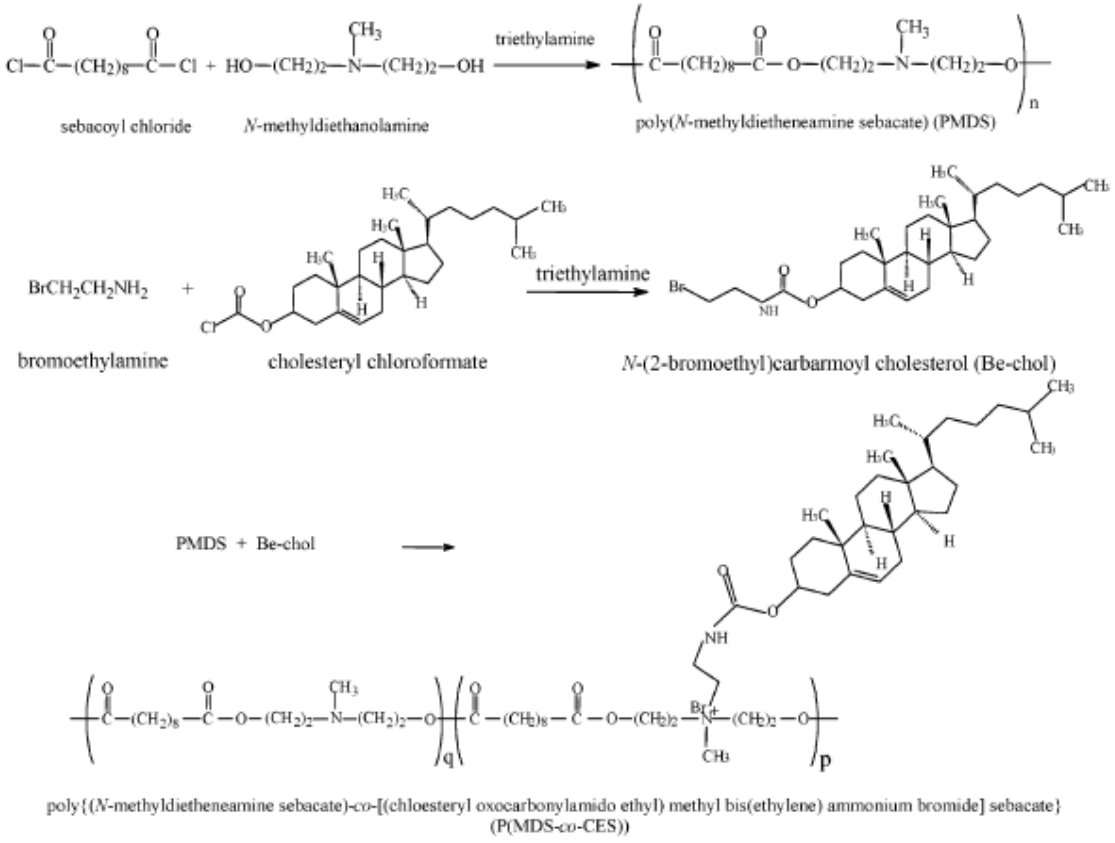

Figure 2.1. Synthesis of cationic amphiphilic polymer P(MDS-*co*-CES) [262].

2.3 Preparation of P(MDS-*co*-CES) micellar nanoparticles

To prepare the cationic micellar nanoparticles, 15.0 mg of P(MDS-*co*-CES) was dissolved in 5.0 ml of DMF, which was placed in a dialysis membrane with a molecular weight cut-off (MWCO) of 2000 Da (Spectrum Laboratories, U.S.A.). The dialysis bag was then immersed in 500 ml of de-ionized water or 20 mM sodium acetate/acetic acid buffer with pH 4.6 at room temperature for 24 hours. The dialysis buffer was replaced hourly with fresh buffer solution for the first 8 hours during the 24 hour course. At the end of the dialysis process, the resulting micelle solution was then filtered through a 0.22 μm filter in a sterile environment to remove large aggregates. The micelles were characterized with respect to their size and zeta potential using a zetasizer with dynamic light scattering capability (scattering angle: 90°) and equipped with a He-Ne laser beam at 658 nm (Malvern Instruments Zetasizer Nano ZS, UK).

2.4 Preparation of drug-loaded P(MDS-co-CES) nanoparticles

Fabrication of drug-loaded P(MDS-co-CES) nanoparticles were carried via the dialysis method whereby the chemotherapeutic drugs were physically entrapped into the hydrophobic core of the micelles. Details of experimental procedures are as follows.

2.4.1 Preparation of Pac-loaded nanoparticles

The polymer (15.0 mg) and pac (3.0 mg) were dissolved together in DMF. The mixture was placed in a dialysis membrane tube with MWCO of 2000 Da (Spectrum Laboratories, U.S.A.). The dialysis bag was then immersed in 500 ml of 20 mM sodium acetate/acetic acid buffer with pH 4.6 at 4°C for 2 days. The dialysis buffer was replaced

3 times per day with fresh buffer solution during the 2-day course. At the end of the dialysis process, the resulting micelle solution was filtered through a 0.45 μm filter in order to remove large aggregates, and then freeze-dried. To determine the encapsulation efficiency and loading level of drug, the drug-loaded micelles were dissolved in 3 ml of chloroform and 9 ml of ether was added to precipitate P(MDS-*co*-CES). The mixture was centrifuged at 4000 rpm for 20 minutes and the supernatant was decanted into a fresh vial, and dried. The deposited drug was dissolved in 1.5 ml of mobile phase consisting of water: methanol: acetonitrile in the volume ratio of 35: 20: 45. Drug content was analyzed using high performance liquid chromatography (HPLC, Waters 996 PDA detector, U.S.A.) at 228 nm UV wavelength. The drug encapsulation efficiency was calculated based on the ratio of the amount of drug successfully encapsulated into the micelles to the amount of drug initially added during the micelle fabrication process.

2.4.2 Preparation of Dox-loaded nanoparticles

5.0 mg powdered Dox was dissolved in 2.0 mL DMAC and vortexed intensely for 20 minutes. Triethanolamine (TEA) was added to the solution in a molar ratio of 3:1 (TEA : Dox) and vortexed intensely for another 20 minutes to allow time for TEA to neutralize the acidic Dox preparation. The Dox solution was then added to 10.0 mg of P(MDS-*co*-CES) pre-dissolved in 2.0 mL DMAc and vortexed to mix. The resulting solution was transferred to a dialysis bag with molecular weight cut-off (MWCO) of 1 kDa, (Spectrum Laboratories, U.S.A). The dialysis bag was then immersed in 500 ml of deionized water at room temperature for 2 days. The dialysis medium was replaced 3 times per day with fresh buffer solution during the 2-day course. At the end of the

dialysis process, the resulting micelle solution was filtered through a 0.45 μm filter in order to remove large aggregates, and then freeze-dried. To determine the encapsulation efficiency and loading level of drug, the drug-loaded micelles were dissolved in DMSO and absorbance was measured against a standard calibration curve of free Dox dissolved in the same solvent at 488 nm wavelength.

2.5 Preparation of P(MDS-*co*-CES) nanoparticle/protein nanocomplexes

Therapeutic proteins used in the experiments were kept in an ice bath during the experiments to prevent disruption to its structural stability caused by temperature changes. The protein was first added to 20 mM sodium acetate/acetic acid buffer at pH 6.0. P(MDS-*co*-CES) nanoparticle/protein nanocomplexes were then formed by adding the freshly prepared micelle solution to the protein solution in varying mass ratios, and mixed gently. The complex solution was left to stand at room temperature for 30 minutes before being characterized and introduced into the cancer cells.

2.6 *In vitro* drug release

To function effectively as drug delivery systems, drug-loaded nanoparticles must be able to provide a sustained and gradual release of their cargo without significant initial burst. It is therefore important to first obtain the *in vitro* release profile of the encapsulated drugs from the P(MDS-*co*-CES) nanoparticles prior to determining its suitability for biomedical application.

2.6.1 *In vitro* release of Pac

Release of Pac from the Pac-loaded micellar nanoaprticles and Pac-loaded nanoparticle/TRAIL complexes was studied using the dialysis method. Dialysis membrane tube with MWCO of 2000 Da (Spectrum Laboratories, U.S.A.) containing 10.5 mg of the micelles was immersed in 40 ml of the release medium, *i.e*. PBS (pH 7.4) containing 0.1% (v/v) Tween 80 to maintain a sink condition. This was kept shaking on an orbital shaker at 120 rpm at 37^{o}C. At designated time intervals, the release medium was removed and replaced with fresh medium. The medium that has been removed was analyzed for its drug content. To do this, 10 ml of dichloromethane (DCM) was added and mixed with the release medium through 3 minutes of vigorous vortexing. The organic layer was left to settle and carefully extracted into a new glass vial. DCM was evaporated by air flow. The deposited drug was dissolved in 1.5 ml of mobile phase and Pac content was analyzed using HPLC at 228 nm as described in Section 2.4.1.

2.6.2 *In vitro* release of Dox

Release of Dox from the Dox-loaded micellar nanoparticles and Dox-loaded nanoparticle/TRAIL complexes was studied using the dialysis method. 4 mL of Dox-loaded micelles was transferred to a dialysis membrane tube with a molecular weight cut-off (MWCO) of 2 kDa (Spectrum Laboratories, U.S.A.) and dialysed against 20 mL of either phosphate buffered saline PBS (pH 7.4) or 20 mM sodium acetate/acetic acid buffer (pH 5.6) solution. The set-up was kept shaking on an orbital shaker at 100 rpm at 37^{o}C. At designated time intervals, the release medium was removed and replaced with

fresh medium. The amount of Dox released into the medium was determined from its absorbance at 488 nm wavelength.

2.7 Native protein gel shift assay on P(MDS-*co*-CES) nanoparticle/protein nanocomplexes

Complex formation was carried out in sodium acetate/acetic acid buffer (pH 6.0) by adding freshly prepared P(MDS-*co*-CES) nanoparticles solution to protein in varying polymer to protein mass ratios between 0.1 to 50. After that, the mixture was left to stand at room temperature for 30 minutes before continuing with native polyacrylamide gel electrophoresis (PAGE). Samples were loaded into 5% (for Lectin A and Herceptin) and 12% (for TRAIL) Tris glycine gel and ran at 200V with Tris glycine running buffer (BioRad, USA) for 35 minutes. Bromophenol blue tracked the fronts and the gel was stained with SYPRO ruby protein gel stain (Invitrogen, U.S.A.). Destaining was carried out in water containing 10% methanol and 7% acetic acid, and the stained gel was imaged under ultraviolet excitation.

2.8 Stability of P(MDS-co-CES) nanoparticle/protein complexes under physiologically-simulating conditions

To determine the stability of nanocomplexes under physiologically-simulating conditions, Herceptin was used as the model protein for this study. The P(MDS-co-CES) nanoparticle/Herceptin complex suspension was diluted 10 times with PBS (pH 7.4) containing 10% (v/v) FBS and incubated at 37^{o}C. Size measurements were taken at 0, 5

minutes, 1 hour, 4 hours and 24 hours. The stability of these complexes is demonstrated by the absence of aggregates formation and maintenance of particle size within the nanometer range.

2.9 Establishment of TRAIL-resistant SW480-TR cell line from parental SW480

In cancer therapy, one of the major problems encountered is the development of drug resistance. In order to investigate the efficacy of the Dox-loaded P(MDS-co-CES) nanoparticle/TRAIL complex against cells that have developed resistance to TRAIL, we first establish TRAIL-resistant cells from parental TRAIL-sensitive SW480 cells. To do this, the cells were cultured in T75 flasks and exposed to increasing doses of TRAIL (1, 2, 4, 8, 10 and 20 nM) for 4 weeks. Cell density was maintained at ~75% confluency and subcultured as needed. Each dose was repeated at least twice by exposing cells to TRAIL-containing medium for 2 to 3 days depending on the amount of cell death induced. The TRAIL-containing medium was then replaced with TRAIL-free medium and incubated for 1 to 2 days before the next treatment with TRAIL. By the end of 4 weeks, the resultant TRAIL-resistant cells (designated SW480-TR) were harvested and kept frozen. In between experiments, cells were maintained in a complete RPMI 1640 medium containing 10 nM TRAIL at 37°C.

2.10 Confocal microscopy and flow cytometry studies on intracellular distribution of nanocomplexes

2.10.1 Preparation of FITC-loaded P(MDS-co-CES) nanoparticles

P(MDS-*co*-CES) nanoparticles was labeled by encapsulating FITC into the hydrophobic core of the nanoparticles. The polymer (15.0 mg) and 1.0 mg of fluorescent dye were dissolved in DMF. The mixture was placed in a dialysis membrane with a molecular weight cut-off of 2000 Da (Spectrum Laboratories, U.S.A.). The dialysis bag was then immersed in 500 ml of 20 mM sodium acetate/acetic acid buffer with pH 4.6 at 4°C for 2 days. The dialysis buffer was replaced 3 times per day with fresh buffer solution during the 2-day course. At the end of the dialysis process, the resulting nanoparticle solution was filtered through a 0.22 μm filter in sterile environment to remove large aggregates.

2.10.2 Preparation of fluorescence-labeled protein

Lectin A-chain and Herceptin were labeled using Alexa Fluor 647 protein labeling kit (Invitrogen, U.S.A.) while TRAIL was labeled using Alexa Fluor 555 protein labeling kit (Invitrogen, U.S.A.). In brief, the Alexa Fluor dye with a tetrapfluorophenyl (TFP) ester moiety was added to the protein in a molar ratio of 15:1 for lectin A-chain, 17:1 for TRAIL and 28:1 for Herceptin. The reaction was carried out at room temperature for 1 hour. Purification of the fluorescent conjugate was carried out using spin columns provided in the labeling kit. The conjugate was then analyzed spectrophotometrically using the NanoDrop ND-1000 spectrophometer (NanoDrop Technologies, USA) and the degree of labeling was determined to be 1.7, 0.1 and 0.1 moles Alexa Fluor dye per mole of Lectin A-chain, TRAIL and Herceptin respectively.

2.10.3 Intracellular uptake and distribution of fluorescence-labeled protein, P(MDS-co-CES) nanoparticles and their nanocomplexes

Cells were seeded onto borosilicate chambered coverglass (Nunc, USA) and cultivated in 500 μl of growth medium. For studies involving Lectin A-chain distribution, HeLa cells were seeded at a density of 2×10^5 cells per well. For studies involving Herceptin distribution, BT474 and HEK293 cells were also seeded at a density of 2×10^5 cells per well while for studies involving TRAIL distribution, 5×10^4 MCF7, T47D, MDA-MB-23 cells were seeded per well. After allowing the cells to adhere overnight, spent growth medium was removed from each well and replaced with 500 μl of the pre-prepared complex solution in serum-free or serum-containing medium. After 1 hour of incubation at 37°C with the nanocomplexes, the growth medium was removed, washed with PBS and fixed with 4% paraformaldehyde. The samples were then imaged at 63× magnification using a LSM 510 DUO confocal unit (Carl Zeiss, USA). Each condition was performed in triplicates.

Flow cytometry was performed to study the cellular uptake of fluorescently-labeled TRAIL into MCF7, T47D and MDA-MB-231 cells. The cells were seeded onto 12-well plates at a density of 1×10^6 cells per well and allowed to adhere overnight. The next day, the spent growth medium was removed from each well and replaced with 1 ml of the pre-prepared complex solution in serum-containing medium, and the cells were incubated for 3 hours at 37°C. Cells were then trypsinized, washed and resuspended in PBS. Cellular uptake of TRAIL was then analyzed with fluorescence-activated cell sorting analysis (FACS) on a Becton Dickinson FACSCalibur flow cytometer using BD FACSDiva™ software (BD Biosciences, U.S.A.).

2.10.4 Confocal microscopy studies on receptor-mediated endocytosis

Confocal microscopy studies were carried out to evaluate receptor-mediated endocytosis of the nanocomplexes by using Dox-loaded nanoparticle/TRAIL complexes as a model system. TRAIL was labeled using Alexa Fluor 647 protein labeling kit (Invitrogen, U.S.A.). Alexa Fluor 647 dye with a tetrafluorophenyl (TFP) ester moiety was added to TRAIL solution in a molar ratio of 15:1 and reacted at room temperature for 0.5 hour. Purification of the fluorescent conjugate was carried out likewise in Section 2.10.2.

Nanocomplexes were fabricated using Dox-loaded nanoparticle and Alexa Fluor 647-labelled TRAIL. SW480 cells were seeded onto borosilicate chambered coverglass (Nunc, U.S.A.) at a density of 5×10^4 cells per well, and cultivated in 500 μl of growth medium. The next day, the spent growth medium was removed from each well and replaced with blocking antibodies anti-DR4 and anti-DR5 in serum-containing medium. After 1 hr, pre-prepared complex solution in serum-containing medium was then added. At designated time points, the growth medium was removed. The cells were then washed with PBS, fixed with 4 w/w% paraformaldehyde in PBS and imaged at 630× magnification using LSM 510 DUO confocal unit (Carl Zeiss, U.S.A.). Each condition was performed in triplicates.

2.11 Cell viability studies

One of the main objectives of this research is to successfully utilize these drug-loaded nanoparticles/protein complexes to induce cell death in cancer cells, either as single agents or enhance cell death when used in combinations. The MTT assay is used as

rapid and convenient method to determine the end-point cell viability remaining after treatment. However, as MTT assay relies on the conversion of membrane-permeant colorless tetrazolium salt into colored formazan crystals by metabolically active mitochondria in viable cells, alterations in metabolic activities may not reflect the actual number of viable cells present. Common situations that can cause changes to mitochondrial functions include overconfluency and/or depletion of culture medium. However, since this method is inexpensive and allows quick screening of cell killing efficiency and effective drug dosages, MTT assay is still suitable for early rounds of investigational studies.

To evaluate the long-term drug effect and proliferation of the cells treated with various formulation, anchorage-dependent clonogenic assay was performed. This assay allows the assessment of irreversible cessation of cell growth that occurs after the removal of therapeutic agents from the cells [271]. The detailed methods for each assay are as follows.

2.11.1 Cytotoxicity study using MTT assay

Depending on the cancer cell lines used, the cells were seeded onto 96-well plates at a density of 1- 1.2 × 10^4 cells per well, and cultivated in 100 μl of growth medium. The plates were then returned to incubator for 24 hours to reach 70%-80% confluency before the administration of nanoparticle/lectin A-chain nanocomplexes. When the desired cell confluency was reached, the spent growth medium was removed from each well and replaced with 100 μl of the pre-prepared complex solution. After 4 hours of incubation with the complexes, the culture medium was replaced with fresh ones. The plates were

then returned to the incubator and maintained in 5% CO_2, at 37°C, for 2 days. Each condition was tested in eight replicates. After 2 days of incubation, the culture medium was removed, and 20 μl of MTT solution was added with 100 μl of fresh medium. The plates were then returned to the incubator and maintained in 5% CO_2, at 37°C, for a further 3 hours. The growth medium and excess MTT in each well were removed. DMSO (200 μl) was added to each well to dissolve the internalised purple formazan crystals. An aliquot of 100 μl was taken from each well and transferred to a new 96-well plate. The plates were then assayed at 550 nm and reference wavelength of 690 nm using a microplate reader (PowerWave X, Bio-tek Instruments, U.S.A.). The absorbance readings of the formazan crystals were taken to be those at 550 nm subtracted by those at 690 nm. The results were expressed as a percentage of the absorbance of the blank.

2.11.2 Anchorage-dependent (monolayer) clonogenicity assay

Monolayer colony assay was performed in drug-free media after exposure to treatment conditions. In a typical assay, cancer cells were first seeded onto 24-well plates at a density of 1-2.5 × 10^5 cells per well, and cultivated in 1ml of growth medium. The plates were then returned to incubators to allow cells to adhere overnight. The spent growth medium was removed from each well and replaced with 1ml of the pre-prepared nanoparticle/TRAIL complex solution. After 48 hour treatment, cells were trypsinized and re-seeded at a density of 1-3 × 10^3 cells per well in 6-well plates in drug and TRAIL-free medium. These cells were incubated at 37°C for 11 to 17 days for colony formation. Media were replaced with fresh (nanoparticle/ TRAIL-free) media every 3 to 4 days. At the end of each assay, cells were stained with 1 ml of 0.5% crystal violet for 1 hour and

washed three times with distilled water. Colonies were counted and imaged using a stereomicroscope (Nikon, U.S.A.) at 10×magnification, in five microscopic fields per well (one central, four peripheral). All assays was performed in triplicate and done independently at least twice.

2.12 Cell cycle analysis

Chemotherapeutic agents, such as Pac and Dox used in this study are known to cause either cell cycle arrest at low dosages or apoptosis at higher dosages. When administered together with therapeutic proteins, they typically exert synergism in apoptosis induction. To determine the effects of single versus combinational therapy, cell cycle analysis was performed. In this assay, cell cycle fractions were determined by propidium iodide nuclear staining. Briefly, cells were harvested, washed in PBS, fixed with 70% ethanol, and stained with 50 µg/ml propidium iodide in the presence of 200 µg/ml RNase and 0.1% Triton X-100 for 45 minutes at room temperature. Data were collected and analyzed with fluorescence-activated cell sorting analysis (FACS) on a Becton Dickinson FACSCalibur flow cytometer using BD FACSDiva™ software (BD Biosciences, U.S.A.).

2.13 Biodistribution of P(MDS-*co*-CES)nanoparticles

To evaluate the biodistribution of P(MDS-*co*-CES) nanoparticles, a near-infrared fluorophore DiR was loaded into the nanoparticles, likewise in Section 2.10.1. Balb/c mice, weighing 20–30 g were injected with 200 µL of a cell suspension containing 1×10^6 4T1 cells subcutaneously. After 2 weeks, when the tumor reached 4–6 mm in diameter, the mice were injected with nanoparticles *via* either tail vein or intratumoral

injection. Non-invasive fluorescent imaging at various times up to 3 days after injection was performed using the IVIS 100 (Caliper Life Sciences, U.S.A.). The mice were then sacrificed at 72 h after injection to estimate the tissue distribution of nanoparticles. All animal handling procedures were conducted in accordance with the approved protocol from the Institutional Animal Care and Use Committee (IACUC) at the Biological Resource Centre of Singapore.

2.14 *In vivo* anti-tumor efficacy studies of P(MDS-*co*-CES)nanoparticles

Female nude mice, weighing 20–25 g were injected with 200 μL of a cell suspension (1:1 with Matrigel) (BD Biosciences, U.S.A.) containing 3×10^6 BT474 cells subcutaneously. 1 month after inoculation (when the tumor volume was ~100 mm^3), the tumor-bearing mice were randomly divided into several groups (six mice per group). In the experiment 1, group 1 mice were used as nontreated control, group 2 and 3 mice were given intratumoral injection of Herceptin (0.5 mg/kg twice weekly) and blank nanoparticles/Herceptin complexes respectively, group 4 and group 5 mice were injected with Pac-loaded nanoparticles (8 mg/kg twice weekly) and Pac-loaded nanoparticles/Her complexes, all on the same schedule. All animal experiments were conducted in accordance with the approved protocol from the Institutional Animal Care and Use Committee (IACUC) at the Biological Resource Centre of Singapore. The tumor size was measured by calipers in two orthogonal diameters and the volume was calculated as $L \times W^2 / 2$, where L and W are the major and minor diameters respectively. Statistical significance in differences was evaluated by Newman-Keuls Method after analysis of variance (ANOVA). $P \leq 0.05$ was considered statistically significant. In addition, the

toxicities of the different formulations were evaluated by monitoring the survival rates over the course of treatment.

2.15 Distribution of nanocomplexes within tumors

To evaluate the biodistribution of nanocomplexes, FITC-loaded nanoparticles and Alexa Fluor 647-Herceptin was fabricated, likewise in Section 2.10. Female nude mice, bearing BT474 xenografts were used. The mice were injected with nanoparticles *via* intratumoral injection and sacrificed at 3 h post-injection to estimate the distribution of nanocomplexes within the tumors. Tissue sections were taken at 3 positions – close to skin, middle and distal to skin, and were imaged at 630× magnification using LSM 510 DUO confocal unit (Carl Zeiss, U.S.A.).

CHAPTER 3

INVESTIGATION OF CATIONIC POLYMERIC NANOPARTICLES AS VEHICLES FOR INTRACELLULAR DELIVERY OF FUNCTIONAL PROTEINS

3.1 Introduction

Over the past few decades, recombinant protein therapeutics has emerged as an important R&D sector for effective treatment against a broad range of human diseases, including cancer, autoimmune diseases and metabolic disorders [74, 272]. However, the main obstacle to achieving *in vivo* efficacy of protein therapy lies in the delivery to targeted diseased sites. The first part of my thesis focuses on the evaluation of using cationic core/shell nanoparticles as carriers for the delivery of therapeutic proteins. Lectin-A chain is selected as the model protein for investigation as it is unable to enter into cells without assistance from delivery carriers but can induce significant cytotoxicity when it gets delivered into the cytoplasm. Therefore, *in vitro* cytotoxicity resulting from Lectin-A chain delivery can be used as an indicator of the protein delivery efficiency of the nanoparticles.

Lectins from *Viscum album coloratum* (Korean Mistletoe) are heterodimeric, consisting of the A-chain with cytotoxic activity and the B-chain with sugar-binding property. They are glycoproteins with rRNA N-glycosidase activity, which inactivates the ribosome, leading to the disruption of the translocation steps of cellular translation during protein biosynthesis and thus cell death [148-150]. Apoptosis induction may also occur through the down-regulation of Bcl-2 and telomerase activity and up-regulation of Bax [273]. Reports have shown that this lectin is cytotoxic to Molt4 cells [149, 274], and is

able to bring about apoptotic death of U937 cells *via* activation of caspase cascades [275]. The counterpart of A-chain, lectin B, serves to mediate the delivery of cytotoxic lectin A-chain by binding to the cell surface and facilitating the subsequent internalization of the A-chain *via* endocytosis [149, 276]. The isolation of these biologically active lectins from plant extract and/or its production *via* recombinant methods encompasses difficulties such as extensive purification and scale-up problems.

A number of methods have been proposed to deliver biologically active proteins into cells, among which are physical methods such as microinjection [277, 278] and electroporation [129, 279]. These physical methods may be difficult to be applied *in vivo* [280]. The protein transduction domains (PTDs) have been conjugated to various active proteins for mediating the cellular uptake of the proteins [281, 282]. Another approach in rational drug delivery research that is becoming increasingly popular involves cationic lipids and polymers [283, 284]. For example, polyethylenimine (PEI)-conjugated proteins are able to enter cells based on ionic charge interactions [285]. The conjugation of proteins with PEI must be conducted under mild conditions to prevent proteins from denaturation. Moreover, cytotoxicity of PEI especially with high molecular weight also limits its *in vivo* applications. In this study, cationic core/shell nanoparticles were fabricated *via* a self-assemly process using biodegradable, cationic and amphiphilic copolymer poly{*N*-methyldietheneamine sebacate)-co-[(cholesteryl oxocarbonylamido ethyl) methyl bis(ethylene) ammonium bromide] sebacate} P(MDS-*co*-CES) [261]. Lectin A-chain interacted with the cationic nanoparticles to form nano-sized complexes, and the lectin A-chain binding ability of the nanoparticles was studied by native gel electrophoresis. The particle size and zeta potential of nanoparticle/lectin A-chain

complexes were measured and compared to those of lectin A-chain complexed with a commercially available cationic lipid-based protein carrier, BioPorter [277, 286]. The cellular uptake and distribution of nanoparticle or BioPorter/lectin A-chain complexes were studied in HeLa cervical cancer cell line by confocal microscopy. The cytotoxicity of lectin A-chain delivered by the nanoparticles was investigated against MDA-MB-231 human breast cancer cell line, HeLa cell line, HepG2 human hepatocellular liver carcinoma cell line and 4T1 mouse breast cancer cell line in comparison with BioPorter. Lectin A-chain delivered by the nanoparticles yielded significantly higher anti-cancer effectiveness when compared to BioPorter. These nano-sized particles may provide a platform for intracellular delivery of biologically active proteins.

3.2 Results and Discussion

3.2.1 Particle size and zeta potential of nanoparticle, BioPorter and their lectin A-chain complexes

As shown in Figure 3.1, the blank nanoparticles and BioPorter particles had an average size of ~ 140 nm and 334 nm with the zeta potential of ~ +28 mV and +22 mV respectively. The size of the nanoparticle/lectin A-chain nanocomplexes decreased but their zeta potential increased as increasing mass ratio of polymer to lectin A-chain (Figure 3.1A). At the mass ratio of 50 or above, their size and zeta potential remained relatively constant at approximately 150 nm and +30 mV respectively, indicating that at these mass ratios, lectin A-chain was well condensed and complexed with the nanoparticles. The small size and positive zeta potential of the complexes rendered them suitable for endocytotic cellular uptake. Complexes formed using commercially available cationic lipid-based carrier, BioPorter were also characterized with respect to their size

and zeta potential. In Figure 3.1B, BioPorter/lectin A-chain complexes were observed to have even larger sizes (>455 nm) and less positive zeta potential (< 20 mV) as compared to the blank P(MDS-*co*-CES) nanoparticles and their lectin A-chain nanocomplexes. Particles of such large sizes were likely to be aggregates. It is expected that the resulting complexes would enter cells less efficiently than the P(MDS-*co*-CES) nanoparticle/lectin A-chain nanocomplexes.

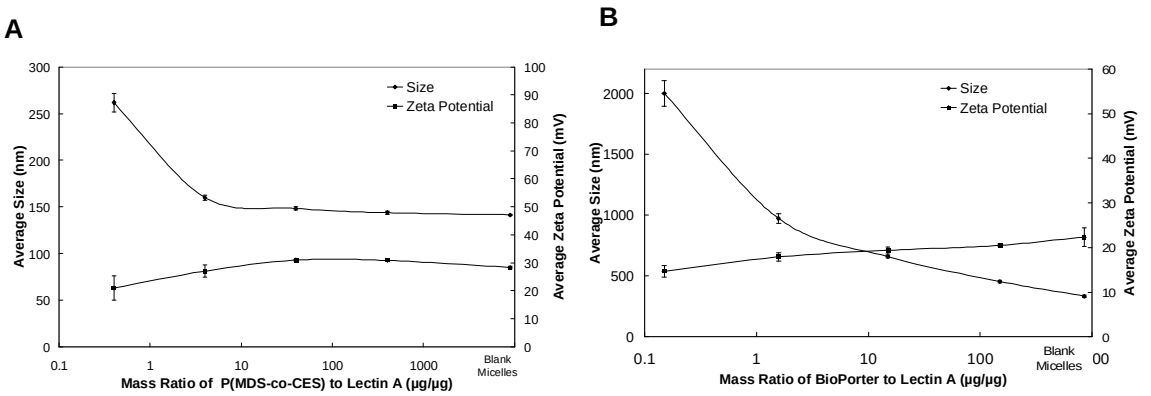

Figure 3.1 Size and zeta potential properties of nanoparticle/lectin A-chain nanocomplexes, and their lectin A-chain binding ability. (A) P(MDS-*co*-CES) nanoparticle/lectin A-chain nanocomplexes and (B) BioPorter/lectin A-chain complexes; Experiments were carried out in triplicates. The standard deviation is presented in error bars.

3.2.2 Lectin A-chain binding of nanoparticles

The protein binding ability of P(MDS-*co*-CES) nanoparticles was studied by native polyacrylamide gel electrophoresis (PAGE) at varying mass ratios. In native PAGE, the mobility of lectin A-chain will depend on both its charge and hydrodynamic size. The interaction between P(MDS-*co*-CES) nanoparticles and lectin A-chain will neutralize the protein's charge and decrease the intensity of protein gel bands. It was observed that electrophoretic mobility of lectin A-chain was increasingly reduced as more P(MDS-*co*-CES) was added for lectin A-chain binding, showing that stronger

nanoparticle/lectin A-chain interaction occurred at higher nanoparticle to protein mass ratios (Figure 3.2). In turn, this correlates to more effective lectin A-chain delivery and apoptosis induction with the use of more P(MDS-*co*-CES) to deliver the protein.

To ensure that native PAGE was carried out in an accurate manner, the process was repeated with lectin A-chain together with bovine serum albumin (BSA). When BSA was used as a model protein, a clear band was observed (data not shown). In contrast, a smear band pattern was observed for lectin A-chain possibly due to the hydrogen bonds formed between the glycoprotein and polyacrylamide gel matrix.

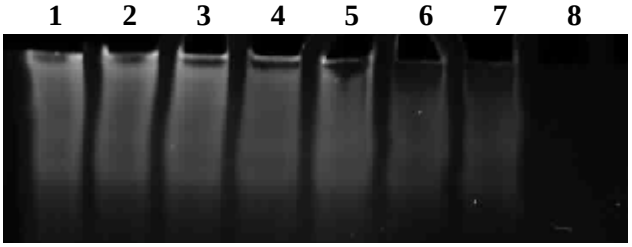

Figure 3.2 Native protein gel assay of P(MDS-*co*-CES) nanoparticle/lectin A nanocomplexes. Lanes 1 – lectin A-chain (8 μg) alone, Lane 8 – P(MDS-*co*-CES) (400 μg) alone, Lanes 2 to 7 – polymer to protein mass ratios: 0.1, 0.5, 1, 5, 10 and 50 respectively.

3.2.3 Intracellular uptake and distribution of nanoparticle/lectin A-chain complexes

To evaluate the efficiency of intracellular lectin A-chain delivery using P(MDS-*co*-CES) nanoparticles, the cellular distribution of protein and nanoparticles was investigated in HeLa cells using confocal microscopy in comparison with BioPorter. Cellular distribution of Alexa Fluor 647-labelled lectin A-chain shows up as red fluorescence in confocal images (Figure 3.3A-C). Low fluorescence present in Figure 3.3C illustrates that lectin A-chain alone was unable to enter cells efficiently without a transport carrier. Comparison between Figure 3.3F and I shows the presence of higher

amount of lectin A-chain in cells treated with P(MDS-*co*-CES) nanoparticle/lectin A-chain nanocomplexes as compared to those treated with BioPorter/lectin A-chain complexes. Lectin A-chain delivery and internalization was significantly more efficient when delivered using P(MDS-*co*-CES) nanoparticles as compared to BioPorter. This is most likely due to the presence of quaternary ammonium groups in P(MDS-*co*-CES) designed for protein binding and tertiary amine groups for endosomal buffering [287] and release of nanocomplexes. Fluorescein isothiocyanate (FITC) was loaded into the nanoparticles. Green and yellow regions in Figure 3.3J and K represent the localization of the nanoparticles, and the co-localization of lectin A-chain and P(MDS-*co*-CES) nanocomplexes in the cytoplasm after one hour of incubation, illustrating that the nanoparticles were able to bring lectin A-chain into the cells together as an associated complex. The nanoparticles, lectin A-chain and their nanocomplexes were also observed in the nuclei, suggesting that lectin A-chain is not only localized in the cytoplasm but also localized in the nucleus. This observation could provide one possible molecular basis of lectin A-chain in modulating telomerase activity in cancer cells as described earlier [276].

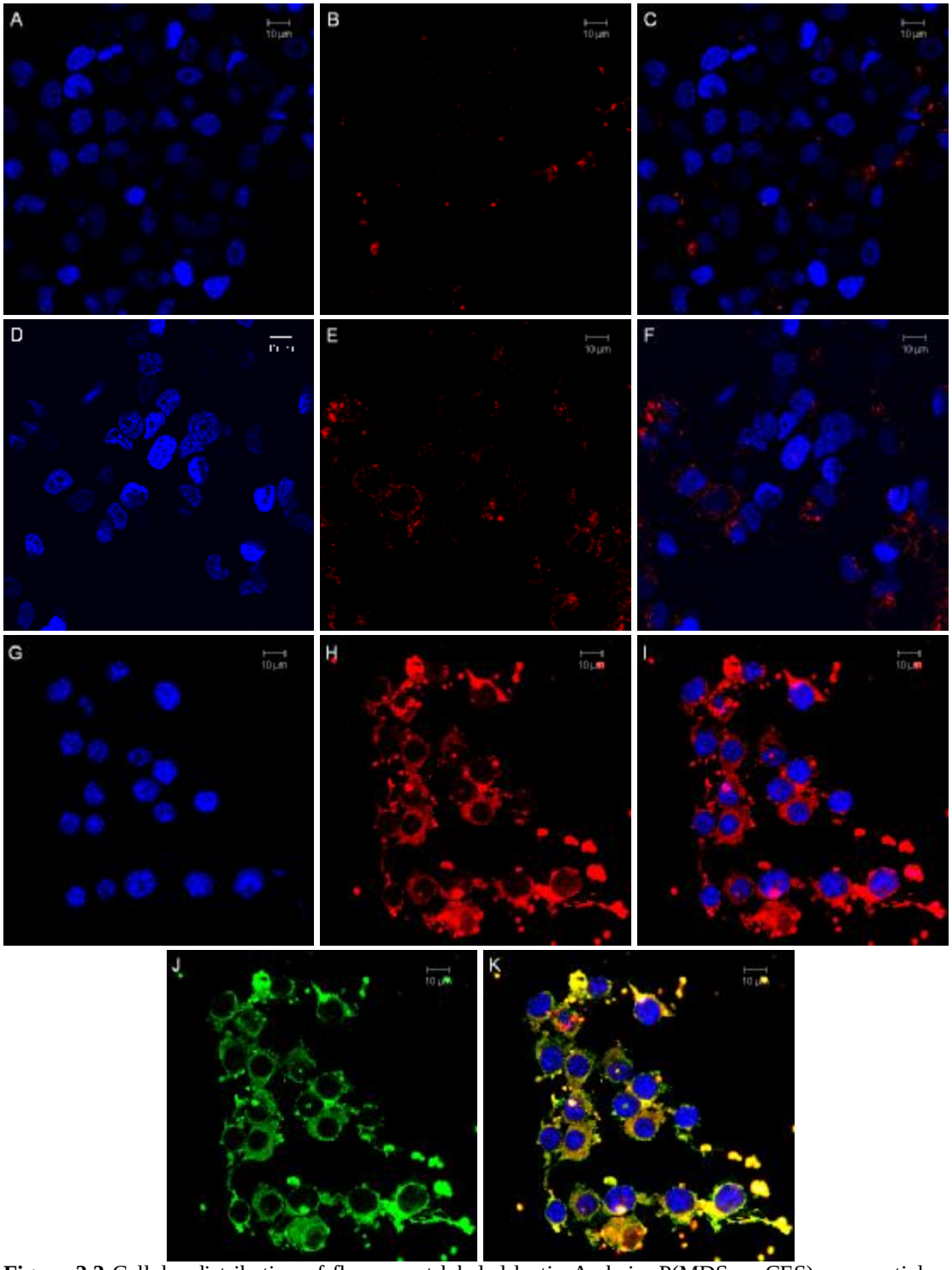

Figure 3.3 Cellular distribution of fluorescent-labeled lectin A-chain, P(MDS-*co*-CES) nanoparticles and their nanocomplexes in comparison with BioPorter/lectin A-chain complexes. Nuclei were stained blue with (A, D, G) DAPI, and cellular distribution of Alexa Fluor 647-lectin A-chain (B, E, H) and FITC-P(MDS-*co*-CES) nanoparticles (J) are shown as red and green fluorescence respectively. (A-C) Control experiments with Alexa Fluor 647-lectin A-chain (5 ppm) only, (D-F) Alexa Fluor 647-lectin A-chain (5 ppm) with BioPorter and (G-K) Alexa Fluor 647-lectin A-chain (5 ppm) with 50 ppm of P(MDS-*co*-CES) nanoparticles. Yellow regions in (K) represent the co-localization of lectin A-chain and P(MDS-*co*-CES) nanoparticles in cells.

3.2.4 Cytotoxicity and IC_{50} of lectin A-chain

Intracellular release of lectin A-chain from the nanocomplexes is essential for it to function as a biologically active protein. To determine whether lectin A-chain retains its cytotoxic property after cellular internalization, cytotoxicity tests were carried out in MDA-MB-231, HeLa, HepG2 and 4T1 cancer cells. Cell viability after treatment was determined *via* the 3-[4,5-Dimethylthiazol-2-yl]-2,5-diphenyl tetrazolium bromide (MTT) assay. For all cell lines tested, lectin A-chain alone did not exhibit significant cytotoxicity since the protein was unable to enter the cells and exert its cytotoxic properties without a transport carrier (Figure 3.4). This correlates with the significantly lower cellular internalization of lectin A-chain seen in confocal images (Figure 3.2A-C). At low P(MDS-*co*-CES) concentrations in the complexes, the cytotoxicity exhibited was insignificant, possibly due to insufficient binding between lectin A-chain and P(MDS-*co*-CES) nanoparticles (Figure 3.2). The size and zeta potential results also indicate that the nanoparticle/lectin A-chain nanocomplexes were too large for efficient cellular uptake at these concentrations (Figure 3.1A). Blank nanoparticles possessed non-selective cytotoxicity probably due to electrostatic interactions with negatively charged glycocalyx of cell surface [288]. To reduce the effects of the non-selective cytotoxicity, polymer concentration for complex preparation was optimized for each cell line, being 20, 50, 40 and 100 ppm for MDA-MB-231, HeLa, HepG2 and 4T1 respectively, at which cell viability was greater than 80%.

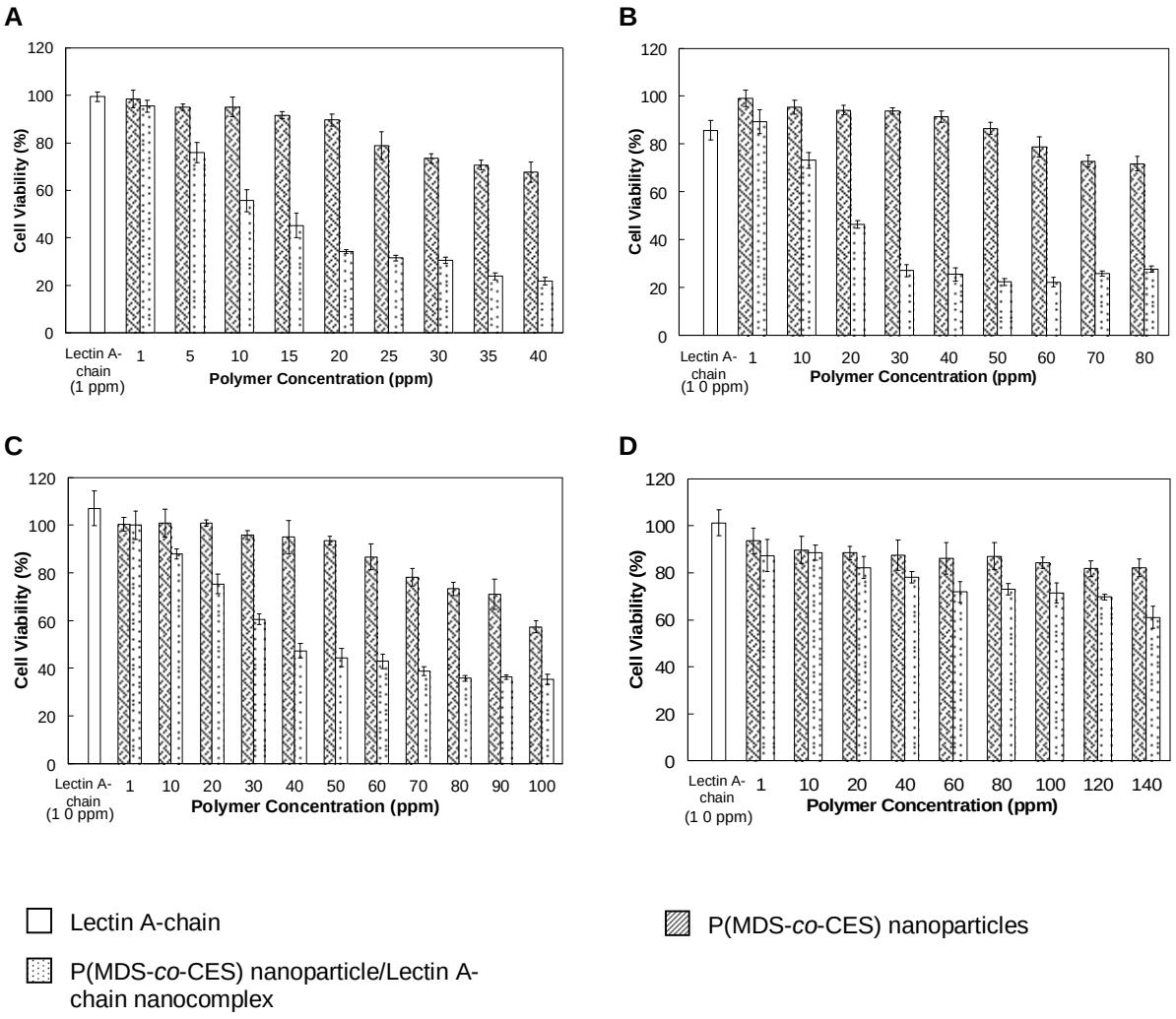

Figure 3.4 Viability of (A) MDA-MB-231, (B) HeLa, (C) HepG2 and (D) 4T1 cells after three days of incubation with nanoparticle/lectin A-chain nanocomplexes containing a fixed concentration of lectin A-chain and P(MDS-*co*-CES) of varying concentration. Lectin A-chain concentrations were fixed at 1, 10, 10 and 10 ppm for (A), (B), (C) and (D) respectively. Each condition was tested in eight replicates. The standard deviation is presented in error bars.

To determine the IC_{50} value of lectin A-chain, the viability of each cell line was tested at varying lectin A-chain concentrations and the optimized polymer concentration, which were 0.2, 0.5, 10 and 50 ppm for MDA-MB-231, HeLa, HepG2 and 4T1 cells respectively (Figure 3.5). Differences in IC_{50} between the various cell lines revealed their different degrees of sensitivity to the cytotoxicity of nanoparticle/lectin A-chain

nanocomplexes. MDA-MB-231 cells showed the least tolerance to the cytotoxic effects of the complexes, followed by HeLa, HepG2 and 4T1 cells.

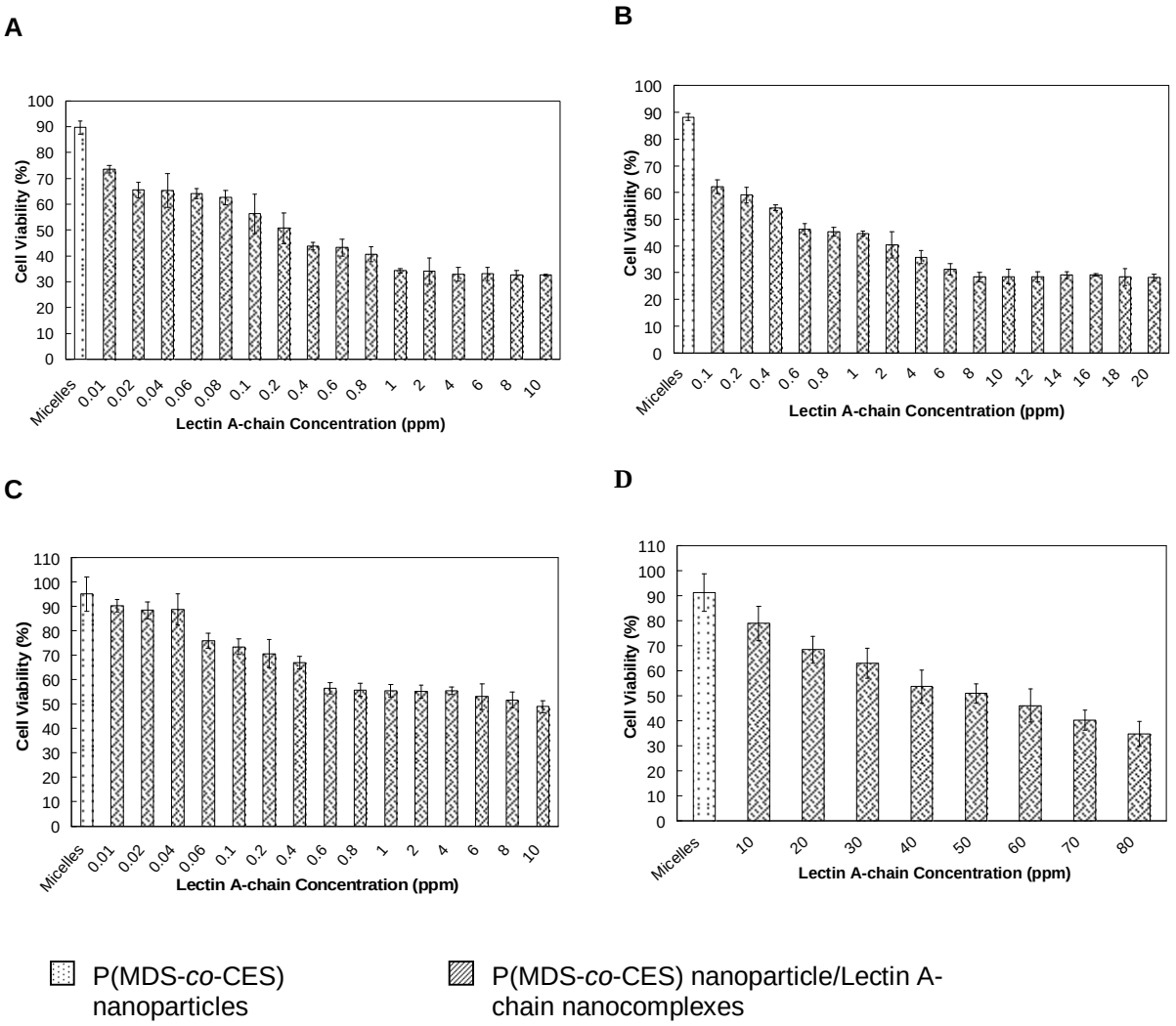

Figure 3.5 Viability of (A) MDA-MB-231, (B) HeLa, (C) HepG2 and (D) 4T1 cells after three days of incubation with nanoparticle/lectin A-chain nanocomplexes containing a varying concentration of lectin A-chain and a fixed concentration of P(MDS-*co*-CES). P(MDS-*co*-CES) concentrations were fixed at 20, 50, 40 and 100 ppm for (A), (B), (C) and (D) respectively. Each condition was tested in eight replicates. The standard deviation is presented in error bars.

The cytotoxicity of nanoparticle/lectin A-chain nanocomplexes was compared to that induced by BioPorter/lectin A-chain complexes (Figure 3.6). In all cell lines tested,

BioPorter mediated lower cytotoxic effects of lectin A-chain in the serum-containing cell culture medium than in the serum-free medium due to its instability in the presence of serum proteins. Comparing the two carriers, cytotoxicity exerted by lectin A-chain delivered *via* P(MDS-*co*-CES) nanoparticles in the serum-containing medium was significantly higher than that attained by BioPorter/lectin A-chain complexes. Under the same serum conditions, P(MDS-*co*-CES) nanoparticle/lectin A-chain resulted in 200 and 500 times lower IC_{50} of lectin A-chain in MDA-MB-231 and HeLa cells respectively. This may be due to greater cellular uptake, stability and endosomal buffering capacity of P(MDS-*co*-CES) nanoparticle/lectin A-chain nanocomplexes.

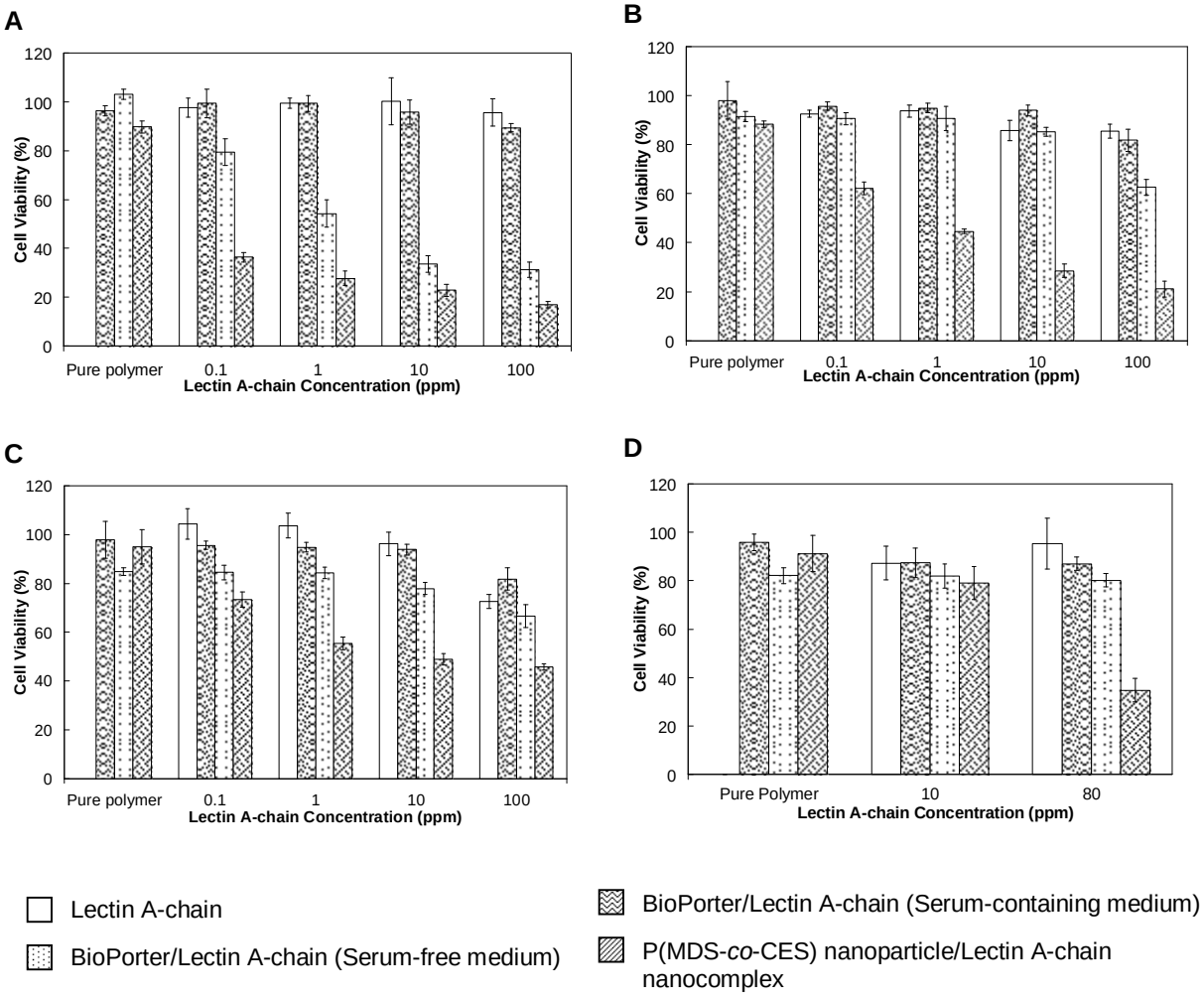

Figure 3.6 Comparison studies of P(MDS-*co*-CES) nanoparticles- and BioPorter-mediated lectin A-chain delivery to (A) MDA-MB-231, (B) HeLa, (C) HepG2 and (D) 4T1 cells. P(MDS-*co*-CES) concentrations were fixed at 20, 50, 40 and 100 ppm for (A), (B), (C) and (D) respectively in serum-containing medium. Each condition was tested in eight replicates. The standard deviation is presented in error bars.

3.3 Conclusion

In this chapter, the possibility of using cationic micelles fabricated from biodegradable, amphiphilic polymers intracellular delivery of proteins was investigated. The P(MDS-*co*-CES) micelles were able to bind to therapeutic glycoprotein, lectin A-chain, to form nanocomplexes that were small enough (~150nm) and positively-charge (+30 mV) for mediating cellular uptake. Intracellular release of the protein from the nanocomplexes and preservation of protein activity is shown from the cytotoxicity studies as protein is only functional when released into the cytoplasm. When compared to commercial delivery agent, BioPorter, the cytotoxicity of lectin A-chain delivered by P(MDS-*co*-CES) nanoparticles was significantly higher even in the serum-containing medium. Hence, these nano-sized particles show great potential to serve as an efficient carrier for intracellular delivery of biologically active proteins.

CHAPTER 4

INVESTIGATION OF CO-DELIVERY OF THERAPEUTIC PROTEIN AND ANTI-CANCER DRUG USING CATIONIC POLYMERIC NANOPARTICLES

4.1 Introduction

Combination therapy with two or more drugs in has been widely reported to show great improvements in cancer treatment efficacy and lower risk of multidrug resistance development. However, current treatment regimens are typically developed using free drugs without delivery carriers and may not be able to bring about the best possible therapeutic efficacy. One of the key aspects of my study is to investigate the possibility of using polymeric micelles as co-delivery vehicles for anti-cancer drugs and proteins for cancer therapy. For this part of my study, investigation was carried out on the delivery of another therapeutic protein of similar molecular weight, i.e. recombinant human tumor necrosis factor-related apoptosis-inducing ligand (TRAIL, MW: 20 kDa) and anti-cancer drugs simultaneously. The cooperative interaction of chemotherapeutic drug and TNF-related apoptosis inducing ligand (TRAIL) is utilized to achieve synergistic anti-cancer effects. TRAIL is an important tumor necrosis factor (TNF)-family protein [269, 289], and it can initiate apoptosis through binding with cell death receptors, TRAIL-R1 (DR4) and TRAIL-R2 (DR5). Briefly, in TRAIL-induced apoptosis, TRAIL first binds to death receptors present on cell surface. Following this, formation of the death-inducing signaling complex (DISC) occurs, which leads to a cascade of caspases activation. There are three additional receptors that act as ‘decoys’: TRAIL-R3 (DcR1), TRAIL-R4 (DcR2), and osteoprotegerin (OPG). These receptors can bind to TRAIL, but are unable

to provide apoptotic signaling [289, 290]. There are other members present in the TNF super family, such as TNFα and Fas ligand (FasL). These TNF family proteins can also initiate apoptosis in solid tumor but their clinical applications have mostly been hampered by hepatotoxicity [268]. On the contrary, native TRAIL is a particularly promising therapeutic member of the TNF-family as its cytotoxic activity is selective to the human tumor cells and does not exhibit considerable toxicity in normal cells. Studies on *in vitro* hepatotoxicity have been documented [291, 292] but they involved the use of different recombinant versions of TRAIL that contains exogenous tags such as polyhistidine (TRAIL-His) or FLAG (TRAIL-FLAG). Tagged versions of TRAIL are different from native TRAIL with regards to biochemical properties such as zinc content and trimeric structure, and such differences have been linked to the variations in their cellular and animal toxicities [293].

Till this date, preclinical models have demonstrated that TRAIL is able to retard the growth of human tumor xenografts in animals, and enhance chemotherapy and radiotherapy effects without evoking lethal toxicities [268, 269, 289, 294]. Previous reports attributed the ability of TRAIL to selectively kill tumor cells largely to the relatively higher expression of decoy receptors on normal cells as compared to tumor cells [293, 295] as these receptors compete for TRAIL binding with the death receptors. In addition, more recent findings have suggested that the relative expression levels between death and decoy receptors do not correlate with TRAIL sensitivity, but other factors involve in the death signaling pathway such as death inhibitors (e.g. cellular-FLICE inhibitory protein (c-FLIP), Fas-associated phosphatase-1 **(**FAP-1) and Inhibitor of Apoptosis (IAP) proteins) may be responsible for differential susceptibility to TRAIL-induced cell death [268, 290, 295, 296].

Although TRAIL is able to induce apoptosis in cancers of diverse origin, therapeutic efficacy of TRAIL may not be optimal when the protein is used as a monotherapy. However, when it is used in combination with conventional chemotherapeutic drugs such as cisplatin, paclitaxel, doxorubicin, 5-fluorouracil, and camptothecin, the effectiveness of combination treatment is greatly increased [297-303].

Sensitivity of cancer cells to combination treatment using TRAIL and chemotherapy vary widely and the underlying mechanism is still unclear. Some cancer cell lines are susceptible to concurrent treatment, while some cancer cells in preclinical studies involving Pac and TRAIL combination treatment require sequential treatment of cells with the chemotherapeutic drug followed by TRAIL [301, 303] as neither concurrent treatment with both agents nor reversal sequence of drug exposure was able to induce comparable levels of apoptosis. In such scenarios, despite the promise for therapeutic improvements, the downside to sequential treatment method is apparent. Some of the potential problems include inconveniences arising from multiple drug administrations and ambiguity in whether co-internalization of the therapeutic drug and TRAIL can occur in the same cells. Pac, which is a commonly used drug against solid tumors, is administered through a vehicle comprising of Cremophor EL (polyethoxylated castor oil) and ethanol due to its low aqueous solubility (less than 2 μg/mL). However, the use of such organic solvents is often related with hypersensitivity issues. Thus, the development of solvent-free formulations such as nanoparticles becomes extremely beneficial for patients with adverse response against such solvents [304-306].

Several types of polymeric micelles/nanoparticles have been developed and used for the delivery of drugs and macromolecular therapeutics such as DNA, siRNA and

proteins [261, 307-314]. Recently, our group reported cationic micelles self-assembled from a biodegradable amphiphilic copolymer P(MDS-*co*-CES) [261], and used them for efficient *in vitro* and *in vivo* co-delivery of drug and gene. In the earlier study, nanocomplexes were successfully fabricated by loading an anti-cancer glycoprotein, lectin A, onto the surface of the micelles. These cationic nanoparticles have been shown to significantly enhance the cellular uptake of the protein and its cytotoxicity against several types of cancer cell lines [313].

For this study, cationic P(MDS-*co*-CES) micelles were used to co-deliver Pac and TRAIL simultaneously. Pac was loaded into the core of the micelles by physical encapsulation and TRAIL was then absorbed onto the surface of these micelles. Simultaneous delivery of Pac and TRAIL using the nanoparticles would facilitate clinical usage by reducing the number of administrations and concurrently delivering both Pac and TRAIL to the same cells. In addition, the dosage of Pac and TRAIL can be conveniently manipulated by adjusting the initial loading level *via* this co-delivery approach. Physical properties of the nanoparticle/TRAIL and Pac-loaded nanoparticle/TRAIL complexes were characterized with regards to particle size, zeta potential, and drug loading as well as release capacities. Cellular localization and uptake of fluorescently-labeled TRAIL delivered using P(MDS-*co*-CES) nanoparticles was studied *via* confocal microscopy and flow cytometry. Co-delivery of Pac and TRAIL using the micellar nanoparticles was also demonstrated to exert significant enhanced cytotoxic and anti-proliferative effects in three human breast cancer cell lines with different TRAIL-sensitivity, namely, MCF7, T47D and MDA-MB-231.

4.2 Results and Discussion

4.2.1 Characterization of Pac-loaded nanoparticles and Pac-loaded nanoparticle/TRAIL complexes

Cationic Pac-loaded P(MDS-*co*-CES) nanoparticles have an average size of 181 nm and zeta potential of about 82 mV (Figure 5.1). Compared to blank P(MDS-*co*-CES) nanoparticles (84 nm), the physical entrapment of Pac in the hydrophobic core of micelles results in an increase in micellular volume. Formation of nanocomplexes between P(MDS-*co*-CES) nanoparticles and TRAIL shields some of the cationicity of the nanoparticles. We observe that as more TRAIL is added for complexation, there is a general increase in size and decrease in zeta potential of the complexes. From zeta potential measurements, TRAIL shows a weak positive charge in 20 mM sodium acetate/acetic acid buffer (pH 6.0) (4 mV). Hence, binding between TRAIL and nanoparticles would most likely be occurring through hydrogen bonding, hydrophobic interaction and van der Waals forces at different regions of TRAIL and P(MDS-*co*-CES). The overall positive charge of P(MDS-*co*-CES) nanoparticle/TRAIL complexes may improve their interaction with negatively-charged cell membranes and increase cellular uptake of the complexes [315, 316]. Moreover, the adsorption of TRAIL molecules on particle surface could also increase the probability of TRAIL molecules interacting with death/TRAIL receptors present on the cell surface.

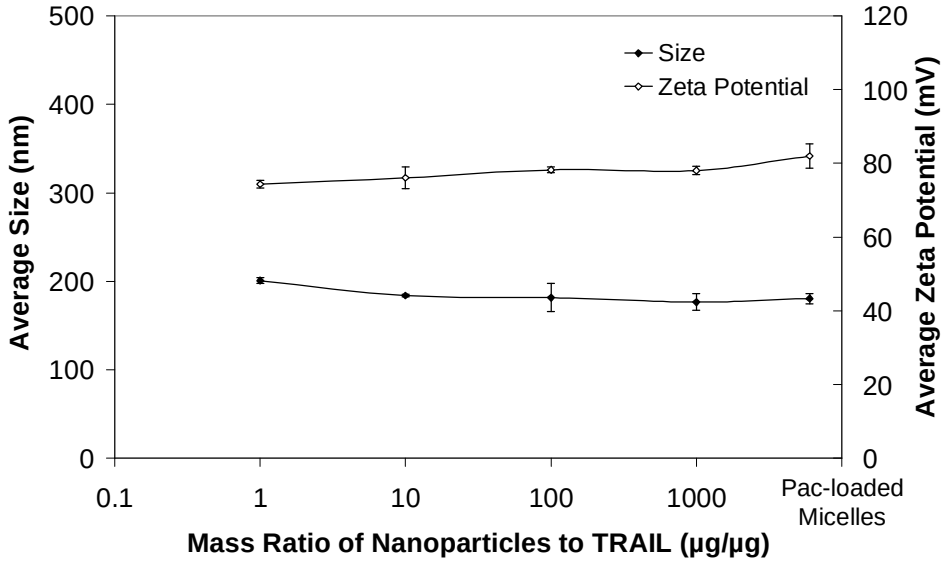

Figure 4.1 Size and zeta potential properties of Pac-loaded P(MDS-*co*-CES) nanoparticle/TRAIL complexes. Experiments were carried out in triplicates. The standard deviation is presented in error bars. Polymer concentration was fixed at 50 µg/mL. All condition was tested in triplicates.

4.2.2 Native protein gel shift assay on TRAIL binding efficiency of P(MDS-*co*-CES) nanoparticles

Increase in size and reduction in zeta potential of Pac-loaded nanoparticles after complexation with TRAIL (Section 4.2.1) illustrates that Pac-loaded nanoparticles are able to bind TRAIL and package the protein to form stable nanocomplexes. Native (non-denaturing) protein gel shift assay was performed to ensure that TRAIL remains in its native confirmation and is not denatured during the complexation process. From this assay, we are also able to compare the ability of P(MDS-*co*-CES) nanoparticles to bind TRAIL at different mass ratios. Pac-loaded nanoparticle/TRAIL complexes were prepared with different mass ratios of nanoparticles to TRAIL, and the resulting mixture was then applied to a native polyacrylamide gel. From Figure 4.2, we observe that with increasing nanoparticles to TRAIL mass ratio from 1 to 20 (Lanes 2 to 5), the electrophoretic mobility of TRAIL is also increasingly reduced. The complete retardation

of TRAIL mobility is achieved at mass ratio of 20. Distinct/non-smeared protein bands on the gel also indicate that TRAIL remains in their native confirmation after complexation with P(MDS-*co*-CES) micelles.

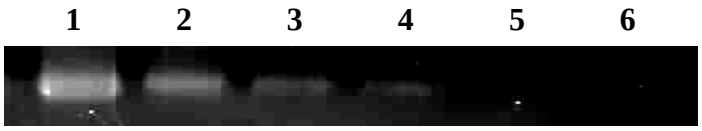

Figure 4.2 Native protein gel assay of Pac-loaded P(MDS-*co*-CES) nanoparticle/TRAIL complexes. Lane 1 – TRAIL (2 μg) alone, Lane 6 – Pac-loaded P(MDS-*co*-CES) nanoparticles (40 μg) alone, Lanes 2 to 5 – nanoparticle to protein mass ratios: 1, 5, 10 and 20 respectively.

4.2.3 Drug loading and *in vitro* release

Encapsulation efficiency and loading level of Pac in P(MDS-*co*-CES) micellar nanoparticles was determined to be 58.3 % and 14.7 % respectively. The release profile of Pac from P(MDS-co-CES) nanoparticles with or without TRAIL was monitored over 191 hours at 37^{o}C (Figure 5.3). Most of the drug molecules are released within the first 72 hours of incubation. After that, release of drug from the micelles tapers and eventually comes to a gradual stop (71.6% and 60.9%, in the absence and presence of TRAIL respectively). The release rate and extent of Pac release are slightly reduced by the presence of TRAIL on the surface of nanoparticles.

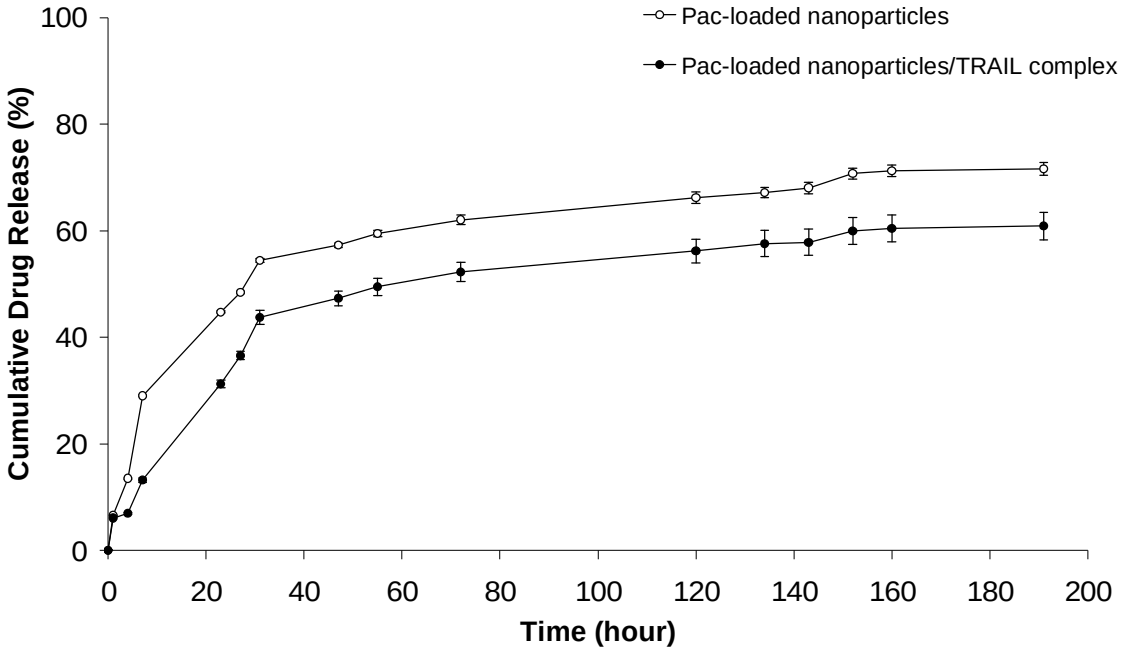

Figure 4.3 Release profiles of Pac from P(MDS-*co*-CES) micellar nanoparticles with and without TRAIL in PBS (pH 7.4) at 37°C. Each condition was tested in triplicates. The standard deviation is presented in error bars.

4.2.4 Cellular trafficking of P(MDS-*co*-CES) nanoparticle/TRAIL complexes

Cellular localization of double-labeled nanoparticle/TRAIL complexes was studied in all three cell lines, MCF7, T47D, MDA-MB-231 ***via*** confocal microscopy. In particular, cellular trafficking of the nanocomplexes was monitored in MDA-MB-231 over a 3 hour period. Nuclei were stained blue with DAPI, and cellular distribution of Alexa Fluor 555-TRAIL and FITC-loaded P(MDS-*co*-CES) nanoparticles are shown as red and green fluorescence respectively. From Figure 4.4, we see that at 5 minutes post-exposure, nanocomplexes form a thin fluorescent lining with small fluorescent clumps (see arrows) along the cell surface membrane. At 30 minutes post-exposure, clumps of fluorescence appear within cytoplasm. And at 1 hour post-exposure clumps of fluorescence become larger and increase in number. Strong co-localization of Alexa

Fluor 555-TRAIL and FITC-loaded P(MDS-*co*-CES) nanoparticles, represented by yellow regions, indicates that TRAIL is delivered to the cells with nanoparticles simultaneously. Some Alexa Fluor 555-TRAIL continues to be present on cell surface probably due to interaction of TRAIL (dissociated from the nanoparticles) with death/TRAIL receptors (see arrows). At 3 hour post-exposure, endocytosis of the nanocomplexes becomes more extensive and the reduction of co-localization (red and green fluorescence appear at different parts of the cells) demonstrates that TRAIL molecules have dissociated from the P(MDS-*co*-CES) nanoparticles.

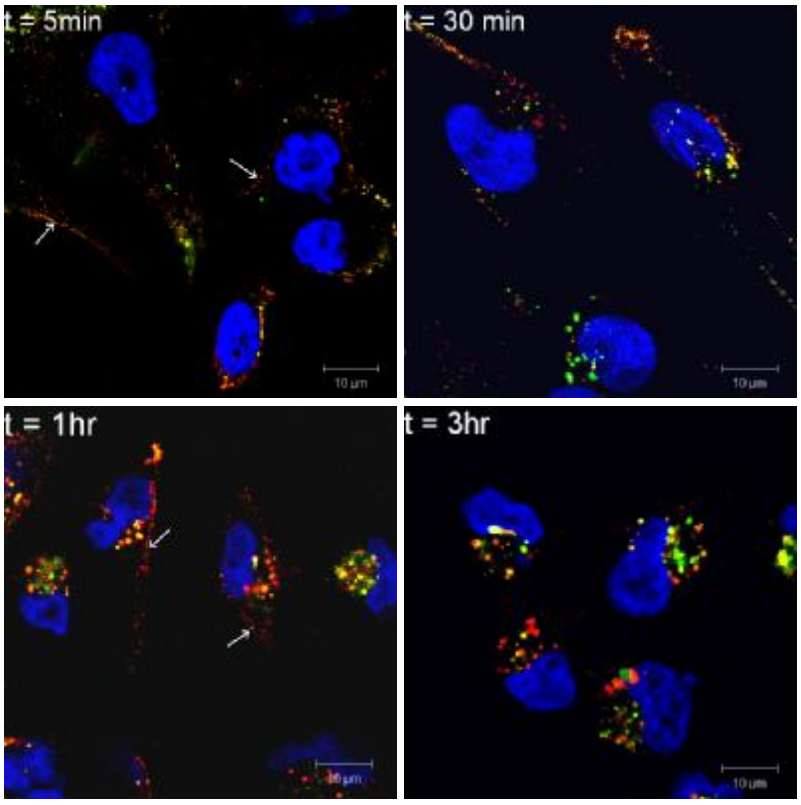

Figure 4.4 Cellular trafficking and distribution of doubled-labeled P(MDS-*co*-CES) nanoparticle/TRAIL nanocomplexes in MDA-MB-231 cells, at 5 minutes, 30 minutes, 1 hour and 3 hours respectively. Nuclei were stained blue with DAPI, and cellular distribution of Alexa Fluor 555-TRAIL and FITC-loaded P(MDS-*co*-CES) nanoparticle appears as red and green fluorescence respectively. 1 mg/l of Alexa Fluor 555-TRAIL and 25 mg/l of FITC-loaded P(MDS-*co*-CES) nanoparticles were used.

4.2.5 Cellular delivery of TRAIL using P(MDS-*co*-CES) nanoparticles

To provide a clearer understanding of the TRAIL delivery capabilities of P(MDS-*co*-CES), fluorescently-labeled TRAIL was delivered using P(MDS-*co*-CES) nanoparticles and the cells were analysed using flow cytometry. From Table 4.1, we observe that the amount of TRAIL delivered to all three cell lines using P(MDS-*co*-CES) nanoparticles is significantly higher compared to TRAIL alone. Furthermore, in all three cell lines, P(MDS-*co*-CES) nanoparticles carrying Pac resulted in higher cellular association and internalization of TRAIL as compared to blank nanoparticles. This indicates that the release of Pac from nanoparticles most likely enhances the expression of death receptors on the cells as previously reported, and this has resulted in greater interaction between TRAIL and the cells.

Table 4.1 Uptake of Alexa Fluor 555-TRAIL into MCF7, T47D and MDA-MB-231 cells at 3 hours after TRAIL delivery using the nanoparticles. The values shown represent the mean ± S.D. (n=3).

Treatments	MCF7	T47D	MDA-MB-231
Control	0.3 ± 0.0	0.2 ± 0.1	0.2 ± 0.1
TRAIL alone	1 ± 0.2	0.2 ± 0.1	1.3 ± 0.2
TRAIL with blank P(MDS-co-CES)	16.3 ± 0.5	8.5 ± 0.6	66.8 ± 2.0
TRAIL with Pac-loaded P(MDS-co-CES)	20.2 ± 0.8	14.2 ± 0.6	74.6 ± 2.6

4.2.6 Sensitization of cancer cells to TRAIL and synergistic cytotoxic effect achieved by simultaneous delivery of Pac and TRAIL using P(MDS-*co*-CES) nanoparticles

Enhancement of cytotoxicity and apoptosis induction of Pac-loaded nanoparticle/TRAIL complexes is studied. For TRAIL delivery, prior cytotoxicity experiments have been performed to optimize P(MDS-*co*-CES) concentrations to enable efficient binding with TRAIL without significant non-specific cytotoxicity from the

cationic polymer. Concentration of P(MDS-*co*-CES) is determined by allowing the maximum possible amount of polymer to be used while maintaining the cell viability to be greater than 85%, which is 10 mg/l.

TRAIL shows certain cytotoxicity towards MDA-MB-231 cells, and cell viability was ~ 80% after 48 hours of incubation with 10 nM TRAIL. However, it does not induce significant cytotoxicity against MCF7 and T47D (cell viability: ~92% for MCF7 and ~98% for T47D at 10 nM TRAIL). This is most likely to do with the different sensitivity of the cells to TRAIL as MDA-MB-231 has been known to be TRAIL-sensitive while MCF7 and T47D are semi-sensitive to TRAIL [301, 302]. Delivery of TRAIL using blank P(MDS-co-CES) nanoparticles resulted in an increase in cytotoxicity compared to TRAIL alone especially for semi-sensitive MCF7 and T47D (Table 4.2). This is probably due to the increase in TRAIL binding and internalization into the cells mediated by the delivery using the nanocarriers (Table 4.1).

From Figure 4.5A-C, when Pac is incorporated into the micelles and co-delivered with TRAIL simultaneously, cytotoxicity is significantly enhanced for all three cell lines tested. This event is observed especially after 48 hours of incubation and we attribute this to the gradual release of Pac within the cells and low initial amount of released Pac during the first 24 hours of incubation. Indeed, co-delivery of Pac sensitizes the cells to TRAIL. For example, in MDA-MB-231 cells, cell viability is significantly reduced by approximately one-fold after being treated with Pac-loaded nanoparticle/TRAIL complexes (TRAIL: 10 nM; Pac: 1.67 μM) to 42% as compared to 78% with TRAIL or 91% with Pac-loaded nanoparticles alone, demonstrating significant synergistic effect in suppressing cell survival. This finding is in agreement with that reported by Singh TR et

al [301]. They observed an enhancement of cytotoxic effect when these three cell lines were pretreated with free Pac followed by TRAIL. To confirm synergism, the dose-response interactions at the IC_{50} level were analyzed by the isobologram method. Synergy between the two compounds is shown as the drug combination dose falls to the left of the line of additivity. Synergistic cytotoxic effects from the co-delivery of Pac and TRAIL was seen in all three cell lines (representative isobologram in Figure 4.5D). With this increase in therapeutic efficacy, the amount of Pac and TRAIL needed to induce the same level of cytotoxicity is successfully reduced and this serves to reduce the adverse side effects of the therapeutic agent. Importantly, the co-delivery approach is more advantageous when compared to the free Pac and TRAIL formulation for future clinical applications as assessed in the introduction section.

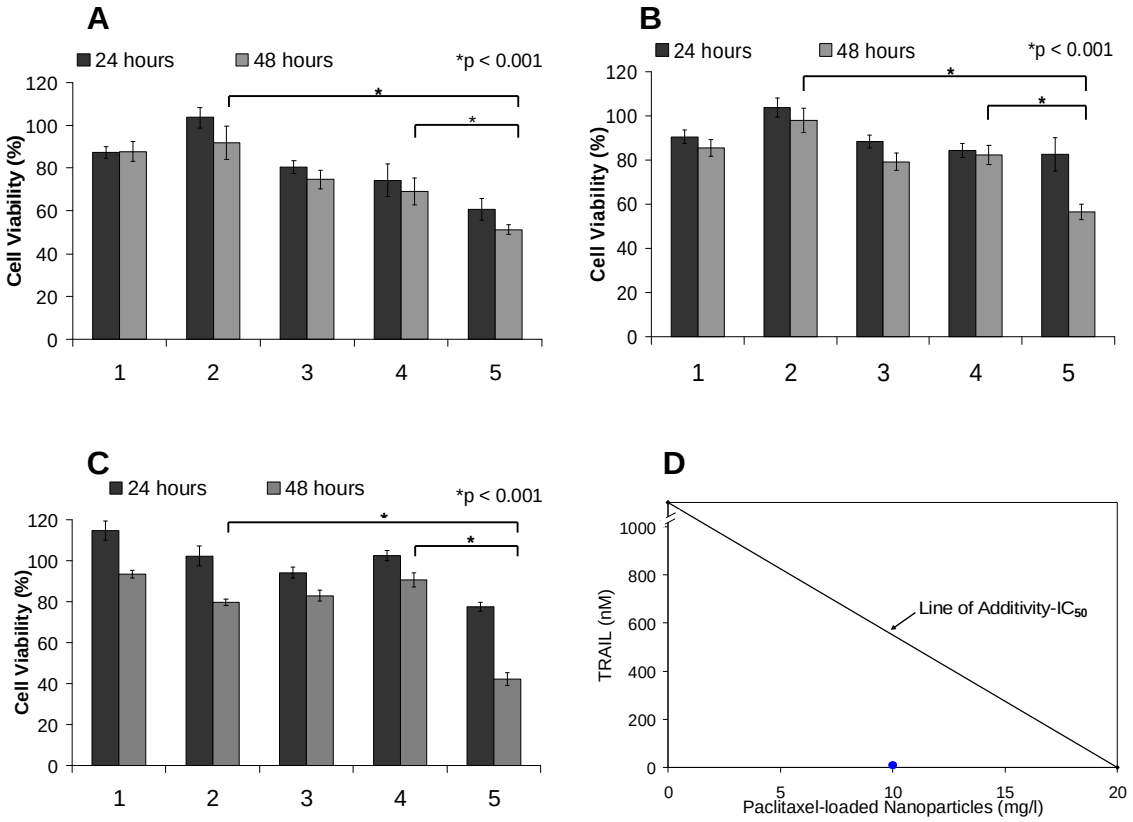

Figure 4.5 Viability of **(A)** MCF7, **(B)** T47D and **(C)** MDA-MB-231 cells after 24 and 48 hours incubation with (1) blank nanoparticles, (2) TRAIL, (3) blank nanoparticle/TRAIL complexes, (4) Pac-loaded nanoparticles (5) Pac-loaded nanoparticle/TRAIL complexes. Cell culture was performed in serum-containing medium. P(MDS-*co*-CES) (10 mg/l), TRAIL (10 nM) and Pac (1.67 µM) were used. The standard deviation is shown by error bars that represent the mean ± S.D. (n=4). Statistical significance in differences was evaluated by Newman–Keuls Multiple Comparison Test after analysis of variance (ANOVA). P≤0.05 was considered statistically significant. **(D)** An isobologram analysis representing the synergy between the two drugs at combination dose of Pac-loaded nanoparticles (10 mg/l) and TRAIL (10 nM) in MCF7.

Cytotoxicity was further compared against treatment with the combination of free Pac and TRAIL (Table 4.2). Unlike the co-delivery formulation using the nanoparticles, the free Pac + TRAIL formulation does not induce any enhancement in cytotoxicity in MCF7 and T47D cells as compared to free Pac. However, in MDA-MB-231 cells, significant enhancement of cytotoxicity is observed after treatment with the free Pac + TRAIL formulation and this is as efficient as the co-delivery of Pac and TRAIL using the

nanoparticles. Although the mechanisms are not clear, we hypothesize that this may be due to the different sensitivity of cells to TRAIL, i.e. MDA-MB-231: TRAIL-sensitive and MCF7/T47D: semi-sensitive [301, 302]. An important point to note is that, the co-delivery of Pac and TRAIL using the nanoparticles is significantly more effective in suppressing the survival of MCF7 and T47D (Table 4.2) compared to free Pac + TRAIL formulation.

Table 4.2 Viability (%) MCF7, T47D and MDA-MB-231 cells after 48 hours incubation with free Paclitaxel (Pac) and Pac-loaded nanoparticles in the presence or absence of TRAIL. P(MDS-*co*-CES) concentration was fixed at 10 mg/l for all cell lines. Cell culture was performed in serum-containing medium. The values shown represent the mean ± S.D. (n=3)

Treatments	MCF7	T47D	MDA-MB-231
Free Pac (1.7μM)	80.7 ± 3.0	77.2 ± 5.4	77.9 ± 3.1
TRAIL (10nM)	91.8 ± 7.8	98.0 ± 5.5	79.6 ± 1.5
Free Pac (1.7μM) + TRAIL (10nM)	76.2 ± 3.5	72.8 ± 4.5	41.2 ± 1.5
Blank P(MDS-co-CES) + TRAIL (10nM)	74.7 ± 4.3	79.1 ± 3.1	73.5 ± 2.7
Pac-loaded P(MDS-co-CES) (1.7μM)	69.1 ± 6.3	82.4 ± 4.3	90.7 ± 8.3
Pac-loaded P(MDS-co-CES) (1.7μM) + TRAIL (10nM)	51.3 ± 2.3	56.6 ± 3.5	42.1 ± 3.2

Apoptotic signaling by TRAIL involves prior binding to cell surface death receptors (DR4 and DR5), followed by DISC formation at cell membrane rafts. In this study, although nanoparticle/TRAIL complexes are internalized after binding to cells (Figure 4.4), proapoptotic functions of TRAIL and synergism with pac are not affected. This is in agreement with a study conducted by Kohlhaas and her co-workers [317], where cellular internalization of TRAIL occurs within a similar time (~ 30 min for complete endocytosis). In addition, although cellular entry of TRAIL has not been shown to be required for cell death signaling, it occurs naturally subsequent to receptor binding. Thus, cell death signaling occurs rapidly after the binding of nanoparticle/TRAIL

complexes to cells and internalization of the nanocomplexes therefore is not likely to interfere with mechanistic action of TRAIL.

4.2.7 Cell cycle and caspase-dependent apoptosis studies

Through cell cycle analysis (Figure 4.6) in MCF7 and MDA-MB-231 cells, we have demonstrated that pac, when released from micelles, is able to induce cell cycle arrest at the G2/M phase. After 48 hours of exposure to Pac-loaded nanoparticles, 67.3% and 42.5% of MCF7 and MDA-MB-231 cells were arrested in G2/M phase respectively. In view of this hallmark cellular response to Pac, it is clear that the drug released from micelles remains active in inducing mitotic arrest. However, although mitotic arrest is often associated with growth delay, it is often not representative of cell death occurrences [318]. With the co-delivery of Pac and TRAIL, we observe a significant increase in the subG1 population in both cell lines, which indicates an increase in apoptotic activity within the cells.

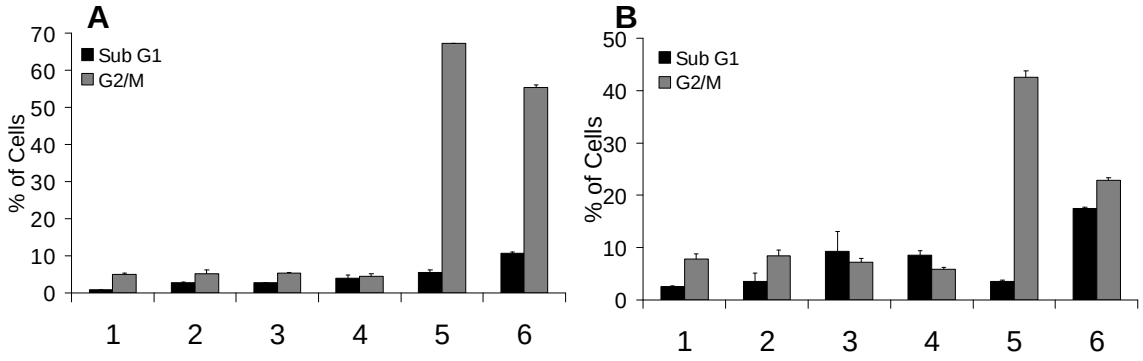

Figure 4.6 Cell cycle analysis of **(A)** MCF7 and **(B)** MDA-MB-231 cells after 48 hours incubation with (1) medium alone, (2) blank nanoparticles, (3) TRAIL, (4) blank nanoparticle/TRAIL complexes, (5) Pac-loaded nanoparticles (6) Pac-loaded nanoparticle/TRAIL complexes. P(MDS-*co*-CES), TRAIL and Pac concentrations were fixed at 10 mg/l, 10 nM and 1.67 µM for both cell lines. Cell culture was performed in serum-containing medium. The error bars represent the mean ± S.D. (n=3).

To determine if the observed apoptotic activity occurs through caspase-dependent mechanisms, all 3 cell lines were treated with nanoparticles, in the presence or absence of the pan-caspase inhibitor, ZVAD-FMK. Cell viability assay reveals that ZVAD-FMK inhibits cell death resulting from Pac-loaded nanoparticles, TRAIL and Pac-loaded nanoparticle/TRAIL complexes, indicating that the cytotoxic activity is based on caspase-dependent mechanisms (Figure 4.7).

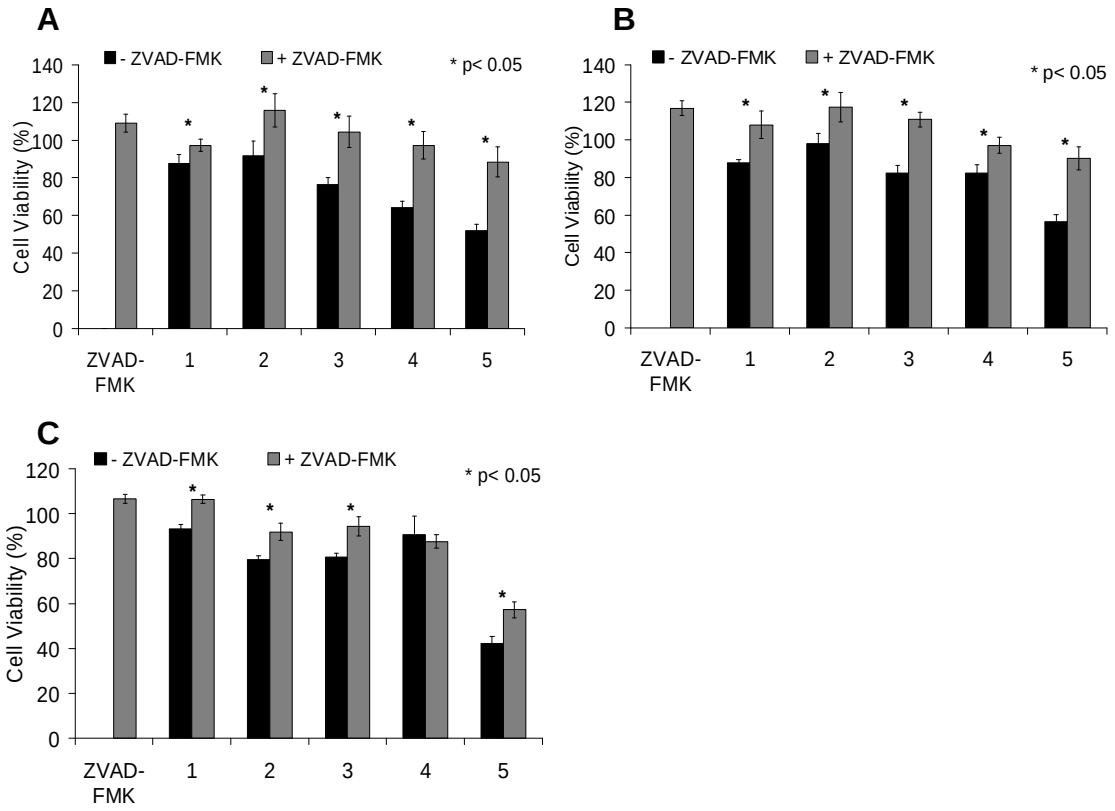

Figure 4.7 Viability of **(A)** MCF7, **(B)** T47D and **(C)** MDA-MB-231 cells in the presence or absence of pan-caspase inhibitor ZVAD-FMK (20μM) pretreatment prior to 48 hour incubation with (1) blank nanoparticles, (2) TRAIL, (3) nanoparticle/TRAIL complexes, (4) Pac-loaded nanoparticles and (5) Pac-loaded nanoparticle/TRAIL complexes. P(MDS-*co*-CES), TRAIL and Pac concentrations were fixed at 10 mg/l, 10 nM and 1.67 μM respectively, for all cell lines. Cell culture was performed in serum-containing medium. The error bars represent the mean ± S.D. (n=4). Statistical significance in differences was evaluated by Student's t-Test. $P \leq 0.05$ was considered statistically significant.

4.2.8 Specificity in cytotoxicity towards cancerous cells

To examine any nonspecific cytotoxicity which the nanocomplexes may have on non-cancerous cells, WI38 was chosen as a representative model cell line. Upon exposure to various treatments that have been applied to the cancer cells, we observe that there is no considerable cytotoxicity to WI38 (Figure 4.8), and the cell viability still exceeds 80% after 48 hours of exposure to Pac-loaded nanoparticle/TRAIL complexes while the viability of MDA-MB-231 human breast cancer cells is reduced to only 42% after the same treatment. This shows that the nanocomplexes have selective killing effects towards cancer cells and not the non-cancerous cells. Similarly, treatment of WI38 with the combination of free Pac and TRAIL does not induce significant cytotoxicity. This is most likely due to the insensitivity of WI38 towards TRAIL [296].

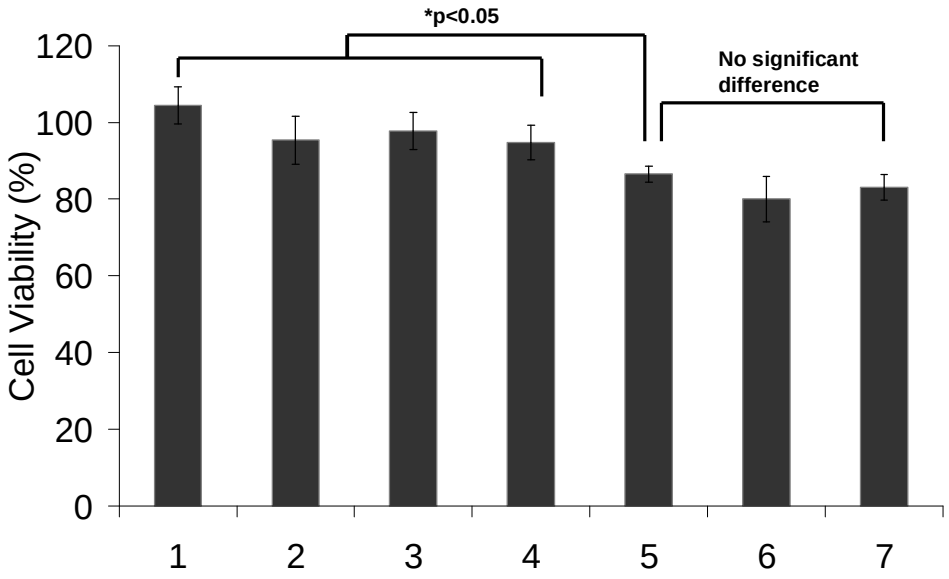

Figure 4.8 Viability of WI38 cells after 48 hours incubation with (1) blank nanoparticles, (2) TRAIL, (3) blank nanoparticle/TRAIL complexes, (4) Pac-loaded nanoparticles, (5) free Pac, (6) free Pac + TRAIL, (7) Pac-loaded nanoparticle/TRAIL complexes. Cell culture was performed in serum-containing medium. P(MDS-*co*-CES) (10 mg/l), TRAIL (10 nM) and Pac (1.67 µM) were used. The standard deviation is shown by error bars that represent the mean ± S.D. (n=3). Statistical significance in differences was evaluated by Newman–Keuls Multiple Comparison Test after analysis of variance (ANOVA). $P \leq 0.05$ was considered statistically significant.

4.2.9 Long-term survival and proliferation assays

From anchorage-dependent clonogenic assay (Figure 4.9A and B), we are able to determine the long-term drug effect and proliferation of the cells treated with various formulations. Pre-exposure of MCF7 and MDA-MB-231 cells to Pac-loaded nanoparticles or Pac-loaded nanoparticle/TRAIL complexes significantly impair subsequent survival and clonogenicity, and cell death continues even after the drugs are removed. In particular, most of the cells treated with the co-delivery system are mitotically arrested or enter into senescence [271]. With prolonged culture, these senescent cells eventually die, leaving very few cells capable of anchorage and survival. In view that Pac-loaded nanoparticle/TRAIL complexes result in significantly higher cytototoxicity within a short culture period (48 hours) and higher impediment to long-term proliferation as compared to TRAIL and Pac-loaded nanoparticles, we have established that this co-delivery system displays excellent effectiveness in inducing rapid cell death and deterring cellular regrowth.

A

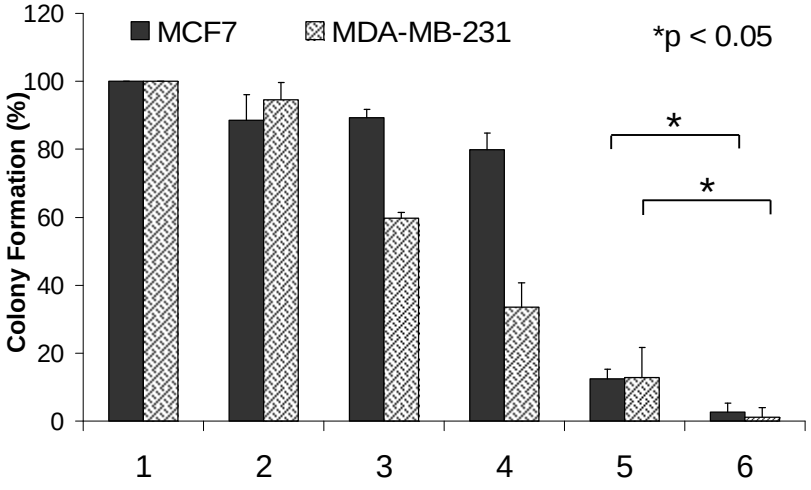

B

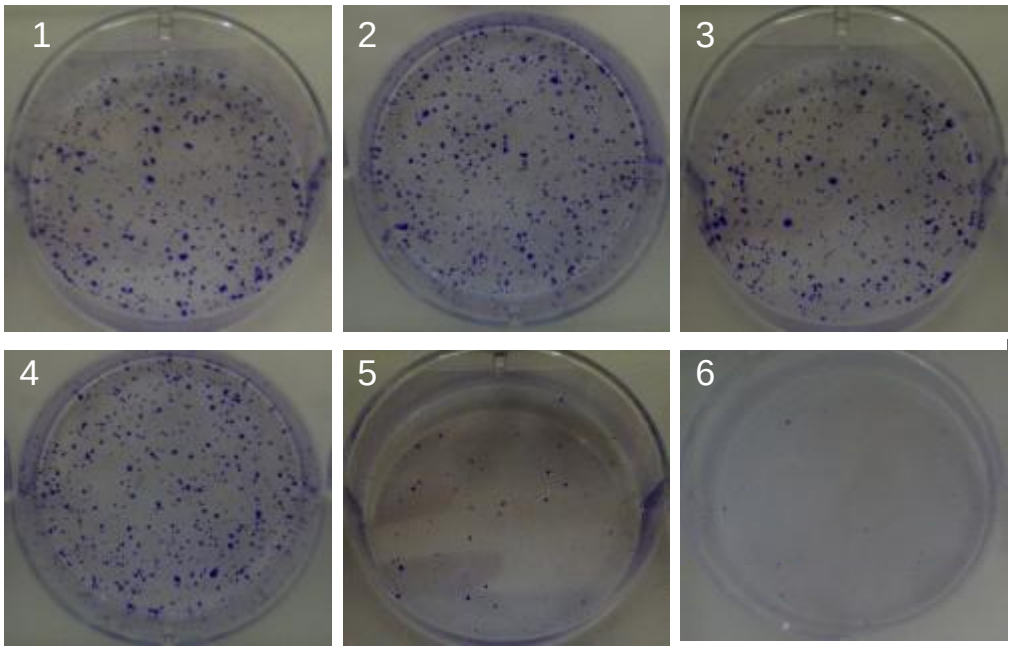

Figure 4.9 (A) Colony formation at Day 17 and 11 in MCF7 and MDA-MB-231 cell lines respectively subsequent to 48 hours treatment with (1) control, (2) blank nanoparticles, (3) TRAIL, (4) blank nanoparticle/TRAIL complexes (5) Pac-loaded nanoparticles (6) Pac-loaded nanoparticle/TRAIL complexes. Colonies were stained with 0.5% w/v crystal violet. Cell culture was performed in serum-containing medium. P(MDS-*co*-CES) (10 mg/l), TRAIL (10 nM) and Pac (1.67 μM) were used. The error bars represent the mean ± S.D. (n=3). Statistical significance in differences was evaluated by Newman–Keuls Multiple Comparison Test after analysis of variance (ANOVA). $P \leq 0.05$ was considered statistically significant. **(B)** Images of MCF7 colony taken at Day 17 subsequent to 48 hours treatment with **(1)** control, **(2)** blank nanoparticles, **(3)** TRAIL, **(4)** nanoparticle/TRAIL complexes, **(5)** Pac-loaded nanoparticles and **(6)** Pac-loaded nanoparticle/TRAIL complexes. P(MDS-*co*-CES), TRAIL and Pac concentrations were fixed at 10 mg/l, 10 nM and 1.67 μM respectively. Colonies were stained with 0.5% w/v crystal violet.

4.3 Conclusion

In this study, cationic micellar nanoparticles self-assembled from a biodegradable amphiphilic copolymer P(MDS-*co*-CES) are used to deliver human tumor necrosis factor-related apoptosis-inducing ligand (TRAIL) and pac simultaneously. The co-delivery of Pac sensitizes human breast cancer cells to TRAIL and achieves synergistic anti-cancer activities. Polyplexes formed between Pac-loaded nanoparticles and TRAIL

are stable with size at ~180 nm and a zeta potential at ~75 mV. P(MDS-*co*-CES) nanoparticles function effectively as a carrier for delivery of TRAIL to cells. Anticancer effects and apoptotic pathway mechanisms of this drug-and-protein co-delivery system are investigated in various human breast cancer cell lines with different TRAIL-sensitivity. The co-delivery of Pac and TRAIL using P(MDS-*co*-CES) nanoparticles induces cell death and deters long-term proliferation of the cells with limited toxicity in non-cancerous cells. Another notable advantage is the synergistic anticancer effects offered by the simultaneous delivery of Pac and TRAIL in nanoparticle system as compared to free drug and protein administration. Thereby, we establish that this co-delivery system represents a comprehensive and effectual approach towards combinational cancer therapy.

CHAPTER 5

SYNERGISTIC ANTI-CANCER EFFECTS IN TRAIL-RESISTANT CANCER CELLS BY THE CO-DELIVERY OF TRAIL AND DOXORUBICN USING CATIONIC POLYMERIC NANOPARTICLES

5.1 Introduction

Colorectal cancer is the third most common cause of cancer-related death throughout the world [57] and for many years, it has served as a prototypic model for research on the role of epigenetic mutations in tumorigenesis [319, 320]. Interventional approaches of the disease are often met with obstacles such as either intrinsic resistance to chemotherapeutic drugs, or the acquirement of drug resistance in those who responded positively during the initial phase of treatment. Like most other human cancers, the development of drug resistance poses a major concern for the eventual failure of chemotherapy. In recent times, most of the cancer treatment approaches involve the use of multiple therapeutic agents as the use of single agent in cancer chemotherapy is largely limited by dose-dependent toxicity and development of drug resistance after repeated administrations. To formulate potent drug combinations, it is therefore important to identify and deliver therapeutic molecules that can overcome cellular resistance mechanisms.

Proapoptotic proteins belonging to the tumor necrosis factor (TNF) family of death ligands, including TNF, Fas ligand (FasL) and TNF related apoptosis-inducing ligand (TRAIL) [321, 322] can be used to overcome resistance to conventional chemotherapeutic drugs. In addition, unlike many conventional anti-cancer agents,

TRAIL can induce apoptosis independent of the p53 tumor suppressor gene status of cancer cells, which is mutated in >50% of human cancers [323].

However, similar to many other chemotherapeutics, resistance to the treatment can eventually develop with repeated administrations of TRAIL. Many studies have shown that the development of resistance to TRAIL may be the result of changes in the expression levels of the various protein factors involved in the apoptotic signaling [324, 325]. As a result, the use of TRAIL as a monotherapy may be futile as an ultimate cure for these cancers. Various attempts have been made to treat patients with TRAIL in combination with small molecular drugs such as doxorubicin, 5-fluorouracil and tunicamycin with reported success in overcoming TRAIL-resistance and enhancing anti-cancer effects [326-330]. In clinics, studies have been performed by sequential treatment with drugs followed by TRAIL or therapeutic antibodies against TRAIL receptors [331, 332]. Such settings usually give rise to several drawbacks. Some of the foreseeable difficulties include patients' compliance and cost incurred from multiple drug administrations. Therapeutic efficacy may also be compromised as a result of uncertainties and inadequacies of co-internalization of the therapeutic drugs and TRAIL into the same cells.

In the previous chapter, Pac and TRAIL were co-delivered using cationic micelles self-assembled from P(MDS-*co*-CES) for investigation of anti-cancer effects in non-drug resistance human breast cancer cells. For this study, the potential of using these drug delivery systems as a solution to tackle the problem drug-resistance is investigated. These micelles are used to deliver another anti-cancer drug, doxorubicin (Dox) and TRAIL simultaneously into colorectal carcinoma SW480 cells with TRAIL-resistance. The

SW480 cell line contains mutations in the p53 gene [323, 333] and is therefore, an excellent model to demonstrate the therapeutic efficacy of co-delivery system. Dox was physically encapsulated into the micelles and TRAIL was then absorbed onto the surface of these cationic micelles. Physical characterization of the nanoparticle/TRAIL and Dox-loaded nanoparticle/TRAIL complexes was performed with respect to particle size, zeta potential, and drug loading as well as release properties. To prove that the cellular uptake of Dox-loaded P(MDS-*co*-CES) nanoparticle/TRAIL complexes occurs through specific interaction between the death receptors and TRAIL present on the nanoparticle surface, receptor-blocking studies were performed in SW480 cells using confocal microscopy studies. In addition, the cytotoxic selectivity of Dox-loaded nanoparticle/TRAIL nanocomplexes towards cancer cells (i.e. SW480) was studied in comparison with a non cancer cell line (i.e. WI38, a human lung fibroblast cell line). Moreover, the cytotoxic and anti-proliferative effects of co-delivery of Dox and TRAIL using the micellar nanoparticles against wild type and TRAIL-resistant SW480 cells were evaluated in comparison with free TRAIL, micelle/TRAIL complexes and Dox-loaded micelles. The results demonstrated that the co-delivery system can synergistically enhance cytotoxic and anti-proliferative effects in both wild type and TRAIL-resistant SW480 cells. Therefore, the nanocomplexes containing Dox and TRAIL are a promising therapeutic formulation that would facilitate clinical applications by delivering both Dox and TRAIL to the same cells and reducing the number of drug administrations. Synergistic cytotoxic effects exerted on TRAIL-resistant cancer cells also reveal the potential of using nanocomplexes as a solution towards drug-resistance in cancers.

5.2 Results and Discussion

5.2.1 Size and zeta potential of nanocomplexes

From Figure 5.1, cationic Dox-loaded P(MDS-*co*-CES) nanoparticles fabricated *via* the dialysis process had an average size of 223 nm and zeta potential of 73 mV. Physical encapsulation of Dox in the micelles resulted in an increase in micellar volume as compared to blank P(MDS-*co*-CES) nanoparticles (194nm). Formation of nanocomplexes between the nanoparticles and TRAIL resulted in slight changes in size (~ 230 nm) and zeta potential (~ 70 mV). In the sodium acetate/acetic acid buffer (pH 6.0) that was used for complexation, TRAIL is slightly positively charged with a zeta potential of 4 mV. Thereby, the association between TRAIL and nanoparticles would most likely be formed through hydrophobic interaction, hydrogen bonding and van der Waals forces. Cationicity of P(MDS-*co*-CES) nanoparticle/TRAIL nanocomplexes is desirable for interacting with cell surface membrane and cellular uptake of the complexes. Dense assembly of TRAIL molecules on the nanoparticle surfaces may also increase the binding between TRAIL and death/TRAIL receptors expressed on cell surface.

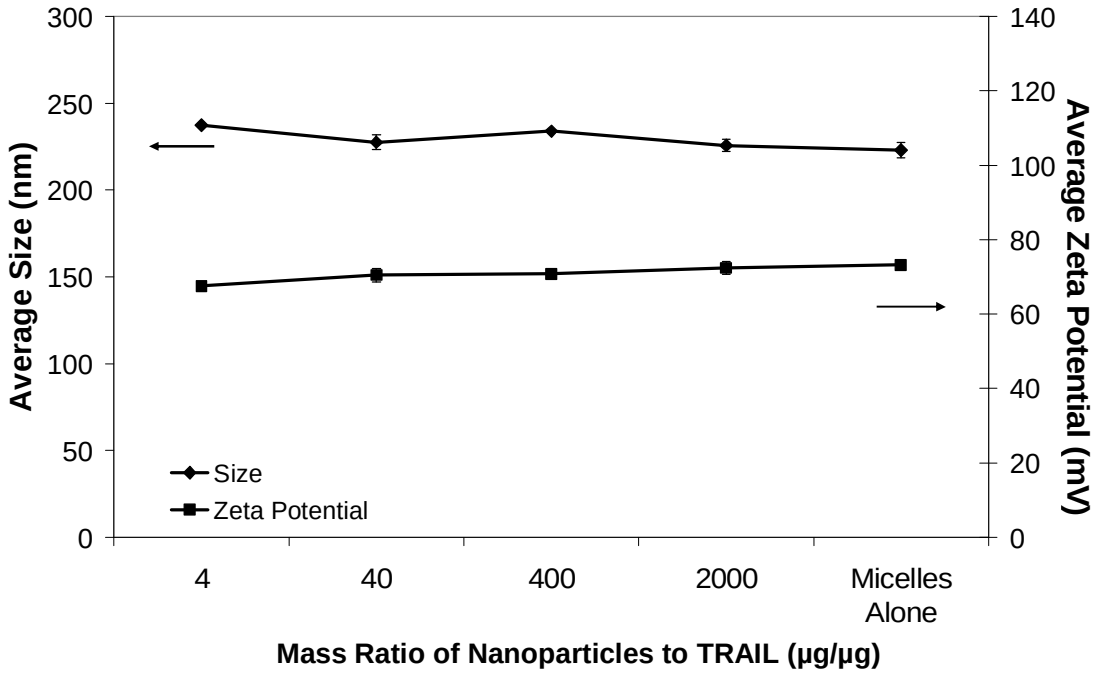

Figure 5.1 Size and zeta potential properties of doxorubicin-loaded P(MDS-*co*-CES) nanoparticle/TRAIL complexes. Experiments were carried out in triplicates. The standard deviation is presented in error bars. Polymer concentration was fixed at 50 µg/mL. All condition was tested in triplicates.

5.2.2 Native protein gel mobility shift assay on Dox-loaded P(MDS-*co*-CES)/TRAIL nanocomplexes

Dox-loaded nanoparticle/TRAIL complexes were first prepared at different mass ratios of nanoparticles to TRAIL, and the resulting mixture was then run on a native polyacrylamide gel. From the changes in protein mobility during the gel electrophoresis process, it is possible to monitor the changes in the binding ability of P(MDS-*co*-CES) nanoparticles to TRAIL at different mass ratios. From Figure 5.2, we observe that increasing the nanoparticles to TRAIL mass ratio from 1 to 20 (Lanes 2 to 5) resulted in a decrease in the electrophoretic mobility of TRAIL. Complete retardation of TRAIL mobility occured at mass ratio of 10. Distinct protein bands on the gel indicate that

TRAIL remained in their native confirmation without degradation after complexation with P(MDS-*co*-CES) nanoparticles.

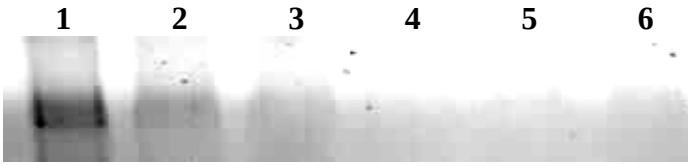

Figure 5.2 Native protein gel assay of Dox-loaded P(MDS-*co*-CES) nanoparticle/TRAIL complexes. Lane 1 – TRAIL (2 μg) alone, Lane 6 – Dox-loaded P(MDS-*co*-CES) nanoparticles (40 μg) alone, Lanes 2 to 5 – nanoparticle to protein mass ratios: 1, 5, 10 and 20 respectively.

5.2.3 Drug loading and *in vitro* release

The loading level of Dox in P(MDS-*co*-CES) micellar nanoparticles is defined as the ratio of the amount of encapsulated drug to the total mass of the micellar product and was determined to be 8.6 ± 2.4%. The *in vitro* release of Dox from P(MDS-co-CES) nanoparticles in the presence or absence of TRAIL was studied for 500 hours at 37^{o}C in two different buffered solutions - PBS (pH 7.4) or 20 mM sodium acetate/acetic acid buffer (pH 5.6) solution. As shown in Figure 5.3, in both buffers, typical two-phase-release profiles are observed, by which, the drug was released at a relatively rapid rate in the initial phase followed by a slow and sustained release over a prolonged period of time. Under both conditions, there was no significant difference in the cumulative amount of Dox released in both the absence and presence of TRAIL. Comparing the drug release profiles at the two pHs shows that the release of Dox from micelles at pH 5.6 was significantly faster than that at pH 7.4 with close to 40% higher amount of Dox released. This is in consistence with the faster release of DOX in acidic conditions as observed by Kataoka and his coworkers [334]. The increase in release rate at the lower pH was likely due to the protonation of the amino group of Dox, which led to the increase in aqueous

solubility of the drug. Micellar nanoparticles are usually internalized by the cells *via* endocytosis [335]. Hence, pH-dependent release would enable preferential release of Dox from the endosome of tumor cells due to the acidic environment in the endosome (pH 5-6.5).[336]

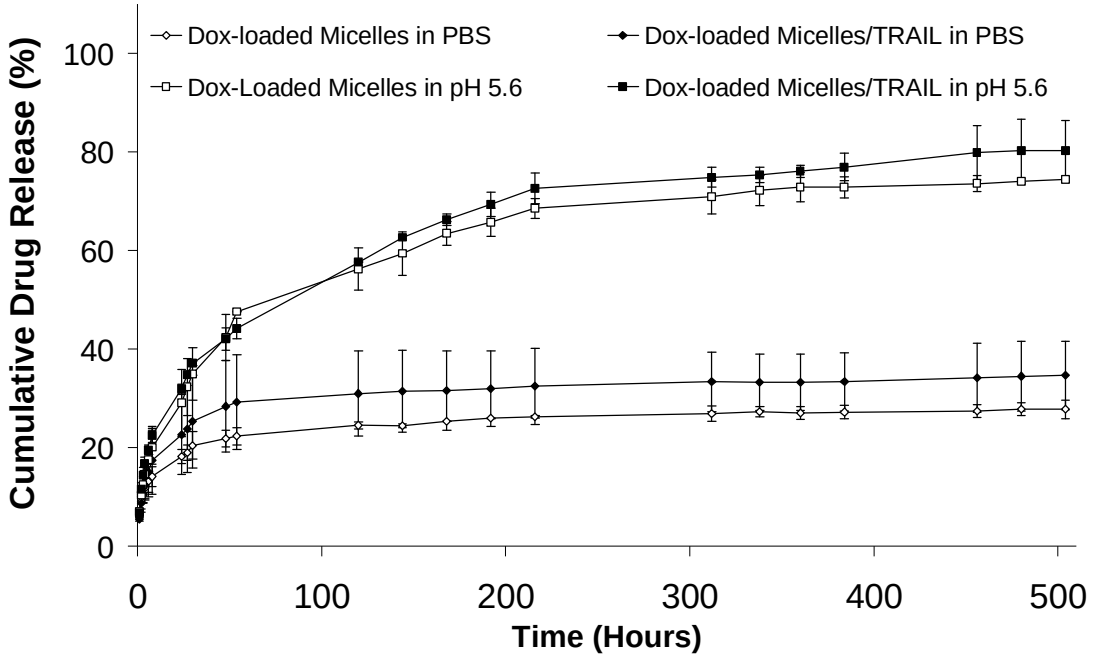

Figure 5.3 Release profiles of Dox from P(MDS-*co*-CES) micellar nanoparticles in the presence and absence of TRAIL in PBS (pH 7.4) and acetate buffer (pH 5.6) at 37°C. Each condition was tested in triplicates. The standard deviation is presented in error bars.

5.2.4 Death receptor-mediated endocytosis of the TRAIL nanocomplexes

Confocal microscopy studies were performed to visualize the cellular localization of fluorescent-labeled Dox-loaded nanoparticle/TRAIL nanocomplexes in SW480 cells over a 4 hour period (Figure 5.4A). Nuclei were stained blue with DAPI, and cellular distribution of Alexa Fluor 647-TRAIL and Dox-loaded P(MDS-*co*-CES) nanoparticles are shown as green and red fluorescence respectively. At 1 hour post-exposure to the TRAIL nanocomplexes, clumps of fluorescence appeared in the cytoplasm and strong co-

localization of Alexa Fluor 647-TRAIL and Dox-loaded P(MDS-*co*-CES) nanoparticles, represented by yellow regions, were observed. This shows that both TRAIL and Dox were delivered to the cells with nanoparticles in a concurrent manner. At 4 hours post-exposure, co-localization of TRAIL and Dox-loaded nanoparticles was reduced as Dox was released from the micelles and moved into the nucleus. However, concurrent uptake of TRAIL and Dox into the same cells was observed at neither 1 hour nor 4 hours when they were administered in free forms (i.e. without the use of the nanoparticles).

TRAIL signals apoptosis through binding with death receptors DR4 and DR5, expressed on cell surface. To prove that uptake of Dox-loaded P(MDS-*co*-CES) nanoparticle/TRAIL complexes occurs through specific interaction between TRAIL present on the nanoparticle surface and the death receptors, receptor-blocking studies were performed. Cells were pre-incubated for 1 hr in the presence (blocked) or absence (unblocked) of blocking antibodies against the death receptors before incubation with nanocomplexes for an additional 1 or 4 hours. Pre-incubation with the anti-DR4 and -DR5 antibodies blocked the cellular uptake of the nanocomplexes extensively, thus demonstrating that the entry of nanocomplexes was dependent on death receptors expressed on cell surface. When the same treatment was performed using free Dox and TRAIL formulation, the uptake of TRAIL was prevented, as expected. However, the uptake of Dox into the cells was unaffected. This further reveals that the specificity of the treatment towards cancer cells expressing death receptors can be conferred by using the TRAIL nanocomplexes.

To elucidate the individual effects of the blocking antibodies on the cellular uptake of the nanocomplexes, SW480 cells were pre-incubated for 1 hr with individual

blocking antibodies against either of the death receptors (DR4 or DR5) before incubation with the TRAIL nanocomplexes for an additional 1 or 4 hours (Figure 5.4B). Confocal images showed that both the antibodies were able to block the cellular uptake of the nanocomplexes to a similar extent.

A

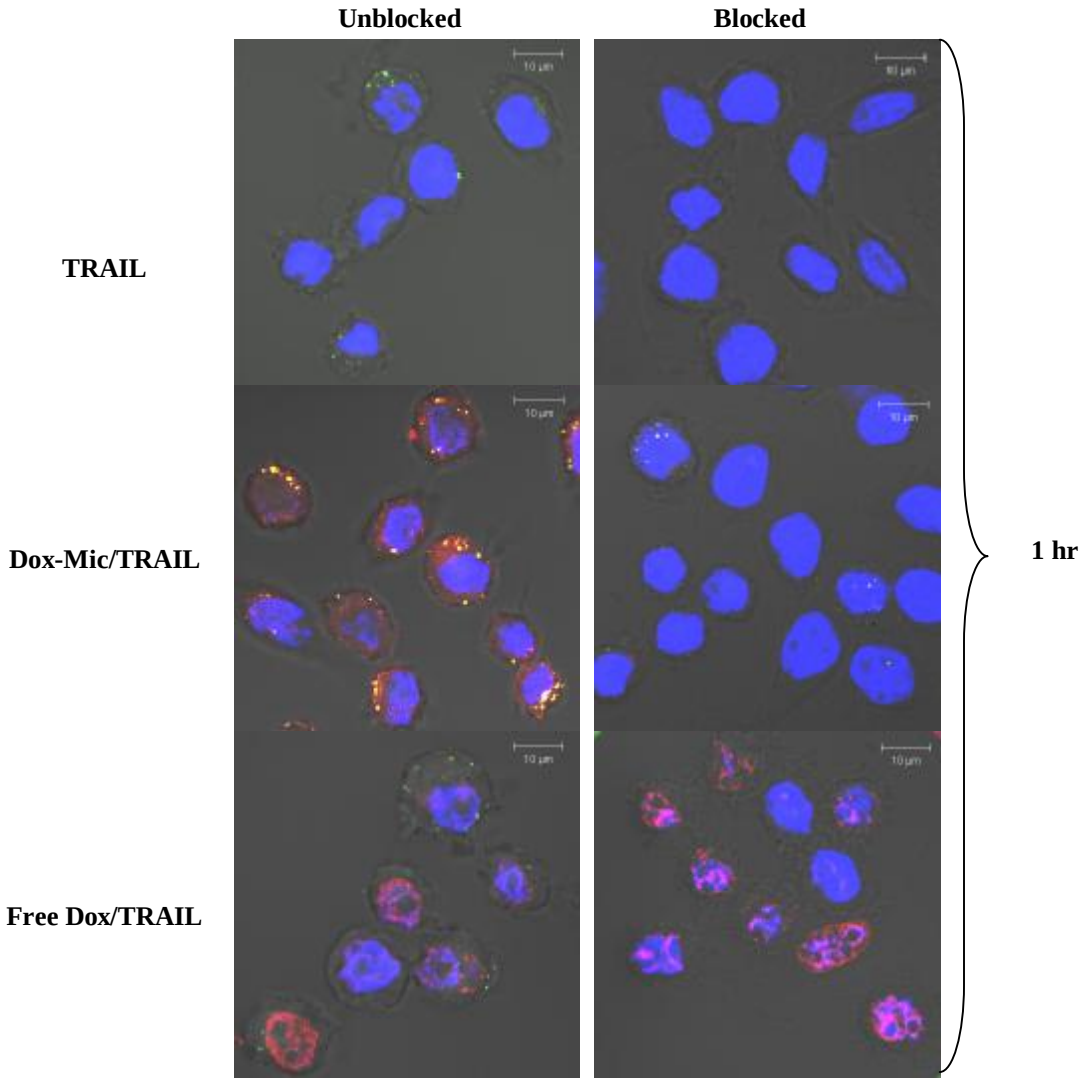

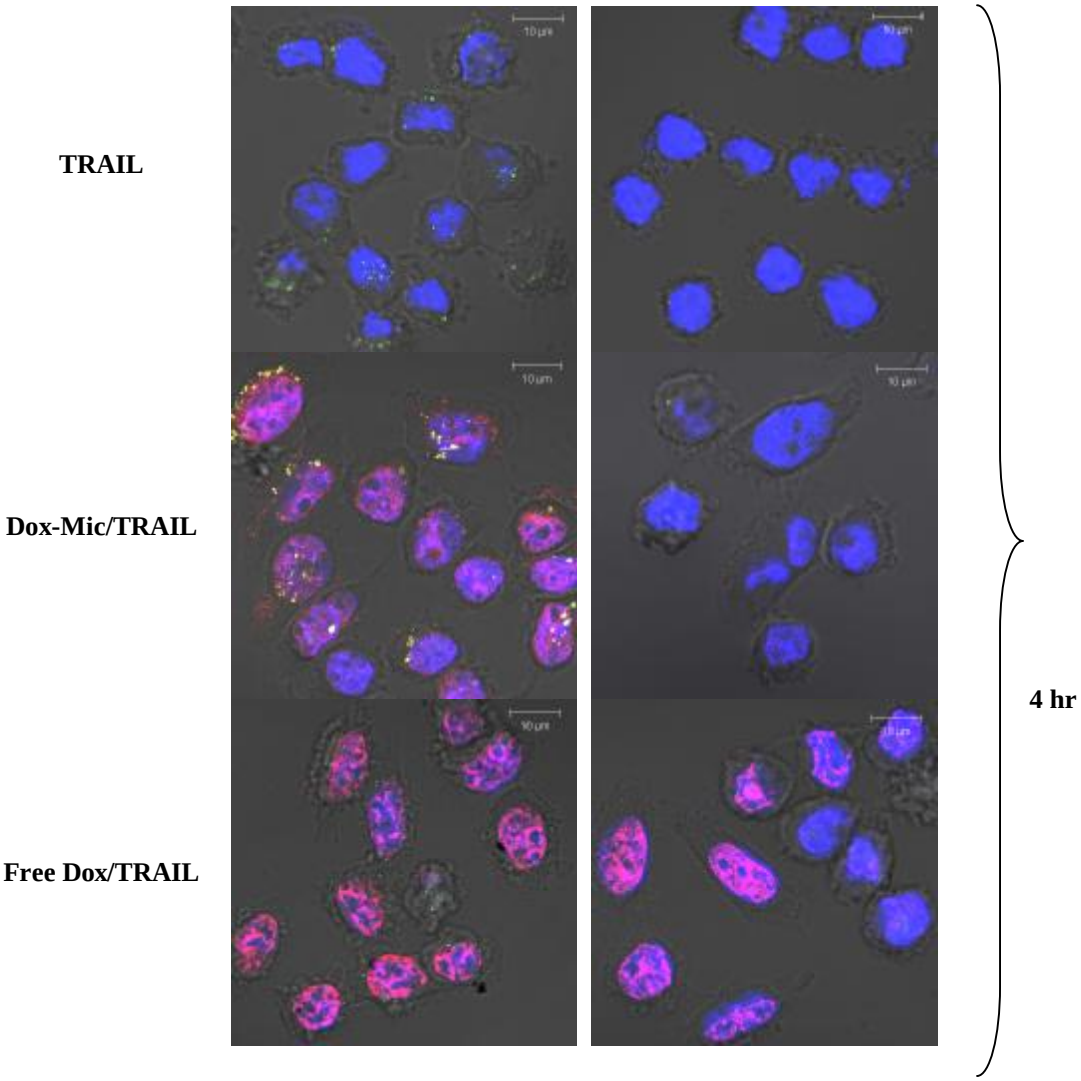
TRAIL
Dox-Mic/TRAIL
Free Dox/TRAIL
4 hr

B

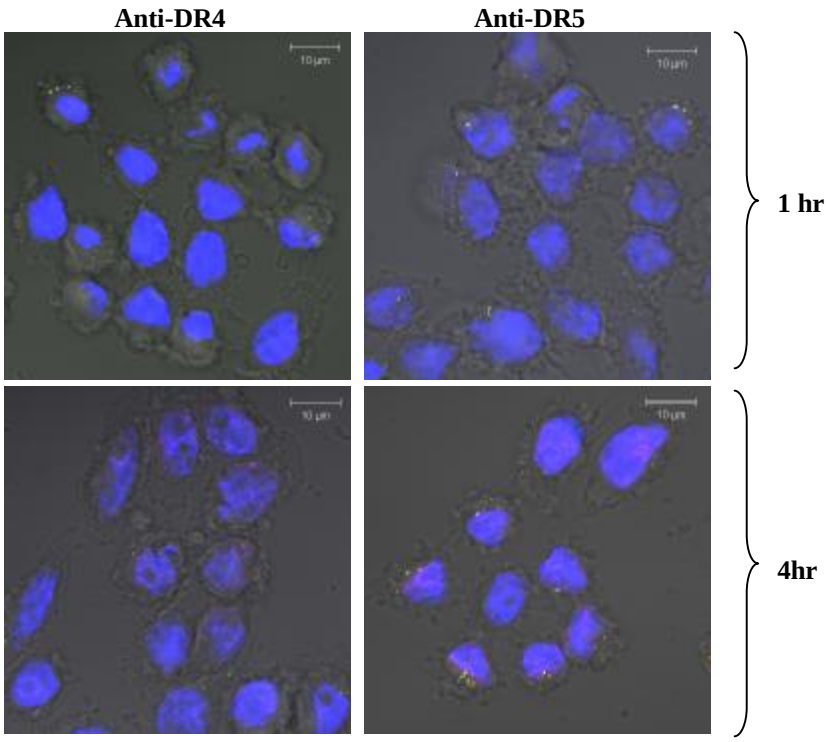

Figure 5.4 (A) Death receptor (DR4 and DR5)-mediated uptake of TRAIL, Dox-loaded P(MDS-*co*-CES) micelle/TRAIL nanocomplexes or free Dox+TRAIL formulation by SW480 cells. Cells were pre-incubated for 1 hour at 37°C in the presence (blocked) or absence (unblocked) of blocking antibodies against the death receptors before incubation with TRAIL, Dox-loaded micelle/TRAIL or free Dox+TRAIL formulation for an additional 1 or 4 hours. **(B)** Death receptor (DR4 or DR5)-mediated endocytosis of P(MDS-*co*-CES) micelle/TRAIL nanocomplexes in SW480 cells. Cells were pre-incubated for 1 hour at 37 °C in the presence (blocked) of antibodies against the death receptors (either DR4 or DR5) before incubation with Dox-loaded micelle/TRAIL nanocomplexes for an additional 1 or 4 hours. Nuclei were stained blue with DAPI, and cellular distribution of Alexa Fluor 647-TRAIL and Dox-loaded P(MDS-*co*-CES) nanoparticle appears as green and red fluorescence respectively. 0.8 mg/l of Alexa Fluor 647-TRAIL and 10 mg/l of Dox-loaded P(MDS-*co*-CES) nanoparticles were used. Dox loading level: 8.6%.

5.2.5 Establishment of TRAIL-resistant cancer cells

The emergence of drug resistance is a major problem, which results from prolonged and repeated treatment with the same drugs. For cancer therapy, such dosage cycles are usually inevitable and success of treatment is jeopardized at times due to the development of resistance to chemotherapeutic drugs. Therefore, in this study we have investigated the effects of Dox-loaded nanoparticle/TRAIL nanocomplexes on both cells

that are sensitive to TRAIL and those that have acquired resistance to TRAIL. To obtain cells resistant to TRAIL, SW480 cells with an IC_{50} of 100 nM TRAIL, were treated repeatedly with subtoxic doses of TRAIL (1 to 20 nM). The selection process is associated with only a low level of cell death (~ 20%) each time, thereby giving rise to a cell population that is representative of the majority of parental cells. The resultant SW480-TR cells were found to be resistant to cytotoxic effects of TRAIL, with even up less than 10% cell death at 1000 nM TRAIL (Figure 5.5A). Cell viability studies of these TRAIL-resistant cells showed that they have also developed slight cross-resistance to Dox-loaded nanoparticles (Figure 5.5B). This minor cross-resistance might be due to some common death signaling intermediates, such as caspases, which were common between TRAIL and doxorubicin in the apoptosis pathways.

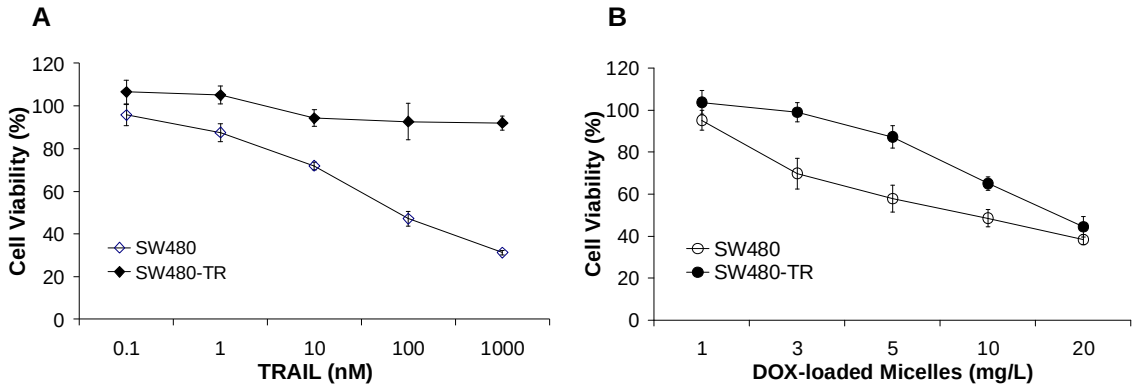

Figure 5.5 Viability of parental SW480 and TRAIL-resistant SW480-TR cells after 48 hours incubation with varying TRAIL (0.1 to 1000 nM) **(A)** and DOX-loaded micelle concentrations (1 to 20 mg/l) **(B)**. Dox loading level: 8.6%. The standard deviation is shown by error bars that represent the mean ± S.D. (n=3).

5.2.6 Synergistic cytotoxic effect of Dox and TRAIL co-delivery using P(MDS-*co*-CES) nanoparticles

Synergism in anti-cancer effects and apoptosis induction of Dox-loaded nanoparticle/TRAIL complexes were investigated in both parental SW480 and TRAIL-

resistant SW480-TR cells in comparison with individual formulations. As shown in Figure 5.6A and B, TRAIL exerted higher cytotoxic effect against SW480 cells when delivered by the nanoparticles at all concentrations tested (e.g. cell viability: 62% at nanoparticle concentration of 1 mg/l *vs.* 72% when TRAIL was used alone). However, in SW480-TR cells, an enhanced cytotoxic effect was only observed at nanoparticle concentration of 10 mg/l. Importantly, the co-delivery of Dox and TRAIL resulted in a significant enhancement of cytotoxicity at all nanoparticle concentrations used. Comparison between the parental and TRAIL-resistant cell lines showed a similar degree of enhancement of cytotoxicity although TRAIL-resistant cells were relatively more difficult to kill. For example, after being treated with Dox-loaded nanoparticle/TRAIL complexes (TRAIL: 10 nM; 5 mg/l nanoparticles with equivalent Dox concentration of 0.8 μM), viability of parental SW480 cells was reduced by 40% more than that when being treated with TRAIL or Dox-loaded nanoparticles alone. Similarly, viability of SW480-TR cells was also reduced by close to 40% after treatment with the nanocomplexes as compared to the individual formulations.

The cytotoxicity of Dox-loaded Micelles was also compared against free Dox in the absence and presence of TRAIL (Table 5.1). In parental SW480, Dox-loaded nanoparticles were more cytotoxic than free Dox with ~19% lower cell viability after the treatment. In SW480-TR cells, Dox-loaded nanoparticles had similar cytotoxicity as compared to free Dox. The Dox-loaded nanoparticle/TRAIL complexes and the free Dox/TRAIL formulation had similar cytotoxicity against both cell lines. However, in normal human lung fibroblasts WI38, Dox-loaded nanoparticles were significantly less cytotoxic than free Dox, both in the absence and presence of TRAIL.

Increase in subG1 population is considered a marker for apoptotic activities [337]. From cell cycle analysis (Figure 5.6 C and D), we observed that the treatment of TRAIL-sensitive SW480 and TRAIL-resistant SW480-TR with free TRAIL or nanoparticle/TRAIL complexes or Dox-loaded nanoparticle/TRAIL complexes (TRAIL concentration: 10 nM) resulted in significantly higher subG1 population compared to the control without treatment, blank micelles and Dox-loaded micelles, indicating that cell death occurred *via* apoptosis when the TRAIL formulations were applied. In addition, treatment with free TRAIL, nanoparticle/TRAIL complexes or Dox-loaded nanoparticle/TRAIL complexes resulted in lesser subG1 population in SW480-TR cells compared to SW480 cells and this is in agreement with the TRAIL resistance developed in SW480-TR. However, the difference in subG1 population between SW480 and SW480-TR cell lines was the smallest when Dox-loaded nanoparticle/TRAIL complexes were used (47 *vs.* 17% for free TRAIL; 48 *vs.* 24% for micelle/TRAIL complexes; 58 *vs.* 49% for Dox-loaded nanoparticle/TRAIL complexes). This demonstrates that the co-delivery formulation is superior to free TRAIL and micelle/TRAIL complex formulations SW380-TR.

To determine if the observed apoptotic activity occurs through caspase-dependent mechanisms, SW480 cells were treated with nanoparticles, in the presence or absence of the pan-caspase inhibitor, ZVAD-FMK. Cell viability assay revealed that ZVAD-FMK indeed inhibits cell death especially resulting from the co-delivery system, indicating that the apoptotic activity was based on caspase-dependent mechanisms (Figure 5.7).

Synergistic cytotoxic effects from the co-delivery of Dox and TRAIL were analyzed using the isobologram method on the drug dose to reduce growth rate by half

(IC_{50}). Synergy between the two compounds is demonstrated as the combination drug dosage falls to the left side of the line of additivity. From Figure 5.6 E and F, the combination dose (indicated by the coloured squares) of TRAIL and Dox delivered using the nanocomplexes was significantly lower than the individual therapeutics, thus demonstrating synergistic cytotoxic effects in both parental SW480 and SW480-TR cell lines. The enhancement in therapeutic efficacy by the co-delivery system will enable the same level of cancer cell death to be induced using a lower dose of Dox and TRAIL. This can reduce the dose-related harmful side effects of the drugs. Such improvements in anti-cancer effects have also been observed in other studies where the combinations of Dox and TRAIL in free-drug formulations were able to induce a much higher level of cytotoxicity in prostrate cancer cells at sub-toxic dosages at which the single drugs were unable to cause significant amount of cancer cell death [338, 339]. In the current system, the co-delivery of Dox and TRAIL using P(MDS-*co*-CES) nanoparticles will enable simultaneous delivery of the two agents in a receptor-mediated manner and thereby inducing higher cytotoxicity selectively to cancer cells. The delivery the multiple therapeutic agents in a single nanoparticle system will also help to reduce the number of drug adminstrations when applied in clinical settings.

Induction of cell death by TRAIL begins by binding of the ligand to cell surface death receptors (DR4 and DR5), followed by a series of death signaling events in the apoptosis pathway. From confocal studies, it is observed that TRAIL alone or when delivered using P(MDS-*co*-CES) nanoparticles entered into cells, most likely *via* receptor-mediated endocytosis. This is in agreement with several studies that reported cellular internalization of TRAIL subsequent to receptor binding [317, 340, 341]. Thus,

internalization of TRAIL delivered using the nanoparticles did not affect its apoptotic signaling functions. This hypothesis is also supported by the successful enhancement of cell death induced by the use of nanoparticles in cell viability study.

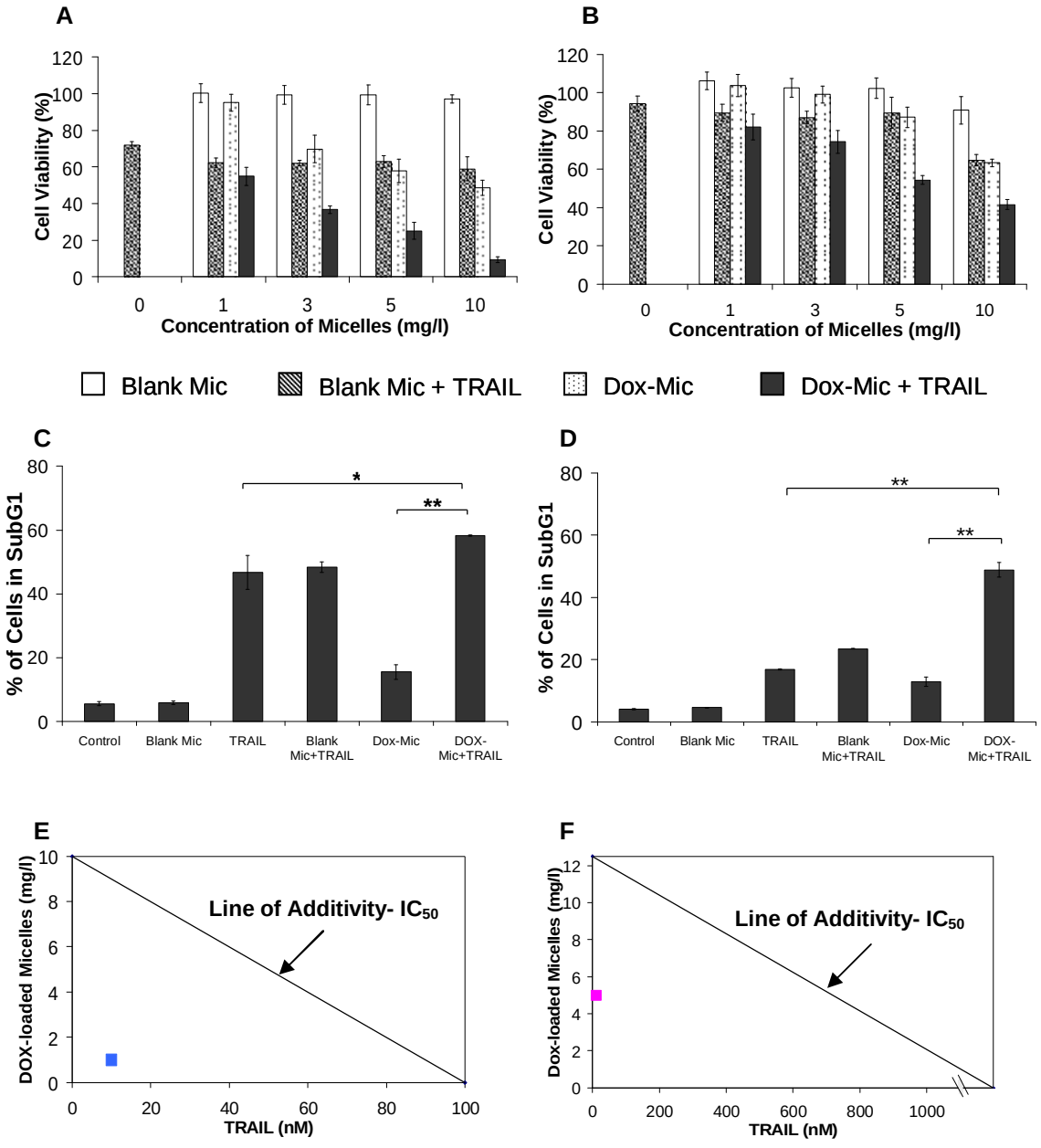

Figure 5.6 Viability of parental SW480 **(A)** and TRAIL-resistant SW480-TR **(B)** cells after 48 hours incubation with various formulations (TRAIL concentration fixed at 10 nM; Dox-loaded nanoparticle concentrations varied from 1 to 10 mg/l; Dox loading level: 8.6%; Free Dox concentrations: 0.086 and 0.43

mg/l (Equivalent Dox concentration in 1 and 5 mg/l of Dox-loaded nanoparticles) for SW480 and SW480-TR respectively. The standard deviation is shown by error bars that represent the mean ± S.D. (n=3). Cell cycle analysis of parental SW480 **(C)** and TRAIL-resistant SW480-TR **(D)** cells after 48 hours incubation. For parental SW480, the concentration of P(MDS-*co*-CES) nanoparticles was 5 mg/l. For TRAIL-resistant SW480-TR, a higher concentration of P(MDS-*co*-CES) nanoparticles (10 mg/l) was used. Dox loading level: 8.6%. TRAIL concentration was fixed at 10 nM. All cell culture experiments were performed in serum-containing medium. The standard deviation is shown by error bars that represent the mean ± S.D. (n=3). Statistical significance in differences was evaluated by Newman–Keuls Multiple Comparison Test after analysis of variance (ANOVA). $P \leq 0.05$ was considered statistically significant. An isobologram analysis representing the synergy between the two drugs at combination dose (colored squares) of Dox-loaded nanoparticles (1 mg/l) and TRAIL (10 nM) in parental SW480 **(E)** and Dox-loaded nanoparticles (5 mg/l) and TRAIL (10 nM) in TRAIL-resistant SW480-TR **(F)** cells.

Table 5.1 Viability (%) of SW480, SW480-TR and WI38 cells after 48-hour incubation with Dox-loaded nanoparticles and free Dox in the presence or absence of TRAIL (10 nM). P(MDS-*co*-CES) concentration was fixed at 5 mg/l for all cell lines (Dox loading level: 8.6%.). Cell culture was performed in serum-containing medium. The values represent the mean ± S.D. (n=3)

	DOX-Mic	Free DOX	Dox-Mic+TRAIL	Free DOX+TRAIL
SW480	57.9 ± 6.3	76.8 ± 4.1	25.1 ± 4.6	22.1 ± 2.2
SW480-TR	87.2 ± 5.4	80.7 ± 4.6	54.4 ± 2.2	52.2 ± 2.4
WI38	76.9 ± 2.9	57.6 ± 2.1	76.4 ± 3.4	47.5 ± 2.3

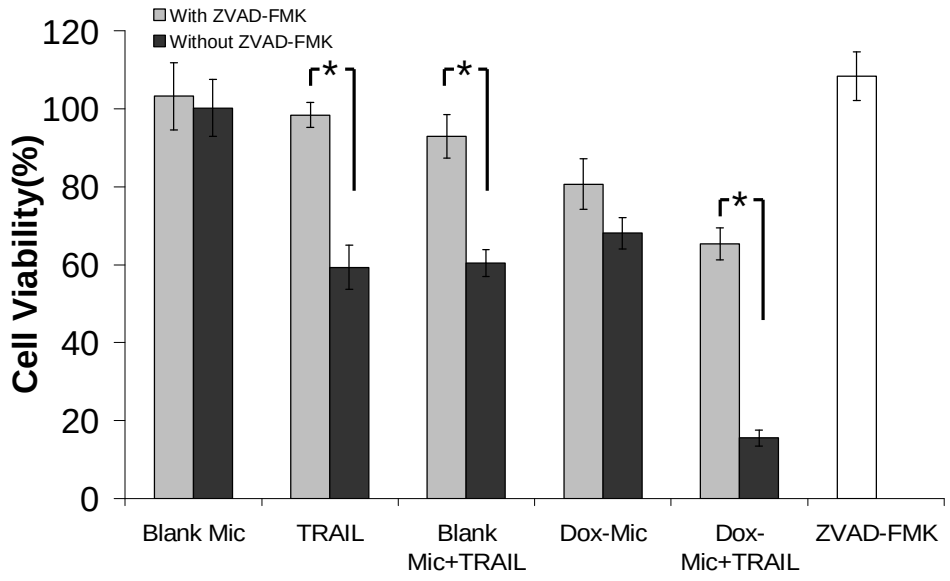

Figure 5.7 Viability of parental SW480 cells in the presence or absence of pan-caspase inhibitor ZVAD-FMK pretreatment (50 μM) prior to 48 hour incubation with nanocomplexes. P(MDS-*co*-CES) and TRAIL concentrations were fixed at 5 mg/l and 10 nM respectively. Dox loading level: 8.6%. Cell culture was performed in serum-containing medium. The error bars represent the mean ± S.D. (n=3). Statistical

significance in differences was evaluated by Student's t-Test. $P \leq 0.05$ was considered statistically significant.

5.2.7 Cytotoxic selectivity towards cancer cells

TRAIL was selected in the current study based on its cytotoxic selectivity towards cancer cells. To investigate if there could be any nonspecific cytotoxicity that the Dox-loaded nanoparticle/TRAIL nanocomplexes may have on normal cells, WI38 was chosen as a representative model cell line. Cell viability assay performed on WI38 cells showed that TRAIL and nanoparticle/TRAIL complexes did not result in substantial cytotoxicity to the cells (Figure 5.8). The viability of the cells after being treated with Dox-loaded nanoparticle/TRAIL complexes was estimated to be 76%, which was similar to that when being treated with Dox-loaded nanoparticles, indicating that 24% cell death was induced by Dox but not TRAIL. As reported in the earlier section, the co-delivery of both therapeutic agents to SW480 cells resulted in 75% cell death. Comparison between these two cell lines showed that the TRAIL nanocomplexes possess high selectivity towards the cancer cells over the normal cells. One of the reasons could be due to the relative differences in expression levels of decoy (TRAIL-R3 (DcR1), TRAIL-R4 (DcR2), and osteoprotegerin (OPG)) and death receptors (TRAIL-R1 (DR4) and TRAIL-R2 (DR5)) in normal *versus* cancer cells [293, 295]. Decoy receptors compete against death receptors for TRAIL binding but do not lead to apoptotic signaling. Other studies have shown that the cancer cells express higher levels of DR5 mRNA and protein than normal cells, which will in turn contribute to greater susceptibility to apoptosis mediated through DR5.[342] More recent findings have also suggested that other factors involved in the apoptotic signaling pathway such as death inhibitors (e.g. cellular-FLICE inhibitory protein

(c-FLIP), Fas-associated phosphatase-1 **(**FAP-1) and Inhibitor of Apoptosis (IAP) proteins) may also be responsible for different susceptibility to TRAIL [268, 290, 295, 296]. The overexpression of cFLIP and IAPs has been reported to play a major role in protecting certain human normal cells, such as melanocytes and lung and foreskin fibroblasts, from TRAIL-induced apoptosis [343].

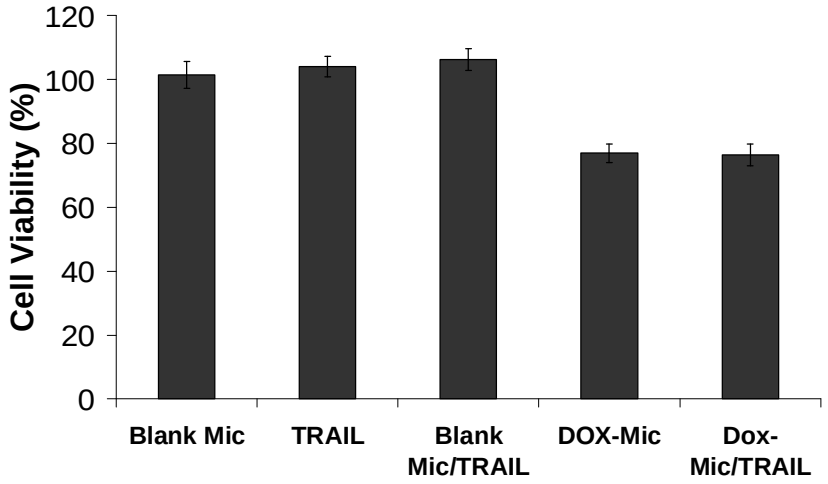

Figure 5.8 Viability of WI38 cells after 48 hours incubation with various formulations. Cell culture was performed in serum-containing medium. P(MDS-*co*-CES) (5 mg/l) and TRAIL (10 nM) were used. Dox loading level: 8.6%. Free Dox concentration: 0.43 mg/l (Equivalent Dox concentration in 5 mg/l of Dox-loaded nanoparticles). The standard deviation is shown by error bars that represent the mean ± S.D. (n=3).

5.2.8 Long-term survival and proliferation assays

Anchorage-dependent clonogenic assay is the method of choice to determine cell survival and proliferation capacities after exposure to chemotherapeutic agents [344]. From Figure 5.9A, treatment with Dox-loaded nanoparticle/TRAIL nanocomplexes significantly lowered the survival and proliferative abilities of SW480 and SW480-TR cells compared to the individual agents. The absence of cell singlets or small clusters remaining in nanocomplexes-treated cultures (Figure 5.9B) indicated that most of the

cells underwent senescence or became mitotically arrested after being treated with the co-delivery formulation. With further culturing, these cells eventually die, resulting in very few cells capable of continual survival. Thus, cytotoxic synergism in co-delivery of Dox and TRAIL with P(MDS-*co*-CES) nanoparticles was further demonstrated in impairing long-term survival and clonogenicity of cancer cells after the treatment.

A

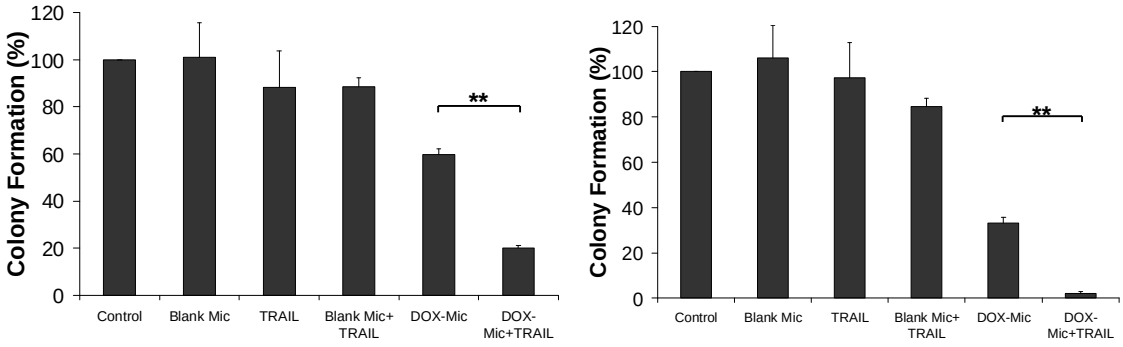

B

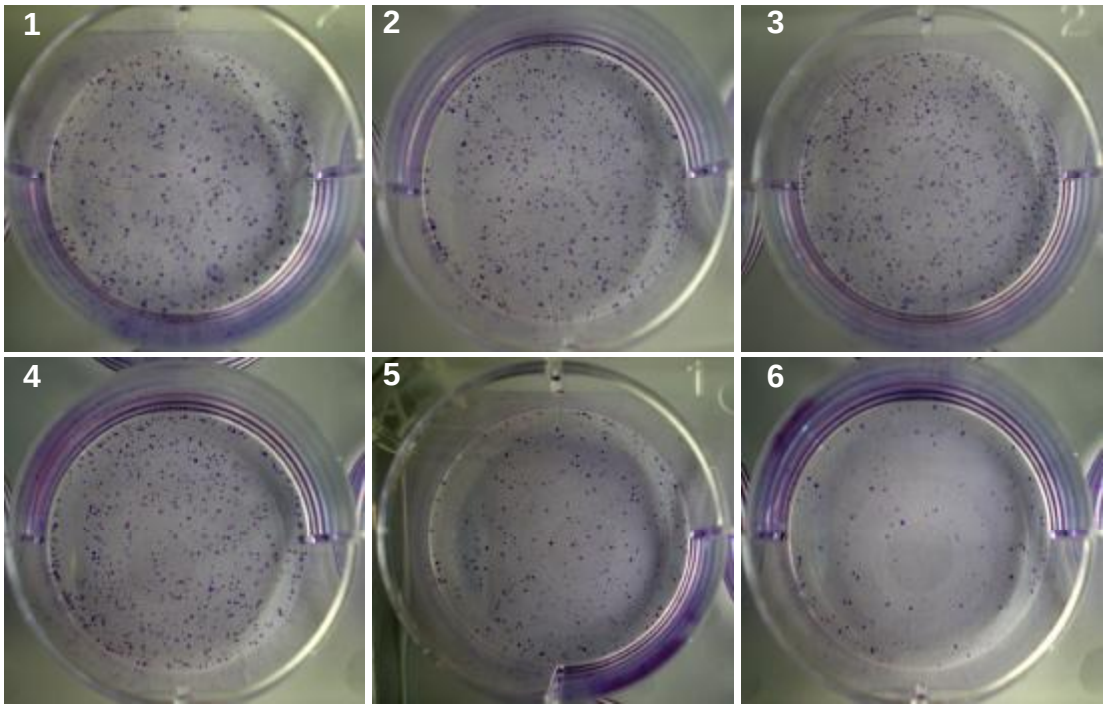

Figure 5.9 (A) Colony formation at Day 9 and 13 in parental SW480 and TRAIL-resistant SW480-TR cell lines respectively subsequent to 48 hours treatment with (1) control, (2) blank nanoparticles, (3) TRAIL, (4) blank nanoparticle/TRAIL complexes, (5) Dox-loaded nanoparticles, (6) Dox-loaded nanoparticle/TRAIL complexes. Colonies were stained with 0.5% w/v crystal violet. Cell culture was performed in serum-containing medium. TRAIL: 10 nM; P(MDS-*co*-CES): 1 and 3 mg/l for SW480 and SW480-TR respectively. Dox loading level: 8.6%. The error bars represent the mean ± S.D. (n=3). Statistical significance in differences was evaluated by Newman–Keuls Multiple Comparison Test after analysis of variance (ANOVA). $P \leq 0.05$ was considered statistically significant. **(B)** Images of SW480 colony taken at Day 9 subsequent to 48 hours treatment with (1) control, (2) blank nanoparticles, (3) TRAIL, (4) nanoparticle/TRAIL complexes, (5) Dox-loaded nanoparticles and (6) Dox-loaded nanoparticle/TRAIL complexes. P(MDS-*co*-CES) and TRAIL were fixed at 1 mg/l and 10 nM respectively. Dox loading level = 8.6%. Colonies were stained with 0.5% w/v crystal violet.

5.3 Conclusion

In the previous chapter, P(MDS-*co*-CES) nanoparticles has shown to be an efficient carrier for co-delivering Pac and TRAIL for treatment of human breast cancer cells. For this chapter, the efficacy of treatment *via* co-delivery of Dox and TRAIL against TRAIL-resistant colorectal carcinoma cells was investigated. Dox-loaded nanoparticles and TRAIL formed stable nanocomplexes with sizes at ~225 nm and zeta potential at ~70 mV. Effects of nanocomplexes were tested on both TRAIL-resistant and wild type SW480 cells. From confocal imaging, the assemblies of Dox and TRAIL with P(MDS-*co*-CES) nanoparticles were shown to be efficiently delivered to cancer cells. Receptor-blocking studies showed that the nanocomplexes entered cells *via* death receptor-mediated endocytosis. Synergism in cell death induction was analysed by the isobologram method to study drug interactions. This co-delivery system was significantly more effective in eliminating cancer cells and preventing reproliferation after drug removal as compared to TRAIL and Dox-loaded nanoparticle formulations. Anti-proliferative effects of nanocomplexes were retained in remaining cancer cells in long-term cultures after treatment with the nanocomplexes. Notably, this system exhibited high cytotoxic selectivity towards cancer cells over normal cells. Therefore, Dox-loaded

nanoparticle/TRAIL nanocomplexes may stand as a potential powerful candidate for colorectal cancer therapy.

CHAPTER 6

HER2-TARGETED CO-DELIVERY OF HERCEPTIN AND PACLITAXEL USING CATIONIC POLYMERIC NANOPARTICLES

6.1 Introduction

One of the widely-accepted methodologies for targeted drug delivery is *via* passive drug targeting based on the enhanced permeability and retention (EPR) effect [178, 336, 345], where nanosized drug-loaded micelles can pass through the leaky tumor blood vessels and accumulate in the tumor tissue for a prolonged period of time. Active targeting can be achieved by incorporating pH and/or temperature-sensitive components [346-349] or biological signals such as folic acid [349, 350], galactose [305, 351], LHRH [352], RGD [353] and antibody [354, 355] into the micelles. Among these biological signals, antibodies are the most promising, and have been used in preclinical and clinical applications as anti-cancer agents [355-357]. In particular, Herceptin is a humanized monoclonal antibody that recognizes the human epidermal growth factor receptor-2 (HER2/neu). HER2/neu is overexpressed in 25-30% of invasive human breast tumors and has been found to be a worse prognosis than those with HER2-negative tumors as measured by significantly lower survival rates [358-360]. Overexpression of HER2/neu in breast cancer cells results in higher resistance against anti-cancer drugs such as pac. This can be counteracted with the use of Herceptin as it displays tumor inhibitory effect through various mechanisms [361, 362], some of which include diminishing signaling from the PI3 kinase and MAP kinase pathways, causing cell cycle arrest at the G1 phase, promoting apoptosis *via* antibody-dependent cellular cytotoxicity (ADCC), inhibiting

angiogenesis and DNA repair in tumors. Biological implications of the use of Herceptin against HER2-overexpressing cells involve the inhibition of HER2-mediated Cdc2-Tyr-15 phosphorylation and upregulation of $p21^{Cip1}$. This allows effective $p34^{Cdc2}$ activation and induction of apoptosis upon pac treatment [363].

In preclinical studies [363, 364] and in Phase II and III clinical trials [365, 366], synergistic chemosensitization effects have been observed with the treatment of subjects using Herceptin together with pac. In these clinical formulations, Pac and Herceptin have been administered through separate injections into patients. To eliminate the inconvenience by reducing the number of injection required for treatment, Herceptin has been conjugated with pac. This conjugate has been reported to target pac to breast tumor bearing scid mice, which was induced with HER2-positive BT474 mammary tumor cells [367]. The co-delivery of Herceptin with pac may not only render the delivery system a targeting ability, but may also sensitize aggressive breast cancer cells to pac and achieve a synergistic effect in suppressing tumor growth. This conjugation approach confers greater advantages over the separate formulations because of the reduction in the number of injections with the possibility of achieving synergistic effect through the simultaneous delivery of Pac and Herceptin to the same cells. However, one of the major disadvantages of this immunoconjugate is the inflexibility of conjugation stoichiometric ratio, which may not be beneficial for achieving drug targeting and synergistic effect since their therapeutic dosage may not be in comparable ranges. Pac and Herceptin have also been reported to be delivered simultaneously to HER2-overexpressing breast cancer cells using negatively-charged PLGA nanoparticles [368]. In this formulation, Pac was loaded inside PLGA nanoparticles by a solvent evaporation method and Herceptin was adsorbed onto

the surface of the nanoparticles *via* electrostatic interaction. In comparison to chemical conjugation, the simultaneous delivery of Pac and Herceptin using nanoparticles represents a better approach as the dosage of Pac and Herceptin can be conveniently adjusted by altering their initial loading level.

In the previous chapters, cationic micellar nanoparticles fabricated from amphiphilic copolymer P(MDS-*co*-CES) have been shown to be efficient carriers for small molecules drugs and proteins such as TRAIL and Lectin-A, either individually or concurrently [313, 369, 370]. For the current study, these micelles are used to co-deliver pac and Herceptin simultaneously to HER2-overexpressing cancer cells. Pac was loaded into the core of the micelles through a membrane dialysis method, and Herceptin was then complexed onto the cationic surface of pac-loaded micelles. Polar groups present in the polymer such as esters and tertiary amine groups as well as relatively hydrophobic alkyl polymer backbone may interact with amide functional groups, primary and secondary amines, carboxylic acid as well as hydrophobic groups in Herceptin through hydrogen bonding and/or hydrophobic interaction. Particle size and zeta potential of the nanoparticle/Herceptin and Pac-loaded nanoparticle/Herceptin complexes were measured in comparison with negatively-charged polystyrene nanoparticle/Herceptin complexes, and the stability of Pac-loaded nanoparticle/Herceptin complexes was investigated in a serum-containing medium *via* particle size analysis. Native protein gel assays were conducted to evaluate Herceptin binding efficiency of the nanoparticles. Pac loading and *in vitro* release profiles from the nanoparticles with or without Herceptin were studied. The intracellular delivery efficiency of Herceptin using these nanoparticles was compared against BioPorter (a commercially available lipid-based protein carrier) through confocal

microscopy and MTT assays. Cytotoxic effects of co-delivery of pac and Herceptin using these nanoparticles was investigated *via* MTT assays in three different human breast cancer cell lines with varying degrees of HER2/neu expression level, namely, MCF7, T47D and BT474, and the effect of Herceptin concentration was also explored. Targeting ability of this co-delivery system was demonstrated through confocal images and cytotoxicity tests of HER2-overexpressing BT474 cells and HER2-negative HEK293 cells [371] after being treated with nanoparticle/Herceptin complexes.

6.2 Results and Discussion

6.2.1 Characterization of pac-loaded nanoparticles and pac-loaded nanoparticle/Herceptin complexes

As shown in Figure 6.1, cationic pac-loaded P(MDS-*co*-CES) nanoparticles have an average size of 115 ± 6 nm and zeta potential of about 60 ± 3 mV. The drug-loaded nanoparticles are larger than blank P(MDS-*co*-CES) nanoparticles (84 ± 5 nm), showing that the presence of pac in the hydrophobic core of the micelles increases micellular volume. As the more nanoparticles is added to complex with Herceptin, there is a general increase in size and decrease in zeta potential of the complexes, indicating complexation between the nanoparticles and Herceptin. From zeta potential measurement, Herceptin molecules show a neutral charge in 20 mM sodium acetate/acetic acid buffer (pH 6.0) (1.8 ± 0.6 mV). Therefore, the interaction between the antibody and nanoparticles would most probably be occurring through hydrogen bonding and/or hydrophobic interaction. These nanocomplexes were compared against cationic BioPorter liposomes [277, 286] (267 ± 25 nm, 18.9 ± 0.4 mV), which after complexation with Herceptin, aggregates to form larger particles (910 ± 46 nm, 12.7 ± 0.6 mV) and (1011 ± 49 nm, 3.7 ± 0.7 mV) at

Herceptin concentrations of 200 nM and 2000 nM respectively as used in *in vitro* experiments (as represented in Figure 6.6).

In comparison, through a similar complex-fabrication method, negatively-charged polystyrene beads (-60.8 ± 4.2 mV) form large aggregates of micrometer sizes with large polydispersities in the presence of Herceptin. Particles of such large sizes are unfavorable because of potential problems associated with aggregation and particle instability.

The small sizes of P(MDS-*co*-CES) nanoparticle/Herceptin complexes may enable them to prolong circulation in blood and slower elimination by the recticuloendothelium system (RES). Herceptin adsorbed on the surface of the nanoparticles may target the complexes to the HER2 receptors on HER2-overexpressing cell surfaces. Attachment of Herceptin to HER2 receptors and the overall positive charge of the complexes may improve their interaction with cell surfaces and increase their cellular uptake.

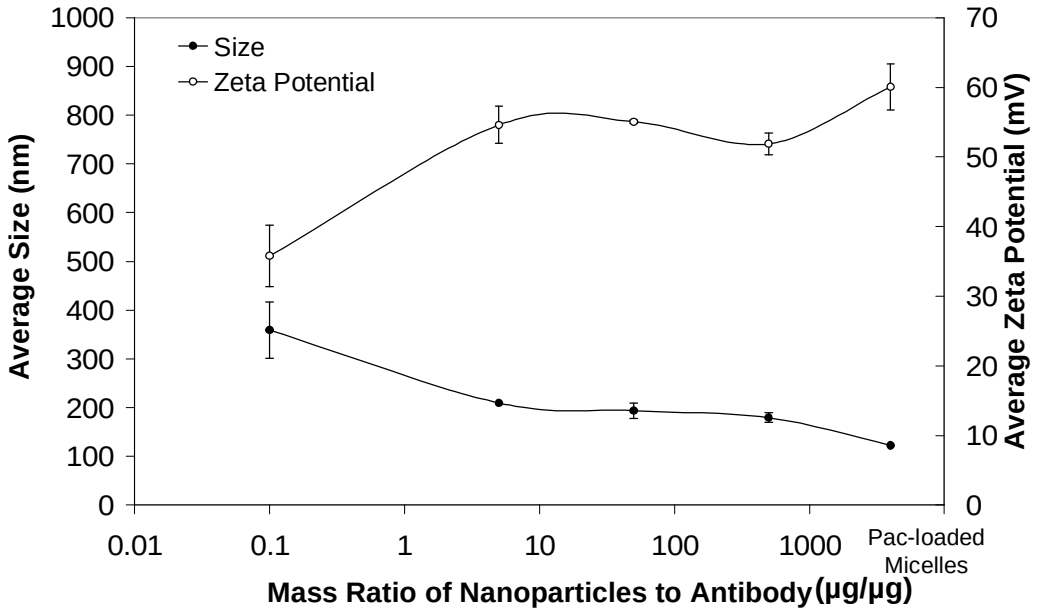

Figure 6.1 Size and zeta potential properties of pac (Pac)-loaded P(MDS-*co*-CES) nanoparticle/Herceptin complexes. Experiments were carried out in triplicates. The standard deviation is presented in error bars.

6.2.2 Native protein gel mobility shift assay on Pac-loaded P(MDS-*co*-CES)/Herceptin nanocomplexes

Size and zeta potential data of Pac-loaded nanoparticle/Herceptin complexes in Section 6.2.1 demonstrate that the Pac-loaded nanoparticles are able to condense and bind to Herceptin to form nanocomplexes with cationic surfaces. Native (non-denaturing) protein gel shift assay was performed to ensure that Herceptin retains its folded confirmation and does not get denatured during the analysis. More importantly, we are able to compare the ability of P(MDS-*co*-CES) nanoparticles to bind Herceptin at different mass ratios. The nanoparticle/Herceptin complexes were prepared with increasing mass ratio of nanoparticles to Herceptin, and the resulting mixture was then applied to a native polyacrylamide gel. Figure 6.2 illustrates the results of this assay, with increasing polymer to protein mass ratio from 0.1 to 50 (Lanes 2 to 7). Electrophoretic mobility of Herceptin is increasingly reduced as more P(MDS-*co*-CES) is added for Herceptin binding. This shows that stronger nanoparticle/Herceptin interaction occurs when there are more polymer molecules available to bind to the antibody.

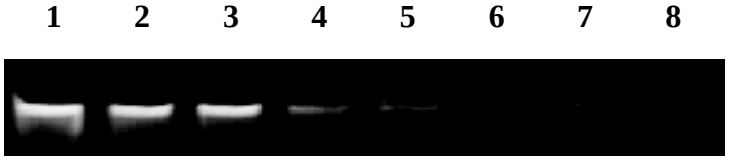

Figure 6.2 Native protein gel assay of Pac-loaded P(MDS-*co*-CES) nanoparticle/Herceptin complexes. Lane 1 – Herceptin (4 μg) alone, Lane 8 – Pac-loaded P(MDS-*co*-CES) nanoparticles (200 μg) alone, Lanes 2 to 7 – nanoparticle to antibody mass ratios: 0.1, 0.5, 1, 5, 10 and 50 respectively.

6.2.3 Drug loading and *in vitro* release

Encapsulation efficiency of Pac in P(MDS-*co*-CES) micellar nanoparticles was determined to be 58.1 ± 1.4% and the loading level as 14.3 ± 0.1%. The release profile of pac from P(MDS-co-CES) nanoparticles with or without Herceptin was monitored over 600 hours at 37°C (Figure 6.3). Most of the drug is released within the first 3 days of incubation as the nanoparticles show drug release of 54.7% by 59 hours and the total release is 69.3%. The presence of Herceptin on the surface of nanoparticles slightly reduces the release rate and amount of Pac released (47.3%) over the first 59 hours. However, the total release is 63.2%, which is not significantly different from that without the antibody.

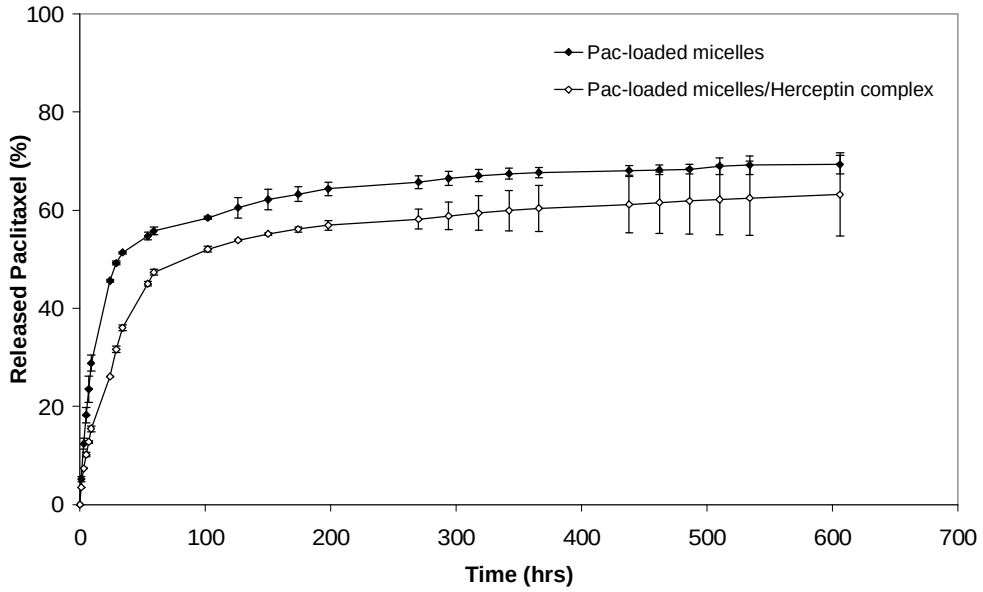

Figure 6.3 Release profiles of paclitaxel (Pac) from P(MDS-*co*-CES) micellar nanoparticles with and without Herceptin in PBS (pH 7.4) at 37°C. Each condition was tested in triplicates. The standard deviation is presented in error bars.

6.2.4 *In vitro* stability of the pac-loaded P(MDS-*co*-CES) nanoparticle/Herceptin complexes

The stability of Pac-loaded P(MDS-*co*-CES) nanoparticle/Herceptin complexes was studied by *in vitro* simulation of physiological conditions that the complexes might be subjected to. Size readings of the complexes were taken at predetermined time intervals after incubation in PBS containing 10% FBS at 37^{o}C (Figure 6.4). After 5 minutes of incubation, the size of the particles increases to 300-350 nm. During this period, the cationic complexes may attract the serum proteins, which may cause aggregation of the nanoparticles. The adsorbed proteins and aggregation of the nanoparticles lead to an increase in particle size. Since the Pac-loaded nanoparticles and complexes formed at mass ratio of 50 have higher zeta potential than the complexes prepared at mass ratio of 0.1 (Figure 6.1), more proteins may be adsorbed onto the nanoparticles and the complexes formed at mass ratio of 50 during the first 5 minutes, resulting in bigger particles. However, as time passes, cationic nanoparticles or complexes form stronger electrostatic interactions with the serum proteins and compact the proteins into tighter structures. Thus, the size of complexes decreases with time. Particle size stabilizes at around 200 nm by 4 hours of incubation and remains unchanged over 24 hours.

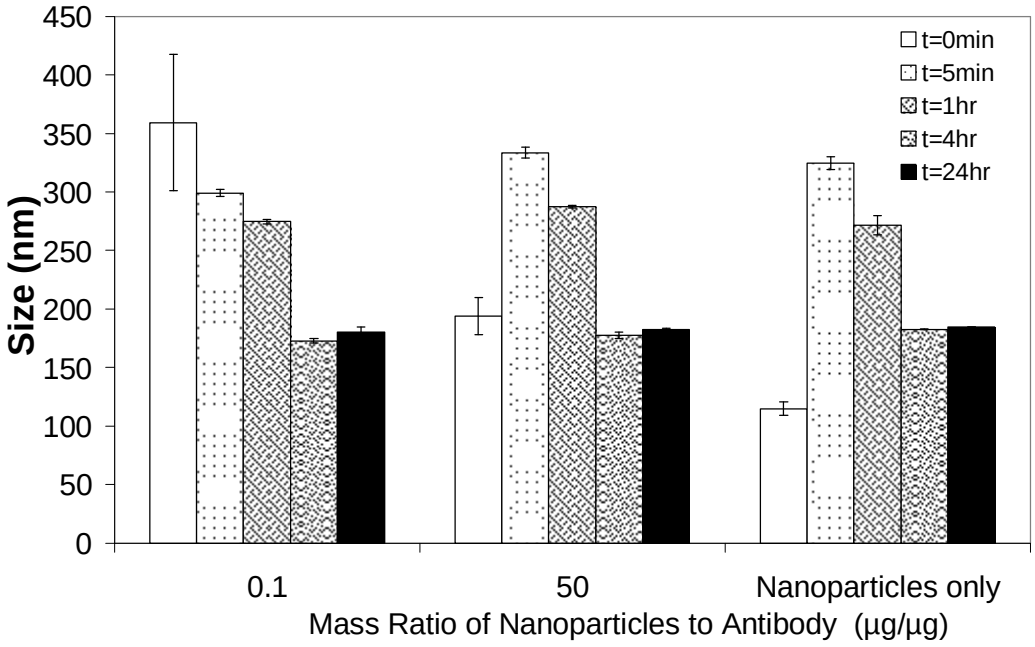

Figure 6.4 Stability of pac-loaded P(MDS-*co*-CES) nanoparticle/Herceptin complexes in PBS containing 10% FBS incubated at 37°C. Each condition was tested in triplicates. The standard deviation is presented in error bars.

6.2.5 Cellular delivery and uptake of Herceptin

Cellular uptake of Herceptin delivered by the nanoparticles was studied in BT474 cells *via* confocal microscopy, in comparison with pure Herceptin and Herceptin transported by BioPorter, a commercially available lipid-based protein carrier. As shown in Figure 6.5A, without any transport carrier, Herceptin mainly appears on the cell membrane with very little uptake into the cells. Similarly, cells treated with BioPorter also did not show any increase in cellular uptake (Figure 6.5C) as compared to the cells treated with Herceptin alone. This may be due to the encapsulation of Herceptin within BioPorter liposomes [372] and entanglement of Herceptin with the Bioporter lipids, which prevents the antibody from recognizing HER2 receptors on the cancer cells and this in turn reduces the translocation of Herceptin into the cells. Cells treated with P(MDS-*co*-CES) nanoparticle/Herceptin show significantly higher internalization of

Herceptin (Figure 6.5B, red regions in the cytosol and purple regions in the nucleus). This may be due to smaller size, higher zeta potential, stability and endosomal buffering capacity of cationic P(MDS-*co*-CES) nanoparticle/Herceptin complexes.

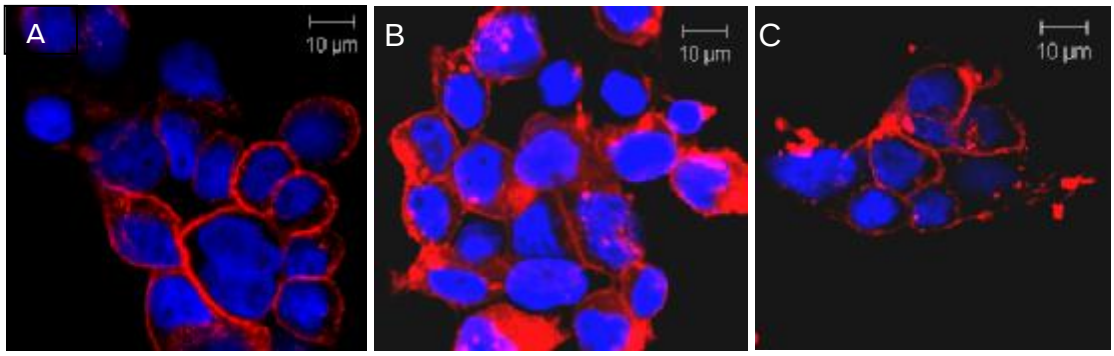

Figure 6.5 Cellular distribution of (A) fluorescence-labeled Herceptin, and (B) nanoparticle/Herceptin complexes in comparison with (C) BioPorter/Herceptin complexes. Nuclei were stained blue with DAPI, and cellular distribution of Alexa Fluor 647-Herceptin is shown as red fluorescence in the cytosol or purple fluorescence in the nucleus. Alexa Fluor 647-Herceptin: 200 nM; P(MDS-*co*-CES) nanoparticles: 40 ppm.

Cytotoxicity of Herceptin delivered by the nanoparticles was also compared against BioPorter in BT474 cells. The cells treated with BioPorter/Herceptin did not show any increase in cytoxicity as compared to the cells treated with Herceptin alone because of low cellular uptake of Herceptin (Figure 6.6). In contrast, Herceptin delivered by the nanoparticles displays significantly higher cytotoxicity as compared to that delivered by BioPorter at both concentrations tested (i.e. 200 and 2000 nM) due to its much higher cellular uptake when delivered by the nanoparticles. The association between suppression of cell prolifertion and internalization of anti-HER2 antibodies and receptors has been reported earlier by Yarden Y. et. al. [373, 374].

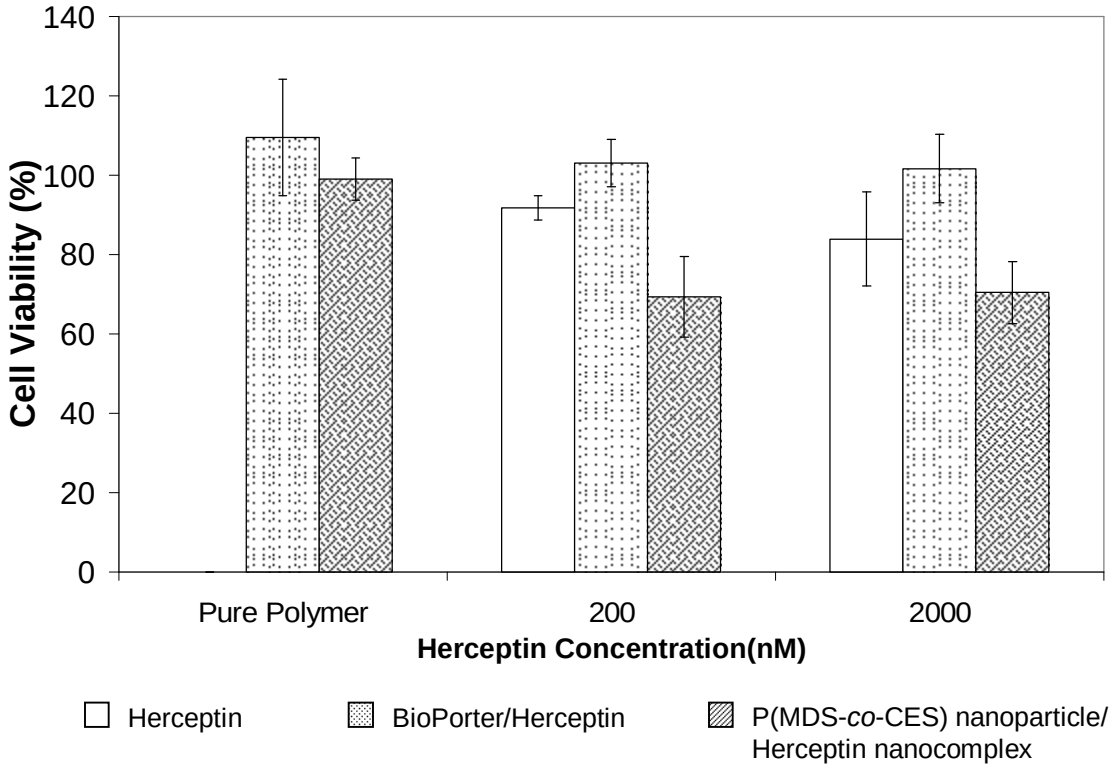

Figure 6.6 Viability of BT474 cells after being incubated with P(MDS-*co*-CES) nanoparticles, BioPorter, BioPorter/Herceptin and P(MDS-*co*-CES) nanoparticle/Herceptin complexes at Herceptin concentrations of 200 and 2000 nM. Concentrations of P(MDS-co-CES) and BioPorter are at 40 ppm and 16 ppm respectively. Each condition was tested in eight replicates. The standard deviation is shown by error bars.

6.2.6 Co-delivery of Pac and Herceptin to human breast cancer cell lines

Cytotoxicity of Pac-loaded nanoparticle/Herceptin complexes was evaluated against three different human breast cancer cell lines with varying degrees of HER2/neu expression levels in comparison with Pac-loaded nanoparticles, pure Herceptin and nanoparticle/Herceptin complexes. HER2/neu is highly expressed in BT474 cells, while the expression is moderate in T47D cells and at low level in MCF7 cells [375]. Polymer concentrations have been optimized to prevent non-selective cytotoxicity, while at the same time, to provide binding for Herceptin to be efficiently delivered. Figure 6.7 shows that at 2000 nM, Herceptin alone does have considerable cytotoxicity against BT474 cells

with 16% loss of cell viability, but the same does not occur in MCF7 and T47D cells. The susceptibility of cells towards Herceptin correlates with their HER2 receptor expression level. We also observe that cytotoxicity is slightly decreased when the dosage of Herceptin is decreased 10-fold from 2000 nM to 200 nM. Instead, with the use of P(MDS-*co*-CES) as a transport carrier for Herceptin, cytotoxicity is significantly increased in all cell lines. In particular, HER2-overexpressing BT474 cells have 22.4% higher cytotoxicity at 200 nM Herceptin delivered using P(MDS-*co*-CES) micelles. P(MDS-*co*-CES) nanoparticles mediate higher cellular uptake of Herceptin, resulting in greater cytotoxic effects.

Cytotoxicity data of Pac-loaded nanoparticle/Herceptin complexes illustrates that the effectiveness of treatment is greatly increased with drug and antibody co-delivery system as compared to delivering Herceptin alone. This system again shows a dependency on the HER2 expression level of the cells as the percentage of the cancer cells killed increases with the HER2 expression level. BT474 cells with the highest HER2 expression level display the greatest susceptibility towards the co-delivery treatment at both 200 and 2000 nM Herceptin concentration (Figure 6.7). Cell viability is reduced to 60.2% after being treated with Pac-loaded nanoparticle/Herceptin complexes (Herceptin: 200 nM; Pac: 6.7 μM) as compared to 92% with 200 nM Herceptin alone or 83% with Pac-loaded nanoparticles, demonstrating a synergistic effect. A similar trend has also been observed for the formulations with 2000 nM Herceptin (Figure 7). With this co-delivery approach, the amount of Pac and Herceptin needed to induce the same level of cytotoxicity is successfully reduced.

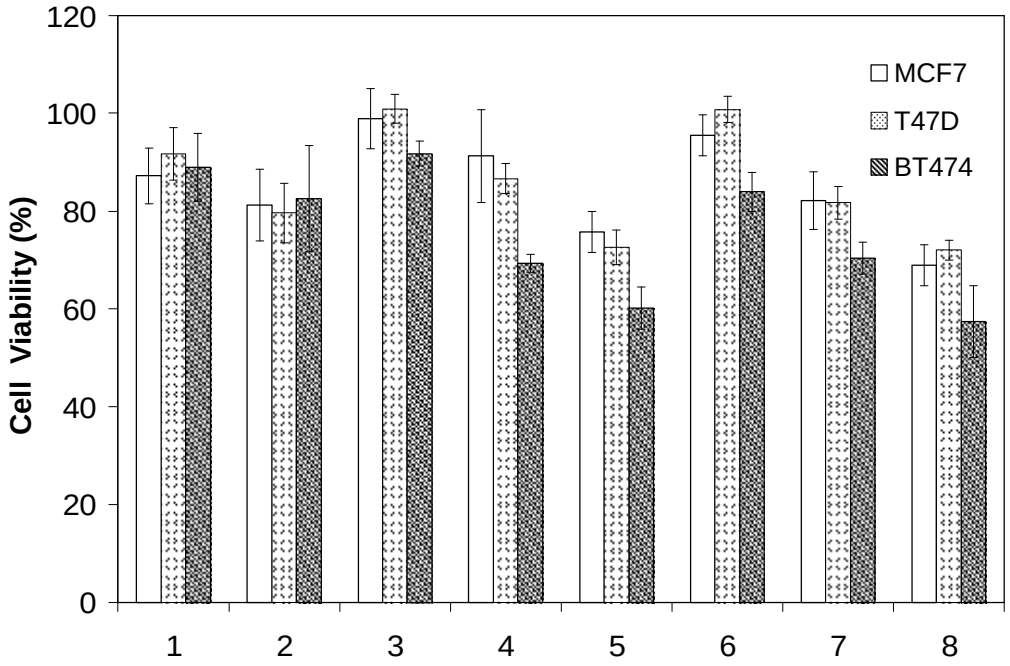

Figure 6.7 Viability of MCF7, T47D and BT474 cells after being treated with different formulations. Cells were treated once with (1) blank nanoparticles, (2) Pac-loaded nanoparticles, (3 and 6) Herceptin at 200 and 2000 nM, (4 and 7) blank nanoparticle/Herceptin complexes at 200 and 2000 nM Herceptin and (5 and 8) Pac-loaded nanoparticle/Herceptin complexes at 200 and 2000 nM Herceptin respectively. P(MDS-*co*-CES) concentrations were fixed at 20 ppm for MCF7 and T47D cells and 40 ppm for BT474 cells respectively. Cell culture was performed in serum-containing medium. Each condition was tested in eight replicates. The standard deviation is shown by error bars. Pac concentration: 3.35 μM for both T47D and MCF7 and 6.7 μM for BT474.

Further experiments were carried out with pretreatment of cells with blank nanoparticle/Herceptin complexes for 24 hours prior to treatment with Pac-loaded/Herceptin complexes. Cell death occurs in a significantly greater extent in cells that have been pretreated with blank nanoparticle/Herceptin complexes (Figure 6.8). Pretreatment results in viability of BT474 cells being almost 1-fold lower than the cells without pretreatment at 32.8% and 28.0% at 200nM and 2000nM Herceptin respectively.

In addition, the pretreated cells were also compared against the cells tested with twice-repeated daily treatment of blank nanoparticle/Herceptin complexes without Pac encapsulation. This is to find out the extent of cytotoxicity induced by the nanocomplexes

without the combined use with Pac. As shown in Figure 6.8, the viability of BT474 cells that underwent twice repeated addition of blank nanoparticle/Herceptin complexes is at 58.8% and 60.1% at 200nM and 2000nM Herceptin respectively, which is a significant improvement from single treatment of blank nanoparticle/Herceptin complexes. However, the cytotoxicity achieved with twice-repeated daily treatment of blank nanoparticle/Herceptin complexes is still much lower as compared to Pac and Herceptin co-delivery. This illustrates that co-delivery of Pac and Herceptin using P(MDS-*co*-CES) nanoparticles is advantageous in enhancing the efficiency of chemotherapeutic treatment against HER2-overexpressing breast cancer cells.

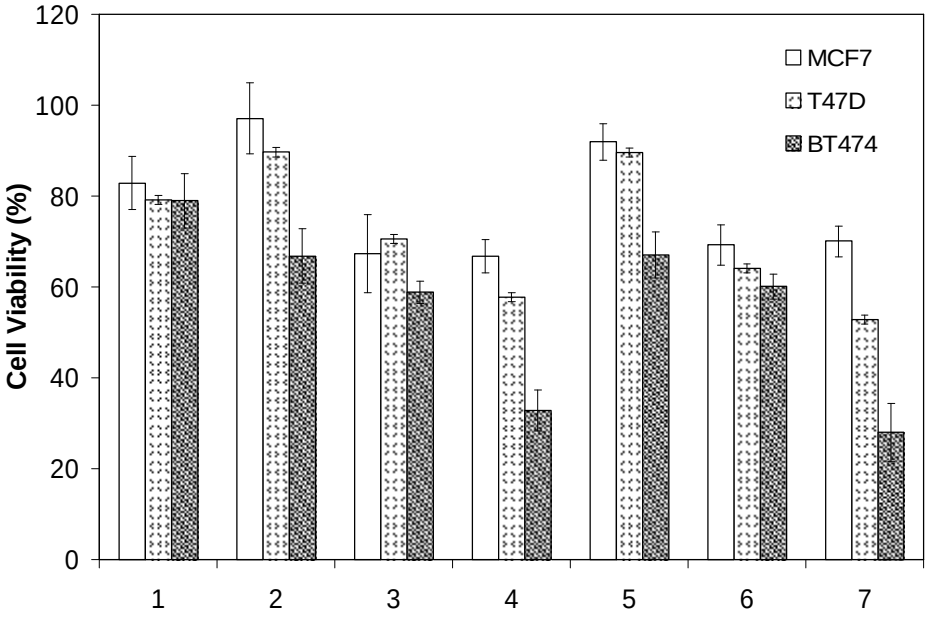

Figure 6.8 Viability of MCF7, T47D and BT474 cells after being treated with different formulations. Twice-repeated daily treatment of (1) blank nanoparticles, (2 and 5) Herceptin at 200 and 2000 nM, (3 and 6) blank nanoparticle/Herceptin complexes at 200 and 2000 nM Herceptin respectively. Cells in (4 and 7) were pretreated with (3 and 6) for 24 hours prior to treatment with Pac-loaded nanoparticle/Herceptin complexes at 200 and 2000 nM Herceptin respectively. P(MDS-*co*-CES) concentrations were fixed at 20 ppm for MCF7 and T47D cells and 40 ppm for BT474 cells respectively. Cell culture was performed in serum-containing medium. Each condition was tested in eight replicates. The standard deviation is shown by error bars. Pac concentration: 3.35 μM for both T47D and MCF7 and 6.7 μM for BT474.

6.2.7 Targeted delivery of drug-loaded nanoparticle/Herceptin complexes

The targeting ability of nanoparticle/Herceptin complexes was evaluated using HER2-overexpressing BT474 cells and HER2-negative HEK293 cells *via* confocal microscopy and cytotoxicity studies. Cellular internalization of P(MDS-*co*-CES) micelle/Herceptin complexes was monitored over two hours to verify if the complexes can be targeted to BT474 cells but not HEK293 cells. Throughout the course of the study, the uptake of the complexes by HEK293 cells is limited and insignificant (Figure 6.9B). In sharp contrast, the uptake of the complexes by BT474 cells increases with time. The complexes are taken up and distributed to the majority of the cells by 30 minutes of incubation (Figure 6.9A). At 2 hours, uptake of complexes continues to increase and some of them begin to dissociate as evidenced by the green and red/purple regions in the cytosol and nucleus of the cells. The significant increase in Herceptin uptake and residence time within BT474 cells as compared to HEK293 cells demonstrates that the uptake of the complexes is favored by the HER2-overexpressing BT474 cells as compared to HER2-negative HEK293 cells, inferring that Herceptin is able to exert HER2-targetting specificity on the complexes. This cellular trafficking study is coherent with the cytotoxicity comparison between the two cell lines (Figure 6.10). HEK293 cells are irresponsive to the treatment of nanoparticle/Herceptin and no significant cytotoxicity is observed with nanoparticle/Herceptin complexes when compared to the blank nanoparticles and Herceptin. In contrast, significant cytotoxicity of Herceptin was found against BT474 cells when the antibody is delivered using P(MDS-*co*-CES) nanoparticles.

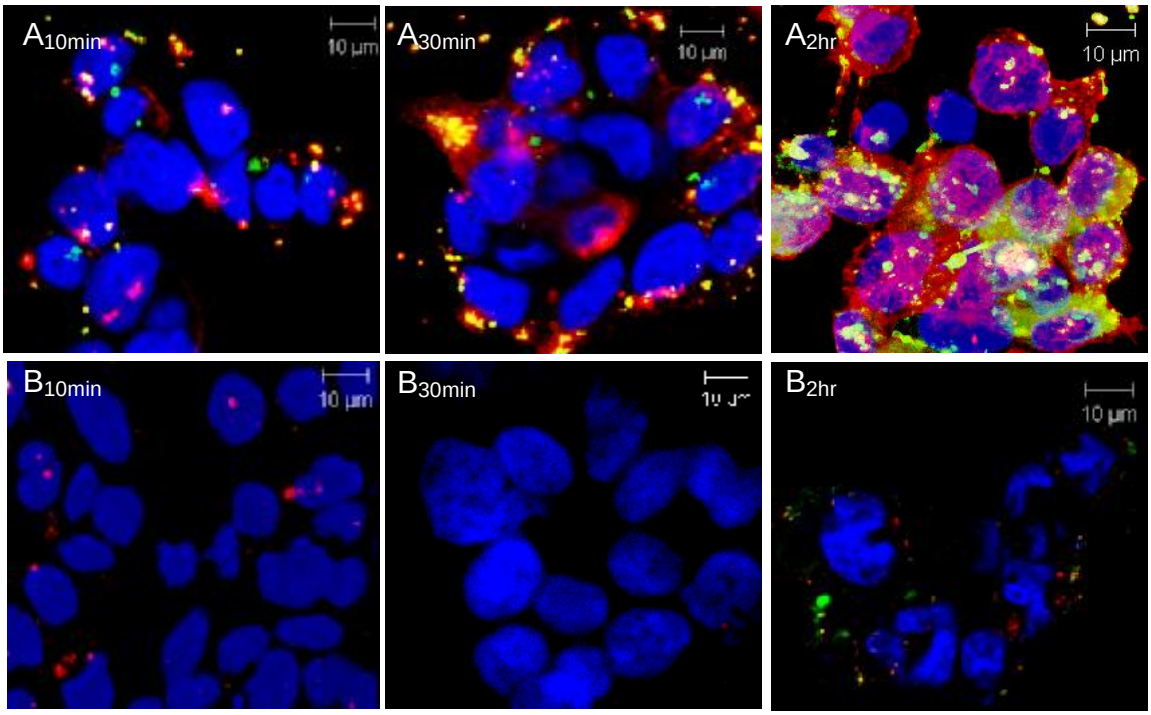

Figure 6.9 Confocal images of cellular internalization of P(MDS-*co*-CES) nanoparticle/Herceptin nanocomplexes in (A) HER2 overexpressing BT474 cells and (B) HER2-negative HEK293 cells at 10 minutes, 30 minutes and 2 hours. Nuclei were stained blue with DAPI, and cellular distribution of Alexa Fluor 647-Herceptin and FITC-loaded P(MDS-*co*-CES) nanoparticles are shown as red and green fluorescence respectively. Yellow regions represent the co-localization of Herceptin and P(MDS-*co*-CES) nanoparticles in cells. In both cell lines, Alexa Fluor 647-Herceptin (200 nM) and 40 ppm of P(MDS-*co*-CES) nanoparticles were used.

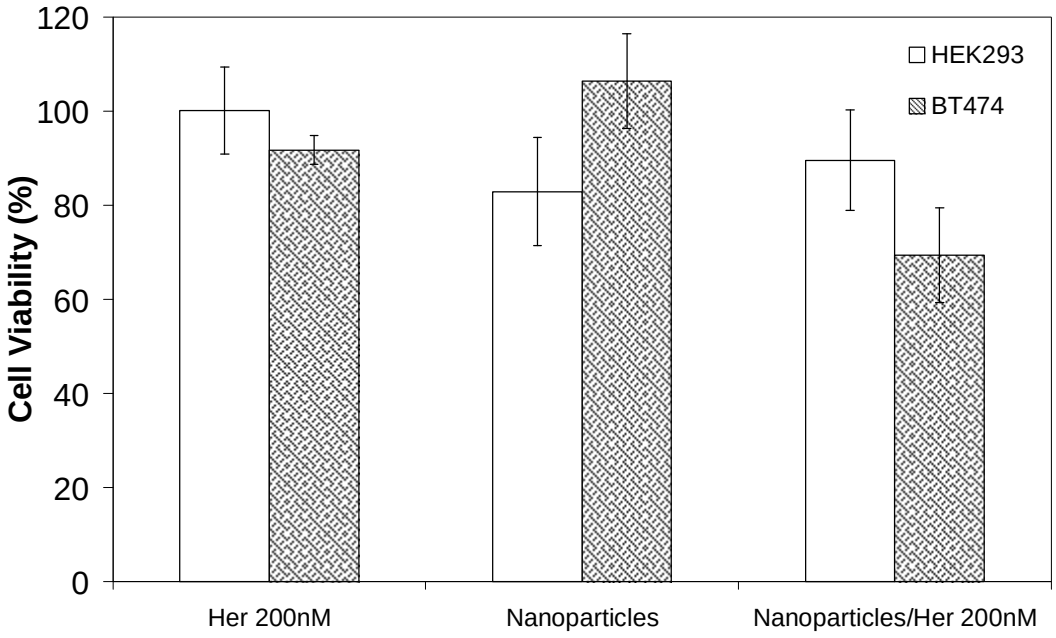

Figure 6.10 Viability of HER2-negative HEK293 and HER2 overexpressing BT474 cells after being treated with different formulations for 48 hours. P(MDS-*co*-CES) concentrations were fixed at 40 ppm for both cell lines. Cell culture was performed in serum-containing medium. Each condition was tested in eight replicates. The standard deviation is shown by error bars.

6.3 Conclusion

We have demonstrated that the cationic micellar nanoparticles self-assembled from P(MDS-*co*-CES) can carry both pacltitaxel and Herceptin simultaneously. The nanoparticles provide high capacity for pac loading, and bind with Herceptin more efficiently than BioPorter and negatively charged polystyrene beads. Pac-loaded nanoparticle/Herceptin complexes are stable over 24 hours under physiologically-simulating conditions. Compared to BioPorter and pure Herceptin, the uptake of Herceptin by HER2 overexpressed BT474 cells are much higher when it is delivered by the cationic nanoparticles, leading to greater cytotoxicity. The co-delivery of Herceptin increases the cytotoxicity of Pac, and the degree of increment in cytotoxicity depends on the level of HER2 expression. The co-delivery of Herceptin yielded greater enhancement

in the cytotoxicity of Pac in the cells with a higher HER2 expression level. The pretreatment of the cells with blank nanoparticle/Herceptin complexes for 24 hours increases the cytotoxicity of Herceptin and enhances the co-delivery efficiency. In addition, significantly higher cellular uptake and cytotoxicity of Herceptin in HER2-overexpressing BT474 as compared to HER2-negative HEK293 demonstrates targeting properties of the nanocomplexes. The Pac-loaded nanoparticle/Herceptin complexes display great potential to be used as targeted therapeutics against HER2-overexpressing breast cancers.

CHAPTER 7
IN VIVO INVESTIGATION OF HERCEPTIN AND PACLITAXEL CO-DELIVERY USING CATIONIC POLYMERIC NANOPARTICLES

7.1 Introduction

With the promising data obtained from *in vitro* investigation of Herceptin and Pac co-delivery (Chapter 6), research efforts were further extended to *in vivo* testing using mice tumor models. The initial phase of the study involves the evaluation of nanoparticles biodistribution following different routes of injection- tail vein *versus* intratumoral injection. Non-invasive fluorescent imaging at various was performed at various times up to 7 days after the mice were then sacrificed at the end of the experiment to estimate the distribution of nanoparticles in individual tissues. Next, tumor efficacy study was performed by treating BT474-tumor bearing nude mice with Pac-loaded nanoparticle/Herceptin complexes, together with the relavant treatmet controls.

7.2 Results and Discussion

7.2.1 Biodistribution of DiR-loaded nanoparticles

Comparison between the two modes of injection shows that intratumoral injection is more favorable compared to tail vein injection (Figure 7.1A and B). The latter injection method resulted in the accumulation of nanoparticles within mainly in the lungs and liver but only very low amount of nanoparticles is present in the tumor tissue. This is may be due to the aggregation of the cationic nanoparticles in the presence of negatively charged serum proteins following intravenous administration. The resultant aggregates could form

transient embolism in lung capillaries [376]. Conversely, intratumoral injection results in accumulation of nanoparticles mainly in the tumors.

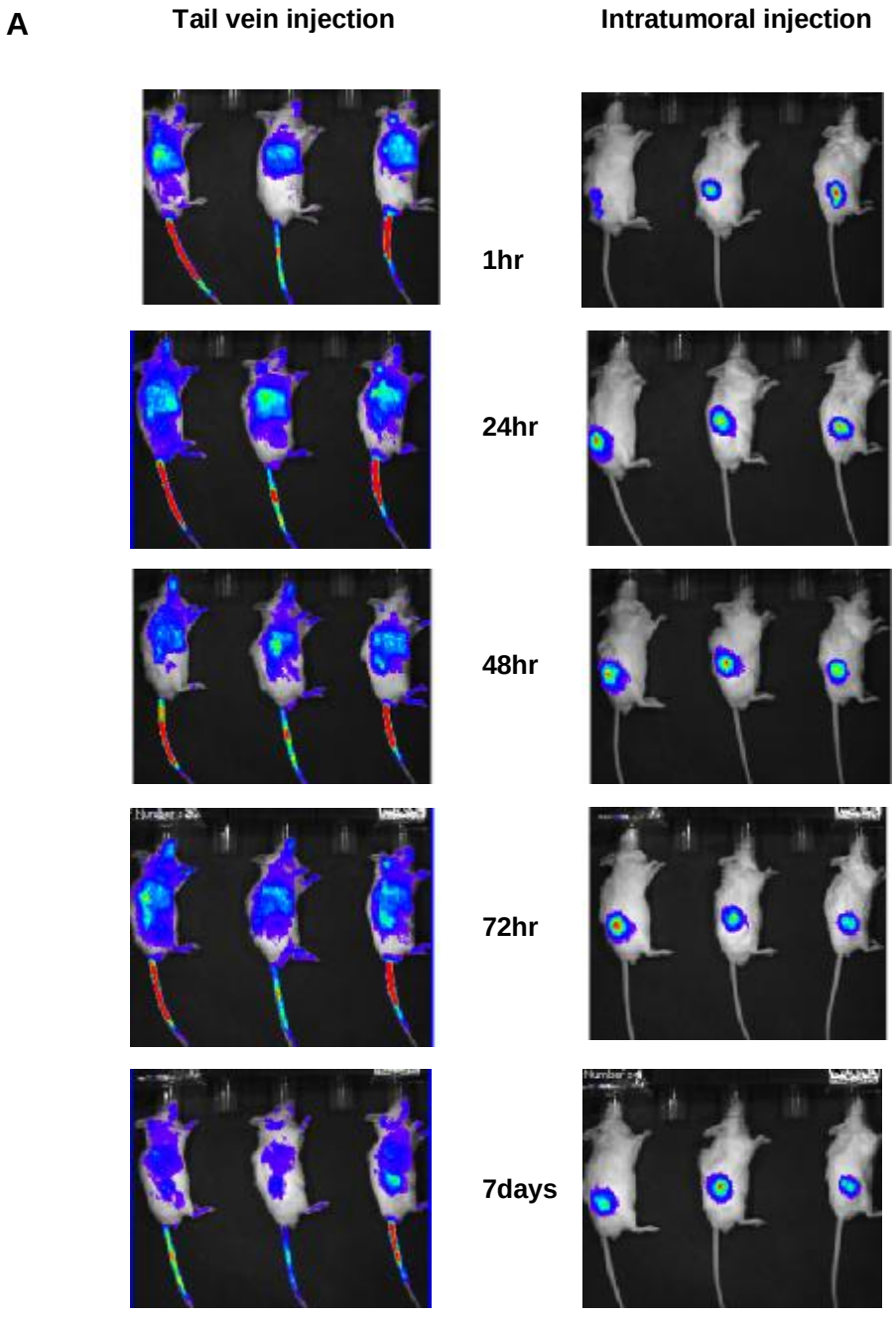

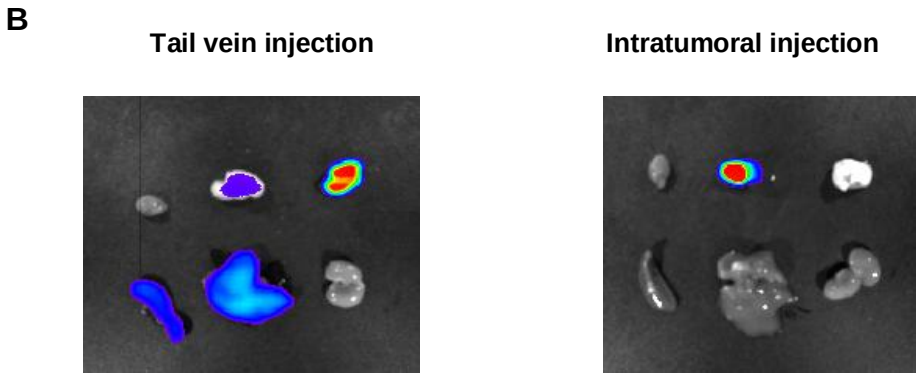

Figure 7.1 (A) *In vivo* biodistribution of P(MDS-*co*-CES) nanoparticles with different injection methods (tail-vein vs. intratumoral). **(B)** Distribution of P(MDS-*co*-CES) nanoparticles in different tissues 7 days post-injection. (Top row, starting from left: heart, tumor and lungs. Bottom row: spleen, liver and kidneys)

7.2.2 *In vivo* anti-tumor efficacy studies of Pac-loaded nanoparticle/Herceptin complexes

To understand the therapeutic effects of Pac and Herceptin codelivery, BT474-tumor bearing mice were used as the animal model for *in vivo* experimentation. The treatment groups consist of: control treated with actete buffer (20 mM, pH 6.0); Herceptin; blank nanoparticles/Herceptin complexes; Pac-loaded nanoparticles and Pac-loaded nanoparticles/Herceptin complexes. The concentration of nanoparticles was carefully chosen as 8 mg/kg, which is much lower compared to the LD_{50} of 27.7 mg/kg (Appendix I). As such, all mice survived the entire course of treatment. Measurements of changes in tumor size (Fig. 7.2) showed that the growth inhibition resulting from the single modality therapies were different. Statistical differences in tumor size at the end of treatment was evaluated by analysis of variance (ANOVA) and followed by Tukey Test. $P \leq 0.05$ was considered statistically significant The mice that were treated with Pac-loaded nanoparticles have similar average tumor volume compared to the control group (P =

0.35). On the other hand, treatment with blank nanoparticles/Herceptin ($P < 0.01$) resulted in tumor reduction of 44% and was not significantly different from Herceptin treatment alone. The anti-tumor efficacy is more profound using combination therapy with Pac-loaded nanoparticle/ Herceptin nanocomplexes, where there is a growth inhibition of 82% versus the control treated mice ($P < 0.01$). In addition, the codelivery of the two therapeutic agents is also statistically superior to Pac-loaded nanoparticles alone ($P < 0.01$). However, there is no statistical difference when compared against blank nanoparticles/Herceptin complexes alone ($P = 0.13$). There may be several contributing factors to the insufficient drug synergism. One of the probable reasons could be the inadequate release of Pac from the nanoparticles *in vivo*, which will weaken the biological actions of the drug with Herceptin. There could also be limited spread of nanoparticles in the tumor tissue as a result of self-aggregation, hindered diffusion due to dense cancer cell packing and extracellular matrix and high interstitial fluid pressure [377, 378]. Investigation of the spread of nanoparticles within the BT474 tumor tissue shows that the nanoparticles self-aggregate within the extracellular space after adminstration. As such, the nanoparticles are unable to penetrate or distribute evenly to the cancer cells (Fig. 7.3), the cellular access and drug effects is inevitably reduced.

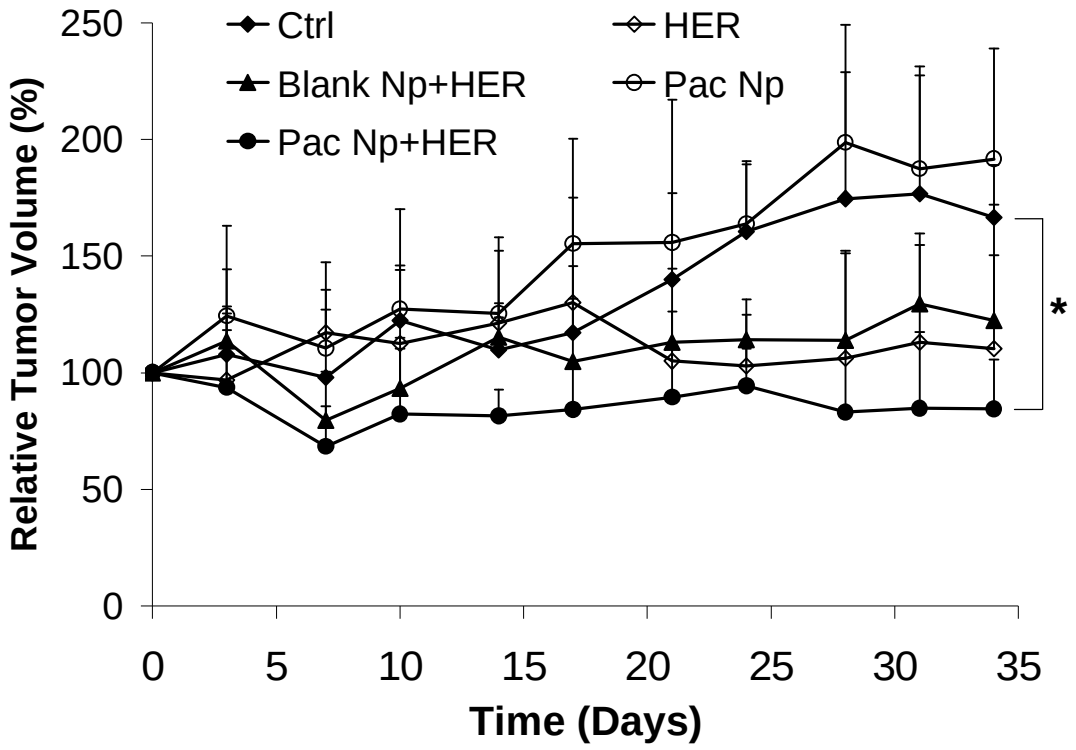

Figure 7.2 Changes in relative tumor size (%) with time. Statistical significance in tumor size differences at the end of treatment was evaluated by Tukey Test after analysis of variance (ANOVA). *$P \leq 0.05$ was considered statistically significant.

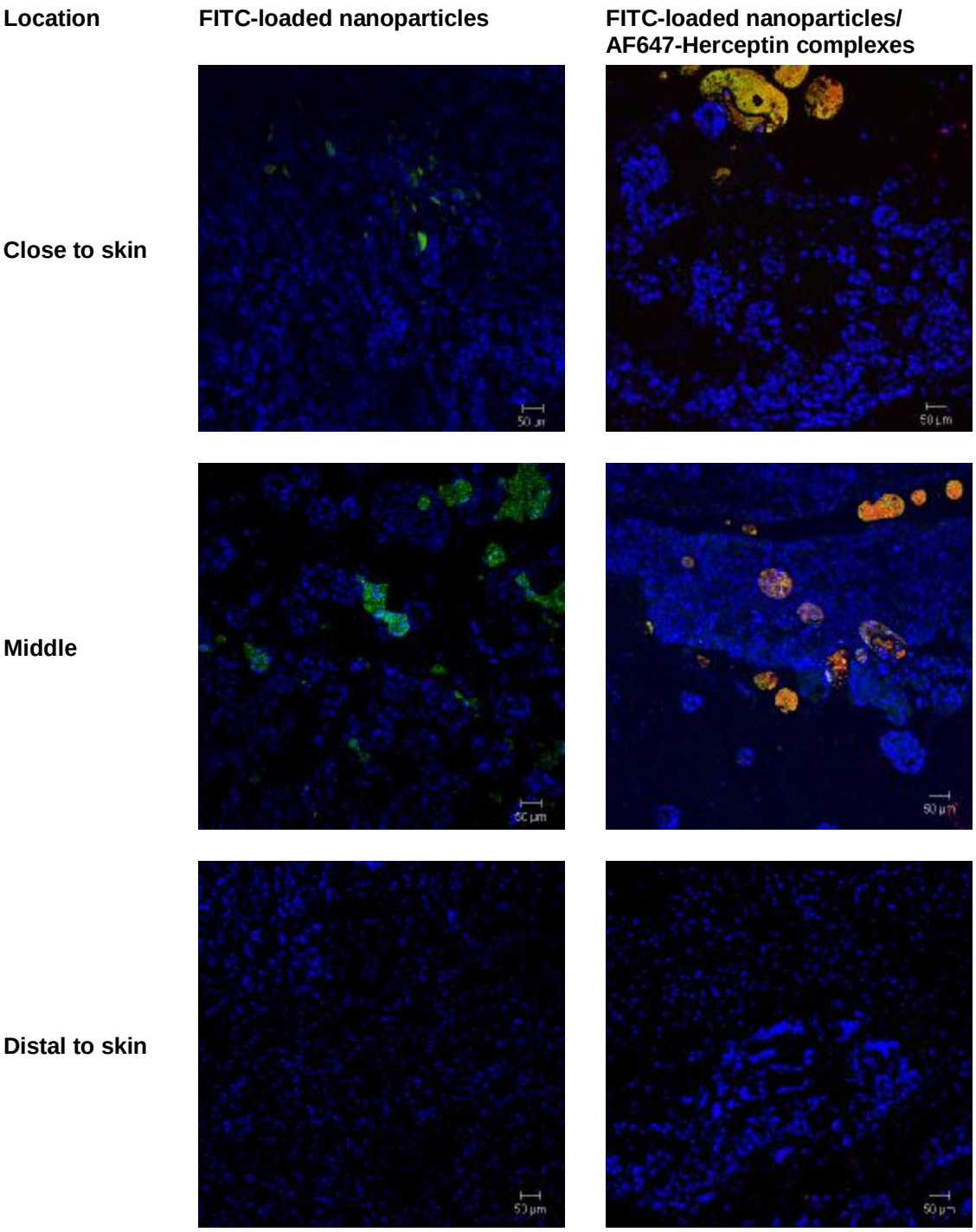

Figure 7.3 Distibution of nanocomplexes within tumor tissue 4 hr after intratumoral injection. Nuclei were stained blue with DAPI, and cellular distribution of Alexa Fluor 647-Herceptin and FITC-loaded P(MDS-*co*-CES) nanoparticles are shown as red and green fluorescence respectively. Yellow regions represent the co-localization of Herceptin and P(MDS-*co*-CES) nanoparticles in cells.

7.3 Conclusion

Non-invasive *in vivo* imaging demonstrates that delivery of nanoparticles using intratumoral injection may be more efficient than tail vein injection as it enables more nanoparticles to be accumulated within the tumor tissue compared to other organs. Treatment of BT474-tumor bearing nude mice shows that the codelivery of Herceptin and Pac shows significantly better anti-tumor efficacy compared to Pac-loaded nanoparticles alone. On the other hand, although the mean relative tumor size is lower for mice treated with the codelivery nanocomplexes compared to blank nanoparticles/Herceptin complexes, no significant difference is observed when assessed using statistical methods. The compromised therapeutic efficacy may be due to the self-aggregation of the nanoparticles within the tumor tissue, which led to limited penetration and non-uniform distribution to the cancer cells.

CHAPTER 8

CONCLUSIONS AND RECOMMENDATIONS

8.1 Conclusion

Over the past few decades, cancer therapy involving two or more therapeutic agents in combination has become widely accepted as a more effective treatment regimen compared to using single drugs. When chosen appropriately, interactions between different drugs can significantly improve the quality of life of patients by enhancing therapeutic efficacy and delaying disease progression. Side effects may also be reduced as lesser drugs of each kind will be required to achieve similar anti-cancer effects as the single drug formulation. Furthermore, based on the postulation that the probability of cancer cells developing resistance to a combination of non-cross-resistant drugs varies as the product of the probabilities of resistance to each of the individual drug, the use of drug combinations may help to lower the chances of developing multi-drug resistance.

This p.h.D. work has been designed to study the application of nanotechnology for advancing cancer treatment, particularly in development of nanoparticles as multifunctional vehicles for therapeutic protein and drug delivery. In my research, cationic core/shell nanoparticles self-assembled from a biodegradable amphiphilic copolymer poly{*N*-methyldietheneamine sebacate)-co-[(cholesteryl oxocarbonylamido ethyl) methyl bis(ethylene) ammonium bromide] sebacate}P(MDS-*co*-CES) have been fabricated and used for the codelivery of various anti-cancer drugs and therapeutic proteins to improve cancer therapy.

In the initial phase, the P(MDS-*co*-CES) cationic nanoparticles are investigated for their capacity to function as protein carriers. A model protein, Lectin A-chain, *Viscum*

album coloratum (Korean Mistletoe) is used for testing. This protein is unable to enter cells alone and its *in vitro* cytotoxicity is minimal when it is delivered without any carrier. Binding assays shows that the polymeric nanoparticles are able to complex with Lectin A-chain to form nano-sized complexes. When P(MDS-*co*-CES) nanoparticles were used to deliver Lectin A-chain, the cytotoxicity of the nanocomplexes is significantly increased. In addition, when compared to a commercially-available protein carrier, BioPorter, P(MDS-*co*-CES) nanoparticles also performed better with regards to particle size and stability as well as the intracellular delivery of the protein.

Protein-and-drug codelivery capabilities of P(MDS-*co*-CES) nanoparticles is then studied by delivering another therapeutic protein with a similar molecular weight, i.e. recombinant human tumor necrosis factor-related apoptosis-inducing ligand (TRAIL, MW: 20 kDa), and an anticancer drug doxorubicin (Dox) simultaneously. TRAIL is a promising therapeutic protein as it is selectively toxic to cancer cells and exerts limited toxicity to normal tissues when introduced *in viv*o. Cellular response towards the P(MDS-*co*-CES) nanoparticle/TRAIL nanocomplexes has been investigated in both wild type and TRAIL-resistant SW480 cells (a human colon adenocarcinoma cell line). Cytotoxicity studies have shown that the co-delivery system synergistically enhances cytotoxic and anti-proliferative effects in both wild type and TRAIL-resistant SW480 cells. Importantly, Dox-loaded nanoparticle/TRAIL nanocomplexes are toxic towards the cancer cells, but they do not exhibit significant cytotoxicity against non-cancerous cells (i.e. WI38, a human lung fibroblast cell line). In a separate study, TRAIL is codelivered with another anti-cancer drug, paclitaxel (Pac) and synergistic anti-cancer effects are observed on various human breast cancer cell lines with different TRAIL-sensitivity.

Cancer cells that are semi-sensitive to TRAIL responded positively to the combination treatment. *In vitro* cytotoxicity of the codelivery system is significantly higher compared to free Pac+TRAIL combination in two out of the three cell lines tested.

In addition, another important feature that is desirable for an effective drug delivery system is target-specificity. A therapeutic antibody, Herceptin (MW: 145 kDa), that recognizes human epidermal growth factor receptor-2 (HER2/neu) receptors, is loaded onto the surface of P(MDS-co-CES) nanoparticles and codelivered with Pac. The binding of herceptin to nanoparticles can confer targeting ability to the nanocomplexes and increase delivery of both the antibody and Pac to HER2-overexpressing cancer cells. When cell lines with different levels of HER2/neu expression are treated with the nanocomplexes, higher therapeutic efficacy is observed in cells with higher expression level. Targeting ability of this co-delivery system is demonstrated through confocal imaging, which shows significantly higher cellular uptake in HER2-overexpressing BT474 cells as compared to HER2-negative HEK293 cells.

Finally, tumor efficacy studies are performed using the Pac/Herceptin codelivery system to treat female athymic mice that bear BT474 tumor xenografts. Mice that are treated with Pac-loaded micelles/herceptin nanocomplexes experience significantly slower tumor growth compared to those treated with Pac-loaded nanoparticle alone. The development of this targeted co-delivery system from self-assembled polymeric nanoparticles demonstrates that it is possible to fabricate multifunctional vehicles that can be used ubiquitously for the simultaneous delivery of therapeutic agents of different chemical nature (i.e. proteins and hydrophobic drugs). Thereby, the realization of this co-

delivery system represents a comprehensive and effectual contribution towards combinational cancer therapy.

8.2 Recommendations

Enhancing therapeutic efficacy

The multifunctional nanoparticles developed from self-assembled P(MDS-*co*-CES) micelles showed that it can used for the simultaneous delivery of both for many therapeutic combinations of anti-cancer drug and proteins. To understand the actual therapeutic efficacy of the codelivery systems, Pac/Herceptin codelivery system has been selected amongst other *in vitro* system for tumor efficacy studies in the final phase of this p.h.D. work. The results obtained showed that treatment with Pac and Herceptin-containing nanocomplexes induced significantly slower tumor growth compared to those treated with Pac-loaded nanoparticle alone. However, the tumor growth difference between the codelivery system and Herceptin delivered using nanoparticles without Pac is not statistically significant. This shows that the *in vitro* synergistic interaction between the therapeutic drug and antibody is not able to translate to similar effects *in vivo* with the current treatment regimen. To improve on this, future studies may be performed by varying the treatment schedule to determine the optimal frequency of administrations. Alternatively, changing the loading levels of Pac and Herceptin may also influence the degree of drug interaction and therapeutic activities of the drug combinations.

Understanding potential immunotoxicity

When nanoparticles enter the bloodstream, they can stimulate and/or suppression of immune responses through binding of proteins in the blood. This is mostly determined by the proteins bound on the surface of these nanoparticles that can influence the interaction with other blood components and uptake of these particles into cells. In order for nanoparticles to enter the mainstream of chemotherapy, it is important to evaluate the potential effects they have will have on the immune system. It is known that several factors such as size, shape, chemical composition and surface modification of the nanoparticles can affect the biocompatibility. However, as the use of nanomaterials is considerably new for biomedical applications, there is still a lack of a universal guide for understanding of the immunotoxicity for such material. Nonetheless, a series of *in vitro* and *in vivo* assays can be performed to understand the biological and toxic properties. Some of the assays that can be performed include - hemolysis assay to test for the potential damage to red blood cells, platelet aggregation and plasma coagulation assays as well as pyrogenicity evaluation. By performing this comprehensive evaluation of immunotoxicity, this will allow a more extensive assessment of the therapeutic potential of the nanomaterial presented in this thesis.

REFERENCES

1. Goodman LS, Wintrobe MM, Dameshek W, Goodman MJ, Gilman A, McLennan MT. Landmark article Sept. 21, 1946: Nitrogen mustard therapy. Use of methyl-bis(beta-chloroethyl)amine hydrochloride and tris(beta-chloroethyl)amine hydrochloride for Hodgkin's disease, lymphosarcoma, leukemia and certain allied and miscellaneous disorders. By Louis S. Goodman, Maxwell M. Wintrobe, William Dameshek, Morton J. Goodman, Alfred Gilman and Margaret T. McLennan. JAMA 1984 May 4;251(17):2255-2261.
2. Farber S. others. Temporary remissions in acute leukemia in children produced by folic acid antagonist, 4-aminopteroylglutamic acid (aminopterin). New Engl J Med 1948;238:787-793.
3. Frei E, 3rd, Karon M, Levin RH, Freireich EJ, Taylor RJ, Hananian J, et al. The effectiveness of combinations of antileukemic agents in inducing and maintaining remission in children with acute leukemia. Blood 1965 Nov;26(5):642-656.
4. Breedveld FC. Therapeutic monoclonal antibodies. Lancet 2000 Feb 26;355(9205):735-740.
5. Allen TM, Cullis PR. Drug delivery systems: entering the mainstream. Science 2004 Mar 19;303(5665):1818-1822.
6. Gregoriadis G, Swain CP, Wills EJ, Tavill AS. Drug-carrier potential of liposomes in cancer chemotherapy. The Lancet 1974;303(7870):1313-1316.
7. Brasseur F, Couvreur P, Kante B, Deckers-Passau L, Roland M, Deckers C, et al. Actinomycin D adsorbed on polymethylcyanoacrylate nanoparticles: increased efficiency against an experimental tumor. European Journal of Cancer (1965) 1980;16(11):1441-1445.
8. Harris L, Batist G, Belt R, Rovira D, Navari R, Azarnia N, et al. Liposome-encapsulated doxorubicin compared with conventional doxorubicin in a randomized multicenter trial as first-line therapy of metastatic breast carcinoma. Cancer 2002 Jan 1;94(1):25-36.
9. Narta UK, Kanwar SS, Azmi W. Pharmacological and clinical evaluation of L-asparaginase in the treatment of leukemia. Crit Rev Oncol Hematol 2007 Mar;61(3):208-221.
10. Ho DH, Brown NS, Yen A, Holmes R, Keating M, Abuchowski A, et al. Clinical pharmacology of polyethylene glycol-L-asparaginase. Drug Metab Dispos 1986 May-Jun;14(3):349-352.
11. Ho EA, Soo PL, Allen C, Piquette-Miller M. Impact of intraperitoneal, sustained delivery of paclitaxel on the expression of P-glycoprotein in ovarian tumors. Journal of Controlled Release 2007;117(1):20-27.
12. Brigger I, Dubernet C, Couvreur P. Nanoparticles in cancer therapy and diagnosis. Advanced drug delivery reviews 2002;54(5):631-651.
13. Chavanpatil MD, Patil Y, Panyam J. Susceptibility of nanoparticle-encapsulated paclitaxel to P-glycoprotein-mediated drug efflux. International journal of pharmaceutics 2006;320(1-2):150-156.
14. Mayer LD, Harasym TO, Tardi PG, Harasym NL, Shew CR, Johnstone SA, et al. Ratiometric dosing of anticancer drug combinations: controlling drug ratios after

systemic administration regulates therapeutic activity in tumor-bearing mice. Molecular cancer therapeutics 2006;5(7):1854.
15. Harasym TO, Tardi PG, Harasym NL, Harvie P, Johnstone SA, Mayer LD. Increased preclinical efficacy of irinotecan and floxuridine coencapsulated inside liposomes is associated with tumor delivery of synergistic drug ratios. Oncology Research Featuring Preclinical and Clinical Cancer Therapeutics 2006;16(8):361-374.
16. Devita VT, Jr., Serpick AA, Carbone PP. Combination chemotherapy in the treatment of advanced Hodgkin's disease. Ann Intern Med 1970 Dec;73(6):881-895.
17. Teicher BA, Bonavida B. Sensitization of Cancer Cells for Chemo/Immuno/Radio-therapy. 2008.
18. Cunningham D, Humblet Y, Siena S, Khayat D, Bleiberg H, Santoro A, et al. Cetuximab monotherapy and cetuximab plus irinotecan in irinotecan-refractory metastatic colorectal cancer. N Engl J Med 2004 Jul 22;351(4):337-345.
19. O'Shaughnessy J, Miles D, Vukelja S, Moiseyenko V, Ayoub JP, Cervantes G, et al. Superior survival with capecitabine plus docetaxel combination therapy in anthracycline-pretreated patients with advanced breast cancer: phase III trial results. J Clin Oncol 2002 Jun 15;20(12):2812-2823.
20. Kabbinavar FF, Hambleton J, Mass RD, Hurwitz HI, Bergsland E, Sarkar S. Combined analysis of efficacy: the addition of bevacizumab to fluorouracil/leucovorin improves survival for patients with metastatic colorectal cancer. J Clin Oncol 2005 Jun 1;23(16):3706-3712.
21. Marty M, Cognetti F, Maraninchi D, Snyder R, Mauriac L, Tubiana-Hulin M, et al. Randomized phase II trial of the efficacy and safety of trastuzumab combined with docetaxel in patients with human epidermal growth factor receptor 2-positive metastatic breast cancer administered as first-line treatment: the M77001 study group. J Clin Oncol 2005 Jul 1;23(19):4265-4274.
22. Marcus R, Imrie K, Belch A, Cunningham D, Flores E, Catalano J, et al. CVP chemotherapy plus rituximab compared with CVP as first-line treatment for advanced follicular lymphoma. Blood 2005 Feb 15;105(4):1417-1423.
23. Sledge GW, Neuberg D, Bernardo P, Ingle JN, Martino S, Rowinsky EK, et al. Phase III trial of doxorubicin, paclitaxel, and the combination of doxorubicin and paclitaxel as front-line chemotherapy for metastatic breast cancer: an intergroup trial (E1193). J Clin Oncol 2003 Feb 15;21(4):588-592.
24. Dancey JE, Chen HX. Strategies for optimizing combinations of molecularly targeted anticancer agents. Nat Rev Drug Discov 2006 Aug;5(8):649-659.
25. Petitjean A, Achatz MI, Borresen-Dale AL, Hainaut P, Olivier M. TP53 mutations in human cancers: functional selection and impact on cancer prognosis and outcomes. Oncogene 2007 Apr 2;26(15):2157-2165.
26. Osborne CK, Shou J, Massarweh S, Schiff R. Crosstalk between estrogen receptor and growth factor receptor pathways as a cause for endocrine therapy resistance in breast cancer. Clin Cancer Res 2005 Jan 15;11(2 Pt 2):865s-870s.
27. Basu A, Castle VP, Bouziane M, Bhalla K, Haldar S. Crosstalk between extrinsic and intrinsic cell death pathways in pancreatic cancer: synergistic action of estrogen metabolite and ligands of death receptor family. Cancer Res 2006 Apr 15;66(8):4309-4318.

28. Kamb A, Wee S, Lengauer C. Why is cancer drug discovery so difficult? Nat Rev Drug Discov 2007 Feb;6(2):115-120.
29. Dean M, Fojo T, Bates S. Tumour stem cells and drug resistance. Nat Rev Cancer 2005 Apr;5(4):275-284.
30. Folkman J. Antiangiogenesis in cancer therapy--endostatin and its mechanisms of action. Exp Cell Res 2006 Mar 10;312(5):594-607.
31. Jonkers J, Berns A. Oncogene addiction: sometimes a temporary slavery. Cancer Cell 2004 Dec;6(6):535-538.
32. Kummar S, Kinders R, Rubinstein L, Parchment RE, Murgo AJ, Collins J, et al. Compressing drug development timelines in oncology using phase '0' trials. Nat Rev Cancer 2007 Feb;7(2):131-139.
33. Miller K, Wang M, Gralow J, Dickler M, Cobleigh M, Perez EA, et al. Paclitaxel plus bevacizumab versus paclitaxel alone for metastatic breast cancer. N Engl J Med 2007 Dec 27;357(26):2666-2676.
34. Skipper HE, Schabel FM, Jr., Wilcox WS. Experimental Evaluation of Potential Anticancer Agents. Xiii. On the Criteria and Kinetics Associated with "Curability" of Experimental Leukemia. Cancer Chemother Rep 1964 Feb;35:1-111.
35. Skipper HE, Griswold DP. Frank M. Schabel 1918-1983. Cancer Res 1984 Feb;44(2):871-872.
36. Chou TC. Theoretical basis, experimental design, and computerized simulation of synergism and antagonism in drug combination studies. Pharmacol Rev 2006 Sep;58(3):621-681.
37. Zimmermann GR, Lehar J, Keith CT. Multi-target therapeutics: when the whole is greater than the sum of the parts. Drug Discov Today 2007 Jan;12(1-2):34-42.
38. Weinstein IB, Joe AK. Mechanisms of disease: Oncogene addiction--a rationale for molecular targeting in cancer therapy. Nat Clin Pract Oncol 2006 Aug;3(8):448-457.
39. Schimke RT. Gene amplification, drug resistance, and cancer. Cancer Res 1984 May;44(5):1735-1742.
40. Jia J, Zhu F, Ma X, Cao Z, Li Y, Chen YZ. Mechanisms of drug combinations: interaction and network perspectives. Nat Rev Drug Discov 2009 Feb;8(2):111-128.
41. Ciardiello F, Caputo R, Bianco R, Damiano V, Pomatico G, De Placido S, et al. Antitumor effect and potentiation of cytotoxic drugs activity in human cancer cells by ZD-1839 (Iressa), an epidermal growth factor receptor-selective tyrosine kinase inhibitor. Clin Cancer Res 2000 May;6(5):2053-2063.
42. Motwani M, Delohery TM, Schwartz GK. Sequential dependent enhancement of caspase activation and apoptosis by flavopiridol on paclitaxel-treated human gastric and breast cancer cells. Clin Cancer Res 1999 Jul;5(7):1876-1883.
43. Huang S, Armstrong EA, Benavente S, Chinnaiyan P, Harari PM. Dual-agent molecular targeting of the epidermal growth factor receptor (EGFR): combining anti-EGFR antibody with tyrosine kinase inhibitor. Cancer Res 2004 Aug 1;64(15):5355-5362.
44. Yokoyama Y, Dhanabal M, Griffioen AW, Sukhatme VP, Ramakrishnan S. Synergy between angiostatin and endostatin: inhibition of ovarian cancer growth. Cancer Res 2000 Apr 15;60(8):2190-2196.

45. Nahta R, Hung MC, Esteva FJ. The HER-2-targeting antibodies trastuzumab and pertuzumab synergistically inhibit the survival of breast cancer cells. Cancer Res 2004 Apr 1;64(7):2343-2346.
46. Maeda H. SMANCS and polymer-conjugated macromolecular drugs: advantages in cancer chemotherapy. Adv Drug Deliv Rev 2001 Mar 1;46(1-3):169-185.
47. Suzuki M, Hori K, Abe I, Saito S, Sato H. A new approach to cancer chemotherapy: selective enhancement of tumor blood flow with angiotensin II. J Natl Cancer Inst 1981 Sep;67(3):663-669.
48. Ganapathi R, Grabowski D. Enhancement of sensitivity to adriamycin in resistant P388 leukemia by the calmodulin inhibitor trifluoperazine. Cancer Res 1983 Aug;43(8):3696-3699.
49. Meerum Terwogt JM, Malingre MM, Beijnen JH, ten Bokkel Huinink WW, Rosing H, Koopman FJ, et al. Coadministration of oral cyclosporin A enables oral therapy with paclitaxel. Clin Cancer Res 1999 Nov;5(11):3379-3384.
50. Tallarida RJ. Drug synergism: its detection and applications. J Pharmacol Exp Ther 2001 Sep;298(3):865-872.
51. Woolverton WL, Balster RL. Behavioral and lethal effects of combinations of oral ethanol and inhaled 1,1,1-trichloroethane in mice. Toxicol Appl Pharmacol 1981 Jun 15;59(1):1-7.
52. Zhao L, Au JL, Wientjes MG. Comparison of methods for evaluating drug-drug interaction. Front Biosci (Elite Ed) 2009
2:241-249.
53. Keith CT, Borisy AA, Stockwell BR. Multicomponent therapeutics for networked systems. Nat Rev Drug Discov 2005 Jan;4(1):71-78.
54. Fitzgerald JB, Schoeberl B, Nielsen UB, Sorger PK. Systems biology and combination therapy in the quest for clinical efficacy. Nat Chem Biol 2006 Sep;2(9):458-466.
55. Zhao L, Au JL, Wientjes MG. Comparison of methods for evaluating drug-drug interaction. Front Biosci (Elite Ed) 2009;2:241-249.
56. Zhao L, Wientjes MG, Au JL. Evaluation of combination chemotherapy: integration of nonlinear regression, curve shift, isobologram, and combination index analyses. Clin Cancer Res 2004 Dec 1;10(23):7994-8004.
57. Parkin DM, Bray F, Ferlay J, Pisani P. Global cancer statistics, 2002. CA Cancer J Clin 2005 Mar-Apr;55(2):74-108.
58. Poh TW, Huang S, Hirpara JL, Pervaiz S. LY303511 amplifies TRAIL-induced apoptosis in tumor cells by enhancing DR5 oligomerization, DISC assembly, and mitochondrial permeabilization. Cell Death Differ 2007 Oct;14(10):1813-1825.
59. Zhou P, Jiang W, Zhang YJ, Kahn SM, Schieren I, Santella RM, et al. Antisense to cyclin D1 inhibits growth and reverses the transformed phenotype of human esophageal cancer cells. Oncogene 1995 Aug 3;11(3):571-580.
60. Alas S, Emmanouilides C, Bonavida B. Inhibition of interleukin 10 by rituximab results in down-regulation of bcl-2 and sensitization of B-cell non-Hodgkin's lymphoma to apoptosis. Clin Cancer Res 2001 Mar;7(3):709-723.
61. Zhou Z, Jia SF, Hung MC, Kleinerman ES. E1A sensitizes HER2/neu-overexpressing Ewing's sarcoma cells to topoisomerase II-targeting anticancer drugs. Cancer Res 2001 Apr 15;61(8):3394-3398.

62. Roth JA, Swisher SG, Meyn RE. p53 tumor suppressor gene therapy for cancer. Oncology (Williston Park) 1999 Oct;13(10 Suppl 5):148-154.
63. Brickelmaier M, Carmillo A, Goelz S, Barsoum J, Qin XQ. Cytotoxicity of combinations of IFN-beta and chemotherapeutic drugs. J Interferon Cytokine Res 2002 Aug;22(8):873-880.
64. Wadler S, Schwartz EL. Antineoplastic activity of the combination of interferon and cytotoxic agents against experimental and human malignancies: a review. Cancer Res 1990 Jun 15;50(12):3473-3486.
65. Browder T, Butterfield CE, Kraling BM, Shi B, Marshall B, O'Reilly MS, et al. Antiangiogenic scheduling of chemotherapy improves efficacy against experimental drug-resistant cancer. Cancer Res 2000 Apr 1;60(7):1878-1886.
66. D'Haeseleer P, Liang S, Somogyi R. Genetic network inference: from co-expression clustering to reverse engineering. Bioinformatics 2000 Aug;16(8):707-726.
67. DeVita VT, Jr., Young RC, Canellos GP. Combination versus single agent chemotherapy: a review of the basis for selection of drug treatment of cancer. Cancer 1975 Jan;35(1):98-110.
68. Cheng MF, Chatterjee S, Berger NA. Schedule-dependent cytotoxicity of topotecan alone and in combination chemotherapy regimens. Oncol Res 1994;6(6):269-279.
69. Hryniuk W, Levine MN. Analysis of dose intensity for adjuvant chemotherapy trials in stage II breast cancer. J Clin Oncol 1986 Aug;4(8):1162-1170.
70. Hryniuk WM, Figueredo A, Goodyear M. Applications of dose intensity to problems in chemotherapy of breast and colorectal cancer. Semin Oncol 1987 Dec;14(4 Suppl 4):3-11.
71. Johnson IS, Armstrong JG, Gorman M, Burnett JP, Jr. The Vinca Alkaloids: A New Class of Oncolytic Agents. Cancer Res 1963 Sep;23:1390-1427.
72. Bensch KG, Malawista SE. Microtubule crystals: a new biophysical phenomenon induced by Vinca alkaloids. Nature 1968 Jun 22;218(5147):1176-1177.
73. Gibbs JB. Mechanism-based target identification and drug discovery in cancer research. Science 2000 Mar 17;287(5460):1969-1973.
74. Pavlou AK, Reichert JM. Recombinant protein therapeutics--success rates, market trends and values to 2010. Nat Biotechnol 2004 Dec;22(12):1513-1519.
75. Reichert JM, Wenger JB. Development trends for new cancer therapeutics and vaccines. Drug Discov Today 2008 Jan;13(1-2):30-37.
76. Reichert JM, Rosensweig CJ, Faden LB, Dewitz MC. Monoclonal antibody successes in the clinic. Nat Biotechnol 2005 Sep;23(9):1073-1078.
77. Banting FG, Best CH, Collip JB, Campbell WR, Fletcher AA. Pancreatic Extracts in the Treatment of Diabetes Mellitus. Can Med Assoc J 1922 Mar;12(3):141-146.
78. Nykiforuk CL, Boothe JG, Murray EW, Keon RG, Goren HJ, Markley NA, et al. Transgenic expression and recovery of biologically active recombinant human insulin from Arabidopsis thaliana seeds. Plant Biotechnol J 2006 Jan;4(1):77-85.
79. Boothe J, Nykiforuk C, Shen Y, Zaplachinski S, Szarka S, Kuhlman P, et al. Seed-based expression systems for plant molecular farming. Plant Biotechnol J 2010 Jun;8(5):588-606.
80. Hitchman RB, Possee RD, King LA. Baculovirus expression systems for recombinant protein production in insect cells. Recent Pat Biotechnol 2009;3(1):46-54.

81. Panahi M, Alli Z, Cheng X, Belbaraka L, Belgoudi J, Sardana R, et al. Recombinant protein expression plasmids optimized for industrial E. coli fermentation and plant systems produce biologically active human insulin-like growth factor-1 in transgenic rice and tobacco plants. Transgenic Res 2004 Jun;13(3):245-259.
82. Vermasvuori R, Koskinen J, Salonen K, Siren N, Weegar J, Dahlbacka J, et al. Production of recombinant HIV-1 nef protein using different expression host systems: a techno-economical comparison. Biotechnol Prog 2009 Jan-Feb;25(1):95-102.
83. Zang M, Trautmann H, Gandor C, Messi F, Asselbergs F, Leist C, et al. Production of recombinant proteins in Chinese hamster ovary cells using a protein-free cell culture medium. Biotechnology (N Y) 1995 Apr;13(4):389-392.
84. Wurm F, Bernard A. Large-scale transient expression in mammalian cells for recombinant protein production. Curr Opin Biotechnol 1999 Apr;10(2):156-159.
85. Baldi L, Hacker DL, Adam M, Wurm FM. Recombinant protein production by large-scale transient gene expression in mammalian cells: state of the art and future perspectives. Biotechnol Lett 2007 May;29(5):677-684.
86. Cereghino GP, Cregg JM. Applications of yeast in biotechnology: protein production and genetic analysis. Curr Opin Biotechnol 1999 Oct;10(5):422-427.
87. Leader B, Baca QJ, Golan DE. Protein therapeutics: a summary and pharmacological classification. Nat Rev Drug Discov 2008 Jan;7(1):21-39.
88. Fussenegger M, Bailey JE, Hauser H, Mueller PP. Genetic optimization of recombinant glycoprotein production by mammalian cells. Trends Biotechnol 1999 Jan;17(1):35-42.
89. Harris JM, Chess RB. Effect of pegylation on pharmaceuticals. Nat Rev Drug Discov 2003 Mar;2(3):214-221.
90. Kuo CJ, Farnebo F, Yu EY, Christofferson R, Swearingen RA, Carter R, et al. Comparative evaluation of the antitumor activity of antiangiogenic proteins delivered by gene transfer. Proc Natl Acad Sci U S A 2001 Apr 10;98(8):4605-4610.
91. Folkman J. Angiogenesis: an organizing principle for drug discovery? Nat Rev Drug Discov 2007 Apr;6(4):273-286.
92. Mountain A. Gene therapy: the first decade. Trends Biotechnol 2000 Mar;18(3):119-128.
93. Reichert JM. Trends in development and approval times for new therapeutics in the United States. Nat Rev Drug Discov 2003 Sep;2(9):695-702.
94. Putney SD, Burke PA. Improving protein therapeutics with sustained-release formulations. Nat Biotechnol 1998 Feb;16(2):153-157.
95. Cleland JL, Daugherty A, Mrsny R. Emerging protein delivery methods. Curr Opin Biotechnol 2001 Apr;12(2):212-219.
96. Morishita M, Peppas NA. Is the oral route possible for peptide and protein drug delivery? Drug Discov Today 2006 Oct;11(19-20):905-910.
97. De Groot AS, Scott DW. Immunogenicity of protein therapeutics. Trends Immunol 2007 Nov;28(11):482-490.
98. Vogel CL, Cobleigh MA, Tripathy D, Gutheil JC, Harris LN, Fehrenbacher L, et al. Efficacy and safety of trastuzumab as a single agent in first-line treatment of HER2-overexpressing metastatic breast cancer. J Clin Oncol 2002 Feb 1;20(3):719-726.

99. Medin JA, Hunt L, Gathy K, Evans RK, Coleman MS. Efficient, low-cost protein factories: expression of human adenosine deaminase in baculovirus-infected insect larvae. Proc Natl Acad Sci U S A 1990 Apr;87(7):2760-2764.
100. Maiorella B, Inlow D, Shauger A, Harano D. Large-scale insect cell-culture for recombinant protein production. Nature Biotechnology 1988;6(12):1406-1410.
101. Wurm FM. Production of recombinant protein therapeutics in cultivated mammalian cells. Nat Biotechnol 2004 Nov;22(11):1393-1398.
102. Linnankoski J, Makela J, Palmgren J, Mauriala T, Vedin C, Ungell AL, et al. Paracellular porosity and pore size of the human intestinal epithelium in tissue and cell culture models. J Pharm Sci Apr;99(4):2166-2175.
103. Goldberg M, Gomez-Orellana I. Challenges for the oral delivery of macromolecules. Nat Rev Drug Discov 2003 Apr;2(4):289-295.
104. Woodley JF. Enzymatic barriers for GI peptide and protein delivery. Crit Rev Ther Drug Carrier Syst 1994;11(2-3):61-95.
105. Fasano A, Uzzau S. Modulation of intestinal tight junctions by Zonula occludens toxin permits enteral administration of insulin and other macromolecules in an animal model. J Clin Invest 1997 Mar 15;99(6):1158-1164.
106. Yen WC, Lee VHL. Penetration enhancement effect of Pz-peptide, a paracellularly transported peptide, in rabbit intestinal segments and Caco-2 cell monolayers. Journal of Controlled Release 1995;36(1-2):25-37.
107. Salamat-Miller N, Johnston TP. Current strategies used to enhance the paracellular transport of therapeutic polypeptides across the intestinal epithelium. Int J Pharm 2005 Apr 27;294(1-2):201-216.
108. Pan Y, Li YJ, Zhao HY, Zheng JM, Xu H, Wei G, et al. Bioadhesive polysaccharide in protein delivery system: chitosan nanoparticles improve the intestinal absorption of insulin in vivo. Int J Pharm 2002 Dec 5;249(1-2):139-147.
109. Ma Z, Lim TM, Lim LY. Pharmacological activity of peroral chitosan-insulin nanoparticles in diabetic rats. International journal of pharmaceutics 2005;293(1-2):271-280.
110. Foss AC, Goto T, Morishita M, Peppas NA. Development of acrylic-based copolymers for oral insulin delivery. Eur J Pharm Biopharm 2004 Mar;57(2):163-169.
111. Van den Mooter G, Kinget R. Oral colon-specific drug delivery: a review. Drug delivery 1995;2(2):81-93.
112. Habberfield A, Jensen-Pippo K, Ralph L, Westwood SW, Russell-Jones GJ. Vitamin B12-mediated uptake of recombinant therapeutic proteins from the gut. Int J Pharm 1996;145:1-8.
113. Han HK, Amidon GL. Targeted prodrug design to optimize drug delivery. AAPS PharmSci 2000;2(1):E6.
114. Elliott S, Lorenzini T, Asher S, Aoki K, Brankow D, Buck L, et al. Enhancement of therapeutic protein in vivo activities through glycoengineering. Nature Biotechnology 2003;21(4):414-421.
115. Osborn BL, Olsen HS, Nardelli B, Murray JH, Zhou JX, Garcia A, et al. Pharmacokinetic and pharmacodynamic studies of a human serum albumin-interferon-alpha fusion protein in cynomolgus monkeys. J Pharmacol Exp Ther 2002 Nov;303(2):540-548.

116. Jin X, Zhang X, Wu Z, Teng D, Wang Y, Wang Z, et al. Amphiphilic Random Glycopolymer Based on Phenylboronic Acid: Synthesis, Characterization, and Potential as Glucose-Sensitive Matrix. Biomacromolecules 2009;10(6):1337-1345.
117. Hoare T, Pelton R. Charge-switching, amphoteric glucose-responsive microgels with physiological swelling activity. Biomacromolecules 2008 Feb;9(2):733-740.
118. Boven K, Stryker S, Knight J, Thomas A, van Regenmortel M, Kemeny DM, et al. The increased incidence of pure red cell aplasia with an Eprex formulation in uncoated rubber stopper syringes. Kidney Int 2005 Jun;67(6):2346-2353.
119. Coscelli C, Lostia S, Lunetta M, Nosari I, Coronel GA. Safety, efficacy, acceptability of a pre-filled insulin pen in diabetic patients over 60 years old. Diabetes Res Clin Pract 1995 Jun;28(3):173-177.
120. Griffin S, Hieronymus L. Insulin delivery devices. Diabetes Self Manag 2007 Jul-Aug;24(4):14, 16, 19-22.
121. Mitragotri S. Current status and future prospects of needle-free liquid jet injectors. Nat Rev Drug Discov 2006 Jul;5(7):543-548.
122. Verhagen A, Ebels JT, Dogterom AA, Jonkman JH. Pharmacokinetics and pharmacodynamics of a single dose of recombinant human growth hormone after subcutaneous administration by jet-injection: comparison with conventional needle-injection. Eur J Clin Pharmacol 1995;49(1-2):69-72.
123. Bareille P, MacSwiney M, Albanese A, De Vile C, Stanhope R. Growth hormone treatment without a needle using the Preci-Jet 50 transjector. Archives of disease in childhood 1997;76(1):65.
124. Suzuki T, Takahashi I, Takada G. Daily subcutaneous erythropoietin by jet injection in pediatric dialysis patients. Nephron 1995;69(3):347.
125. Karande P, Jain A, Ergun K, Kispersky V, Mitragotri S. Design principles of chemical penetration enhancers for transdermal drug delivery. Proc Natl Acad Sci U S A 2005 Mar 29;102(13):4688-4693.
126. Ledger PW. Skin biological issues in electrically enhanced transdermal delivery. Advanced Drug Delivery Reviews 1992;9(2-3):289-307.
127. Denet AR, Vanbever R, Préat V. Skin electroporation for transdermal and topical delivery. Advanced Drug Delivery Reviews 2004;56(5):659-674.
128. Mitragotri S, Blankschtein D, Langer R. Ultrasound-mediated transdermal protein delivery. Science 1995 Aug 11;269(5225):850-853.
129. Banga AK, Prausnitz MR. Assessing the potential of skin electroporation for the delivery of protein- and gene-based drugs. Trends Biotechnol 1998 Oct;16(10):408-412.
130. Prausnitz MR, Mitragotri S, Langer R. Current status and future potential of transdermal drug delivery. Nat Rev Drug Discov 2004 Feb;3(2):115-124.
131. McAllister DV, Wang PM, Davis SP, Park JH, Canatella PJ, Allen MG, et al. Microfabricated needles for transdermal delivery of macromolecules and nanoparticles: fabrication methods and transport studies. Proceedings of the National Academy of Sciences of the United States of America 2003;100(24):13755.
132. Prausnitz MR, Langer R. Transdermal drug delivery. Nat Biotechnol 2008 Nov;26(11):1261-1268.
133. Donner B, Zenz M, Strumpf M, Raber M. Long-term treatment of cancer pain with transdermal fentanyl. Journal of pain and symptom management 1998;15(3):168-175.

134. Sloan PA, Moulin DE, Hays H. A clinical evaluation of transdermal therapeutic system fentanyl for the treatment of cancer pain. J Pain Symptom Manage 1998 Aug;16(2):102-111.
135. Hussain A, Arnold JJ, Khan MA, Ahsan F. Absorption enhancers in pulmonary protein delivery. J Control Release 2004 Jan 8;94(1):15-24.
136. Shoyele SA, Slowey A. Prospects of formulating proteins/peptides as aerosols for pulmonary drug delivery. International journal of pharmaceutics 2006;314(1):1-8.
137. Quattrin T, Belanger A, Bohannon NJ, Schwartz SL. Efficacy and safety of inhaled insulin (Exubera) compared with subcutaneous insulin therapy in patients with type 1 diabetes: results of a 6-month, randomized, comparative trial. Diabetes Care 2004 Nov;27(11):2622-2627.
138. Hollander PA, Blonde L, Rowe R, Mehta AE, Milburn JL, Hershon KS, et al. Efficacy and safety of inhaled insulin (exubera) compared with subcutaneous insulin therapy in patients with type 2 diabetes: results of a 6-month, randomized, comparative trial. Diabetes Care 2004 Oct;27(10):2356-2362.
139. Steckel H, Eskandar F, Witthohn K. The effect of formulation variables on the stability of nebulized aviscumine. International journal of pharmaceutics 2003;257(1-2):181-194.
140. Bitonti AJ, Dumont JA, Low SC, Peters RT, Kropp KE, Palombella VJ, et al. Pulmonary delivery of an erythropoietin Fc fusion protein in non-human primates through an immunoglobulin transport pathway. Proceedings of the National Academy of Sciences of the United States of America 2004;101(26):9763.
141. Patton JS. Pulmonary delivery of drugs for bone disorders. Adv Drug Deliv Rev 2000 Aug 31;42(3):239-248.
142. Sharma S, White D, Imondi AR, Placke ME, Vail DM, Kris MG. Development of inhalational agents for oncologic use. Journal of Clinical Oncology 2001;19(6):1839.
143. Aulton ME, Cooper JW. Pharmaceutics: the science of dosage form design. 2002.
144. Timsina MP, Martin GP, Marriott C, Ganderton D, Yianneskis M. Drug delivery to the respiratory tract using dry powder inhalers. International journal of pharmaceutics 1994;101(1-2):1-13.
145. von Pawel J, Gatzemeier U, Pujol JL, Moreau L, Bildat S, Ranson M, et al. Phase ii comparator study of oral versus intravenous topotecan in patients with chemosensitive small-cell lung cancer. J Clin Oncol 2001 Mar 15;19(6):1743-1749.
146. Eckardt JR, von Pawel J, Pujol JL, Papai Z, Quoix E, Ardizzoni A, et al. Phase III study of oral compared with intravenous topotecan as second-line therapy in small-cell lung cancer. Journal of Clinical Oncology 2007;25(15):2086.
147. O'Neill VJ, Twelves CJ. Oral cancer treatment: developments in chemotherapy and beyond. Br J Cancer 2002 Oct 21;87(9):933-937.
148. Yoon TJ, Yoo YC, Kang TB, Shimazaki K, Song SK, Lee KH, et al. Lectins isolated from Korean mistletoe (Viscum album coloratum) induce apoptosis in tumor cells. Cancer Lett 1999 Feb 8;136(1):33-40.
149. Vervecken W, Kleff S, Pfuller U, Bussing A. Induction of apoptosis by mistletoe lectin I and its subunits. No evidence for cytotoxic effects caused by isolated A- and B-chains. Int J Biochem Cell Biol 2000 Mar;32(3):317-326.

150. Endo Y, Tsurugi K, Franz H. The site of action of the A-chain of mistletoe lectin I on eukaryotic ribosomes. The RNA N-glycosidase activity of the protein. FEBS Lett 1988 Apr 25;231(2):378-380.
151. Lee SC, Huh KM, Lee J, Cho YW, Galinsky RE, Park K. Hydrotropic polymeric micelles for enhanced paclitaxel solubility: in vitro and in vivo characterization. Biomacromolecules 2007;8(1):202-208.
152. Gelderblom H, Verweij J, Nooter K, Sparreboom A. Cremophor EL: the drawbacks and advantages of vehicle selection for drug formulation. Eur J Cancer 2001 Sep;37(13):1590-1598.
153. Weiss RB, Donehower RC, Wiernik PH, Ohnuma T, Gralla RJ, Trump DL, et al. Hypersensitivity reactions from taxol. J Clin Oncol 1990 Jul;8(7):1263-1268.
154. Eisenhauer EA, ten Bokkel Huinink WW, Swenerton KD, Gianni L, Myles J, Van der Burg ME, et al. European-Canadian randomized trial of paclitaxel in relapsed ovarian cancer: high-dose versus low-dose and long versus short infusion. Journal of Clinical Oncology 1994;12(12):2654.
155. Hidalgo M, Aylesworth C, Hammond LA, Britten CD, Weiss G, Stephenson J, Jr., et al. Phase I and pharmacokinetic study of BMS-184476, a taxane with greater potency and solubility than paclitaxel. J Clin Oncol 2001 May 1;19(9):2493-2503.
156. Plummer R, Ghielmini M, Calvert P, Voi M, Renard J, Gallant G, et al. Phase I and pharmacokinetic study of the new taxane analog BMS-184476 given weekly in patients with advanced malignancies. Clin Cancer Res 2002 Sep;8(9):2788-2797.
157. Pasut G, Veronese FM. PEG conjugates in clinical development or use as anticancer agents: An overview. Advanced Drug Delivery Reviews 2009;61(13):1177-1188.
158. Nakanishi T, Fukushima S, Okamoto K, Suzuki M, Matsumura Y, Yokoyama M, et al. Development of the polymer micelle carrier system for doxorubicin. Journal of Controlled Release 2001;74(1-3):295-302.
159. Kim TY, Kim DW, Chung JY, Shin SG, Kim SC, Heo DS, et al. Phase I and pharmacokinetic study of Genexol-PM, a cremophor-free, polymeric micelle-formulated paclitaxel, in patients with advanced malignancies. Clinical cancer research 2004;10(11):3708.
160. Lee KS, Chung HC, Im SA, Park YH, Kim CS, Kim SB, et al. Multicenter phase II trial of Genexol-PM, a Cremophor-free, polymeric micelle formulation of paclitaxel, in patients with metastatic breast cancer. Breast cancer research and treatment 2008;108(2):241-250.
161. Yoo HS, Park TG. Folate receptor targeted biodegradable polymeric doxorubicin micelles. Journal of Controlled Release 2004;96(2):273-283.
162. Vasey PA, Kaye SB, Morrison R, Twelves C, Wilson P, Duncan R, et al. Phase I clinical and pharmacokinetic study of PK1 [N-(2-hydroxypropyl) methacrylamide copolymer doxorubicin]: first member of a new class of chemotherapeutic agents—drug-polymer conjugates. Clinical cancer research 1999;5(1):83.
163. Meerum Terwogt JM, ten Bokkel Huinink WW, Schellens JHM, Schot M, Mandjes IAM, Zurlo MG, et al. Phase I clinical and pharmacokinetic study of PNU166945, a novel water-soluble polymer-conjugated prodrug of paclitaxel. Anti-Cancer Drugs 2001;12(4):315.

164. Boddy AV, Plummer ER, Todd R, Sludden J, Griffin M, Robson L, et al. A phase I and pharmacokinetic study of paclitaxel poliglumex (XYOTAX), investigating both 3-weekly and 2-weekly schedules. Clinical cancer research 2005;11(21):7834.
165. Kojima C, Kono K, Maruyama K, Takagishi T. Synthesis of polyamidoamine dendrimers having poly (ethylene glycol) grafts and their ability to encapsulate anticancer drugs. Bioconjugate Chem 2000;11(6):910-917.
166. Singh P, Gupta U, Asthana A, Jain NK. Folate and Folate- PEG- PAMAM Dendrimers: Synthesis, Characterization, and Targeted Anticancer Drug Delivery Potential in Tumor Bearing Mice. Bioconjugate chemistry 2008;19(11):2239-2252.
167. Mrozek E, Rhoades CA, Allen J, Hade EM, Shapiro CL. Phase I trial of liposomal encapsulated doxorubicin (Myocet™; D-99) and weekly docetaxel in advanced breast cancer patients. Annals of Oncology 2005;16(7):1087.
168. Gibbs DD, Pyle L, Allen M, Vaughan M, Webb A, Johnston SRD, et al. A phase I dose-finding study of a combination of pegylated liposomal doxorubicin (Doxil), carboplatin and paclitaxel in ovarian cancer. British journal of cancer 2002;86(9):1379-1384.
169. Yang T, Choi MK, Cui FD, Kim JS, Chung SJ, Shim CK, et al. Preparation and evaluation of paclitaxel-loaded PEGylated immunoliposome. Journal of Controlled Release 2007;120(3):169-177.
170. Kirpotin DB, Drummond DC, Shao Y, Shalaby MR, Hong K, Nielsen UB, et al. Antibody targeting of long-circulating lipidic nanoparticles does not increase tumor localization but does increase internalization in animal models. Cancer research 2006;66(13):6732.
171. Tong GJ, Hsiao SC, Carrico ZM, Francis MB. Viral capsid DNA aptamer conjugates as multivalent cell-targeting vehicles. Journal of the American Chemical Society 2009;131(31):11174-11178.
172. Destito G, Yeh R, Rae CS, Finn MG, Manchester M. Folic acid-mediated targeting of cowpea mosaic virus particles to tumor cells. Chem Biol 2007 Oct;14(10):1152-1162.
173. Feazell RP, Nakayama-Ratchford N, Dai H, Lippard SJ. Soluble single-walled carbon nanotubes as longboat delivery systems for platinum (IV) anticancer drug design. J Am Chem Soc 2007;129(27):8438-8439.
174. Liu Z, Sun X, Nakayama-Ratchford N, Dai H. Supramolecular chemistry on water-soluble carbon nanotubes for drug loading and delivery. Acs Nano 2007;1(1):50-56.
175. Liu Z, Chen K, Davis C, Sherlock S, Cao Q, Chen X, et al. Drug delivery with carbon nanotubes for in vivo cancer treatment. Cancer research 2008;68(16):6652.
176. Morgillo F, Lee HY. Resistance to epidermal growth factor receptor-targeted therapy. Drug Resistance Updates 2005;8(5):298-310.
177. Chen CD, Welsbie DS, Tran C, Baek SH, Chen R, Vessella R, et al. Molecular determinants of resistance to antiandrogen therapy. Nature medicine 2003;10(1):33-39.
178. Cho K, Wang X, Nie S, Chen ZG, Shin DM. Therapeutic nanoparticles for drug delivery in cancer. Clin Cancer Res 2008 Mar 1;14(5):1310-1316.
179. Choi HS, Liu W, Misra P, Tanaka E, Zimmer JP, Ipe BI, et al. Renal clearance of quantum dots. Nature Biotechnology 2007;25(10):1165-1170.

180. Storm G, Belliot SO, Daemen T, Lasic DD. Surface modification of nanoparticles to oppose uptake by the mononuclear phagocyte system. Advanced Drug Delivery Reviews 1995;17(1):31-48.
181. Veronese FM, Pasut G. PEGylation, successful approach to drug delivery. Drug discovery today 2005;10(21):1451-1458.
182. Gref R, Domb A, Quellec P, Blunk T, Müller RH, Verbavatz JM, et al. The controlled intravenous delivery of drugs using PEG-coated sterically stabilized nanospheres. Advanced Drug Delivery Reviews 1995;16(2-3):215-233.
183. Duncan R. The dawning era of polymer therapeutics. Nature Reviews Drug Discovery 2003;2(5):347-360.
184. Li C. Poly (-glutamic acid)-anticancer drug conjugates. Advanced Drug Delivery Reviews 2002;54(5):695-713.
185. Soppimath KS, Aminabhavi TM, Kulkarni AR, Rudzinski WE. Biodegradable polymeric nanoparticles as drug delivery devices. Journal of Controlled Release 2001;70(1-2):1-20.
186. Lavasanifar A, Samuel J, Kwon GS. Poly (ethylene oxide)-block-poly (-amino acid) micelles for drug delivery. Advanced Drug Delivery Reviews 2002;54(2):169-190.
187. Nagarajan R, Barry M, Ruckenstein E. Unusual selectivity in solubilization by block copolymer micelles. Langmuir 1986;2(2):210-215.
188. Puri S, Kallinteri P, Higgins S, Hutcheon GA, Garnett MC. Drug incorporation and release of water soluble drugs from novel functionalised poly (glycerol adipate) nanoparticles. Journal of Controlled Release 2008;125(1):59-67.
189. Oh I, Lee K, Kwon HY, Lee YB, Shin SC, Cho CS, et al. Release of adriamycin from poly ([gamma]-benzyl--glutamate)/poly (ethylene oxide) nanoparticles. International journal of pharmaceutics 1999;181(1):107-115.
190. Kukowska-Latallo JF, Candido KA, Cao Z, Nigavekar SS, Majoros IJ, Thomas TP, et al. Nanoparticle targeting of anticancer drug improves therapeutic response in animal model of human epithelial cancer. Cancer research 2005;65(12):5317.
191. Yuan F, Dellian M, Fukumura D, Leunig M, Berk DA, Torchilin VP, et al. Vascular permeability in a human tumor xenograft: molecular size dependence and cutoff size. Cancer research 1995;55(17):3752.
192. Maeda H, Matsumura Y. Tumoritropic and lymphotropic principles of macromolecular drugs. Critical reviews in therapeutic drug carrier systems 1989;6(3):193.
193. Hobbs SK, Monsky WL, Yuan F, Roberts WG, Griffith L, Torchilin VP, et al. Regulation of transport pathways in tumor vessels: role of tumor type and microenvironment. Proceedings of the National Academy of Sciences of the United States of America 1998;95(8):4607.
194. Shubik P. Vascularization of tumors: a review. Journal of cancer research and clinical oncology 1982;103(3):211-226.
195. Carmeliet P, Jain RK. Angiogenesis in cancer and other diseases. Nature 2000 Sep 14;407(6801):249-257.
196. Iyer AK, Khaled G, Fang J, Maeda H. Exploiting the enhanced permeability and retention effect for tumor targeting. Drug discovery today 2006;11(17-18):812-818.

197. Sinha R, Kim GJ, Nie S, Shin DM. Nanotechnology in cancer therapeutics: bioconjugated nanoparticles for drug delivery. Molecular cancer therapeutics 2006;5(8):1909.
198. Thurston G, McLean JW, Rizen M, Baluk P, Haskell A, Murphy TJ, et al. Cationic liposomes target angiogenic endothelial cells in tumors and chronic inflammation in mice. J Clin Invest 1998 Apr 1;101(7):1401-1413.
199. Krasnici S, Werner A, Eichhorn ME, Schmitt Sody M, Pahernik SA, Sauer B, et al. Effect of the surface charge of liposomes on their uptake by angiogenic tumor vessels. International journal of cancer 2003;105(4):561-567.
200. Byrne JD, Betancourt T, Brannon-Peppas L. Active targeting schemes for nanoparticle systems in cancer therapeutics. Advanced Drug Delivery Reviews 2008;60(15):1615-1626.
201. Allen TM. Ligand-targeted therapeutics in anticancer therapy. Nature Reviews Cancer 2002;2(10):750-763.
202. Zhang Z, Huey Lee S, Feng SS. Folate-decorated poly (lactide-co-glycolide)-vitamin E TPGS nanoparticles for targeted drug delivery. Biomaterials 2007;28(10):1889-1899.
203. Soppimath KS, Liu LH, Seow WY, Liu SQ, Powell R, Chan P, et al. Multifunctional Core/Shell Nanoparticles Self Assembled from pH Induced Thermosensitive Polymers for Targeted Intracellular Anticancer Drug Delivery. Advanced Functional Materials 2007;17(3):355-362.
204. Kobayashi T, Ishida T, Okada Y, Ise S, Harashima H, Kiwada H. Effect of transferrin receptor-targeted liposomal doxorubicin in P-glycoprotein-mediated drug resistant tumor cells. International journal of pharmaceutics 2007;329(1-2):94-102.
205. De Villiers MM, Aramwit P, Kwon GS. Nanotechnology in drug delivery: Springer Verlag, 2008.
206. Kakizawa Y, Kataoka K. Block copolymer micelles for delivery of gene and related compounds. Advanced drug delivery reviews 2002;54(2):203-222.
207. Yezhelyev MV, Qi L, O'Regan RM, Nie S, Gao X. Proton-sponge coated quantum dots for siRNA delivery and intracellular imaging. Journal of the American Chemical Society 2008;130(28):9006-9012.
208. Popielarski SR, Hu-Lieskovan S, French SW, Triche TJ, Davis ME. A nanoparticle-based model delivery system to guide the rational design of gene delivery to the liver. 2. In vitro and in vivo uptake results. Bioconjugate Chem 2005;16(5):1071-1080.
209. Jeong YI, Seo SJ, Park IK, Lee HC, Kang IC, Akaike T, et al. Cellular recognition of paclitaxel-loaded polymeric nanoparticles composed of poly ([gamma]-benzyl l-glutamate) and poly (ethylene glycol) diblock copolymer endcapped with galactose moiety. International journal of pharmaceutics 2005;296(1-2):151-161.
210. Bellocq NC, Pun SH, Jensen GS, Davis ME. Transferrin-containing, cyclodextrin polymer-based particles for tumor-targeted gene delivery. Bioconjugate Chem 2003;14(6):1122-1132.
211. Ishida O, Maruyama K, Tanahashi H, Iwatsuru M, Sasaki K, Eriguchi M, et al. Liposomes bearing polyethyleneglycol-coupled transferrin with intracellular targeting property to the solid tumors in vivo. Pharmaceutical research 2001;18(7):1042-1048.

212. Yamazaki N, Kojima S, Bovin NV, Andre S, Gabius S, Gabius HJ. Endogenous lectins as targets for drug delivery. Advanced Drug Delivery Reviews 2000;43(2-3):225-244.
213. Pirollo KF, Chang EH. Does a targeting ligand influence nanoparticle tumor localization or uptake? Trends in biotechnology 2008;26(10):552-558.
214. Goren D, Horowitz AT, Zalipsky S, Woodle MC, Yarden Y, Gabizon A. Targeting of stealth liposomes to erbB-2 (Her/2) receptor: in vitro and in vivo studies. British journal of cancer 1996;74(11):1749.
215. Park JW, Kirpotin DB, Hong K, Shalaby R, Shao Y, Nielsen UB, et al. Tumor targeting using anti-her2 immunoliposomes. Journal of Controlled Release 2001;74(1-3):95-113.
216. Chapman AP. PEGylated antibodies and antibody fragments for improved therapy: a review. Advanced Drug Delivery Reviews 2002;54(4):531-545.
217. Kumar S, Li C. Targeting of vasculature in cancer and other angiogenic diseases. Trends in immunology 2001;22(3):129.
218. Ishihara K, Kamata M, Hayashi I, Yamashina S, Majima M. Roles of bradykinin in vascular permeability and angiogenesis in solid tumor. International immunopharmacology 2002;2(4):499-509.
219. Zambaux MF, Bonneaux F, Gref R, Maincent P, Dellacherie E, Alonso MJ, et al. Influence of experimental parameters on the characteristics of poly (lactic acid) nanoparticles prepared by a double emulsion method. Journal of Controlled Release 1998;50(1-3):31-40.
220. Tan CJ, Wangrangsimakul S, Bai R, Tong YW. Defining the interactions between proteins and surfactants for nanoparticle surface imprinting through miniemulsion polymerization. Chemistry of Materials 2007;20(1):118-127.
221. Bilati U, Allémann E, Doelker E. Development of a nanoprecipitation method intended for the entrapment of hydrophilic drugs into nanoparticles. European Journal of Pharmaceutical Sciences 2005;24(1):67-75.
222. Allemann E, Leroux JC, Gurny R, Doelker E. In vitro extended-release properties of drug-loaded poly (DL-lactic acid) nanoparticles produced by a salting-out procedure. Pharmaceutical research 1993;10(12):1732-1737.
223. Bilati U, Allémann E, Doelker E. Sonication Parameters for the Preparation of Biodegradable Nanocapsulesof Controlled Size by the Double Emulsion Method. Pharmaceutical development and technology 2003;8(1):1-9.
224. Zambaux MF, Bonneaux F, Gref R, Dellacherie E, Vigneron C. Preparation and characterization of protein C-loaded PLA nanoparticles. Journal of Controlled Release 1999;60(2-3):179-188.
225. Davda J, Labhasetwar V. Characterization of nanoparticle uptake by endothelial cells. International journal of pharmaceutics 2002;233(1-2):51-59.
226. Barichello JM, Morishita M, Takayama K, Nagai T. Encapsulation of hydrophilic and lipophilic drugs in PLGA nanoparticles by the nanoprecipitation method. Drug development and industrial pharmacy 1999;25(4):471-476.
227. Cai C, Bakowsky U, Rytting E, Schaper AK, Kissel T. Charged nanoparticles as protein delivery systems: a feasibility study using lysozyme as model protein. European journal of pharmaceutics and biopharmaceutics 2008;69(1):31-42.

228. Bayraktar H, You CC, Rotello VM, Knapp MJ. Facial control of nanoparticle binding to cytochrome C. J Am Chem Soc 2007 Mar 14;129(10):2732-2733.
229. Lee Y, Fukushima S, Bae Y, Hiki S, Ishii T, Kataoka K. A protein nanocarrier from charge-conversion polymer in response to endosomal pH. J Am Chem Soc 2007;129(17):5362-5363.
230. Becker JC, Varki N, Gillies SD, Furukawa K, Reisfeld RA. An antibody-interleukin 2 fusion protein overcomes tumor heterogeneity by induction of a cellular immune response. Proceedings of the National Academy of Sciences of the United States of America 1996;93(15):7826.
231. Sharma SK, Pedley RB, Bhatia J, Boxer GM, El-Emir E, Qureshi U, et al. Sustained tumor regression of human colorectal cancer xenografts using a multifunctional mannosylated fusion protein in antibody-directed enzyme prodrug therapy. Clinical Cancer Research 2005;11(2):814.
232. Boado RJ, Zhang Y, Pardridge WM. Genetic engineering, expression, and activity of a fusion protein of a human neurotrophin and a molecular Trojan horse for delivery across the human blood-brain barrier. Biotechnology and bioengineering 2007;97(6):1376-1386.
233. Roberts MJ, Bentley MD, Harris JM. Chemistry for peptide and protein PEGylation. Advanced drug delivery reviews 2002;54(4):459-476.
234. Bontempo D, Heredia KL, Fish BA, Maynard HD. Cysteine-reactive polymers synthesized by atom transfer radical polymerization for conjugation to proteins. J Am Chem Soc 2004;126(47):15372-15373.
235. Al-Tahami K, Singh J. Smart polymer based delivery systems for peptides and proteins. Recent Patents on Drug Delivery &# 38; Formulation 2007;1(1):65-71.
236. Stefanadis C, Chrysochoou C, Markou D, Petraki K, Panagiotakos DB, Fasoulakis C, et al. Increased temperature of malignant urinary bladder tumors in vivo: the application of a new method based on a catheter technique. Journal of Clinical Oncology 2001;19(3):676.
237. Gerweck LE, Seetharaman K. Cellular pH gradient in tumor versus normal tissue: potential exploitation for the treatment of cancer. Cancer research 1996;56(6):1194.
238. Chung JE, Yokoyama M, Yamato M, Aoyagi T, Sakurai Y, Okano T. Thermo-responsive drug delivery from polymeric micelles constructed using block copolymers of poly (N-isopropylacrylamide) and poly (butylmethacrylate). Journal of Controlled Release 1999;62(1-2):115-127.
239. Liu XM, Pramoda KP, Yang YY, Chow SY, He C. Cholesteryl-grafted functional amphiphilic poly (N-isopropylacrylamide-co-N-hydroxylmethylacrylamide): synthesis, temperature-sensitivity, self-assembly and encapsulation of a hydrophobic agent. Biomaterials 2004;25(13):2619-2628.
240. Alarcón CH, Pennadam S, Alexander C. Stimuli responsive polymers for biomedical applications. Chemical Society Reviews 2005;34(3):276-285.
241. Idziak I, Avoce D, Lessard D, Gravel D, Zhu XX. Thermosensitivity of aqueous solutions of poly (N, N-diethylacrylamide). Macromolecules 1999;32(4):1260-1263.
242. Verdonck B, Goethals EJ, Du Prez FE. Block Copolymers of Methyl Vinyl Ether and Isobutyl Vinyl Ether With Thermo Adjustable Amphiphilic Properties. Macromolecular Chemistry and Physics 2003;204(17):2090-2098.

243. Vihola H, Laukkanen A, Valtola L, Tenhu H, Hirvonen J. Cytotoxicity of thermosensitive polymers poly (N-isopropylacrylamide), poly (N-vinylcaprolactam) and amphiphilically modified poly (N-vinylcaprolactam). Biomaterials 2005;26(16):3055-3064.
244. Schmaljohann D. Thermo-and pH-responsive polymers in drug delivery. Advanced drug delivery reviews 2006;58(15):1655-1670.
245. Meewes M, Ricka J, De Silva M, Nyffenegger R, Binkert T. Coil-globule transition of poly (N-isopropylacrylamide): a study of surfactant effects by light scattering. Macromolecules 1991;24(21):5811-5816.
246. Kuckling D, Adler HJP, Arndt KF, Ling L, Habicher WD. Temperature and pH dependent solubility of novel poly (N-isopropylacrylamide)-copolymers. Macromolecular Chemistry and Physics 2000;201(2):273-280.
247. Feil H, Bae YH, Feijen J, Kim SW. Effect of comonomer hydrophilicity and ionization on the lower critical solution temperature of N-isopropylacrylamide copolymers. Macromolecules 1993;26(10):2496-2500.
248. Yoo HS, Park TG. Biodegradable polymeric micelles composed of doxorubicin conjugated PLGA-PEG block copolymer. Journal of Controlled Release 2001;70(1-2):63-70.
249. Li C, Yu DF, Newman RA, Cabral F, Stephens LC, Hunter N, et al. Complete regression of well-established tumors using a novel water-soluble poly (L-glutamic acid)-paclitaxel conjugate. Cancer research 1998;58(11):2404.
250. Mitra S, Gaur U, Ghosh PC, Maitra AN. Tumour targeted delivery of encapsulated dextran-doxorubicin conjugate using chitosan nanoparticles as carrier. Journal of Controlled Release 2001;74(1-3):317-323.
251. Lee H, Lee K, Park TG. Hyaluronic Acid- Paclitaxel Conjugate Micelles: Synthesis, Characterization, and Antitumor Activity. Bioconjugate chemistry 2008;19(6):1319-1325.
252. Shuai X, Merdan T, Schaper AK, Xi F, Kissel T. Core-cross-linked polymeric micelles as paclitaxel carriers. Bioconjugate Chem 2004;15(3):441-448.
253. Jiang X, Ge Z, Xu J, Liu H, Liu S. Fabrication of multiresponsive shell cross-linked micelles possessing pH-controllable core swellability and thermo-tunable corona permeability. Biomacromolecules 2007;8(10):3184-3192.
254. Liggins RT, Burt HM. Polyether-polyester diblock copolymers for the preparation of paclitaxel loaded polymeric micelle formulations. Advanced drug delivery reviews 2002;54(2):191-202.
255. Nishiyama N, Okazaki S, Cabral H, Miyamoto M, Kato Y, Sugiyama Y, et al. Novel cisplatin-incorporated polymeric micelles can eradicate solid tumors in mice. Cancer research 2003;63(24):8977.
256. Xu Y, Du Y. Effect of molecular structure of chitosan on protein delivery properties of chitosan nanoparticles. International journal of pharmaceutics 2003;250(1):215-226.
257. Calvo P, Remunan-Lopez C, Vila-Jato JL, Alonso MJ. Chitosan and chitosan/ethylene oxide-propylene oxide block copolymer nanoparticles as novel carriers for proteins and vaccines. Pharmaceutical research 1997;14(10):1431-1436.

258. Sun B, Ranganathan B, Feng SS. Multifunctional poly (D, L-lactide-co-glycolide)/montmorillonite (PLGA/MMT) nanoparticles decorated by Trastuzumab for targeted chemotherapy of breast cancer. Biomaterials 2008;29(4):475-486.
259. Li YP, Pei YY, Zhang XY, Gu ZH, Zhou ZH, Yuan WF, et al. PEGylated PLGA nanoparticles as protein carriers: synthesis, preparation and biodistribution in rats. Journal of Controlled Release 2001;71(2):203-211.
260. Diwan M, Park TG. Pegylation enhances protein stability during encapsulation in PLGA microspheres. Journal of Controlled Release 2001;73(2-3):233-244.
261. Wang Y, Gao S, Ye WH, Yoon HS, Yang YY. Co-delivery of drugs and DNA from cationic core-shell nanoparticles self-assembled from a biodegradable copolymer. Nat Mater 2006 Oct;5(10):791-796.
262. Wang Y, Wang LS, Goh SH, Yang YY. Synthesis and characterization of cationic micelles self-assembled from a biodegradable copolymer for gene delivery. Biomacromolecules 2007;8(3):1028-1037.
263. Beh CW, Seow WY, Wang Y, Zhang Y, Ong ZY, Ee PLR, et al. Efficient delivery of Bcl-2-targeted siRNA using cationic polymer nanoparticles: downregulating mRNA expression level and sensitizing cancer cells to anticancer drug. Biomacromolecules 2008;10(1):41-48.
264. Wang Y, Ke CY, Weijie Beh C, Liu SQ, Goh SH, Yang YY. The self-assembly of biodegradable cationic polymer micelles as vectors for gene transfection. Biomaterials 2007;28(35):5358-5368.
265. Qiu LY, Bae YH. Self-assembled polyethylenimine-graft-poly(epsilon-caprolactone) micelles as potential dual carriers of genes and anticancer drugs. Biomaterials 2007 Oct;28(28):4132-4142.
266. Patil Y, Sadhukha T, Ma L, Panyam J. Nanoparticle-mediated simultaneous and targeted delivery of paclitaxel and tariquidar overcomes tumor drug resistance. Journal of Controlled Release 2009;136(1):21-29.
267. Kim C, Shah BP, Subramaniam P, Lee KB. Synergistic induction of apoptosis in brain cancer cells by targeted codelivery of siRNA and anticancer drugs. Mol Pharm Oct 3;8(5):1955-1961.
268. Srivastava RK. TRAIL/Apo-2L: mechanisms and clinical applications in cancer. Neoplasia 2001 Nov-Dec;3(6):535-546.
269. Johnstone RW, Frew AJ, Smyth MJ. The TRAIL apoptotic pathway in cancer onset, progression and therapy. Nat Rev Cancer 2008 Oct;8(10):782-798.
270. Ye W, Nanga RPR, Kang CB, Song J, Song SK, Yoon HS. Molecular characterization of the recombinant A-chain of a type II ribosome-inactivating protein (RIP) from Viscum album coloratum and structural basis on its ribosome-inactivating activity and the sugar-binding properties of the B-chain. Journal of Biochemistry and Molecular Biology 2006;39(5):560.
271. Galluzzi L, Aaronson SA, Abrams J, Alnemri ES, Andrews DW, Baehrecke EH, et al. Guidelines for the use and interpretation of assays for monitoring cell death in higher eukaryotes. Cell Death Differ 2009 Aug;16(8):1093-1107.
272. Krejsa C, Rogge M, Sadee W. Protein therapeutics: new applications for pharmacogenetics. Nat Rev Drug Discov 2006 Jun;5(6):507-521.
273. Bussing A, Multani AS, Pathak S, Pfuller U, Schietzel M. Induction of apoptosis by the N-acetyl-galactosamine-specific toxic lectin from Viscum album L. is associated

with a decrease of nuclear p53 and Bcl-2 proteins and induction of telomeric associations. Cancer Lett 1998 Aug 14;130(1-2):57-68.
274. Lee HS, Kim YS, Kim SB, Choi BE, Woo BH, Lee KC. Isolation and characterization of biologically active lectin from Korean mistletoe, Viscum album var. Coloratum. Cell Mol Life Sci 1999 Apr;55(4):679-682.
275. Kim MS, So HS, Lee KM, Park JS, Lee JH, Moon SK, et al. Activation of caspase cascades in Korean mistletoe (Viscum album var. coloratum) lectin-II-induced apoptosis of human myeloleukemic U937 cells. Gen Pharmacol 2000 May;34(5):349-355.
276. Bantel H, Engels IH, Voelter W, Schulze-Osthoff K, Wesselborg S. Mistletoe lectin activates caspase-8/FLICE independently of death receptor signaling and enhances anticancer drug-induced apoptosis. Cancer Res 1999 May 1;59(9):2083-2090.
277. Zelphati O, Wang Y, Kitada S, Reed JC, Felgner PL, Corbeil J. Intracellular delivery of proteins with a new lipid-mediated delivery system. J Biol Chem 2001 Sep 14;276(37):35103-35110.
278. Brustugun OT, Fladmark KE, Doskeland SO, Orrenius S, Zhivotovsky B. Apoptosis induced by microinjection of cytochrome c is caspase-dependent and is inhibited by Bcl-2. Cell Death Differ 1998 Aug;5(8):660-668.
279. Fenton M, Bone N, Sinclair AJ. The efficient and rapid import of a peptide into primary B and T lymphocytes and a lymphoblastoid cell line. J Immunol Methods 1998 Mar 1;212(1):41-48.
280. Luo D, Saltzman WM. Enhancement of transfection by physical concentration of DNA at the cell surface. Nat Biotechnol 2000 Aug;18(8):893-895.
281. Ford KG, Souberbielle BE, Darling D, Farzaneh F. Protein transduction: an alternative to genetic intervention? Gene Ther 2001 Jan;8(1):1-4.
282. Wadia JS, Dowdy SF. Protein transduction technology. Curr Opin Biotechnol 2002 Feb;13(1):52-56.
283. Sang Yoo H, Gwan Park T. Biodegradable nanoparticles containing protein-fatty acid complexes for oral delivery of salmon calcitonin. J Pharm Sci 2004 Feb;93(2):488-495.
284. Kim YH, Park JH, Lee M, Park TG, Kim SW. Polyethylenimine with acid-labile linkages as a biodegradable gene carrier. J Control Release 2005 Mar 2;103(1):209-219.
285. Futami J, Kitazoe M, Maeda T, Nukui E, Sakaguchi M, Kosaka J, et al. Intracellular delivery of proteins into mammalian living cells by polyethylenimine-cationization. J Biosci Bioeng 2005 Feb;99(2):95-103.
286. Zheng X, Lundberg M, Karlsson A, Johansson M. Lipid-mediated protein delivery of suicide nucleoside kinases. Cancer Res 2003 Oct 15;63(20):6909-6913.
287. Wood KC, Little SR, Langer R, Hammond PT. A family of hierarchically self-assembling linear-dendritic hybrid polymers for highly efficient targeted gene delivery. Angew Chem Int Ed Engl 2005 Oct 21;44(41):6704-6708.
288. Fischer D, Li Y, Ahlemeyer B, Krieglstein J, Kissel T. In vitro cytotoxicity testing of polycations: influence of polymer structure on cell viability and hemolysis. Biomaterials 2003 Mar;24(7):1121-1131.
289. de Vries EG, Gietema JA, de Jong S. Tumor necrosis factor-related apoptosis-inducing ligand pathway and its therapeutic implications. Clin Cancer Res 2006 Apr 15;12(8):2390-2393.

290. Wang S, El-Deiry WS. TRAIL and apoptosis induction by TNF-family death receptors. Oncogene 2003 Nov 24;22(53):8628-8633.
291. Jo M, Kim TH, Seol DW, Esplen JE, Dorko K, Billiar TR, et al. Apoptosis induced in normal human hepatocytes by tumor necrosis factor-related apoptosis-inducing ligand. Nat Med 2000 May;6(5):564-567.
292. Ganten TM, Koschny R, Sykora J, Schulze-Bergkamen H, Buchler P, Haas TL, et al. Preclinical differentiation between apparently safe and potentially hepatotoxic applications of TRAIL either alone or in combination with chemotherapeutic drugs. Clin Cancer Res 2006 Apr 15;12(8):2640-2646.
293. Lawrence D, Shahrokh Z, Marsters S, Achilles K, Shih D, Mounho B, et al. Differential hepatocyte toxicity of recombinant Apo2L/TRAIL versions. Nat Med 2001 Apr;7(4):383-385.
294. Hao C, Song JH, Hsi B, Lewis J, Song DK, Petruk KC, et al. TRAIL inhibits tumor growth but is nontoxic to human hepatocytes in chimeric mice. Cancer Res 2004 Dec 1;64(23):8502-8506.
295. Lee YJ, Amoscato AA. TRAIL and ceramide. Vitam Horm 2004;67:229-255.
296. Kim K, Fisher MJ, Xu SQ, el-Deiry WS. Molecular determinants of response to TRAIL in killing of normal and cancer cells. Clin Cancer Res 2000 Feb;6(2):335-346.
297. Naka T, Sugamura K, Hylander BL, Widmer MB, Rustum YM, Repasky EA. Effects of tumor necrosis factor-related apoptosis-inducing ligand alone and in combination with chemotherapeutic agents on patients' colon tumors grown in SCID mice. Cancer Res 2002 Oct 15;62(20):5800-5806.
298. Gliniak B, Le T. Tumor necrosis factor-related apoptosis-inducing ligand's antitumor activity in vivo is enhanced by the chemotherapeutic agent CPT-11. Cancer Res 1999 Dec 15;59(24):6153-6158.
299. Frese S, Brunner T, Gugger M, Uduehi A, Schmid RA. Enhancement of Apo2L/TRAIL (tumor necrosis factor-related apoptosis-inducing ligand)-induced apoptosis in non-small cell lung cancer cell lines by chemotherapeutic agents without correlation to the expression level of cellular protease caspase-8 inhibitory protein. J Thorac Cardiovasc Surg 2002 Jan;123(1):168-174.
300. Yamamoto T, Nagano H, Sakon M, Wada H, Eguchi H, Kondo M, et al. Partial contribution of tumor necrosis factor-related apoptosis-inducing ligand (TRAIL)/TRAIL receptor pathway to antitumor effects of interferon-alpha/5-fluorouracil against Hepatocellular Carcinoma. Clin Cancer Res 2004 Dec 1;10(23):7884-7895.
301. Singh TR, Shankar S, Chen X, Asim M, Srivastava RK. Synergistic interactions of chemotherapeutic drugs and tumor necrosis factor-related apoptosis-inducing ligand/Apo-2 ligand on apoptosis and on regression of breast carcinoma in vivo. Cancer Res 2003 Sep 1;63(17):5390-5400.
302. Keane MM, Ettenberg SA, Nau MM, Russell EK, Lipkowitz S. Chemotherapy augments TRAIL-induced apoptosis in breast cell lines. Cancer Res 1999 Feb 1;59(3):734-741.
303. Nimmanapalli R, Perkins CL, Orlando M, O'Bryan E, Nguyen D, Bhalla KN. Pretreatment with paclitaxel enhances apo-2 ligand/tumor necrosis factor-related apoptosis-inducing ligand-induced apoptosis of prostate cancer cells by inducing death receptors 4 and 5 protein levels. Cancer Res 2001 Jan 15;61(2):759-763.

304. Ibrahim NK, Desai N, Legha S, Soon-Shiong P, Theriault RL, Rivera E, et al. Phase I and pharmacokinetic study of ABI-007, a Cremophor-free, protein-stabilized, nanoparticle formulation of paclitaxel. Clin Cancer Res 2002 May;8(5):1038-1044.
305. Wang YC, Liu XQ, Sun TM, Xiong MH, Wang J. Functionalized micelles from block copolymer of polyphosphoester and poly(epsilon-caprolactone) for receptor-mediated drug delivery. J Control Release 2008 May 22;128(1):32-40.
306. Ranganath SH, Fu Y, Arifin DY, Kee I, Zheng L, Lee HS, et al. The use of submicron/nanoscale PLGA implants to deliver paclitaxel with enhanced pharmacokinetics and therapeutic efficacy in intracranial glioblastoma in mice. Biomaterials Jul;31(19):5199-5207.
307. Jabr-Milane L, van Vlerken L, Devalapally H, Shenoy D, Komareddy S, Bhavsar M, et al. Multi-functional nanocarriers for targeted delivery of drugs and genes. J Control Release 2008 Sep 10;130(2):121-128.
308. Al-Abd AM, Lee SH, Kim SH, Cha JH, Park TG, Lee SJ, et al. Penetration and efficacy of VEGF siRNA using polyelectrolyte complex micelles in a human solid tumor model in-vitro. J Control Release 2009 Jul 20;137(2):130-135.
309. Peddada LY, Harris NK, Devore DI, Roth CM. Novel graft copolymers enhance in vitro delivery of antisense oligonucleotides in the presence of serum. J Control Release 2009 Dec 3;140(2):134-140.
310. Cheng H, Li YY, Zeng X, Sun YX, Zhang XZ, Zhuo RX. Protamine sulfate/poly(L-aspartic acid) polyionic complexes self-assembled via electrostatic attractions for combined delivery of drug and gene. Biomaterials 2009 Feb;30(6):1246-1253.
311. Chirila TV, Rakoczy PE, Garrett KL, Lou X, Constable IJ. The use of synthetic polymers for delivery of therapeutic antisense oligodeoxynucleotides. Biomaterials 2002 Jan;23(2):321-342.
312. Campolongo MJ, Luo D. Drug delivery: Old polymer learns new tracts. Nat Mater 2009 Jun;8(6):447-448.
313. Lee AL, Wang Y, Ye WH, Yoon HS, Chan SY, Yang YY. Efficient intracellular delivery of functional proteins using cationic polymer core/shell nanoparticles. Biomaterials 2008 Mar;29(9):1224-1232.
314. Lee AL, Wang Y, Cheng HY, Pervaiz S, Yang YY. The co-delivery of paclitaxel and Herceptin using cationic micellar nanoparticles. Biomaterials 2009 Feb;30(5):919-927.
315. Kuo JH, Lo YL, Shau MD, Cherng JY. A thermodynamic study of cationic polymer-plasmid DNA complexes by highly-sensitive differential scanning calorimetry. J Control Release 2002 Jun 17;81(3):321-325.
316. Tang R, Palumbo RN, Nagarajan L, Krogstad E, Wang C. Well-defined block copolymers for gene delivery to dendritic cells: probing the effect of polycation chain-length. J Control Release 2009 Mar 3;142(2):229-237.
317. Kohlhaas SL, Craxton A, Sun XM, Pinkoski MJ, Cohen GM. Receptor-mediated endocytosis is not required for tumor necrosis factor-related apoptosis-inducing ligand (TRAIL)-induced apoptosis. J Biol Chem 2007 Apr 27;282(17):12831-12841.
318. Milross CG, Mason KA, Hunter NR, Chung WK, Peters LJ, Milas L. Relationship of mitotic arrest and apoptosis to antitumor effect of paclitaxel. J Natl Cancer Inst 1996 Sep 18;88(18):1308-1314.

319. Jones PA, Baylin SB. The fundamental role of epigenetic events in cancer. Nat Rev Genet 2002 Jun;3(6):415-428.
320. Wong JJ, Hawkins NJ, Ward RL. Colorectal cancer: a model for epigenetic tumorigenesis. Gut 2007 Jan;56(1):140-148.
321. Mitsiades CS, Treon SP, Mitsiades N, Shima Y, Richardson P, Schlossman R, et al. TRAIL/Apo2L ligand selectively induces apoptosis and overcomes drug resistance in multiple myeloma: therapeutic applications. Blood 2001 Aug 1;98(3):795-804.
322. de Jong S, Timmer T, Heijenbrok FJ, de Vries EG. Death receptor ligands, in particular TRAIL, to overcome drug resistance. Cancer Metastasis Rev 2001;20(1-2):51-56.
323. Bossi G, Lapi E, Strano S, Rinaldo C, Blandino G, Sacchi A. Mutant p53 gain of function: reduction of tumor malignancy of human cancer cell lines through abrogation of mutant p53 expression. Oncogene 2006 Jan 12;25(2):304-309.
324. Zobalova R, McDermott L, Stantic M, Prokopova K, Dong LF, Neuzil J. CD133-positive cells are resistant to TRAIL due to up-regulation of FLIP. Biochem Biophys Res Commun 2008 Sep 5;373(4):567-571.
325. Van Geelen CM, de Vries EG, de Jong S. Lessons from TRAIL-resistance mechanisms in colorectal cancer cells: paving the road to patient-tailored therapy. Drug Resist Updat 2004 Dec;7(6):345-358.
326. Strater J, Walczak H, Pukrop T, Von Muller L, Hasel C, Kornmann M, et al. TRAIL and its receptors in the colonic epithelium: a putative role in the defense of viral infections. Gastroenterology 2002 Mar;122(3):659-666.
327. Komdeur R, Meijer C, Van Zweeden M, De Jong S, Wesseling J, Hoekstra HJ, et al. Doxorubicin potentiates TRAIL cytotoxicity and apoptosis and can overcome TRAIL-resistance in rhabdomyosarcoma cells. Int J Oncol 2004 Sep;25(3):677-684.
328. Zhu H, Zhang L, Huang X, Davis JJ, Jacob DA, Teraishi F, et al. Overcoming acquired resistance to TRAIL by chemotherapeutic agents and calpain inhibitor I through distinct mechanisms. Mol Ther 2004 May;9(5):666-673.
329. Jin Z, McDonald ER, 3rd, Dicker DT, El-Deiry WS. Deficient tumor necrosis factor-related apoptosis-inducing ligand (TRAIL) death receptor transport to the cell surface in human colon cancer cells selected for resistance to TRAIL-induced apoptosis. J Biol Chem 2004 Aug 20;279(34):35829-35839.
330. Jalving M, de Jong S, Koornstra JJ, Boersma-van Ek W, Zwart N, Wesseling J, et al. TRAIL induces apoptosis in human colorectal adenoma cell lines and human colorectal adenomas. Clin Cancer Res 2006 Jul 15;12(14 Pt 1):4350-4356.
331. Soria JC, Smit E, Khayat D, Besse B, Yang X, Hsu CP, et al. Phase 1b study of dulanermin (recombinant human Apo2L/TRAIL) in combination with paclitaxel, carboplatin, and bevacizumab in patients with advanced non-squamous non-small-cell lung cancer. J Clin Oncol Mar 20;28(9):1527-1533.
332. Mom CH, Verweij J, Oldenhuis CN, Gietema JA, Fox NL, Miceli R, et al. Mapatumumab, a fully human agonistic monoclonal antibody that targets TRAIL-R1, in combination with gemcitabine and cisplatin: a phase I study. Clin Cancer Res 2009 Sep 1;15(17):5584-5590.
333. Rodrigues NR, Rowan A, Smith ME, Kerr IB, Bodmer WF, Gannon JV, et al. p53 mutations in colorectal cancer. Proc Natl Acad Sci U S A 1990 Oct;87(19):7555-7559.

334. Kataoka K, Matsumoto T, Yokoyama M, Okano T, Sakurai Y, Fukushima S, et al. Doxorubicin-loaded poly(ethylene glycol)-poly(beta-benzyl-L-aspartate) copolymer micelles: their pharmaceutical characteristics and biological significance. J Control Release 2000 Feb 14;64(1-3):143-153.
335. Torchilin VP. Multifunctional nanocarriers. Adv Drug Deliv Rev 2006 Dec 1;58(14):1532-1555.
336. Duncan R. The dawning era of polymer therapeutics. Nat Rev Drug Discov 2003 May;2(5):347-360.
337. Darzynkiewicz Z, Bruno S, Del Bino G, Gorczyca W, Hotz MA, Lassota P, et al. Features of apoptotic cells measured by flow cytometry. Cytometry 1992;13(8):795-808.
338. Voelkel-Johnson C, King DL, Norris JS. Resistance of prostate cancer cells to soluble TNF-related apoptosis-inducing ligand (TRAIL/Apo2L) can be overcome by doxorubicin or adenoviral delivery of full-length TRAIL. Cancer Gene Ther 2002 Feb;9(2):164-172.
339. Kelly MM, Hoel BD, Voelkel-Johnson C. Doxorubicin pretreatment sensitizes prostate cancer cell lines to TRAIL induced apoptosis which correlates with the loss of c-FLIP expression. Cancer Biol Ther 2002 Sep-Oct;1(5):520-527.
340. Zhang XD, Franco AV, Nguyen T, Gray CP, Hersey P. Differential localization and regulation of death and decoy receptors for TNF-related apoptosis-inducing ligand (TRAIL) in human melanoma cells. J Immunol 2000 Apr 15;164(8):3961-3970.
341. Zhang Y, Yoshida T, Zhang B. TRAIL induces endocytosis of its death receptors in MDA-MB-231 breast cancer cells. Cancer Biol Ther 2009 May;8(10):917-922.
342. Ichikawa K, Liu W, Zhao L, Wang Z, Liu D, Ohtsuka T, et al. Tumoricidal activity of a novel anti-human DR5 monoclonal antibody without hepatocyte cytotoxicity. Nat Med 2001 Aug;7(8):954-960.
343. Zhang L, Fang B. Mechanisms of resistance to TRAIL-induced apoptosis in cancer. Cancer Gene Ther 2005 Mar;12(3):228-237.
344. Franken NA, Rodermond HM, Stap J, Haveman J, van Bree C. Clonogenic assay of cells in vitro. Nat Protoc 2006;1(5):2315-2319.
345. Bae Y, Nishiyama N, Kataoka K. In vivo antitumor activity of the folate-conjugated pH-sensitive polymeric micelle selectively releasing adriamycin in the intracellular acidic compartments. Bioconjug Chem 2007 Jul-Aug;18(4):1131-1139.
346. Wei H, Zhang XZ, Zhou Y, Cheng SX, Zhuo RX. Self-assembled thermoresponsive micelles of poly(N-isopropylacrylamide-b-methyl methacrylate). Biomaterials 2006 Mar;27(9):2028-2034.
347. Seow WY, Xue JM, Yang YY. Targeted and intracellular delivery of paclitaxel using multi-functional polymeric micelles. Biomaterials 2007 Mar;28(9):1730-1740.
348. Lee ES, Oh KT, Kim D, Youn YS, Bae YH. Tumor pH-responsive flower-like micelles of poly(L-lactic acid)-b-poly(ethylene glycol)-b-poly(L-histidine). J Control Release 2007 Oct 18;123(1):19-26.
349. Liu SQ, Wiradharma N, Gao SJ, Tong YW, Yang YY. Bio-functional micelles self-assembled from a folate-conjugated block copolymer for targeted intracellular delivery of anticancer drugs. Biomaterials 2007 Mar;28(7):1423-1433.
350. Yoo HS, Park TG. Folate receptor targeted biodegradable polymeric doxorubicin micelles. J Control Release 2004 Apr 28;96(2):273-283.

351. Zhang XQ, Wang XL, Zhang PC, Liu ZL, Zhuo RX, Mao HQ, et al. Galactosylated ternary DNA/polyphosphoramidate nanoparticles mediate high gene transfection efficiency in hepatocytes. J Control Release 2005 Feb 16;102(3):749-763.
352. Chandna P, Saad M, Wang Y, Ber E, Khandare J, Vetcher AA, et al. Targeted proapoptotic anticancer drug delivery system. Mol Pharm 2007 Sep-Oct;4(5):668-678.
353. Huang G, Zhou Z, Srinivasan R, Penn MS, Kottke-Marchant K, Marchant RE, et al. Affinity manipulation of surface-conjugated RGD peptide to modulate binding of liposomes to activated platelets. Biomaterials 2008 Apr;29(11):1676-1685.
354. Schrama D, Reisfeld RA, Becker JC. Antibody targeted drugs as cancer therapeutics. Nat Rev Drug Discov 2006 Feb;5(2):147-159.
355. Carter P. Improving the efficacy of antibody-based cancer therapies. Nat Rev Cancer 2001 Nov;1(2):118-129.
356. Reichert JM, Valge-Archer VE. Development trends for monoclonal antibody cancer therapeutics. Nat Rev Drug Discov 2007 May;6(5):349-356.
357. Wu AM, Senter PD. Arming antibodies: prospects and challenges for immunoconjugates. Nat Biotechnol 2005 Sep;23(9):1137-1146.
358. Allred DC, Clark GM, Tandon AK, Molina R, Tormey DC, Osborne CK, et al. HER-2/neu in node-negative breast cancer: prognostic significance of overexpression influenced by the presence of in situ carcinoma. J Clin Oncol 1992 Apr;10(4):599-605.
359. Hynes NE, Stern DF. The biology of erbB-2/neu/HER-2 and its role in cancer. Biochim Biophys Acta 1994 Dec 30;1198(2-3):165-184.
360. Press MF, Bernstein L, Thomas PA, Meisner LF, Zhou JY, Ma Y, et al. HER-2/neu gene amplification characterized by fluorescence in situ hybridization: poor prognosis in node-negative breast carcinomas. J Clin Oncol 1997 Aug;15(8):2894-2904.
361. Nahta R, Esteva FJ. Herceptin: mechanisms of action and resistance. Cancer Lett 2006 Feb 8;232(2):123-138.
362. Nahta R, Esteva FJ. Trastuzumab: triumphs and tribulations. Oncogene 2007 May 28;26(25):3637-3643.
363. Lee S, Yang W, Lan KH, Sellappan S, Klos K, Hortobagyi G, et al. Enhanced sensitization to taxol-induced apoptosis by herceptin pretreatment in ErbB2-overexpressing breast cancer cells. Cancer Res 2002 Oct 15;62(20):5703-5710.
364. Baselga J, Norton L, Albanell J, Kim YM, Mendelsohn J. Recombinant humanized anti-HER2 antibody (Herceptin) enhances the antitumor activity of paclitaxel and doxorubicin against HER2/neu overexpressing human breast cancer xenografts. Cancer Res 1998 Jul 1;58(13):2825-2831.
365. Burstein HJ, Harris LN, Gelman R, Lester SC, Nunes RA, Kaelin CM, et al. Preoperative therapy with trastuzumab and paclitaxel followed by sequential adjuvant doxorubicin/cyclophosphamide for HER2 overexpressing stage II or III breast cancer: a pilot study. J Clin Oncol 2003 Jan 1;21(1):46-53.
366. Slamon DJ, Leyland-Jones B, Shak S, Fuchs H, Paton V, Bajamonde A, et al. Use of chemotherapy plus a monoclonal antibody against HER2 for metastatic breast cancer that overexpresses HER2. N Engl J Med 2001 Mar 15;344(11):783-792.
367. Gilbert CW, McGowan EB, Seery GB, Black KS, Pegram MD. Targeted prodrug treatment of HER-2-positive breast tumor cells using trastuzumab and paclitaxel linked by A-Z-CINN Linker. J Exp Ther Oncol 2003 Jan-Feb;3(1):27-35.

368. Sun B, Ranganathan B, Feng SS. Multifunctional poly(D,L-lactide-co-glycolide)/montmorillonite (PLGA/MMT) nanoparticles decorated by Trastuzumab for targeted chemotherapy of breast cancer. Biomaterials 2008 Feb;29(4):475-486.
369. Lee ALZ, Wang Y, Pervaiz S, Yang YY. Synergistic Anticancer Effects Achieved by Co Delivery of TRAIL and Paclitaxel Using Cationic Polymeric Micelles. Macromolecular Bioscience.
370. Lee ALZ, Dhillon SHK, Wang Y, Pervaiz S, Fan W, Yang YY. Synergistic anti-cancer effects via co-delivery of TNF-related apoptosis-inducing ligand (TRAIL/Apo2L) and doxorubicin using micellar nanoparticles. Mol BioSyst.
371. Xu YM, Wang LF, Jia LT, Qiu XC, Zhao J, Yu CJ, et al. A caspase-6 and anti-human epidermal growth factor receptor-2 (HER2) antibody chimeric molecule suppresses the growth of HER2-overexpressing tumors. J Immunol 2004 Jul 1;173(1):61-67.
372. Boyle DL, Carman P, Takemoto L. Translocation of macromolecules into whole rat lenses in culture. Mol Vis 2002 Jul 10;8:226-234.
373. Hurwitz E, Stancovski I, Sela M, Yarden Y. Suppression and promotion of tumor growth by monoclonal antibodies to ErbB-2 differentially correlate with cellular uptake. Proceedings of the National Academy of Sciences 1995;92(8):3353.
374. Klapper LN, Waterman H, Sela M, Yarden Y. Tumor-inhibitory antibodies to HER-2/ErbB-2 may act by recruiting c-Cbl and enhancing ubiquitination of HER-2. Cancer research 2000;60(13):3384.
375. McCabe A, Dolled-Filhart M, Camp RL, Rimm DL. Automated quantitative analysis (AQUA) of in situ protein expression, antibody concentration, and prognosis. J Natl Cancer Inst 2005 Dec 21;97(24):1808-1815.
376. Li SD, Huang L. Pharmacokinetics and biodistribution of nanoparticles. Molecular Pharmaceutics 2008;5(4):496-504.
377. Minchinton AI, Tannock IF. Drug penetration in solid tumours. Nature Reviews Cancer 2006;6(8):583-592.
378. Goodman TT, Olive PL, Pun SH. Increased nanoparticle penetration in collagenase-treated multicellular spheroids. Int J Nanomedicine 2007;2(2):265-274.

APPENDIX I

SYNTHESIS AND CHARACTERIZATION OF P(MDS-*co*-CES)

The amphiphilic copolymer poly{*N*-methyldietheneamine sebacate)-co-[(cholesteryl oxocarbonylamido ethyl) methyl bis(ethylene) ammonium bromide] sebacate}P(MDS-*co*-CES) has been synthesized and characterized with regards to its chemical and physical properties [262].

Synthesis Method of P(MDS-*co*-CES)

Synthesis of PMDS

N-Methyldiethanolamine (5.958 g, 0.05 mol) and 50.5 g of triethylamine (0.5 mol) were added to a 250-mL round-bottom flask with freshly dried 50 mL of THF in a dry ice/ acetone bath (below -30 °C). Freshly dried THF (40 mL) containing 11.945 g of sebacoyl chloride (0.05 mol) was added dropwise to the flask with stirring. The flask was removed 1 h later, and the reaction was allowed to proceed at room temperature overnight. The solvent and residual triethylamine were removed using a rotavapor. The solid was washed three times with 300 mL of THF and the solution was collected by filtration. The solvent was then removed using the rotavapor. The crude product was semisolid, which was put in a vacuum oven overnight to further remove residual solvents. The crude product dissolved in 100 mL of toluene was extracted four times with 50 mL of NaCl saturated aqueous solution and then was dried with anhydrous NaCO3. It was further dialyzed in acetone using a membrane with a molecular weight cutoff of 3.5 kDa. Acetone was subsequently removed from the dialysate using the rotavapor, and the final product was dried in a vacuum oven for 2 days.

Synthesis of Be-chol

Chloroform (50 mL) dried with a molecular sieve was put into a 100-mL round-bottom flask in a dry ice/acetone bath. Cholesteryl chloroformate (4.34 g, 0.0097 mol) and 2.18 g of 2-bromoethylamine hydrobromide (0.0106 mol) were then added with stirring. Next, 3 mL of freshly dried triethylamine was added to the flask. The dry ice/acetone bath was removed after 30 min for the reaction to proceed at room temperature for 12 h. The organic solution was washed three times with 20 mL of 1 N HCl solution saturated with NaCl and once with 30 mL of NaCl saturated aqueous solution to remove residual triethylamine. The organic phase was collected and dried with 5 g of anhydrous magnesium sulfate. The solution was then filtered and distilled. The crude product was recrystallized with anhydrous ethanol once and with anhydrous acetone twice. The final product was dried with a vacuum oven for 24 h.

Synthesis of P(MDS-co-CES)

PMDS (2.85 g, 0.01 mol) and 5.5 g of *N*-(2-bromoethyl) carbarmoyl cholesterol (0.01 mol) were dissolved in 50 mL of dry toluene and were refluxed for 2 days under argon. Diethyl ether (250 mL) was then added to precipitate the product. To completely remove unreacted *N*-(2-bromoethyl) carbarmoyl cholesterol, the product was washed with diethyl ether four more times.

Methods of characterization of P(MDS-*co*-CES)

^{1}H NMR Measurements

The ^{1}H NMR spectra of polymers dissolved in CDCl3 were recorded on a Bruker AVANCE 400 spectrometer (400 MHz). Chemical shifts were expressed in parts per million (δ) using tetramethyl silicane in the indicated solvent as the internal standard.

FT-IR Measurements

The polymers were analyzed using a Fourier transform infrared spectrometer (FT-IR, Perkin-Elmer Spectrum 2000, United States). The samples were dissolved in chloroform, and the solution was then dropped onto a NaCl crystal. The solvent was allowed to evaporate completely prior to the measurements.

Molecular Weight Determination

The molecular weights of polymers were determined using a gel permeation chromatography (GPC) (Waters 2690, MA) with a differential refractometer detector (Waters 410, MA). The polymer sample (10 mg) was dissolved in 5 mL of THF, and the solution was then filtered. The mobile phase was THF at a flow rate of 1 mL/min. Weight and number-average molecular weights were calculated from a calibration curve using a series of polystyrene standards (Polymer Laboratories Inc., MA, with molecular weight ranging from 1300 to 30 000).

CMC Determination

The critical micelle concentration (CMC) of the polymer in deionized (DI) water and sodium acetate buffer of varying concentration and pH was estimated by fluorescence spectroscopy using pyrene as a probe. Fluorescence spectra were recorded on a LS 50B luminescence spectrometer (Perkin-Elmer, United States) at room temperature (22 °C).

Aliquots of pyrene solution (1.54 x 10-5 M in acetone, 400 µL) were added to containers, and the acetone was allowed to evaporate. Polymer solutions (10 mL) at different concentrations were then added to the containers. The final pyrene concentration was 6.17 x 10-7 M. The solutions were kept on a shaker for 20 h at room temperature and then at 60 °C for another 4 h to reach the solubilization equilibrium of pyrene into the aqueous phase. The emission spectra were scanned from 360 to 410 nm at the excitation wavelength of 339 nm while the excitation spectra were scanned from 300 to 360 nm at the emission wavelength of 395 nm. Both excitation and emission bandwidths were 4.5 nm. Fluorescence spectra of pyrene solutions contain a vibrational band exhibiting high sensitivity to the polarity of the pyrene environment. The intensity (peak height) ratio (I_3/I_1) of the third band (385 nm, I_3) to the first band (374 nm, I_1) from the emission spectra and I_{338}/I_{333} ratio from the excitation spectra were analyzed as a function of polymer concentration. The CMC value was taken from the intersection of the tangent to the curve at the inflection with the horizontal tangent through the points at low concentrations.

Transmission Electron Microscopy (TEM) Examinations

The morphology of the micelles was analyzed by TEM (Philips CM300, Holland). One drop of the freshly prepared micelle solution containing 0.01% phosphotungstic acid was placed onto a copper grid coated with carbon film and was self-dried at room temperature (22 °C). The TEM observations were carried out with an electron kinetic energy of 300 k eV.

Synthesis and characterization of P(MDS-*co*-CES)

Synthesis and Characterization of PMDS

Poly(*N*-methyldiethylamine sebacate) (PMDS) is the main chain of the designed polymer (Figure 2.1A). The successful synthesis of PMDS was verified by ^{1}H NMR and FT-IR spectra as shown in Figure A1. ^{1}H NMR peaks at δ 2.71-2.73 (signal a), δ 1.62 (signal b), and δ 1.32 (signals c and d) were attributed to the protons of four different $–CH_2-$ groups from the sebacate units (Figure S1A). Peaks at δ 4.17-4.19 (signal e) and δ 2.30- 2.37 (signals f and g) were due to protons of two different $-CH_2-$ groups and the $–CH_3$ group linked to the nitrogen atom. FT-IR spectrum also confirmed the polyester formation (Figure A1B). The –C=O stretching shifted to a lower wave number (1736 cm^{-1}) compared to carbonyl halide (1805 cm^{-1}) because of the inductive effect of halide. The peak at 1172 cm^{-1} was attributed to C-O.

Synthesis and Characterization of Be-chol

N-(2-Bromoethyl)carbarmoyl cholesterol (Be-chol) has a bromoethyl group that was used to quaternize the main chain at the amino group and to produce positive charges at the same sites. Bechol was also designed as the randomly dispersed hydrophobic pendent chains. It was synthesized by connecting 2-bromoethylamine hydrobromide onto cholesteryl chloroformate through an amidation reaction as shown in Figure 2.1. TLC analysis showed one point at R_f of 0.68 in the mixture of toluene, hexane, and methanol (8:8:1 in volume), indicating that Be-chol was pure. Figure A2 displays the ^{1}H NMR and FT-IR spectra of Be-chol. The ^{1}H peak at δ 5.10 (signal HN) was due to the amide groups

(CON*H*) (Figure A2A). δ 3.50 (signal H_4) and 3.61 (signal H_5) were attributed to the 2-

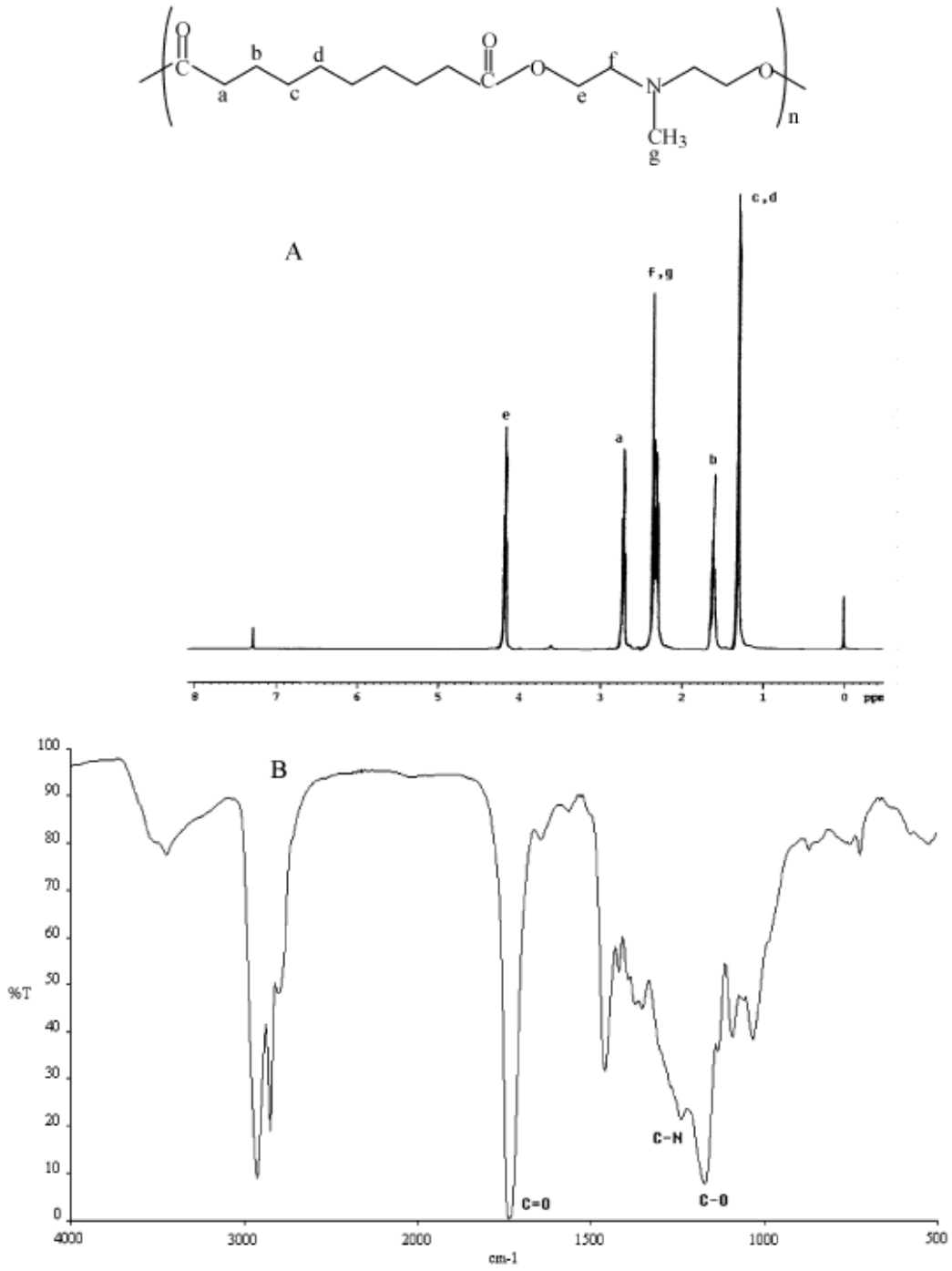

Figure A1. (A) ^{1}H NMR and **(B)** FT-IR spectra of PMDS.

bromoethyl groups. *ä* 4.52 (H_1) and 5.40 (H_2) were associated with the cholesterol units. The ratio of the H_1, H_2, HN, H_4, and H_5 peak areas was determined to be 1:1:1:2:2, confirming the successful synthesis of Be-chol. The FT-IR spectrum of Be-chol further evidenced its successful synthesis. The IR peak at 3325 cm^{-1} was due to –NH stretching.

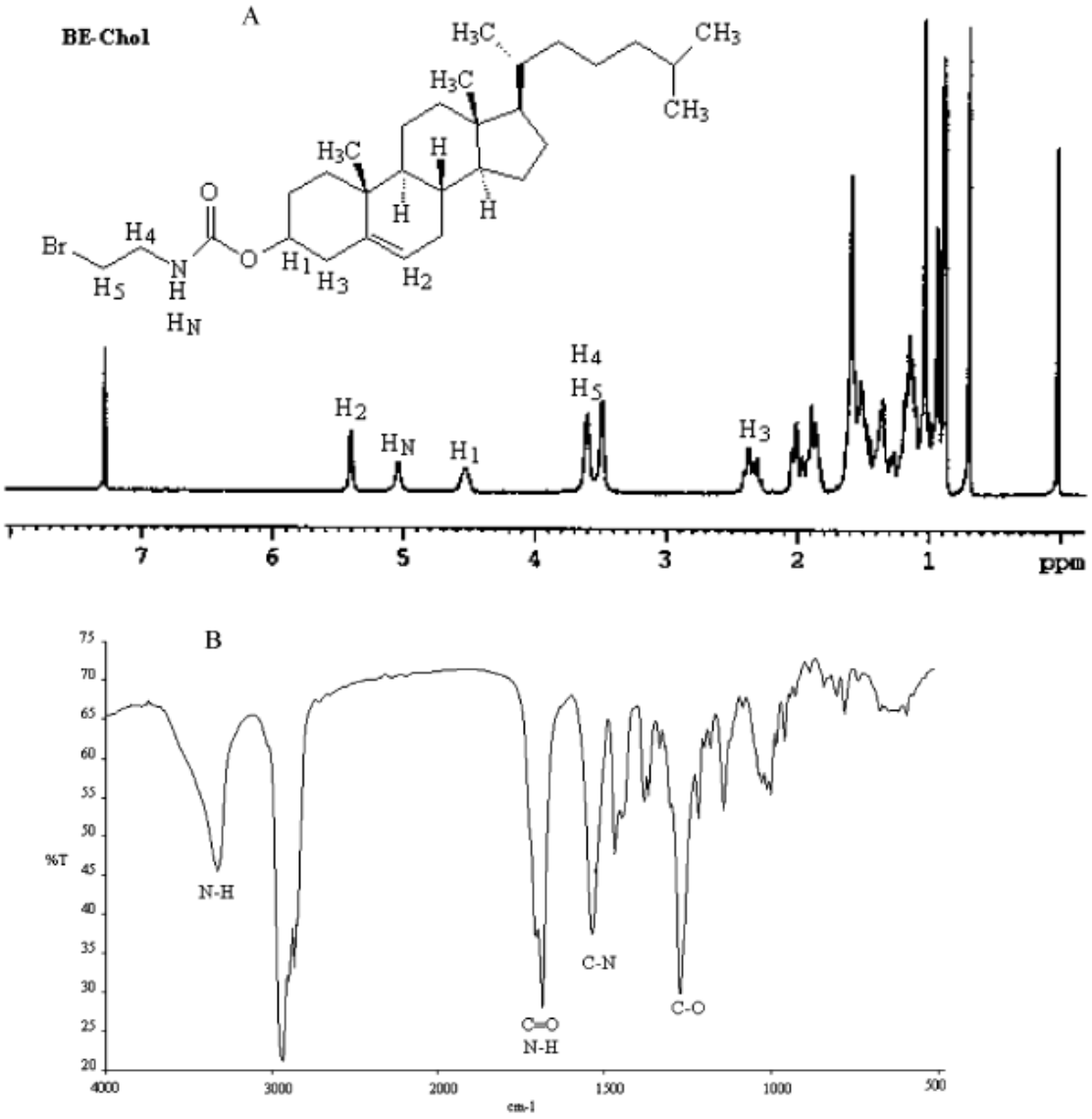

Figure A2. (A) ^{1}H NMR and **(B)** FT-IR spectra of Be-chol.

Peaks from –C=O stretching and -NH- bending overlapped at 1685 cm^{-1}. The peak at 1536 cm^{-1} was attributed to -C-N- stretching.

Synthesis and Characterization of P(MDS-co-CES)

P-(MDS-*co*-CES) was synthesized by grafting Be-chol onto PMDS through a quaternization reaction (Figure 2.1). This reaction needs to be performed at a relatively high temperature when alkyl bromide is used as the reagent for quaternization. The successful synthesis of P(MDS-*co*-CES) was verified by ^{1}H NMR and FT-IR spectra as shown in Figure A3. The ^{1}H NMR spectrum of P(MDS-*co*-CES) displays peaks at δ 2.7-2.8 (signal a), 1.5-1.7 (signal b), 1.2-1.4 (signals c and d), 4.0-4.2 (signal e), and 2.2-2.4 (signals f and g) because of the protons on the PMDS main chain. Various peaks at δ 0.7-1.2 were attributed to the cholesterol groups. The peak at δ 5.38 arose from the proton of =CH- in the cholesterol groups (signal h). The peak at δ 0.7 was from the methyl group directly linked to the cyclic hydrocarbon (signal i). The information provided by the ^{1}H NMR spectrum of P(MDS-*co*-CES) proved that the cholesteryl group was successfully grafted onto the PMDS mainchain. IR spectrum of P(MDS-*co*-CES) showed a peak at 1252 cm^{-1} because of C-N stretching of amine. The shift and increased intensity of this peak compared with that of PMDS (1240 cm^{-1}) illustrated the formation of a quaternary ammonium salt.

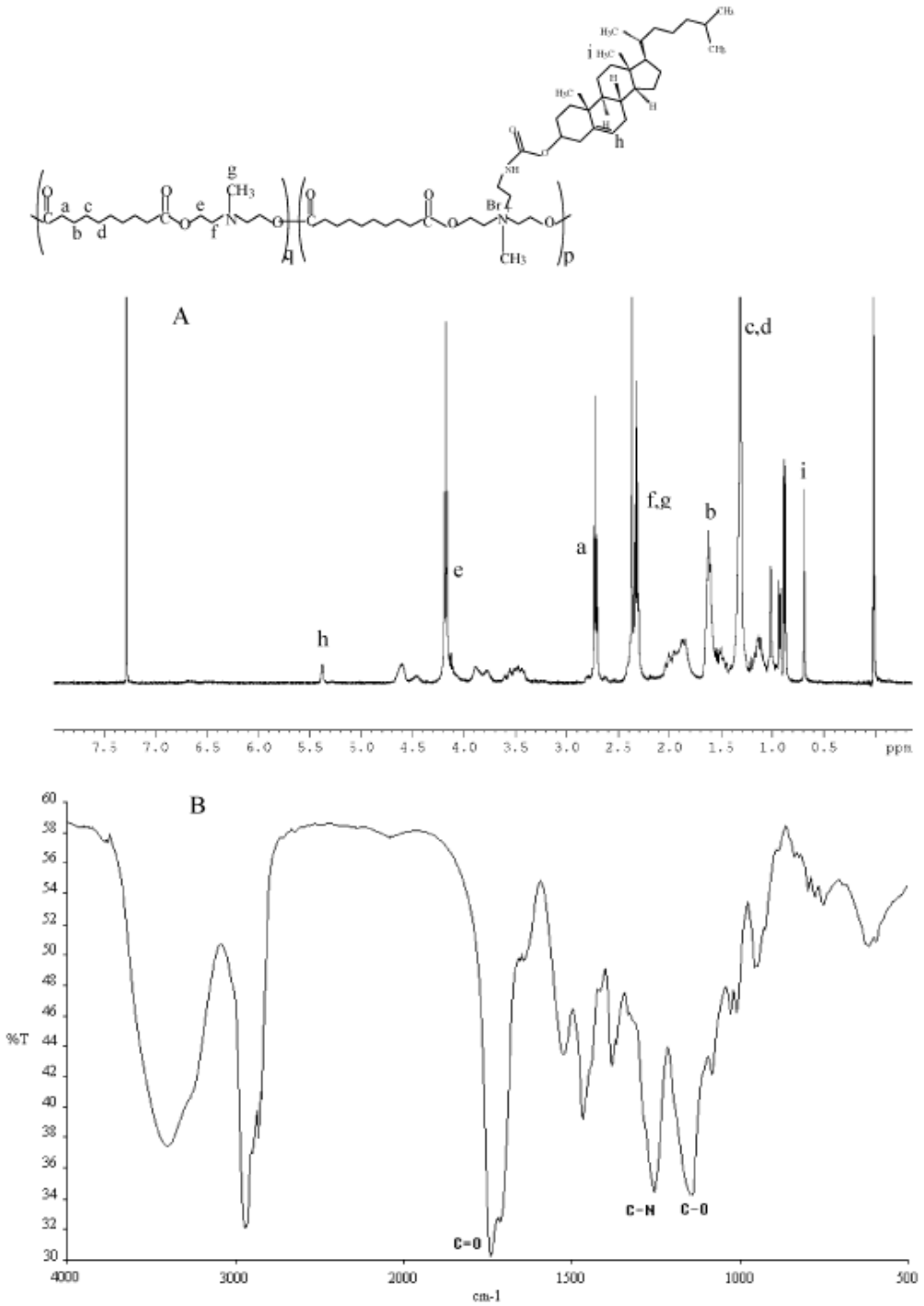

Figure A3. (A) ^{1}H NMR and **(B)** FT-IR spectra of P(MDS-*co*-CES).

Molecular Weight and Grafting Degree

The molecular weight of the polymer was measured by GPC while the grafting degree was obtained from ^{1}H NMR spectra. The weight average molecular weight (Mw) of

PMDS could reach as high as 18.5kDa while the Mw of P(MDS-*co*-CES) could be up to about 9.1 kDa. The molecular weight of P(MDS-*co*-CES) was usually lower than the PMDS, from which the P(MDS-*co*-CES) was synthesized. This indicates that the grafting reaction at the high temperature might cause the degradation of the main chain, resulting in a lower molecular weight. The degree of cholesterol grafting (*R*g), defined as the ratio of the number of amines quaternized by *N*-(2-bromoethyl) carbarmoyl cholesterol to the total number of amines on the PMDS main chain, can be estimated as follows

$$R_g = (\Delta A_p N_{Hm}/\Delta A_m N_{Hp}) \times 100\%$$

where ΔA_p is the area of the selected peak from the pendent chain, ΔA_m is the area of the selected peak from the main chain, N_{Hp} is the number of hydrogen atoms in the selected group from the pendent chain, and N_{Hm} is the number of hydrogen atoms in the selected group from the main chain. Only suitable protons from the pendent chain and the main chain of the polymers were selected in the calculation. The proton signal selected should not overlap with signals from other protons. Furthermore, those protons affected by the quaternized amines should not be used. For P(MDS-*co*-CES), the proton of the methylene group linked to the carbonyl group of the main chain (signal a), the proton of the methylidyne group (-CH=) linked to the double bond (signal h), and the proton of the methyl group linked to the hexane and pentane cycles of the pendent chain (signal i) were considered suitable for use in the estimation of *R*g. On the basis of the peak areas of signal a and signal i (Figure S3), *R*g for P(MDS-*co*-CES) was estimated to be about 27.0% (i.e., $R_g = \Delta A_i \times 4 \times 100\% / 3 \times \Delta A_{Ha}$) 2.046 x 4 x 100%/3 x 10.1 = 27.0% . By changing the molar ratio of the pendent chain to the PMDS main chain, *R*g of the cholesterol moiety and the positive charge of P(MDS-*co*-CES) could be modulated. The

cholesteryl grafting degree of P(MDS-*co*-CES) ranged from 9.4% to 56.2%, depending on the purity of PMDS and the amount of Be-chol added. However, the grafting degree seldom exceeded 60% even though the molar ratio of Be-chol to PMDS unit increased to 1.5. This is possibly because the structure of the cholesteryl group provided steric hindrance for the reaction.

TEM imaging of the micelles

Figure A4 shows a TEM image of P(MDS-*co*-CES) micelles that have been fabricated by the membrane dialysis method in DI water. The micelles had a regular shape in nature. Particle size of the micelles shown in the TEM image was smaller than that measured by dynamic light scattering because the micelles shown in the TEM image were in a dry state and the structure shrank after water was removed.

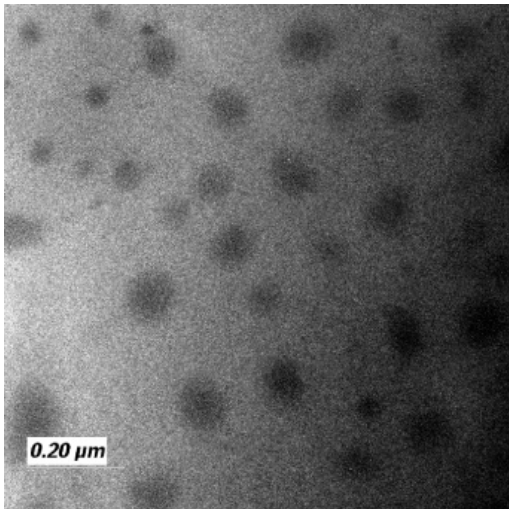

Figure A4. A typical TEM image of micelles prepared using P(MDS-*co*- CES) in DI water with a polymer concentration of 2 mg/mL.

APPENDIX II

ACUTE TOXICITY TEST REPORT IN MICE MODEL

This part of the research has been conducted in collaboration with Prof. Fan Weiming at Zhejiang University School of Medicine, Department of Cardiology, China. The objective of the study was to investigate the dose-related-acute toxicity, animal mortality and evaluate the safety of a single intravenous administration of P(MDS-co-CES) nanoparticles into mice.

Materials and Methods

40 Imprinting Control Region (ICR) mice were randomly divided into 4 groups (n = 10). Each group was given different dosages of the polymeric nanoparticles at 34.6, 26.3, 20.0 and 15.2 mg/kg respectively. After injection, the mice were observed for changes in physiology, behaviour, appetite, defecation, production of abnormal discharge from nose, eyes and mouth as well as mortality. The mice were first observed at 0.5 hr post-injection and subsequently every 0.5 – 1 hr. After the 1st day, the mice were monitored once a day for 7 consecutive days. The acute median lethal dose (LD50) was calculated by the Bliss method with 95% confidence limits. SPSS17.0 software was used for analyzing the experimental data and statistical analysis between groups was conducted with One-Way ANOVA.

Results

Effects on animal physiology

Mice treated with different dosages of nanoparticles experience changes in their physiology in different degrees. Those administered with 15.2 mg/kg nanoparticles were observed to decrease their movement and experience abdominal breathing 3 min post-injection, but the symptoms disappeared in 30 min. Mice injected with 20 mg/kg dose experienced immediate symptoms such as sunken eyes, erected haircoat and abdominal breathing, but the symptoms ease 1 h after the administration. Within the group, one male mouse died and post-mortem examination revealed that cause of death to be lung congestion. In the 26.3 mg/kg dose group, the mice to decrease their movement and experienced abdominal breathing, hunched posture and trembling immediately after administration. A day later, 3 male and 2 female mice died and 1 female mouse died the following day. Post-mortem examination revealed large areas of lung congestion, and foamy fluid secretion in the nose and mouth. In particular, one of the mice had yellowish-brown coloration on its kidneys. In the highest dose group 34.6 mg/kg, 5 male and 1 female mice died within 5 min post-injection and another female mice died 4 hr later. Post-mortem examination of the lungs showed large areas of congestion, while the kidneys, heart and spleen were of darker color than usual. All mice that survived for 2 days after the injections were able to return back to normal.

Table A1: Mortality of mice at different post-treatment time points.

Dose	**Mortality, Dead**								
(mg/kg)	**<24hr**	**Day 1**	**Day 2**	**Day 3**	**Day 4**	**Day 5**	**Day 6**	**Day 7**	**Total (%)**
34.6	7	0	0	0	0	0	0	0	7 (70%)
26.3	5	1	0	0	0	0	0	0	6 (60%)
20	1	0	0	0	0	0	0	0	1 (10%)
15.2	0	0	0	0	0	0	0	0	0 (0%)

Determining the median lethal dose LD_{50}

Tail vein injection of the tested mice resulted in 70%, 60%, 10% and 0% mortality in the 34.6, 26.3, 20.0 and 15.2 mg/kg dose groups respectively (Table A1). The median lethal dose, $LD_{50,}$ determined by Bliss method, was 27.7 mg/kg with 95 % confidence interval of 23.9 ~ 32.1 mg/kg.

Effect on body weight

After treatment, the body weights of the tested mice were monitored on Day 1, 3 and 7. The mean body weight of the 34.6 mg/kg dose group was found to be slightly lower compared to other groups. However, no statistically significant difference was found with when One-Way ANOVA analysis was conducted (P> 0.05).

Table A3: Mean body weight of mice after treatment.

Dose (mg/kg)	**Mean Body Weight（g）**		
	Day 1	**Day 3**	**Day 7**
34.6	19.8 ± 0.97	25.0 ± 1.06	26.6 ± 1.74
26.3	19.7 ± 1.15	26.0 ± 1.94	27.2 ± 2.56
20	19.9 ± 1.35	27.3 ± 1.93	28.9 ± 2.70
15.2	19.9 ± 1.24	26.9 ±2.52	28.7 ± 3.34